NASA CONTRACTOR REPORT

NASA CR-548

DATA REQUIREMENTS FOR IN-FLIGHT SYNTHESIS AND MULTIPLE BLENDER STUDIES

by L. D. Edinger and G. D. White

Prepared by
HONEYWELL, INC.
St. Paul, Minn.
for George C. Marshall Space Flight Center

NATIONAL AERONAUTICS AND SPACE ADMINISTRATION • WASHINGTON, D. C. • AUGUST 1966

DATA REQUIREMENTS FOR IN-FLIGHT SYNTHESIS AND MULTIPLE BLENDER STUDIES

By L. D. Edinger and G. D. White

Prepared under Contract No. NAS 8-11206 by
HONEYWELL, INC.
St. Paul, Minn.

for George C. Marshall Space Flight Center

NATIONAL AERONAUTICS AND SPACE ADMINISTRATION

For sale by the Clearinghouse for Federal Scientific and Technical Information
Springfield, Virginia 22151 – Price $6.00

FOREWORD

This document partially comprises the final report prepared by Honeywell, Incorporated for George C. Marshall Space Flight Center, Huntsville, Alabama, 35812 under contract NAS 8-11206.

This report contains results of studies conducted to (1) define data requirements for in-flight synthesis and (2) evaluate a multiple gyro blender technique with respect to control of a large flexible launch booster.

The work on this contract was supervised by Mr. C. R. Stone and Dr. E. R. Rang. Mr. L. D. Edinger and Mr. G. White are the authors of this report.

ABSTRACT

This document reports the analysis performed in the following studies:

(1) Data Requirements for In-Flight Synthesis
(2) Multiple Blender Study

The objective of the two studies was to develop improved techniques for the control of large flexible boosters of the Saturn class. The flight control problem was broken into two parts: (1) identification and (2) synthesis. Work in the Data Requirements for In-Flight Synthesis Study concentrated on solving the synthesis problem. By so doing, it was possible to establish design requirements for an identification process.

Work in the multiple blender study was concerned with extending the basic Honeywell rate gyro blender concept to provide control of two independent structural bending modes. This was accomplished by blending three rate sensors using three adaptive blenders.

As a result of the work performed in the In-Flight Synthesis study, a control system was defined which met all performance requirements including damping augmentation requirements on the first two bending modes. Data to be regulated by an identification process and the accuracy of the regulation was also defined.

The concept of multiple blending was found to be feasible, however, several problem areas were encountered in extending the single blender concept to use in a multiple blender system. As a result, an improved blender logic was suggested for application to a multiple blender system.

CONTENTS

ILLUSTRATIONS

SECTION 1
INTRODUCTION

This document, Volume I of a two-volume report, describes the analysis conducted in the following areas:

(1) Definition of data requirements for in-flight synthesis

(2) Evaluation of a multiple blender technique

The general objective of these studies was to develop means for controlling flexible boosters of the Saturn class.

Current efforts of research in the area of flexible booster control may be categorized as being concerned with (a) the identification problem and (b) the synthesis problem. In general, a flight control system consists of both an identification process and a synthesis process (i.e., a control law).

The danger in considering either process separately is that often the objectives of the research are not clearly defined. This situation is evident in much of the work on plant identification. Often the relative importance of the vehicle characteristics being identified and the required accuracy of the definition have not been established. Even if a complete on-line identification of the vehicle transfer functions was available, a satisfactory in-flight synthesis technique might not exist. It follows that there is a clear need for research on the problem directed towards an application having relatively formidable control requirements. Fulfilling this need is the objective of the first study, i.e., definition of data requirements for in-flight synthesis. Definition of a synthesis technique will make it possible to specify the data requiring regulation by an identification process. This information can, then, in turn be used to specify requirements for design of an identification process.

One well-developed identification technique is known as the rate gyro blender. This technique uses a implicit identification to provide the required rigid-body signal and favorable bending signals to the control system. It does this by adaptively combining the outputs of two rate gyros according to their relative bending content. This technique has been used successfully to control a flexible vehicle with only one significant bending mode. However, this concept must be extended to provide control of vehicles with more than one significant bending mode. The purpose of the second study (i. e. evaluation of a multiple blender) was to evaluate the extension of the blender concept by using a combination of blenders. Three blenders were used together with three rate gyros to provide implicit identification of the rate-sensor rigid-body content and the bending content for the 1st and 2nd modes. It was the objective of the study to define the advantages and requirements for the implementation of such an approach. The NASA model vehicle No. 2 was used as the vehicle for both the multiple blender study and for the synthesis study.

This document first presents a summary of each of the studies. The balance of this volume is a detailed discussion of the vehicle performance requirements, rigid body analysis and flexible vehicle analysis. Nomenclature is defined in Appendix A. Vehicle data and equations are summarized in Appendix B, and performance results in terms of analog computer traces are presented in Appendix C. Appendix D contains the root locus plots and Appendix E the frequency response plots.

SECTION 2
SUMMARY AND CONCLUSIONS

In this section each study is reviewed by first considering the design objectives and design philosophy. Next, the nominal systems are summarized together with the conclusions and recommendations made as a result of the studies.

DATA REQUIREMENTS FOR IN-FLIGHT SYNTHESIS

Design Objectives

The study had three objectives:

- Determine a satisfactory control law for Model Vehicle No. 2 (see reference no. 2) considering performance requirements which stipulate positive control of two bending modes. Positive control of a bending mode is interpreted to mean that either the bending frequency or damping or both will be artificially augmented by the control system.

- Define data requirements for the control law established. The purpose for defining the data requirements was to establish the parameters requiring regulation by a plant, identification process. By so doing, it should be possible to use the data to establish design objectives for an identification process.

- Define a control law which does not depend on any time schedules for regulation of the variable control parameters. Time scheduling of parameters cannot adapt to unpredicted changes in the trajectory or cope with unknown vehicle characteristics. An additional objective

of the study was, then, to derive the necessary relationships for regulating the variable control parameters independent of time scheduling.

Design Philosophy

The study objectives can be approached in several ways. In order to determine the most reasonable approach, let us first consider the over-all flight control system shown in Figure 1. Design of the flight control systems consists of defining the control law and the identification process. The control law senses a set of state variables (e. g. pitch rate), shapes each of the signals and sums them together to generate a corrective gimbal deflection command through added shaping. An identification process determines certain plant characteristics and in turn modifies the control law as needed to assure proper control. The over-all objective of the study, then, is to define an effective control law and by so doing, define the data required by the control law which must in turn be regulated or modified by an identification process. If the data requiring regulation or modification by an identification process can be minimized, then the requirements for an identification process should be reduced.

Two approaches may be taken in the design of the control law. One approach is to design a control law assuming that explicit rigid body signals and body bending signals are available. To do this implies that either ideal sensors are used (which is unrealistic) or else an explicit identification process is used. Explicit identification is one which pure rigid body signals and pure bending signals are extracted from sensor outputs. While use of input data in an explicit form may somewhat simplify the design of the control law, it greatly increases the complexity of the identification process. Experience has shown that explicit identification is difficult to achieve especially in the presence of noise and unpredictable disturbances such as wind inputs. Thus, requiring input data in an explicit form places the burden of design on the identification process.

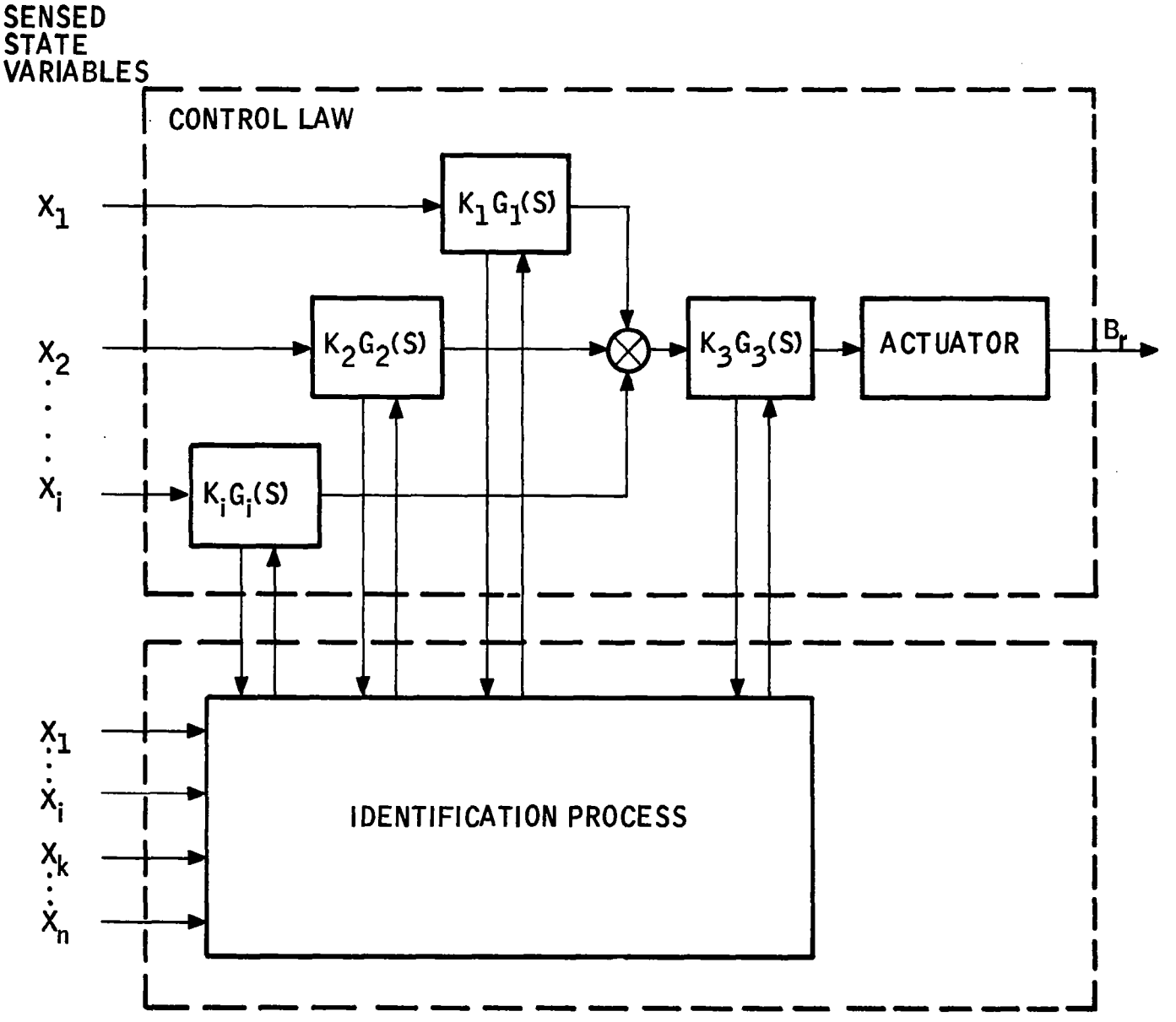

Figure 1. General Flight Control System

The second design approach is to assume that realistic sensors and implicit identification are used to provide data for the control law. If realistic sensors are assumed and only implicit identification is required, then it seems reasonable to assume that the complexity of the control law may be increased because of added shaping which may be required. However, this second approach should greatly reduce the complexity of the identification process. In general, it is easier to obtain implicit identification rather than explicit identification, and the accuracy requirements of the identification may often be relaxed. This approach, then, is believed to minimize the complexity of the over-all flight control system and result in the best over-all performance.

To summarize, the philosophy to be used in the design of the control process is one in which only realistic sensors and implicit identification processes are considered. The use of this philosophy should result both in the minimization of data requiring regulation by an identification process and in a practical and relatively simple flight control system.

Description of Nominal Control System

A block diagram of the nominal control system defined in the study is shown in Figure 2. It is basically an attitude hold control system with acceleration feedback added to provide just enough weathercocking to assure that the bending moment is kept within allowable limits. The attitude sensor location was specified by NASA. The accelerometer location of 90 meters was based solely on rigid body requirements. The forward loop filter is a third over a fifth order filter. Its primary function is to gain stabilize the third and higher bending modes.

Definition of Data Required

With this system, the only data required to be regulated by an identification process is the forward loop gain, K_c, and the bending content of the rate feedback, $\dot{\phi}_B$.

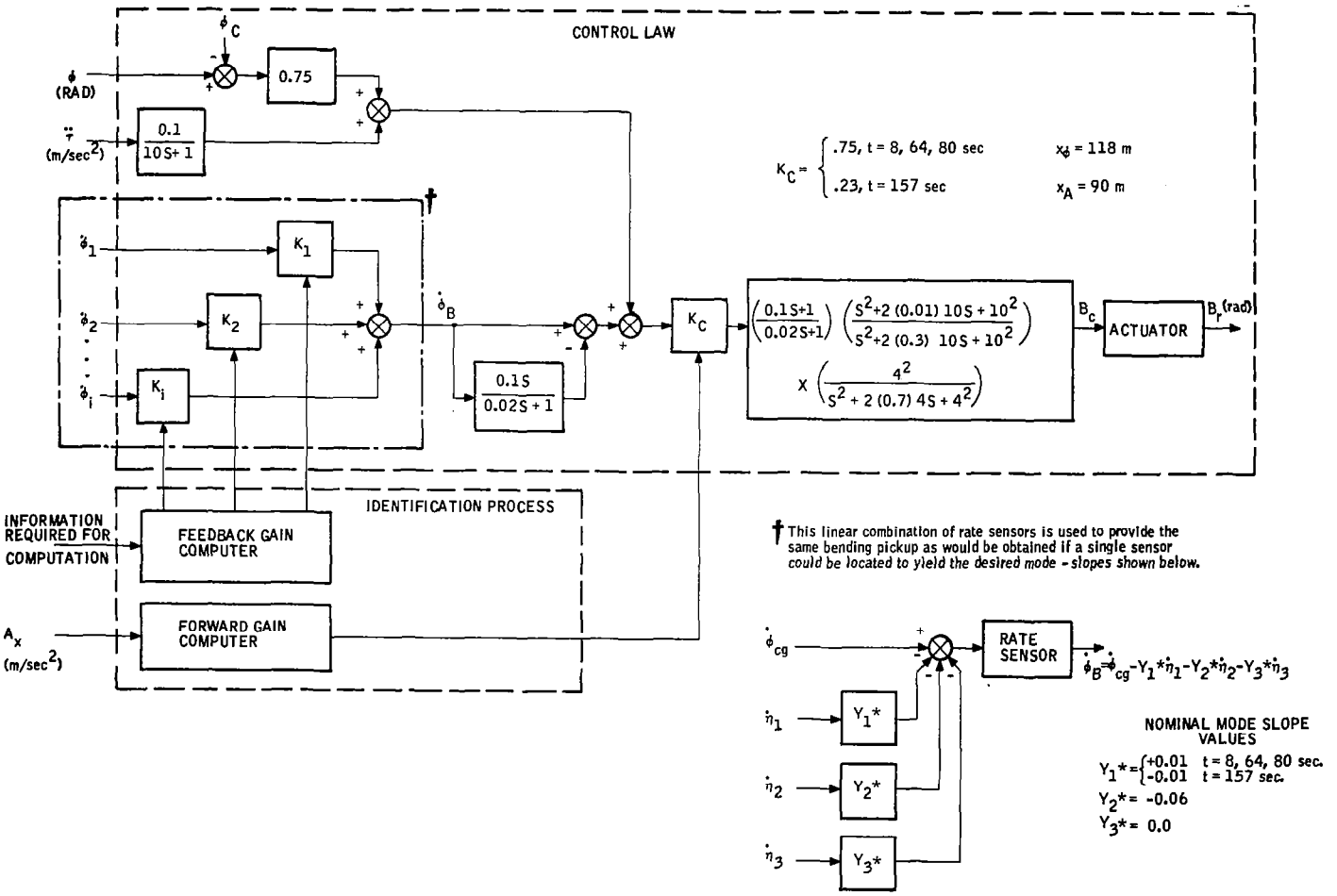

Figure 2. Nominal Flight Control System for Synthesis Study

An axial acceleration sensor is used as the intelligence for changing the forward loop gain, K_C. The forward loop gain takes on two discrete values over the flight trajectory. The gain is switched from a value of 0.75 to a value of 0.23 when the axial acceleration increases above a set value. The actual value of the axial acceleration at which the gain is switched and the accuracy required in measuring the acceleration could not be definitely established by the study since only four flight conditions were considered.

The rate feedback signal is a linear combination of rigid body rate and bending rate feedback signals. These signals can be thought of as being provided by a single sensor. For the nominal system, the rate sensor would have to be placed at a hypothetical position on the vehicle such that the bending mode slopes at the sensor location would have the following values:

$$y_1' = \begin{cases} .01 & t = 8,\ 64,\ 157 \text{ seconds} \\ -.01 & t = 157 \text{ seconds} \end{cases}$$

$$y_2' = -.06$$

$$y_3' = 0$$

These are the nominal values of the slopes necessary to provide the required damping on the 1st and 2nd bending modes and gain stability on the 3rd modes. Examination of the mode shapes for the vehicle will quickly show there is no single rate sensor location which will provide these mode slopes. Thus, to provide these mode slopes two or more rate sensors will have to be combined in some fashion by the identification process. The values of the mode slopes given above are the desired nominal values. Figures 3 - 6 are plots of the allowable ranges of these mode slopes which still assure the required bending mode damping and the gain stability of 6 db on the 3rd mode.

It was assumed in the study that an identification process would generate the desired mode slope on the 1st and 2nd bending modes by actively identifying

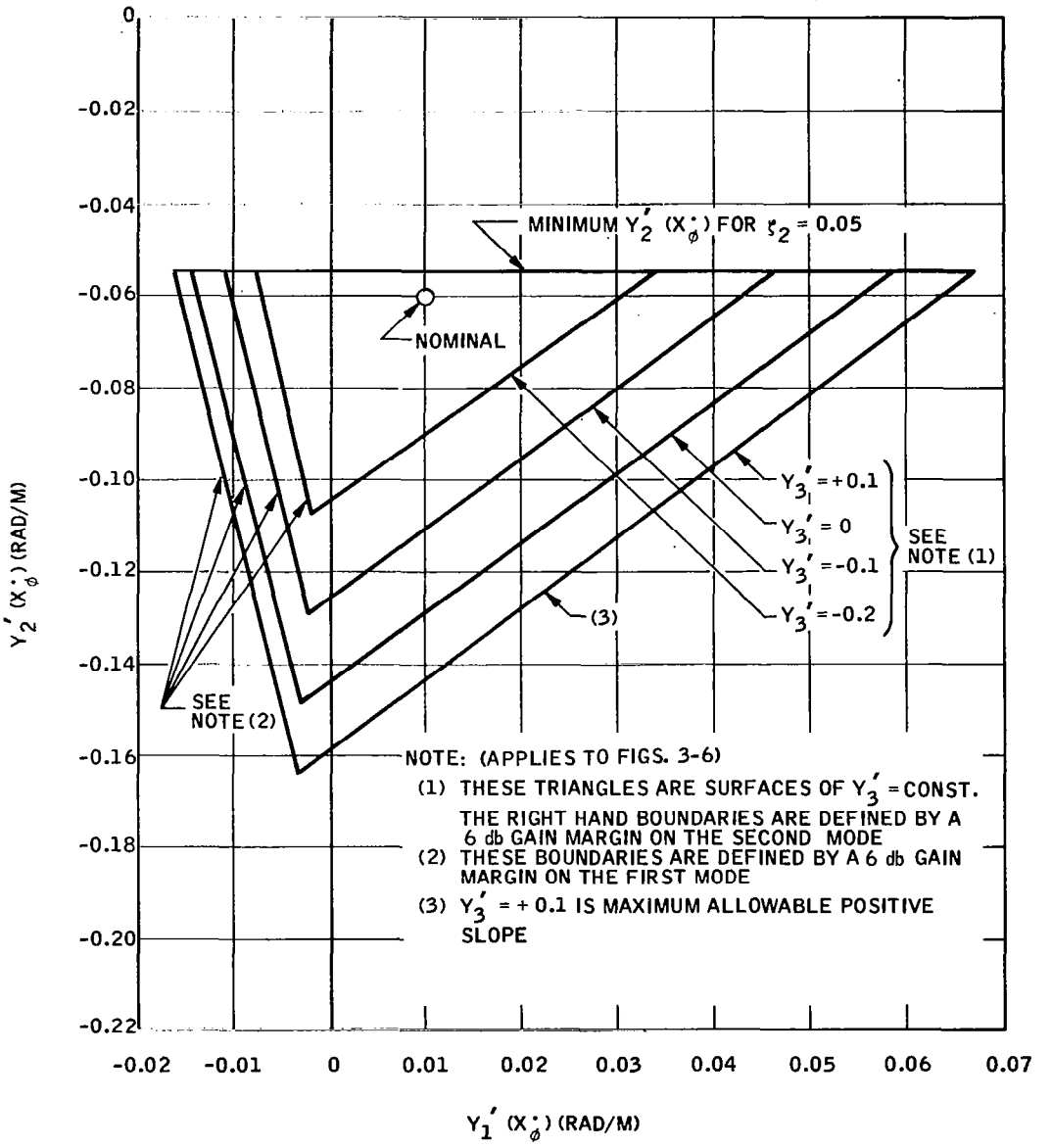

Figure 3. Range of Allowable Mode Slopes, t = 8 seconds

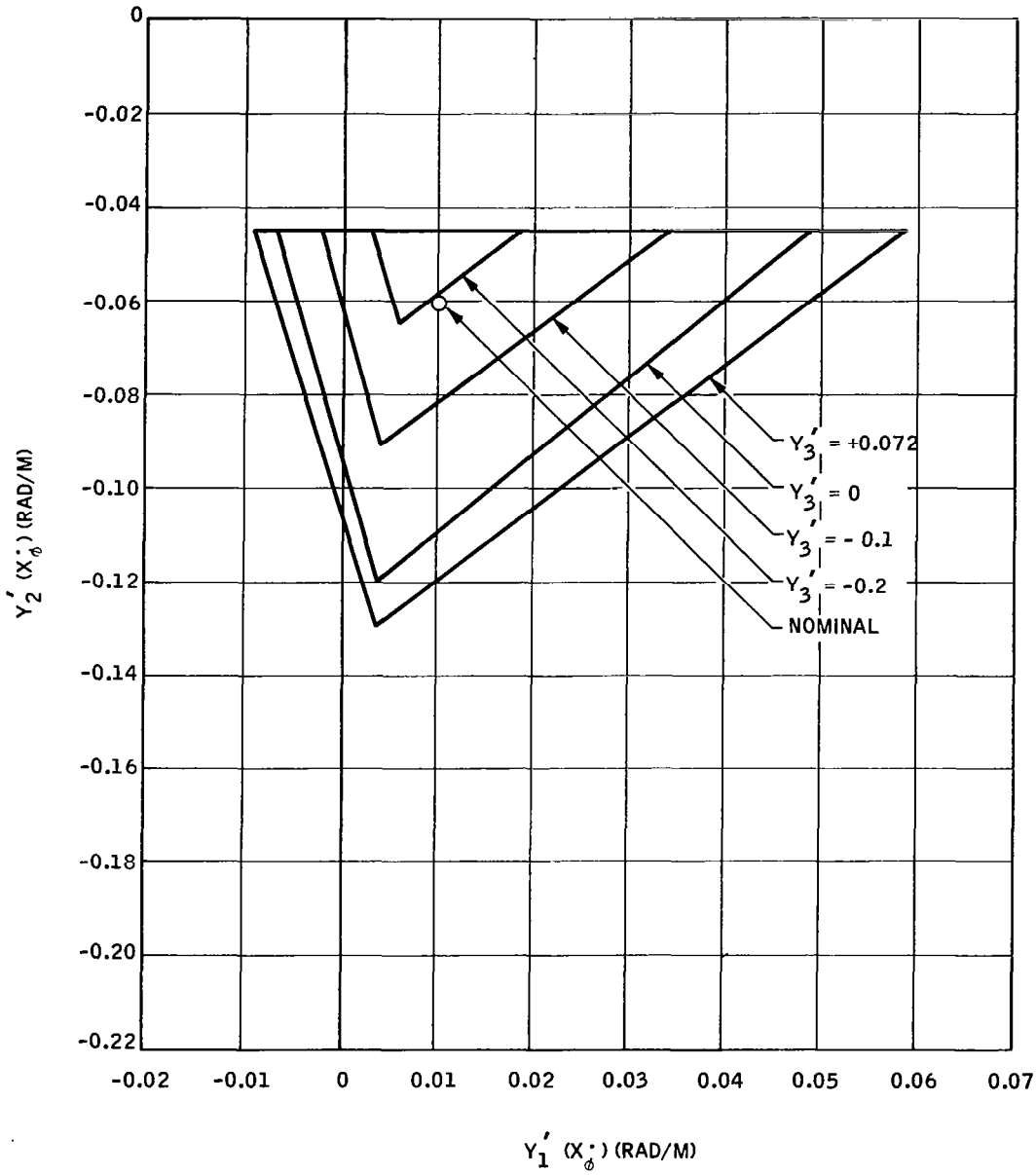

Figure 4. Range of Allowable Mode Slopes, t = 64 seconds

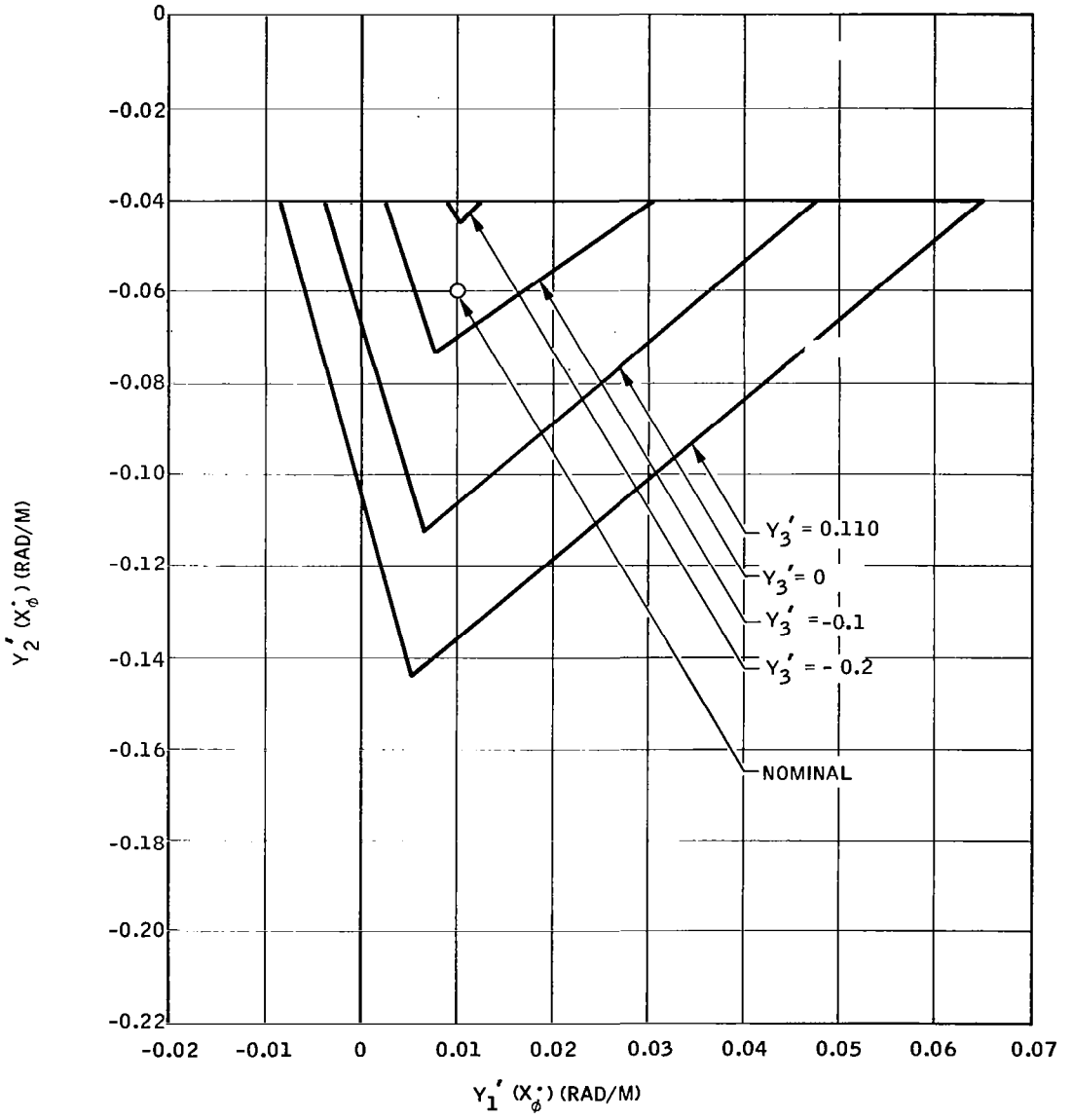

Figure 5. Range of Allowable Mode Slopes, t = 80 seconds

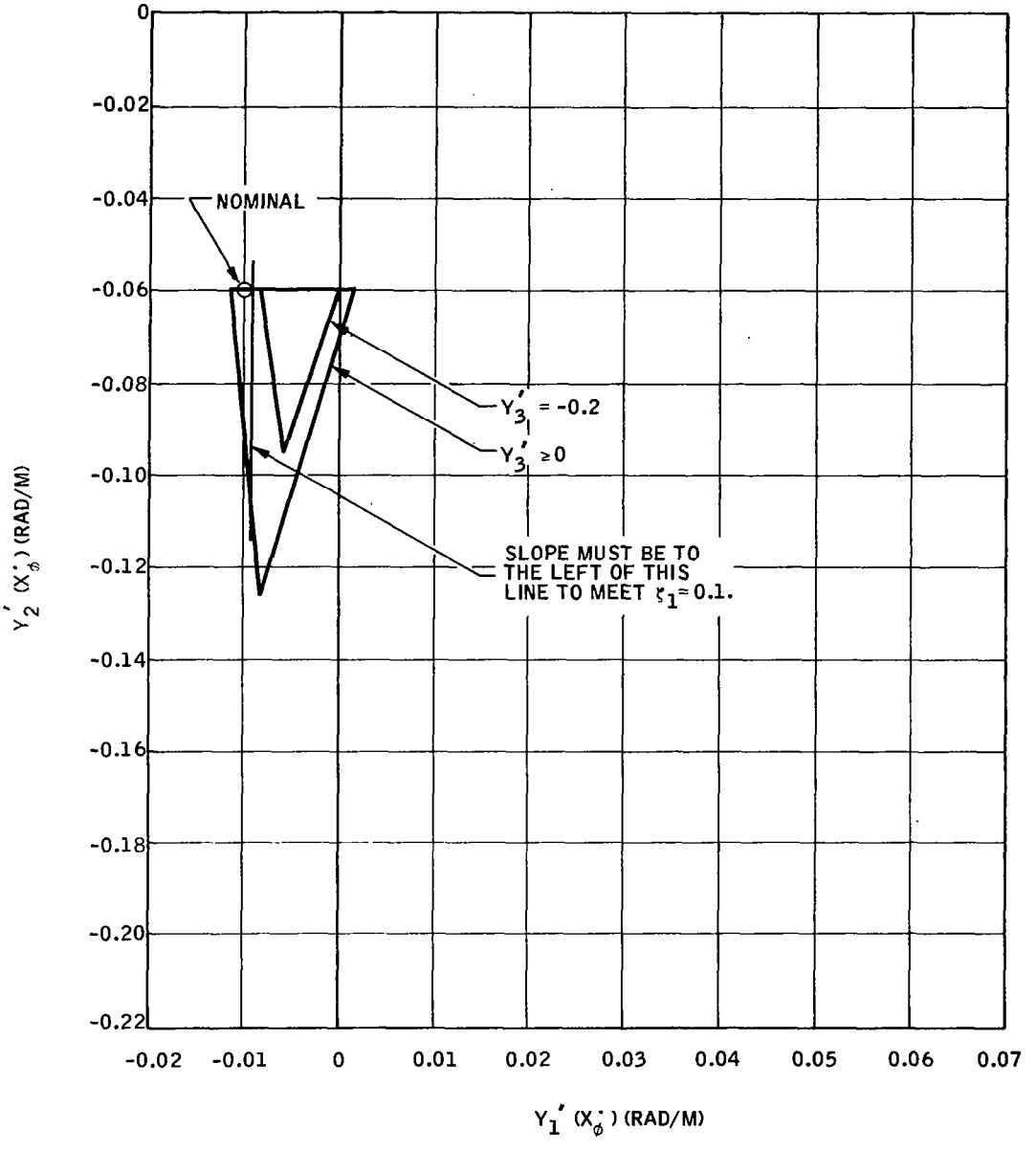

Figure 6. Range of Allowable Mode Slopes, t = 157 seconds

the modes. Thus, the third mode slope would have to be obtained passively by suitable placement of the sensors. However, it is also conceivable that the identification process could also be used to actively identify a desired slope on the 3rd mode. To determine whether this is necessary or not was beyond the scope of the study. The objective of the study was to define the allowable ranges on the mode slopes (as shown in Figures 3-6). This data is to be used in future studies to define an identification process. A future study could establish how many modes must be actively identified in order to assure the slopes are within the allowable ranges.

Conclusions and Recommendations

Conclusions

The control system developed during this study met or exceeded the performance requirements. The required damping ratios on the 1st and 2nd bending modes were attained while gain stabilizing the 3rd and higher modes (for the range of allowable mode slopes). The only input data requiring regulation by an identification process was the rate feedback and the forward loop gain, K_c. The system was designed to maximize the tolerance on this data. Several significant results were obtained in the study but were not necessarily reflected in the final control system. They are as follows:

- A rigid body controller was defined which met the rigid-body performance requirements at all flight conditions with fixed control parameters. A fixed-parameter rigid-body controller was attained primarily through the use of a heavy lag on the accelerometer feedback. This lag not only increased the gain margin but also significantly reduced the bending moment during a wind disturbance.

- The attitude sensor and accelerometer were located on the vehicle without regard to vehicle bending considerations. The attitude sensor location was specified by NASA and the accelerometer location was determined only by the rigid body analysis.

- Although the requirements stipulated that the 3rd mode need only be phase stabilized, the resulting system actually gain stabilized the 3rd and higher modes while providing a damping ratio of 0.05 on the 2nd bending mode and 0.1 on the 1st bending mode. The forward loop filter required to do this was relatively simple, being only a 3rd over 5th order.

- A means for regulating the forward loop gain independent of a time schedule and the vehicle environment was defined. While the gain changing technique must still be considered to be an open loop process it also should be tolerant to a wide variety of parameter variations. Probably the greatest concern over the use of time-scheduled parameters is in the case of an engine failure. In that event the burn time of the remaining engines would be extended to obtain the desired total impulse. A time scheduled parameter could not adapt to this change. However, by using axial acceleration this change in conditions would be accommodated.

- A useful relationship was developed between the bending mode zero locations and the control system feedback configurations. It was found that the location of the bending zero for each mode could be established simply by a hand analysis of the control system feedback configuration. This proved to be a useful tool in the development of the controller.

Recommendations

- In the design of the control system, a considerable price was paid to achieve . 05 damping on the 2nd mode, gain stability on the 4th and higher modes, and a large tolerance to variations in the third mode slope. It is felt that perhaps a damping ratio requirement of.. 05 on the 2nd mode, while desirable, could be relaxed without significantly reducing the over-all performance. This requirement was rather arbitrarily defined so there is no real physcal basis for it. A value in the range . 01 - . 02 might be more practical. If this requirement were relaxed, a much simpler and more tolerant control system could be realized.

  The damping ratio requirement of 0. 1 on the first mode was not difficult to achieve. No added system complexity was required to meet this requirement. However, as with the damping requirement on the second mode, there was no definite basis for the 0. 1 damping requirement. Thus, it is recommended that some realistic criteria be derived for the damping required.

- The development of an off-line synthesis technique is recommended for future study. More often than not, a designer is faced with trying to define a good control system in a short time span. Using the present day synthesis techniques, namely trial and error, the designer is able to investigate only a relatively small number of control system configurations. In so doing, it is not always possible to derive the most effective solution to a control problem. Since it is not likely that the development time will be increased, a means must be found for speeding up the synthesis procedure. Current research in optimal control is directed towards this end. However, the optimal control approach using the cost function or a performance index is deficient because the relationships between the cost function and the basic performance requirements are not well established. Hence a system that is optimum in the sense of the assumed cost function may not satisfy the basic requirements.

- It is recommended that the input data defined by this study be used as a design objective for future identification schemes applicable to the type of vehicle analyzed herein. It should be noted that the data is to be used primarily to define what parameters must be identified and the required accuracy of identification. This does not necessarily mean these numbers will be valid for all future applications of this type.

MULTIPLE BLENDER STUDY

Study Objectives

The use of a single rate-gyro blender to control bending mode effects in a large flexible booster has been shown in earlier studies (Ref. 2) to be a promising approach. The original objectives of the current study were to determine the advantages to be gained by extending this concept to the use of two or more rate gyro blenders and to determine the requirements for implementation including the required accuracy of computation.

During the course of the study, certain problem areas became apparent in attempting to extend the use of a single blender logic to a multiple blender. These problem areas were presented at a coordination meeting with NASA, Huntsville. It was agreed at this meeting that the remaining effort on the blender study should be directed towards elimination of these problem areas by developing a new logic circuitry. It was agreed that this new effort would replace the tolerance studies and parameter variations which had been planned for the existing blender and associated logic scheme to determine computational accuracy requirements.

Design Philosophy

The basic aim of the multiple blender design was to provide phase stabilization of the first two structural bending modes by suitably blending signals from three rate sensors. The design was to be based on multiple use of the present single adaptive blender and its associated logic circuitry (Ref. 2). The approach was to demonstrate the feasibility of multiple blending by blending three rate sensors with a combination of these single adaptive blenders to provide the desired control of two bending modes. Further aims of the study were to refine and simplify the adaptive logic for the particular application of multiple blending.

Description of Nominal System

The nominal control system configuration, including the multiple adaptive rate gyro blender, is shown in block diagram form in Figure 7. Figure 8 is a block diagram of the multiple blender alone which shows the form of the adaptive logic. Attitude and attitude rate feedbacks are used to provide an attitude hold system. A normal acceleration feedback and an angular acceleration feedback are added to provide a load relief capability to assure that the maximum allowable bending moments are not exceeded.

The attitude sensor was specified by NASA to be at station 118 meters. The three rate sensor locations were established by the study to be at stations 118 meters, 90 meters, and 46 meters. The accelerometer location was determined by the study to be at station 60 meters.

A fourth order notch filter was used in the forward loop to represent (at the 1st and 2nd bending mode frequencies) the gain and phase characteristics of a filter designed to gain stabilize the fourth and higher structural modes. The fourth order filter shown in the diagram does not provide gain stability for bending modes above the fourth mode. A complete higher mode filter was not defined as it was unnecessary in order to establish the multiple-blender feasibility.

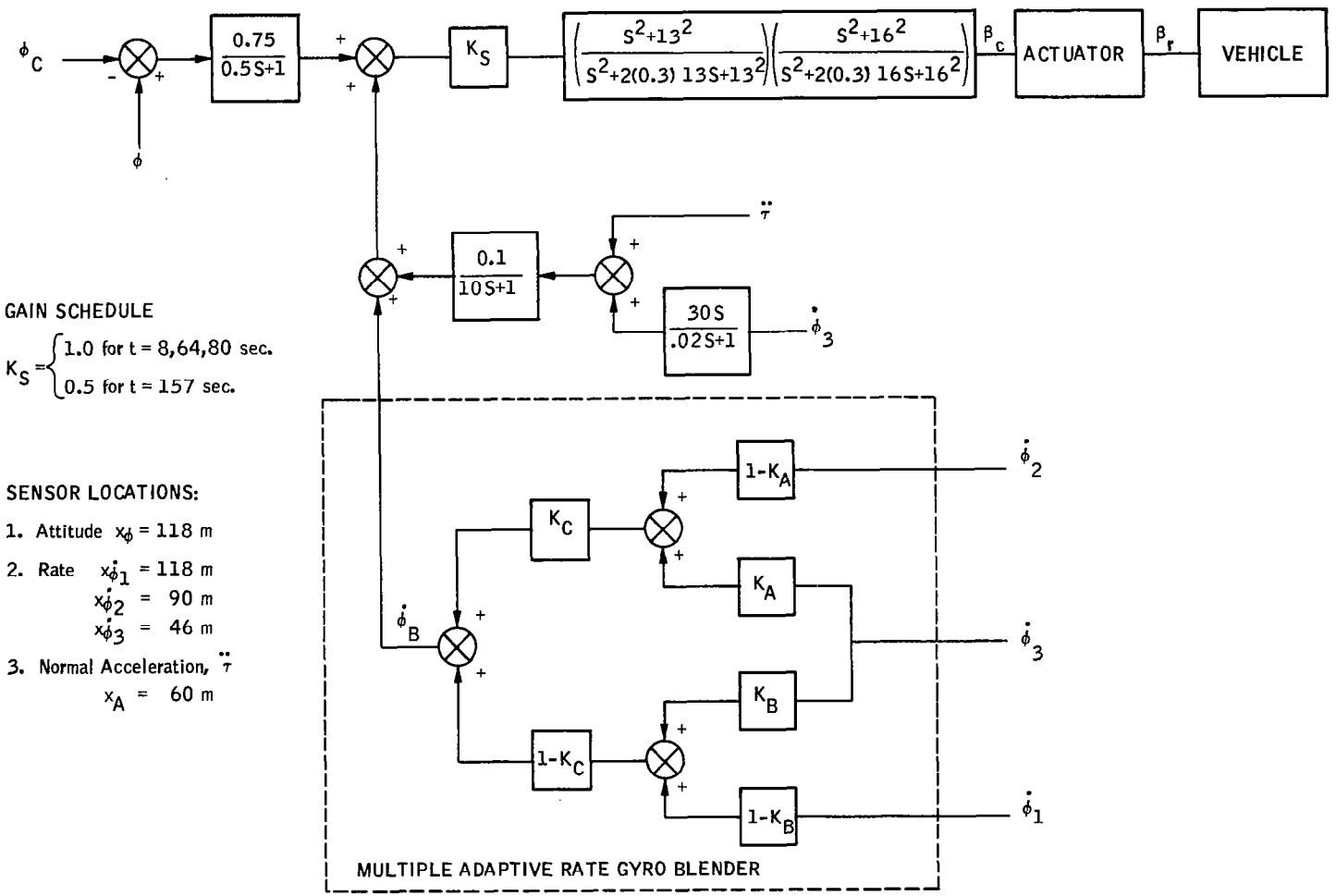

Figure 7. System Block Diagram for Multiple Blender Study

Since the forward loop gain must take on two discrete gain values over a flight trajectory some means must be provided for scheduling this gain. However, since the objective of the study was to evaluate the feasibility of multiple blending, no effort was made to define a means for scheduling the forward loop gain. It was assumed that any scheduling of this gain would have no effect on the operation of the multiple blender. However, time scheduling would probably be the most likely candidate for this job since it is a well-proven technique.

The multiple blender configuration (shown in Figure 8) consists of three single-blender logics which operate on rate signals from three rate gyros. Blenders one and two (see Figure 8) operate to provide the required first bending mode slope. Blender no. 3 (see Figure 8) operates to provide the required mode slope for the second mode. Each of the single blender logics contains two complex seventh order bandpass filters. The blender integration rates, K_1, K_2, K_3 were defined by the study to be 0.05 units/unit error, ϵ. The constant factors K_1', K_2', and K_3' shown in each logic (see Figure 8) are used to bias the logics to generate the desired mode slopes. The following values of these constants were: $K_1' = 1.88$, $K_2' = 1.52$, $K_3' = 2.28$.

As was indicated in the study objectives, during the multiple blender study several problem areas were encountered in defining a multiple blender configuration. Problems inherent in the single blender logic were compounded by combining three blenders together. These basic problems were:

- System complexity. Each blender contains two complex bandpass filters, an integration, and two multiplications.

- Restricted blender operating range. Each blender attenuation factor can take on values only between zero and one. This limitation in turn requires a set of constraints to be placed on sensor locations in terms of allowable ranges of the bending input to each sensor (e. g. slopes and deflections). Many of these constraints could be eliminated, along with a reduction

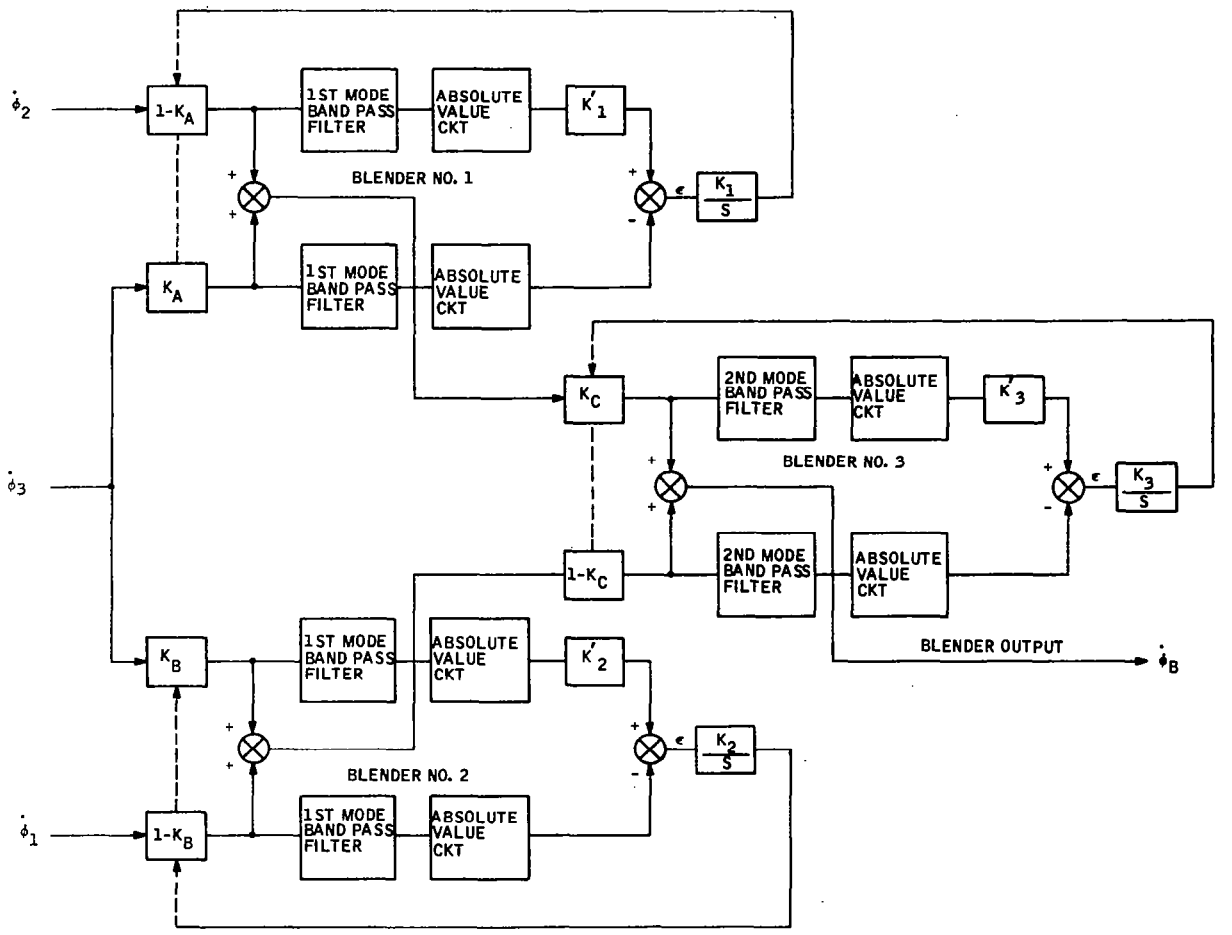

Figure 8. Multiple Adaptive Rate Gyro Blender Logic

in the required accuracy of the bending data, if the limitation on blender position could be removed.

- Blender logic contamination. Unwanted signals (e.g. rigid body rate) appearing in the logic tend to drive the blenders away from the desired values.

To overcome these problems, effort was directed towards the development of a new single blender. As a result of this effort, a new blender was defined. A block diagram of it appears in Figure 9. This logic was designed to eliminate the restriction on the blender operating range, reduce the complexity and to alleviate the problem of logic contamination by unwanted signals, primarily the rigid body signal. This logic is based on using the difference of two rate gyros and measuring the rate of change of the bending amplitude to compute the blender attenuation factor, K, (see Figure 9).

Conclusions and Recommendations

Since the objective of this study was to investigate the feasibility of a concept, the conclusions and recommendations derived from the study are of a qualitative rather than a quantitative nature.

Conclusions

- Multiple blending is a feasible concept. It is possible to provide positive control of more than one bending mode of a flexible vehicle by utilizing the combined signals of a series of single adaptive rate gyro blenders.

- The adaptive logic of the single blender used in the multiple blender study and defined in Reference 2 contains critical problem areas which become even more critical when it is used in a multiple blender configuration.

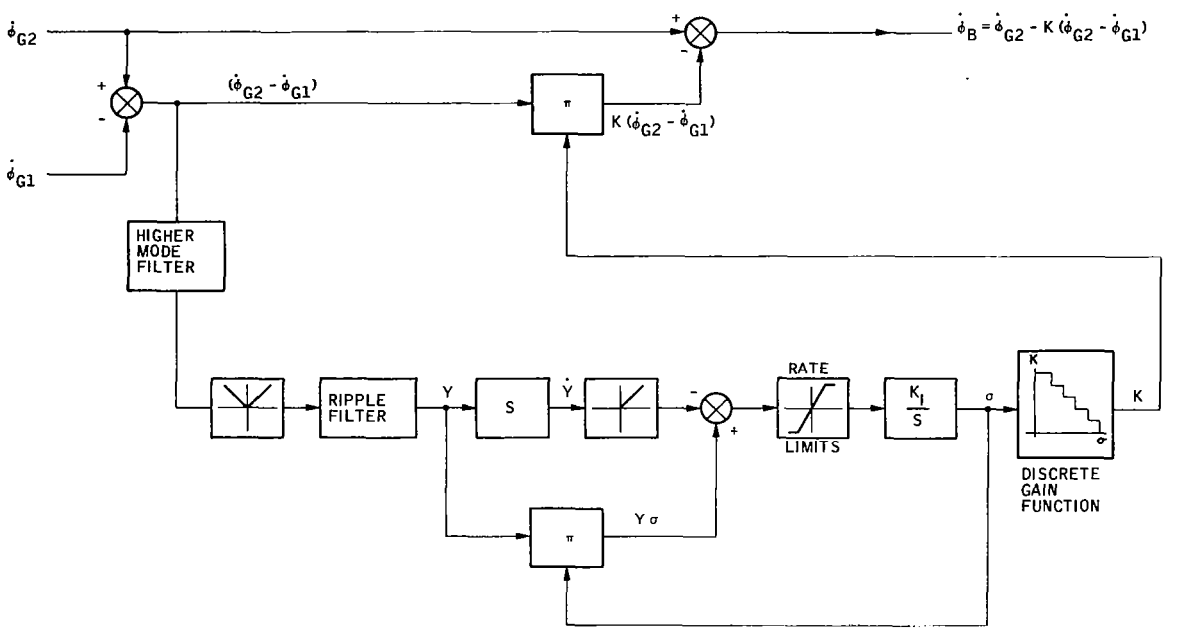

Figure 9. Block Diagram of New Blender Configuration and Adaptive Logic

- The adaptive logic of the blender defined in Reference 2 is suitable for a single blender operation in which it is required to control one bending mode only.

- A new adaptive logic has been defined. Preliminary performance results obtained from a blender utilizing the new logic appear promising.

Recommendation

Further investigation and refinement of the new adaptive logic defined in this study should be conducted with a view towards utilization of the logic in a multiple blender.

SECTION 3
PROBLEM DEFINITION

STUDY VEHICLE

The vehicle used in this booster research study was the NASA "Model Vehicle #2" (see reference 1). This model is intended to be respresentative of large flexible space vehicles (similar to or larger than Saturn V) but is not intended to represent any specific vehicle. It was originally stipulated that Saturn V data, furnished for a past study (see reference 2), would be modified. The modifications would essentially consist of reducing bending frequencies by a factor of two and elimination of fuel sloshing and engine inertia dynamics. However, the "Model Vehicle #2" data contained bending mode dynamics with frequencies which were roughly half of those encountered in the Saturn V data. Thus, since the model vehicle No. 2 data was also readily available, it was agreed this would serve the purpose of the study.

CONDITIONS ANALYZED

The work statement also stated that three flight conditions would be analyzed. They were the launch condition (t = 8 sec), the maximum dynamic pressure condition (t = 80 sec) and the burnout condition (t = 157 seconds). However, upon examination of the data it was decided to add a fourth condition, namely, the Mach 1 condition (t = 64 seconds). Originally it was assumed that the maximum bending moment would occur at the maximum dynamic pressure condition. But it was found that at Mach 1, the bending moment due to angle of attack, M'_{α}, is a maximum and the wind gradient appeared to be a maximum. Hence, it was assumed that the maximum bending moment would occur at this condition and not at the maximum dynamic pressure condition. Therefore, to encompass the extreme flight conditions, the Mach 1 condition was added.

It was assumed that a controller designed to provide satisfactory vehicle performance at these extreme conditions would likewise provide acceptable performance for the entire flight trajectory.

The bending moment was evaluated with respect to the NASA model wind at the flight times of 64 and 80 seconds. Graphs of the model winds which were used at these two conditions are shown in Figures B-2 and B-3. Two points should be noted concerning these wind models. The models included both the wind shear and the gust as suggested in the data package (see reference 1). It was also suggested in the data package that the wind be reduced in amplitude a short time after it reaches its peak value. However, in the model used for this study the wind amplitude was not reduced after the peak occurred (see figures B-2 and B-3). This results in a slightly more severe wind condition but it was felt that this simplification would not affect the validity of the study.

SIMPLIFICATION

Various simplifying assumptions were made concerning the model vehicle No. 2 data. They are as follows:

- Fuel sloshing and engine inertia dynamics were not included.
- Only three structural bending modes were considered.
- Third order actuator dynamics were used but rate and deflection limits were not included in the simulation. However, the effect on performance was qualitatively analyzed.
- Sensor dynamics were not included in the simulation, but their effect on performance was considered.

The vehicle equations of motion and vehicle data appear in Appendix B. The equations are essentially identical to those given in the data package (see reference 1) except for the following corrections and simplifications:

- The aerodynamic term

$$13.2\ qA\ \frac{(\ell cg - 41.5)}{Ixx}\ \sin^2\alpha$$

was neglected in the pitch angular acceleration equation. Correspondingly the term

$$13.2\ qA\ \frac{\sin^2\alpha}{\alpha}$$

was neglected in the expression defining N'. It was concluded that inclusion of these terms would only increase the complexity of the simulation and would not contribute to attainment of the study objectives.

- For clarification, a subscript F was added to the term $\ddot{\phi}_B$ in the equation for angular acceleration about the center of gravity. This was done to distinguish this component of angular acceleration from the $\ddot{\phi}_B$ term defined in the angular relationships.

- A subscript "X" was added to the normal acceleration terms $\ddot{Z}_R$ and $\ddot{Z}_b$ to distinguish between components of normal acceleration measured at the center of gravity and those measured by an accelerometer at the accelerometer location, X_A.

- In the definition of angular relationships in the vehicle equations, the terms ϕ_R, $\dot{\phi}_R$ and $\ddot{\phi}_R$ were changed to ϕ_{cg}, $\dot{\phi}_{cg}$ and $\ddot{\phi}_{cg}$ respectively in order to include the coupling terms between the bending modes and rigid body dynamics. These changes make for a more realistic representation of the vehicle.

- The definition of ℓ_A was given in the data package to be:

$$\ell_A = X_{cg} - X_A$$

However, the term was redefined to be:

$$\ell_A = X_A - X_{cg}$$

to assure a positive value for ℓ_A to avoid possible confusion.

- The aerodynamic coupling term

$$Qin = \sum_i qA \frac{\partial(Cz\alpha)}{\partial (X/D)} \Delta Xn \; Y_i(Xn)\alpha$$

was included only at the 64 second and 80 second conditions. It was assumed, in the computation of Qin, that distribution of normal force as defined in Figure 11 of the data package (see reference 1) would be applicable to both the 64 and 80 second conditions.

- The bending moment was assumed to be defined by the expression

$$I = M'_\alpha \; \alpha + M'_\beta \; \beta$$

This was a simplified expression but it was agreed that it would be sufficient for this study.

PERFORMANCE REQUIREMENTS

Performance requirements were agreed upon with NASA to be the following:

Rigid Body

- Minimum frequency of equivalent second order response to attitude commands shall be 0. 5 rad/sec with a design objective of 0. 63 rad/sec.
- Maximum allowable bending moment shall be 2.7×10^6 kp-m.
- Minimum upper and lower gain margins shall be 5 db with a design objective of 6 db.
- Minimum rigid body damping ratio shall be 0. 1 with a design objective of 0. 25.

Flexible Vehicle - In-Flight Synthesis Study

- As a design objective, the following closed loop damping ratios should be obtained:

  1st mode - 0. 1

  2nd mode - 0. 05

  One objective of the study was to define a system to provide positive control of the first two bending modes. It should be pointed out that these desired damping ratios were chosen to make the problem more challenging. There was no physical constraint which demanded these requirements. It was not known at the start of the study whether or not these requirements would prove unrealistic.

- Minimum phase margin of the third mode shall be 30 degrees with 60 degrees as a design objective. While it was required that the third mode be only phase stabilized it was a design goal to actually gain stabilize the third mode. It was assumed that the first two modes would be actively controlled by the system and that phase stability of the third mode would be attained by suitable placement of the sensors. But since an objective of the study was to minimize the need for an accurate knowledge of mode shapes it was considered most desirable to gain stabilize the third mode. This would hopefully relieve any constraint imposed on sensor placement according to mode shapes.

- The fourth and higher modes were to be gain stabilized with a gain margin of 6 db. To accomplish this without including higher mode dynamics in the analysis a high frequency gain constraint was imposed on the rigid vehicle control system configuration.

  The following criterion was used to define this gain constraint. Examination of a second order pole with 0.005 damping (i.e. the bending mode model) on a Bode plot shows that the amplitude curve will peak up by 40 db at its natural frequency relative to the low frequency. Thus to gain stabilize the mode by 6 db an attenuation of 46db is required at the bending frequency. This constraint assumes there are no compensating bending mode zeros in the vicinity of the pole. This is felt to be a conservative assumption. Nevertheless for want of a better criterion, a 46db attenuation at frequencies above the 4th mode was imposed on the rigid body control system combination to assure gain stability. Thus, if the third mode were to be gain stabilized then the system-vehicle combination must exhibit an attenuation of 46db at the third mode frequency.

Flexible Vehicle - Multiple Blender Study

- The first three modes shall be phase stabilized by 30 degrees. However, it was a design objective to achieve 60 degrees phase margin.

- The fourth and higher modes shall be gain stabilized by 6 db. It was originally stipulated that the 3rd mode would be gain stabilized. However, for the system considered it was later decided to phase stabilize the third mode.

SECTION 4
RIGID BODY ANALYSIS

DEFINITION OF CANDIDATE CONTROL SYSTEMS

Four rigid body candidate control systems were evaluated at the 64 second flight condition using the NASA supplied wind model (see reference 1) and attitude commands as disturbances. Two of the four systems were drift-minimum controllers, one provided pure attitude control, and one provided a combination of attitude control and load relief compensation. The four control laws were as follows:

System 1: Drift minimum using angle of attack

$$\beta_c = 2.95\,\phi + 4.1\,\dot{\phi} + 1.08\alpha, \quad l_\alpha = 104\text{m}$$

System 2: Drift minimum using normal acceleration

$$\beta_c = 3.75\,\phi + 5\,\dot{\phi} + 0.194\,\ddot{\tau}, \quad l_A = 25\text{m}$$

System 3: Attitude Hold

$$\beta_c = \frac{2.5}{S+1}\,\phi + 5\dot{\phi}$$

System 4: Attitude Hold with Load Relief

$$\beta_c = \frac{1}{2S+1}\,\phi + 5\dot{\phi} + \frac{0.3}{10S+1}\,\ddot{\tau}, \quad l_A = 25\text{m}$$

The drift minimum controller using angle of attack feedback (system 1) was identical with a drift minimum controller that had been designed by NASA except the gain on the angle of attack term was increased by a factor of 1.5 over that used by NASA. Figure 10 illustrates the performance of the controller at the 64 second condition using both gains on the angle of attack.

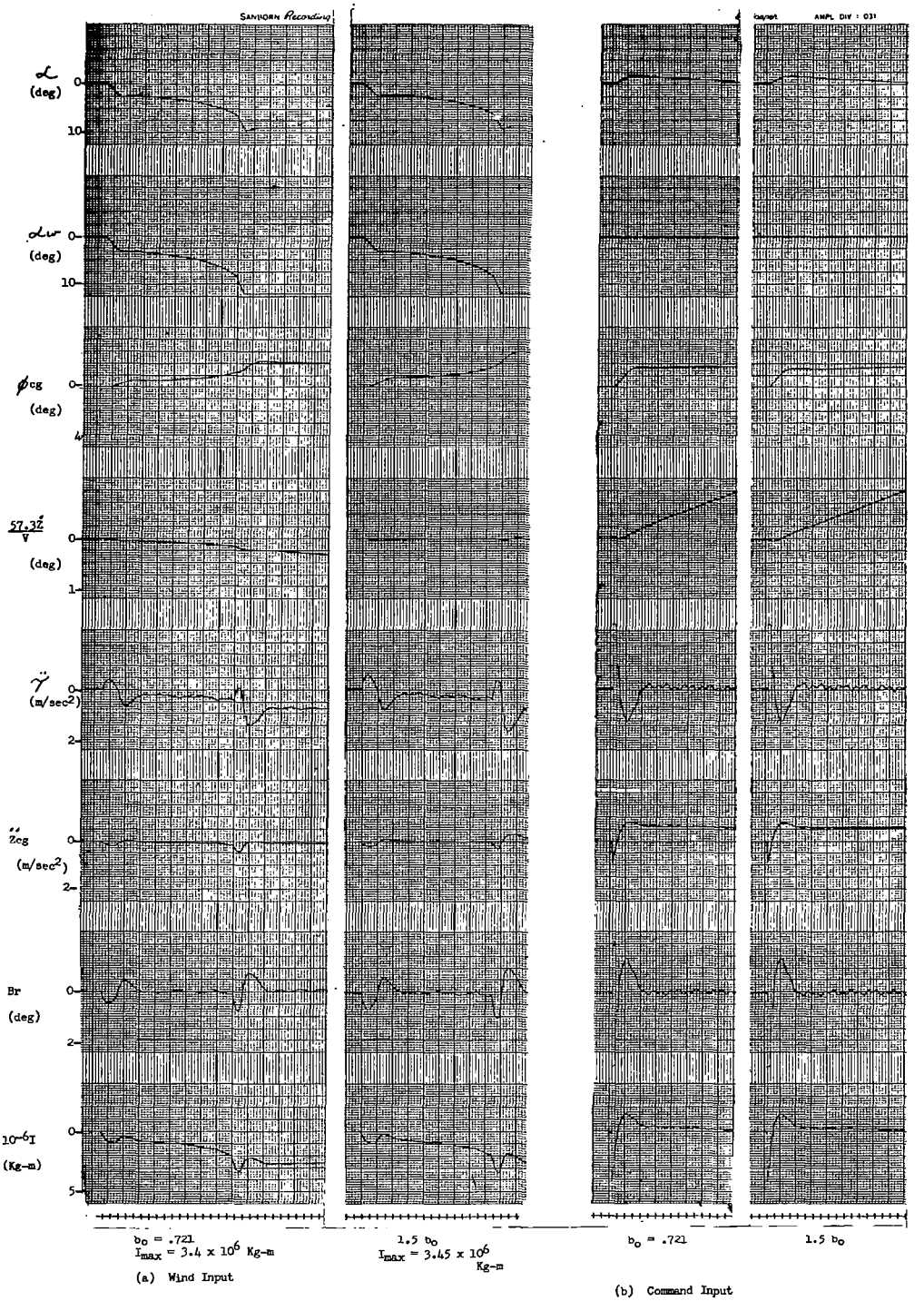

Figure 10. Response of Drift Minimum Controller to Wind Inputs and Command Inputs, t = 64 seconds and $B_C = a_o\phi + a_1\dot{\phi} + b_o\alpha$ ($a_o = 2.95$, $a_1 = 4.1$, $b_o = 0.721$, $\ell\alpha = 144 - 39.6 = 104.4$m)

It should be noted that the lateral velocity is smaller during a wind disturbance with the larger gain on the angle of attack. This system met the attitude response requirements but the resulting maximum bending moment for the wind disturbance was 3.45×10^6 Kp-m which is larger than the allowed 2.7×10^6 Kp-m. Figure 11 compares the performance of the remaining three systems. The only system which met the bending moment constraint was system 4. The results also show that with the attitude controller (system 3) a smaller bending moment resulted than with the drift minimum controller. Figure 12 shows the response of system 4 to a wind input as obtained by a digital computer routine.

The corresponding analog trace (Figure 11) indicated a larger maximum bending moment (2.85×10^6 Kp-m) than did the digital computer result (2.65×10^6 Kp-m). However, upon comparison of the wind models it was evident that for this case the analog wind model was slightly larger than the NASA model. The comparison of the four controllers showed that system 4 was the best system in terms of meeting the bending moment and the attitude response requirements at the 64-second condition. On this basis system 4 was selected as the basic control system configuration.

DEFINITION OF RIGID BODY CONTROL SYSTEM PARAMETERS

Based on the evaluation of the candidate control systems the controller took the form shown in Figure 13. Variations in each of the control parameters were evaluated to determine the most tolerant configuration. The discussion that follows describes the rationale for selection of the parameters.

Attitude Sensor Location

It was stipulated in the NASA vehicle data package (see reference 1) that the attitude sensor be located between body stations 118 meters and 122 meters.

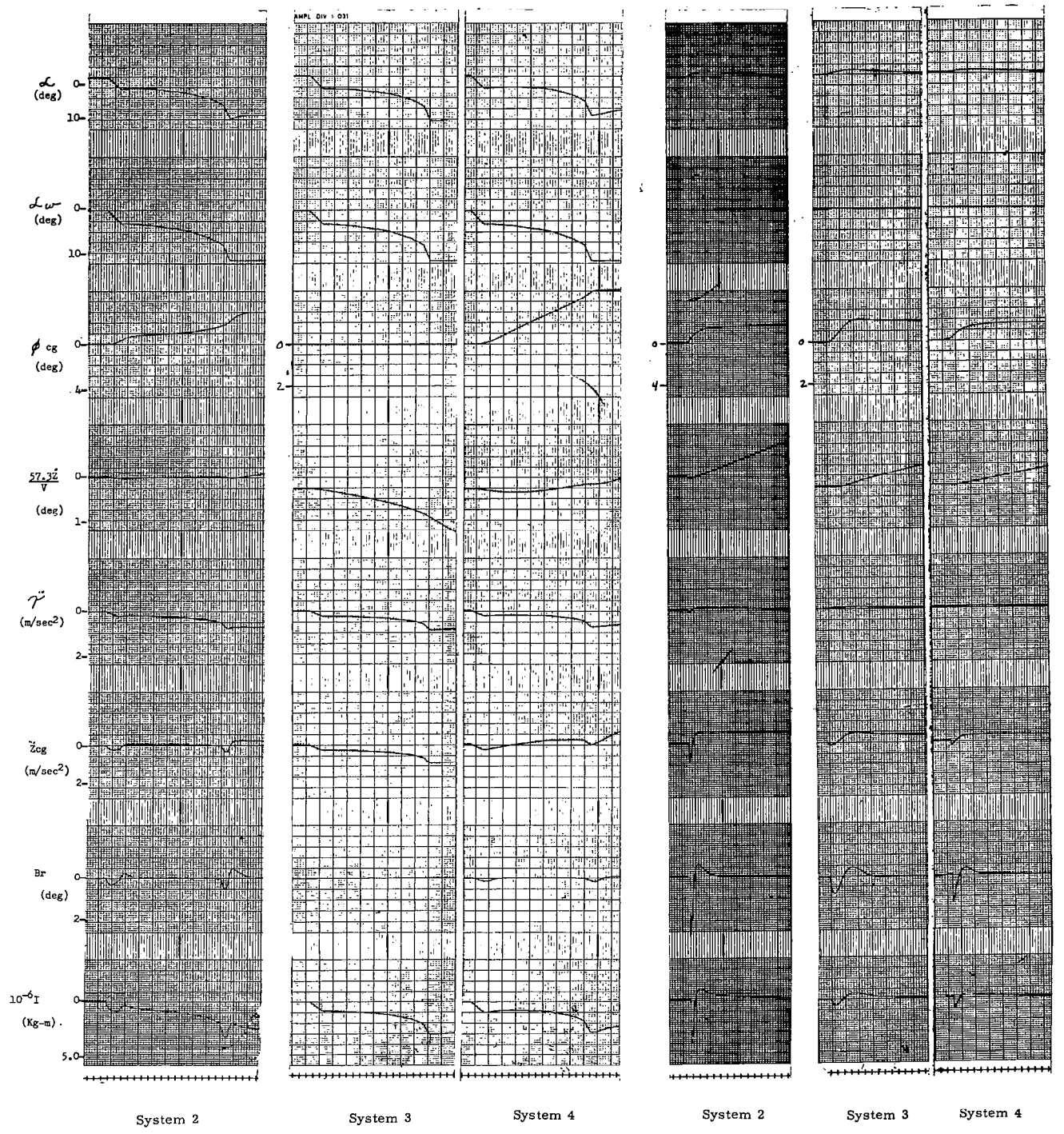

(a) Response to a Wind Input

(b) Response to an Attitude Command

Figure 11. Response of Systems 2, 3 and 4 to Wind Inputs and Command Inputs, t = 64 seconds

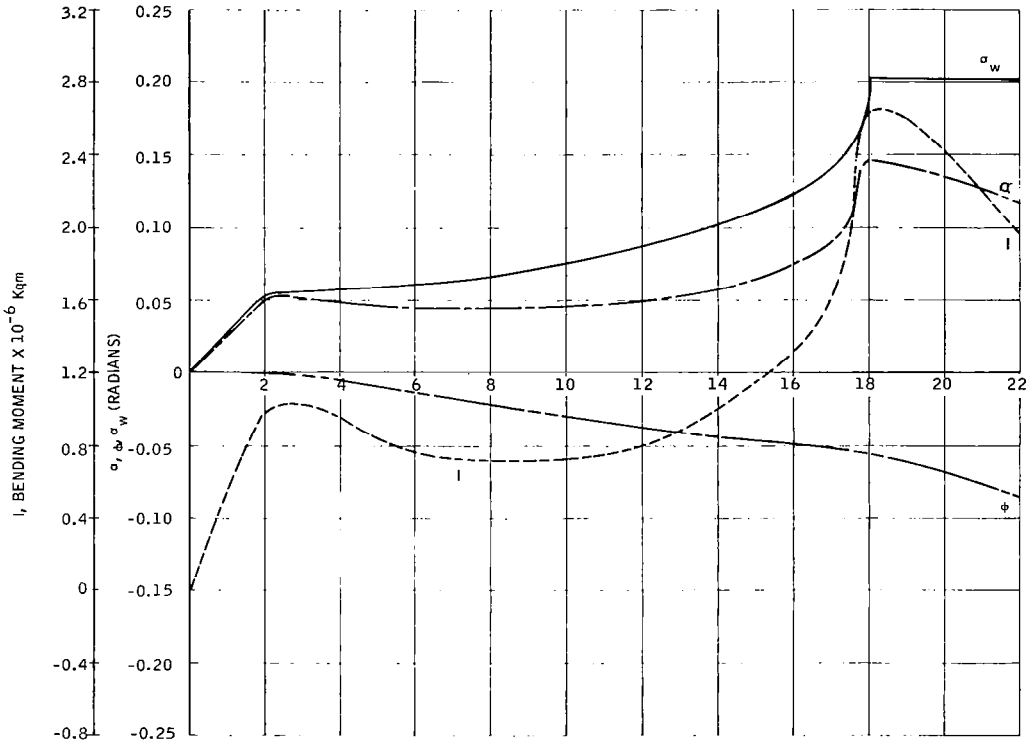

Figure 12. System 4 Response to Wind Input, t = 64 seconds

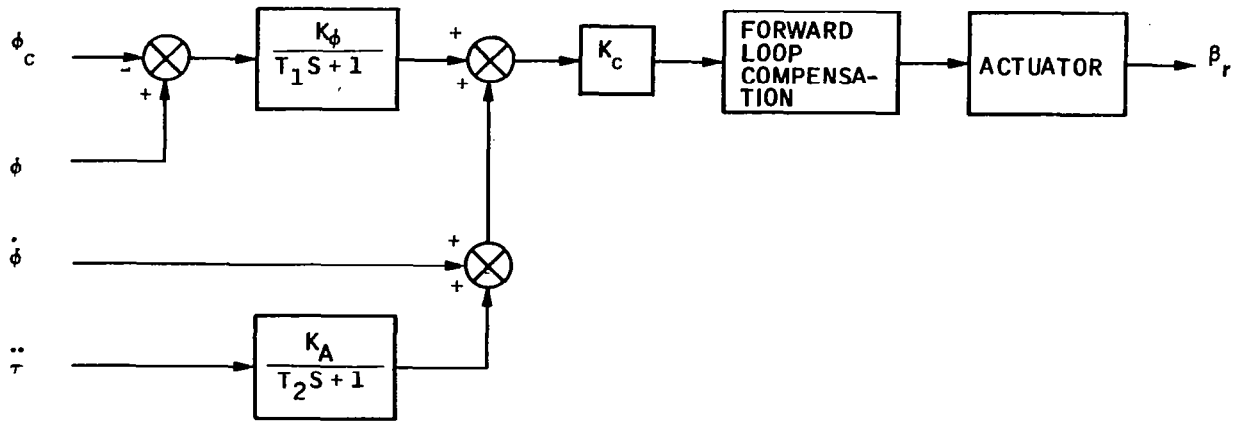

Figure 13. General Rigid Body Controller

Body station 118 meters was selected arbitrarily. It could be placed anywhere within this region without degrading the performance.

Accelerometer Location

The accelerometer location was determined by evaluation of the following factors:

- Allowable locations as defined by Figure B-D.
- Most forward center of gravity location. It was desirable for stability reasons to place the accelerometer ahead of the center of gravity. Since the most forward center of gravity location was body station 68 meters only those allowable locations ahead of body station 76 meters (see Figure B-D) were considered feasible from the standpoint of the center of gravity location.
- Maximum stable gain as a function of accelerometer location. Analysis showed that the maximum stable forward loop gain decreased as the accelerometer was moved forward.

- Attitude Command Response as a function of Accelerometer Location. Analysis showed the attitude response could be improved by moving the accelerometer forward.

- Bending moment as a function of Accelerometer Location. Some reduction in the bending moment during a wind disturbance was noted when the accelerometer was moved forward.

These factors were traded off to determine the best over-all accelerometer location. Considering only accelerometer locations ahead of body station 76 meters, the only two significant factors to be compared were the change in maximum stable forward loop gain and the response to attitude commands. Body station 90 meters was selected as a satisfactory compromise between these factors. The exact location is not considered crucial. Placement of the accelerometer location further aft will result in some degradation of the attitude response. Placement further forward would result in some reduction of the maximum stable forward loop gain. It should be noted that the accelerometer was located without regard to the bending mode shapes.

Rate Sensor Location(s)

For the rigid body analysis the rate sensor could be placed in any of the allowable locations (see Figure B-D). Since the location of the rate sensor has no effect on rigid body performance the location was not specified. Thus, the location of a rate sensor or sensors was left to be defined by the analysis of the flexible vehicle.

Attitude Feedback Compensation

Selection of the attitude gain, K_{ϕ} (see Figure 13) was determined by two factors: (1) attitude command response time and (2) the corresponding

acceleration feedback gain required to meet the bending moment constraint. The ratio of attitude gain, K_ϕ, to acceleration gain, K_a, determines to a large extent the load relief capability of the system. In addition a large accelerometer gain is undesirable since it lowers the damping on the attitude command response. Thus, it was desirable to make the accelerometer feedback gain as small as possible. This implies that for a given bending moment constraint it is, therefore, desirable to keep the attitude feedback gain as small as possible since it is the ratio of these gains which determines the bending moment. On the other hand the extent to which the attitude gain can be reduced is defined by the attitude command response requirements. The attitude feedback gain essentially determines the speed of the response. Analysis showed that if the attitude gain were reduced below a value of 0.75 the response time would no longer be acceptable. Thus, a value of 0.75 was selected for the attitude feedback gain, K_ϕ, to assure an adequate response time and to minimize the value of the accelerometer feedback gain.

A first order lag was added to the attitude error feedback for two reasons: 1) to smooth the command input and 2) to filter the bending pickup by the attitude sensor. The lag increased the frequency of the attitude command response but it also lowered the damping. A value of 0.5 seconds was finally selected as a compromise between the attitude response characteristics and the anticipated filtering of bending signals.

Accelerometer Feedback Compensation

The accelerometer feedback gain was defined by the following constraints:

- The ratio of attitude to acceleration feedback gain required to meet the bending moment constraint
- The degradation in the attitude command response with increased accelerometer feedback gain

- The compensation on the acceleration feedback

For a given compensation on the accelerometer feedback and a given value of the attitude feedback gain, the minimum allowable value of the accelerometer feedback gain required to meet the bending moment constraint is automatically determined. Since increasing the accelerometer gain degrades the response to attitude commands, it was desirable to use the smallest value of K_A possible which would still satisfy the bending moment constraint. Thus, for a given value of the attitude feedback gain the accelerometer gain was a function of the accelerometer feedback compensation. Therefore, to define the accelerometer gain, the compensation had to be defined. It was found in the analysis, that the addition of a first order lag to the accelerometer feedback resulted in the following advantages:

- Increased maximum stable forward loop gain
- For a given accelerometer gain, K_A, the bending moment during a wind disturbance was reduced by increasing the lag time constant.
- The lag provided desirable shaping on the bending feedback through the accelerometer.

Figures 14 and 15 illustrate the effect on the maximum stable forward loop gain as a function of the lag time constant, T_2 (see Figure 13) for various accelerometer locations. From these plots it was clear that a large lag will be advantageous in maximizing the range of stable control gain. Also, use of a large time constant permitted the accelerometer feedback gain, K_A to be reduced and still meet the bending moment constraint.

These considerations led to selecting a lag time constant, T_2, of 10 seconds and a corresponding accelerometer gain of 0.4 rad/m/sec^2. The use of a pure integrator was also analyzed in place of the first order lag. It was

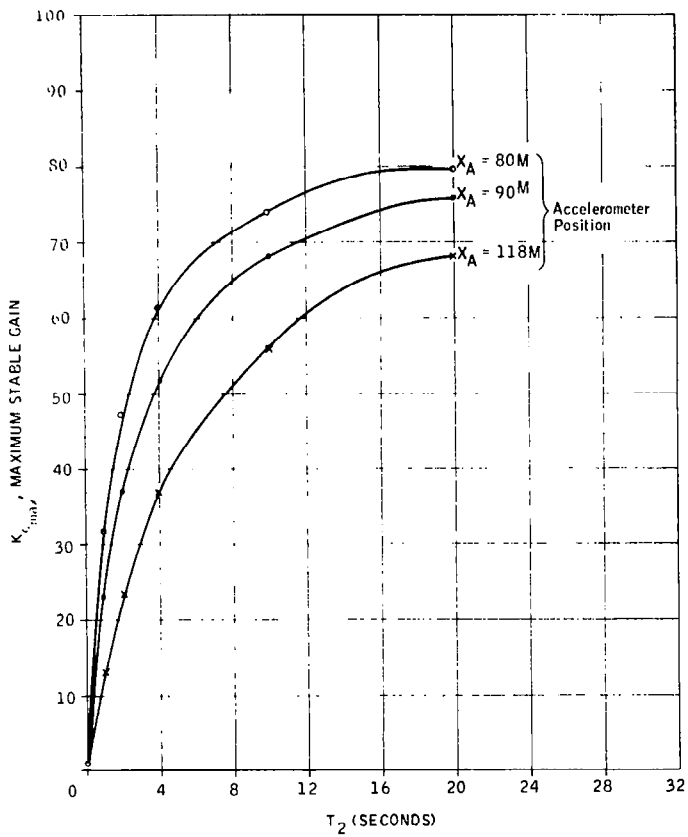

Figure 14. T = 64 Sec. Maximum Stable Gain versus Accelerometer Lag Time Constant, T_2

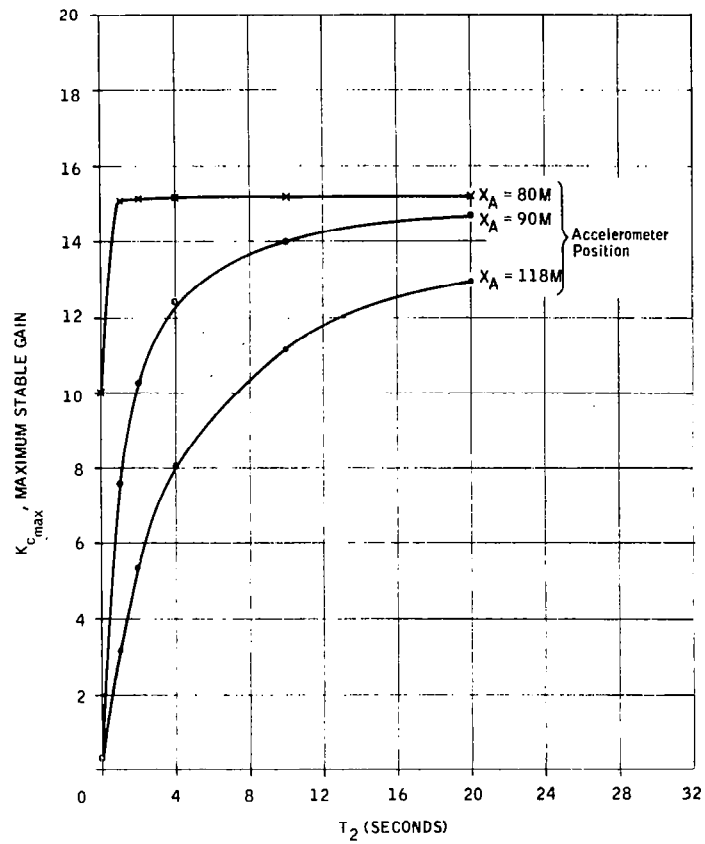

Figure 15. T = 157 Sec. Maximum Stable Gain versus Accelerometer Lag Time Constant, T_2

found that even greater reductions in the bending moment were possible. As a result, the accelerometer gain could have been greatly reduced. However, deterioration of the attitude response at the maximum dynamic pressure condition due to the integrator and probable drift problems ruled out the use of the integrator. A ten second lag provided a good compromise between achieving an acceptable attitude response and meeting the bending moment constraint. Higher order filters were investigated briefly. No immediate advantage was apparent from the analysis so they were not considered in any detail.

Forward Loop Compensation

For the rigid body control system, a proportional-plus-integral compensation was added to the forward loop. It was added primarily to provide a high low frequency gain.

Forward Loop Gain

The forward loop gain, K_C, (see Figure 13) was fixed at 2.5 for all four flight conditions for the rigid body control system. This gain value assured a satisfactory attitude command response, acceptable values of bending moment during a wind disturbance, and adequate (6 db) gain margins at all flight conditions.

SUMMARY OF RIGID BODY CONTROL SYSTEM

Figure 16 is a block diagram of the final rigid body control system. Performance of the system at all four flight conditions is demonstrated in Figures 17 through 21. The system met all rigid body performance requirements without scheduling any of the parameters.

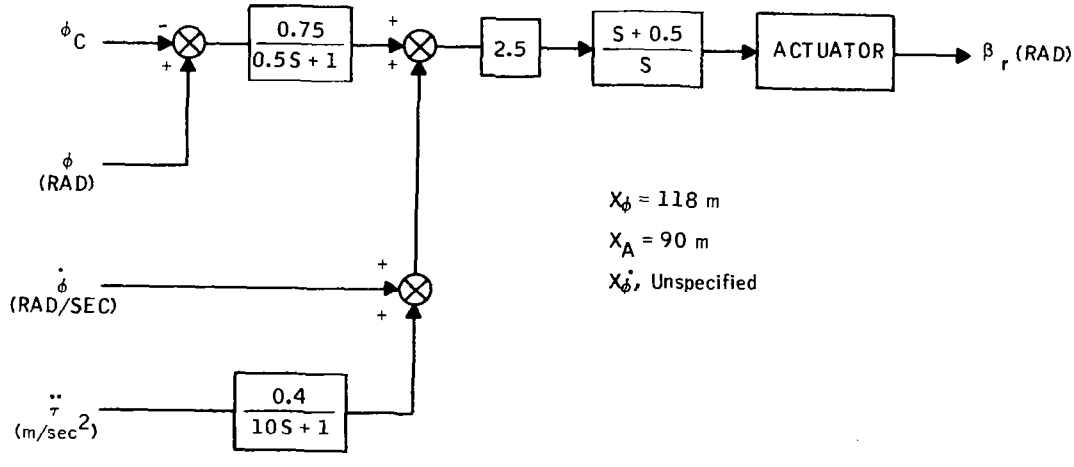

Figure 16. Block Diagram of Nominal Rigid Body Control System

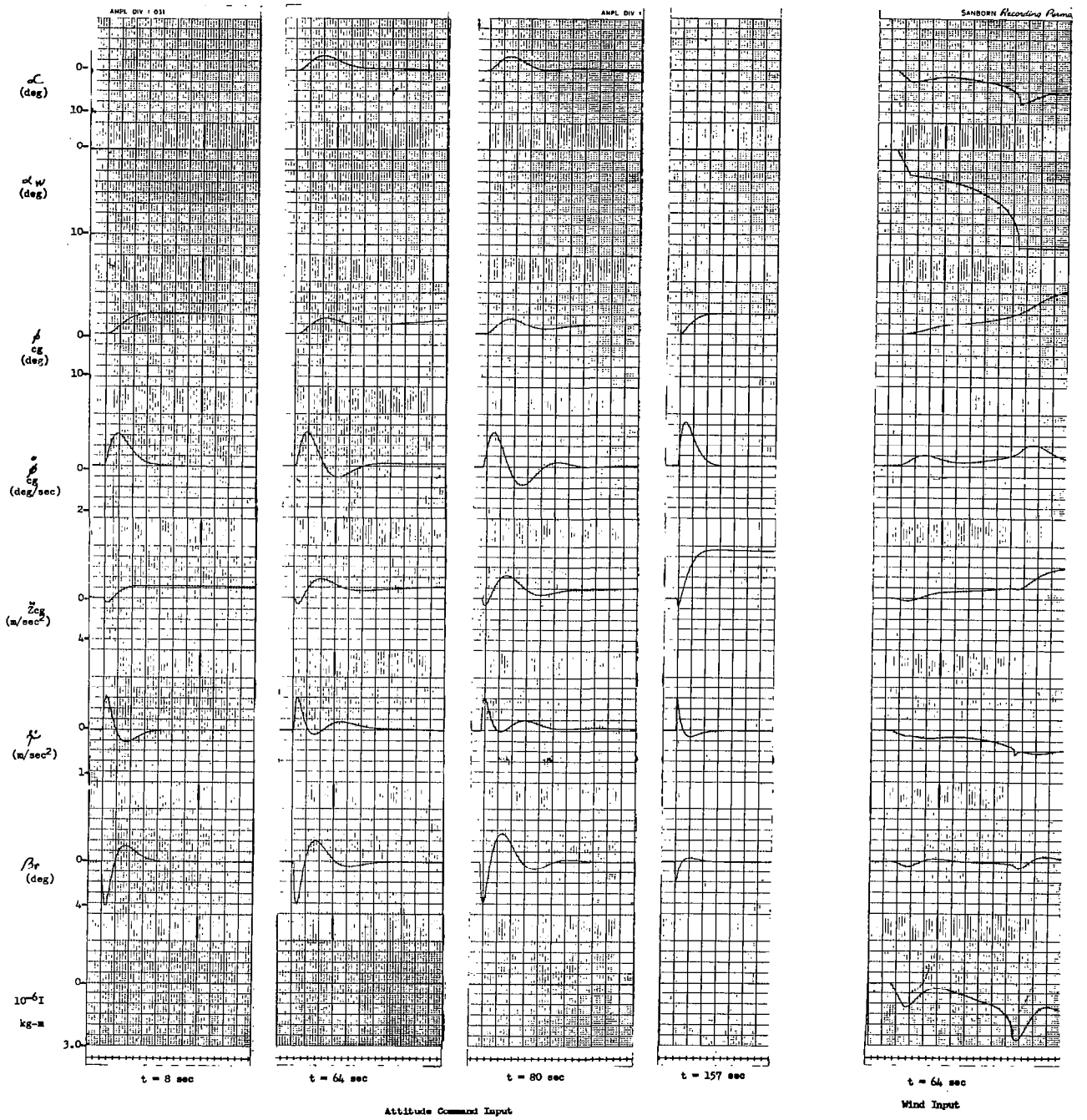

$$\beta_c = 2.5 \left[\frac{s+.5}{s}\right] \left[\frac{.75}{.5s+1} (\phi - \phi_c) + \dot{\beta} + \frac{.4}{10s+1} \dot{\gamma}\right]$$

$X_{cg} = 118$ m, $X_A = 90$m

Figure 17. Nominal Rigid Body Control System Response to Attitude Commands and Wind Disturbances

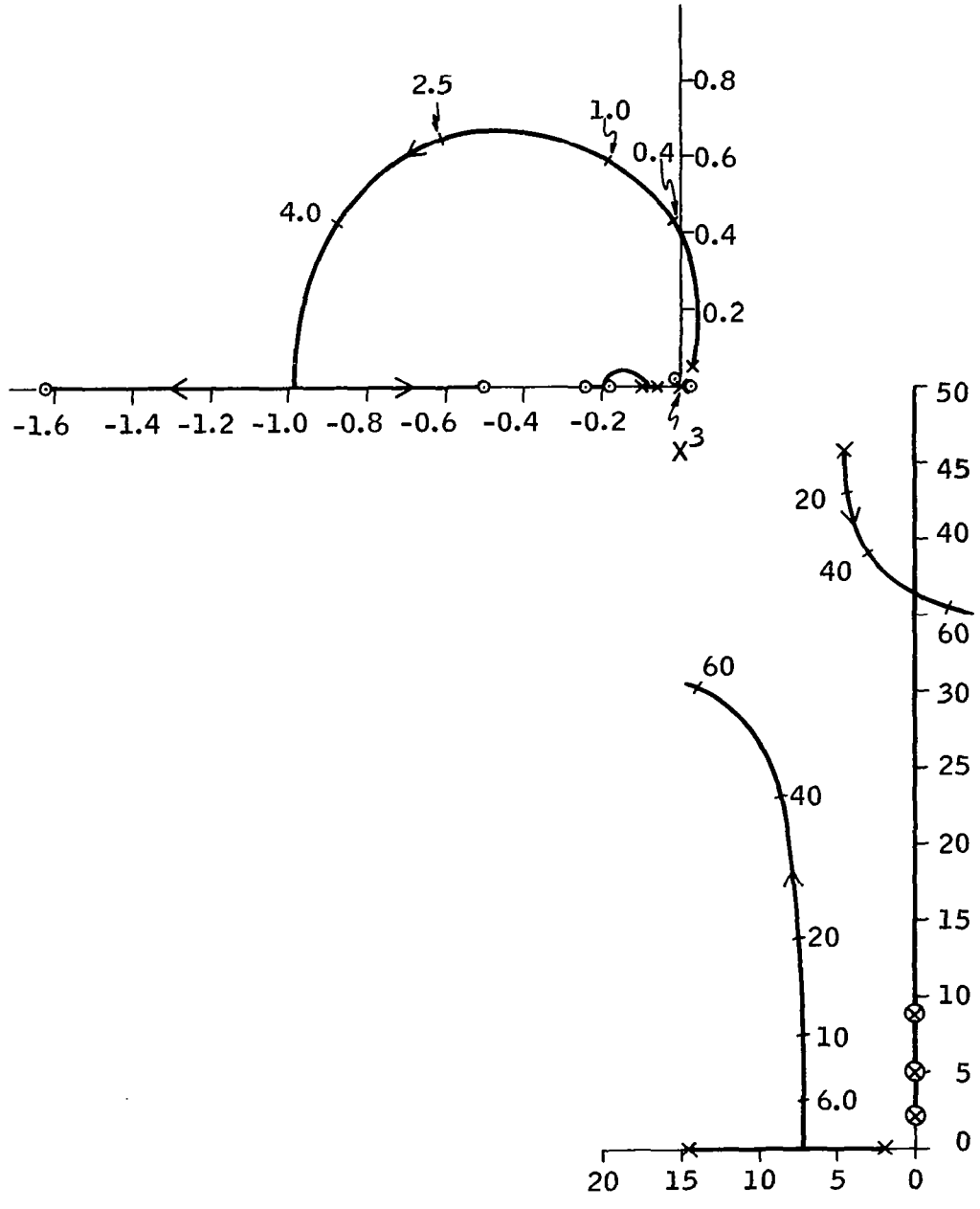

Figure 18. Rigid Body Control System Root Locus, t = 8 seconds

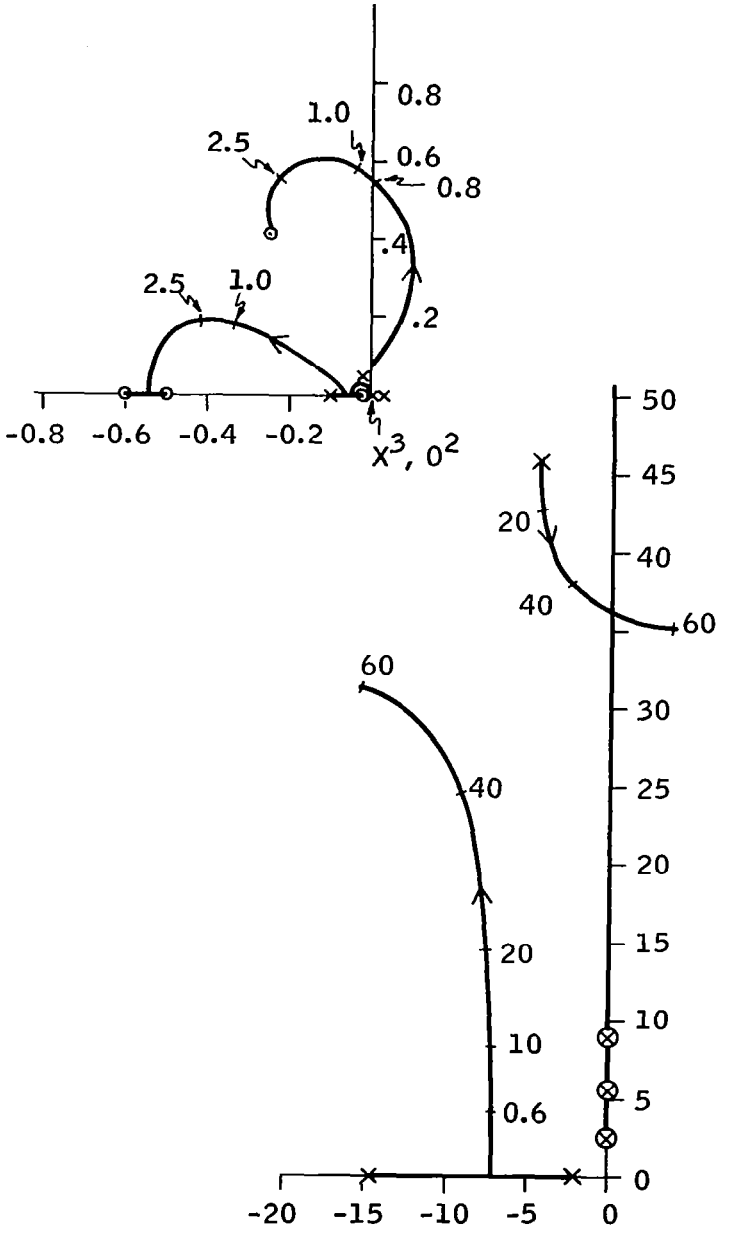

Figure 19. Rigid Body Control System Root Locus
t = 64 seconds

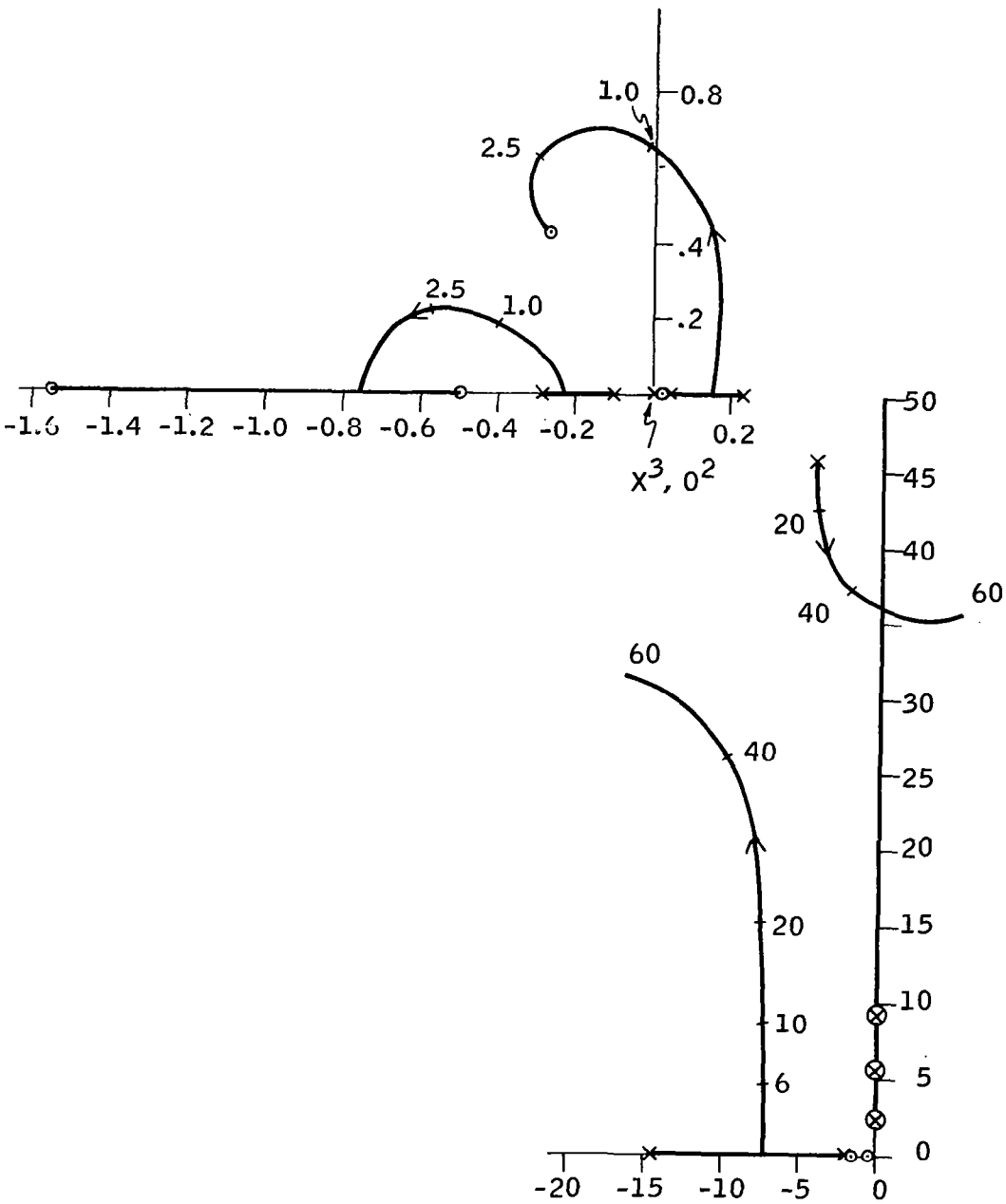

Figure 20. Rigid Body Control System Root Locus, t = 80 seconds

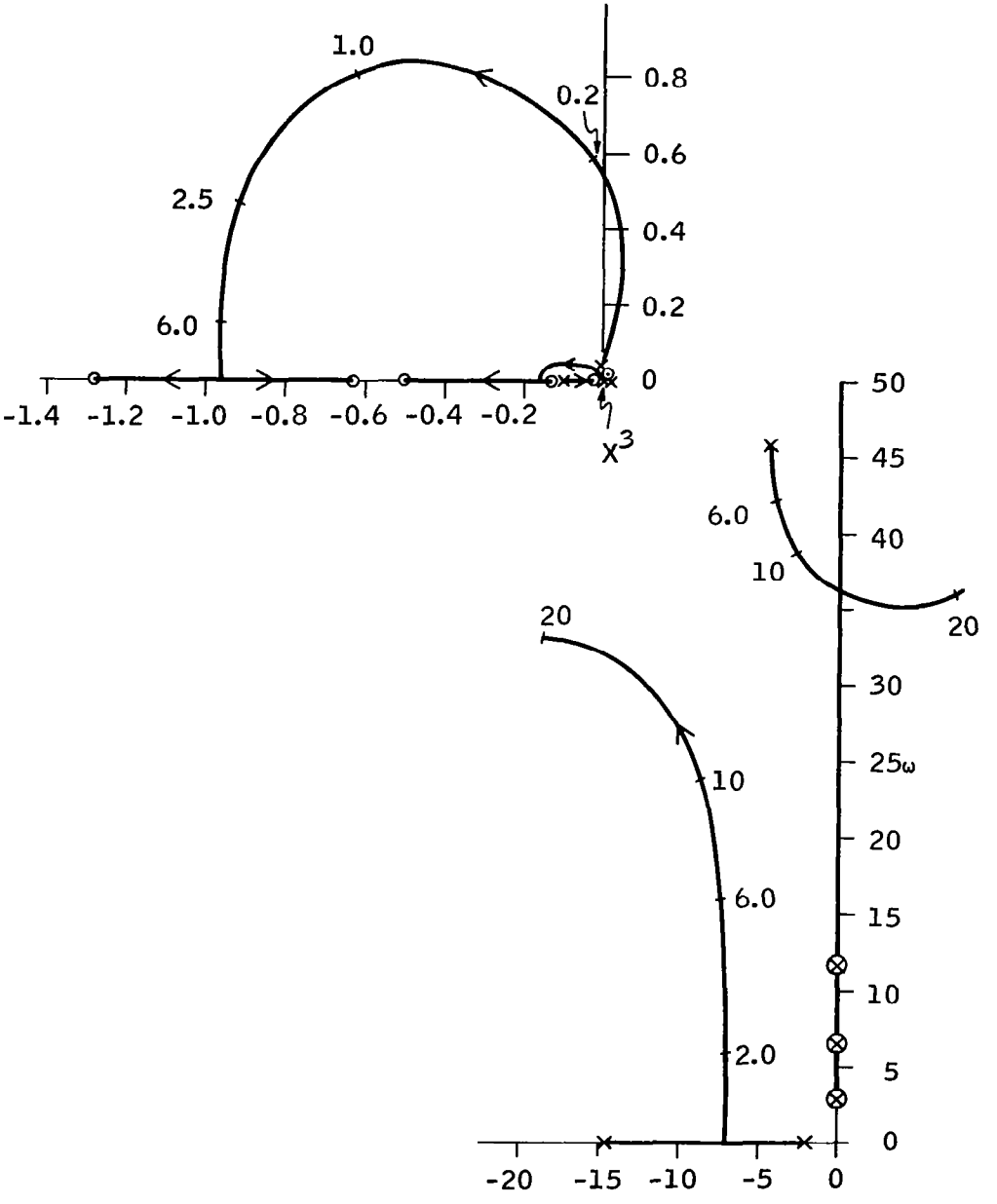

Figure 21. Rigid Body Control System Root Locus, t = 157 seconds

SECTION 5
DATA REQUIREMENTS FOR IN-FLIGHT SYNTHESIS

A brief literature study of flexible vehicle control techniques was made. The objective of the study was to obtain information which might serve as a guideline in the development of a controller. The articles and papers reviewed are listed in the references. It was the objective of practically all the systems reviewed to stabilize the structural bending without relying on an accurate knowledge of the mode shapes. These systems generally employed some form of on-line identification in order to adjust the system compensation. In each case, the identification schemes relied upon conventional sensing techniques. Each of the adaptive techniques measured the bending content of the sensor outputs (using an identification scheme) and either adaptively blended sensor outputs or else adjusted a forward loop filter. Those techniques which adjusted a forward loop filter provided only cancellation of the bending feedback and required explicit identification (e.g. measurement of a bending frequency). However, sensor blending techniques were used to provide either cancellation or phase stabilization. The conclusion drawn from the literature study, then, was that sensor blending would be the most probable means of providing positive control of the bending modes. Thus, the design of a control system should be based on the use of sensor blending techniques to control the flexible vehicle.

Consideration of sensor blending led to the development of a relationship between the control system feedback configuration and the location of bending mode zeros on a root locus plot. Figure 22 is a block diagram of a typical control system. A transfer function of $H/_{\eta i}$ (see Figure 22) can be written for each bending mode signal on each feedback, neglecting coupling through the rigid body. If the transfer functions are evaluated at the bending frequency for the mode of interest, a complex number is obtained for each

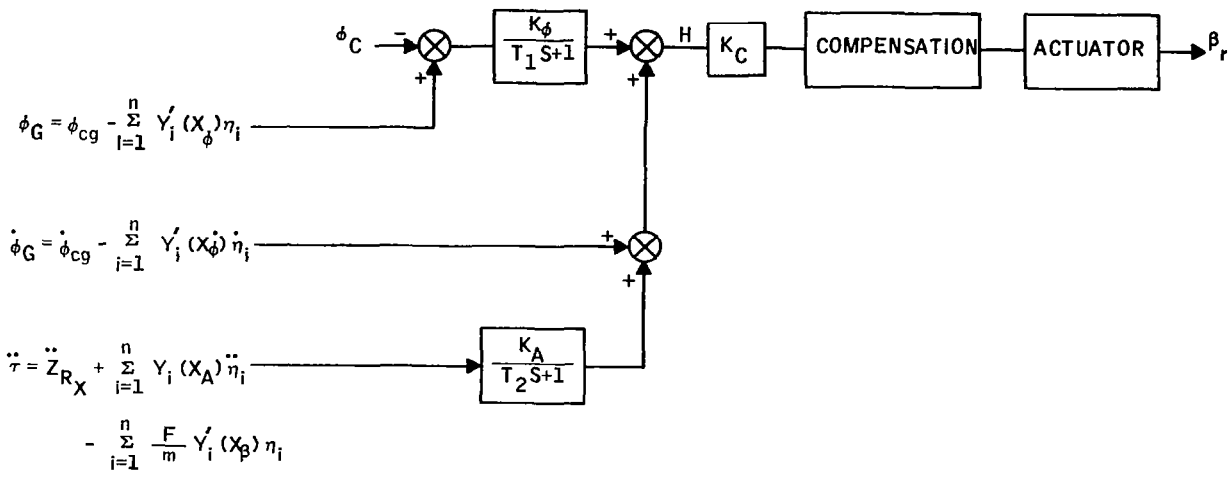

$$\left.\frac{H}{\eta_i}\right)_{\text{attitude}} = \frac{-K_\phi}{T_1 S+1} \; Y_i'(X_\phi) = \frac{-K_\phi Y_i'(X_\phi)}{1+(T_1\omega_i)^2} \left[1 - T_1\omega_i j\right]$$

$$\left.\frac{H}{\eta_i}\right)_{\text{rate}} = -Y_i'(X_{\dot{\phi}})\, S = -Y_i'(X_{\dot{\phi}})\, \omega_i j$$

$$\left.\frac{H}{\eta_i}\right)_{\text{accel.}} = \frac{K_A}{T_2 S+1}\left[Y_i(X_A)\, S^2 - \frac{F}{m} Y_i'(X_\beta)\right] = \frac{-K_A}{1+(\omega_i T_2)^2}\left[Y_i(X_A)\,\omega_i^2 + \frac{F}{m} Y_i'(X_\beta)\right]\left[1 - \omega_i T_2 j\right]$$

where $\dot{\eta}_i = \eta_i S$, $\ddot{\eta}_i = \eta_i S^2$

Figure 22. Typical Control System Block Diagram

feedback (see Figure 22). If these numbers are plotted as vectors, one can readily determine the gain and phase contribution from each feedback. In fact, if the vectors are added, the resultant vector will lie in the direction of the corresponding bending mode zero relative to the bending mode pole on the root locus (see Figure 23). No attempt was made, however, to establish a more direct correlation between the magnitude and direction of the vector and the exact zero location. However, the equations defining the vectors show the phasing and gain desired on each feedback in order to place a bending zero in a favorable position. If one assumes a particular attitude and accelerometer feedback compliment, these equations yield explicit relationships for the minimum value of the bending mode slope required at a rate sensor station to assure phase stability. The maximum value of the slopes still must be determined by computer analysis. However, using this feedback analysis it was possible to obtain quickly the ballpark range of the required mode slopes.

The only control parameters not specified by the rigid vehicle analysis were the number and location of rate sensors. It appeared that a possible approach to the control problem would be to design a system without regard to the number and location of rate sensors. This design would yield a set of mode slopes for a hypothetical rate sensor required to meet the damping requirements on the first and second modes and the phase stability requirement on the third mode. Examination of these mode slopes would determine whether a single sensor placed at a particular station could provide the slopes. If not, then a combination of rate sensors would have to be used. It was assumed for the study that the range of these mode slopes would be defined. This information could be used to define an identification process (if required). This process would generate a synthetic rate feedback signal consisting of the rigid body rate and the bending rates with these artificial mode slopes. If only a single sensor or a fixed combination of rate sensors were required then no active identification process would be needed. There are several appealing factors to this design approach:

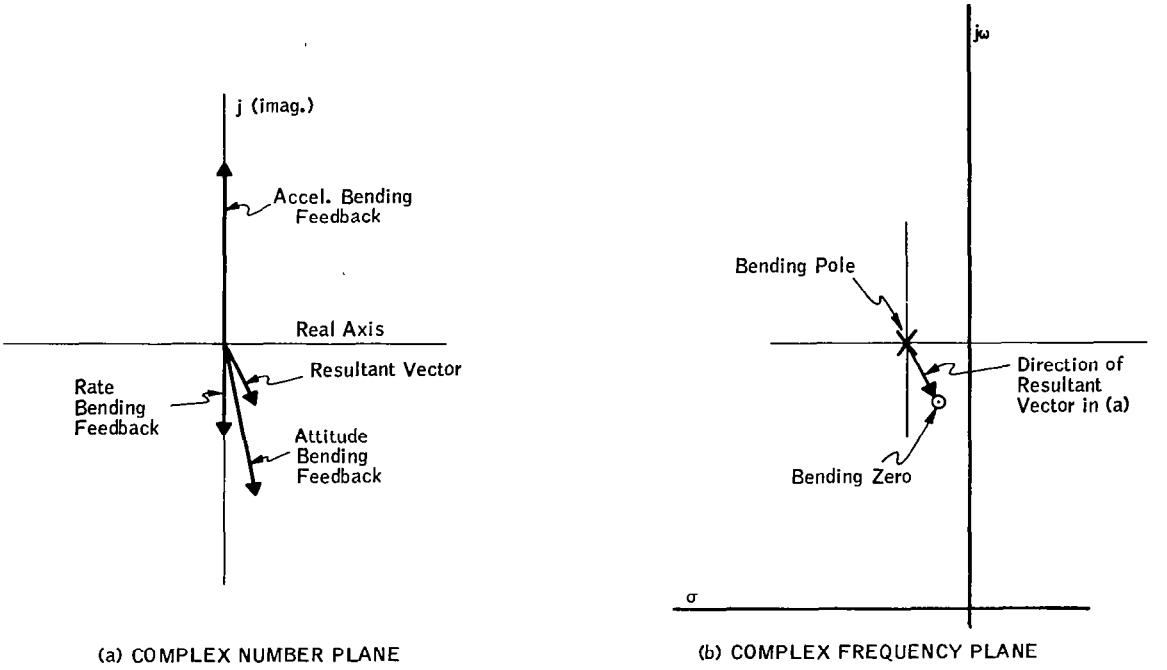

Figure 23. Correlation Between Bending Feedback Vectors ($H/\dot{\eta}_1$)

- The number and location of rate sensors does not affect the rigid body performance. Thus, definition of the flexible vehicle control process in the above manner will not degrade the rigid body performance.

- The accelerometer and attitude sensor could be placed on the vehicle without regard to bending mode shapes.

- The analysis of the control system feedback configuration to define mode slopes can be used extensively as a design tool.

- A factor apparent from the feedback analysis was that with this design approach the shaping required on the feedbacks is completely compatible with rigid body requirements. For example, a large lag was desirable on the accelerometer feedback to align the accelerometer feedback vector with the rate feedback vector.

- Design of a flexible vehicle controller in this manner should result in a system which minimizes the need for an identification scheme. All that would be required from the identification scheme would be a synthetic rate feedback signal. This could be generated by using an implicit identification technique.

DEFINITION OF THE NOMINAL CONTROL LAW

The rigid body control system had to be modified to meet the performance requirements for the flexible vehicle. The following discussion describes the necessary modifications.

Accelerometer Feedback Compensation

Addition of structural bending made it possible to reduce the accelerometer feedback gain, K_A, (see Figure 16) from 0.4 rad/m/sec^2 to 0.1 rad/m/sec^2 and still meet the bending moment constraint. Coupling, particularly with the first mode, reduced the bending moment during a wind disturbance. Reduction in this gain resulted in an improved response to attitude command.

Forward Loop Gain

The forward loop gain, K_c was reduced from a fixed value of 2.5 to a scheduled value ranging from 0.75 at launch to 0.23 at burnout. This reduction in gain was necessary because the range of stable forward loop gain was reduced by the addition of structural bending modes and a forward loop filter. The gain required at each flight condition was as follows:

$$K_c = \begin{cases} 0.75, & t = 8, 64, 80 \text{ seconds} \\ 0.23, & t = 157 \text{ seconds} \end{cases}$$

Actually, the gain at t = 80 seconds should have been 0.80. With a value of 0.75 at t = 80 seconds, the attitude command response was slightly slower than required. But, using $K_c = 0.75$, resulted in requiring only two discrete gain values thus simplifying the gain scheduling. The gain at the 8 and 64 seconds conditions could not be increased without reducing the gain margin to less than 6 db.

Attitude Feedback Compensation

Reduction of the nominal forward loop gain resulted in removal of the lag on the attitude feedback (see Figure 16). The lag was removed to compensate for a degraded command response which resulted when the nominal value of

the forward loop gain was reduced. It was concluded the lag did not provide sufficient bending mode compensation to warrant the reduction in damping on the attitude command response obtained by including it.

Forward Loop Compensation

The proportional-plus-integral compensation was removed as a result of the flexible vehicle analysis. While it provided a high low-frequency gain, it also provided an undesirable phase shift.

The performance requirements stated that the fourth and higher modes be gain stabilized. While it was stipulated that the third mode be phase stabilized it was considered a design objective to gain stabilize it. It was reasoned that the identification scheme could be simplified if gain stabilization of the third mode could be attained. If it were attained, then only ideal mode slopes for the first and second modes would have to be actively regulated by an identification process. If only phase stabilization could be attained on the third mode, however, then the identification scheme would either have to actively generate an artificial third mode slope or else passively obtain it by careful placement of the rate sensors. The latter approach would require a more accurate knowledge of the mode shapes. The former approach would increase the complexity of the identification process.

To establish a design criterion for the forward loop filter, a tradeoff had to be made between the range of stable control gain, K_c, and the cutoff frequency of the system with the filter. The cutoff frequency was defined as the frequency at which the system would go unstable if the control gain were raised above its maximum stable value. In general, as the cutoff frequency is lowered the range of stable gain is reduced. However, as the cutoff frequency is lowered, increased attenuation of high frequency signals is made possible.

Preliminary filter designs were defined to provide a system crossover frequency between the second and third bending mode frequencies. With a crossover frequency in this range a 6db system gain margin could still be obtained. A constraint was imposed on the design of the filter by the damping ratio requirement on the second mode. The filter could not contribute more than sixty degrees of phase lag at the second mode frequency if the damping requirement was to be met. Further, the filter could not attribute any significant attenuation at the second mode frequency. These design constraints all but ruled out gain stabilization of the third mode. Several filters were designed according to this criterion. Figures 24-28 illustrate some of the filters investigated. The filters shown in Figures 24-27 assumed a forward loop gain, K_c, of one. Figure 28 shows a filter for a system with K_c reduced by 3db. There were three basic problems with each filter:

- Complexity
- The resulting small range of allowable third mode slopes to assure phase stability
- Second mode damping was at best, only marginally acceptable.

While it was concluded that the performance requirements could have been met, the resulting filter complexity, the marginal performance and the accuracy requirements on the third mode slope made each of these filters an undesirable solution.

To improve the system, modifications to the feedback configuration were analyzed. Several configurations were tried but none proved to be of any significant advantage for the added complexity. Finally, forward loop filters were examined which provided a cross-over frequency below the second bending mode frequency. It was found that if the forward loop gain, K_c, were lowered slightly to accommodate the loss in bandwidth, then a more tolerant and less complex filter could be defined. This analysis yielded the following filter:

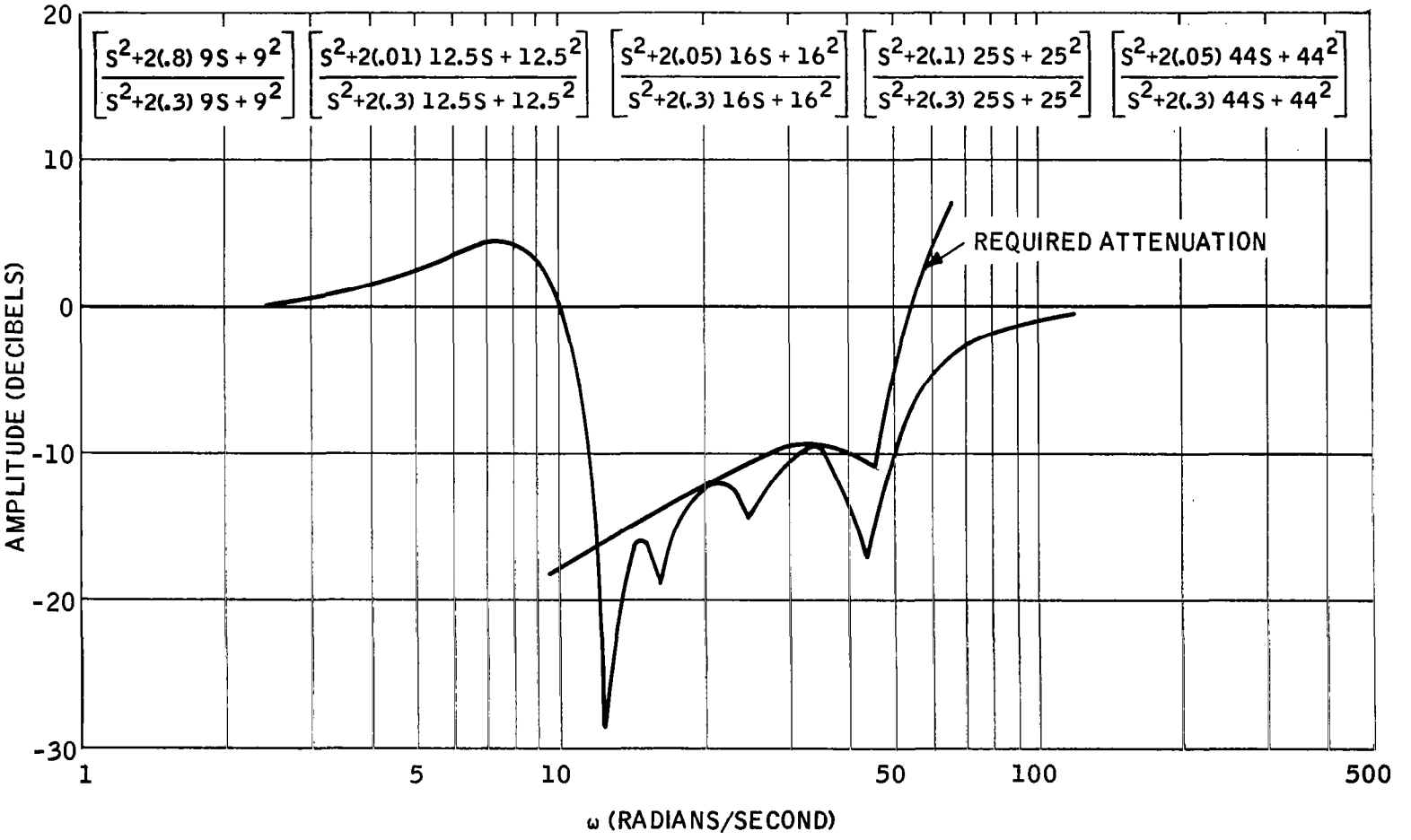

Figure 24. Notch Filter No. 1

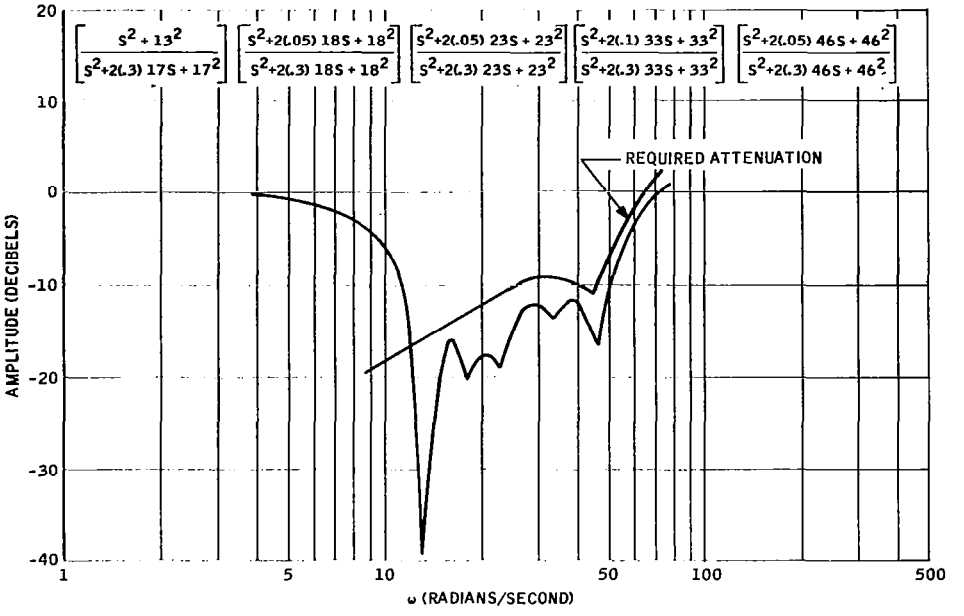

Figure 25. Notch Filter No. 2

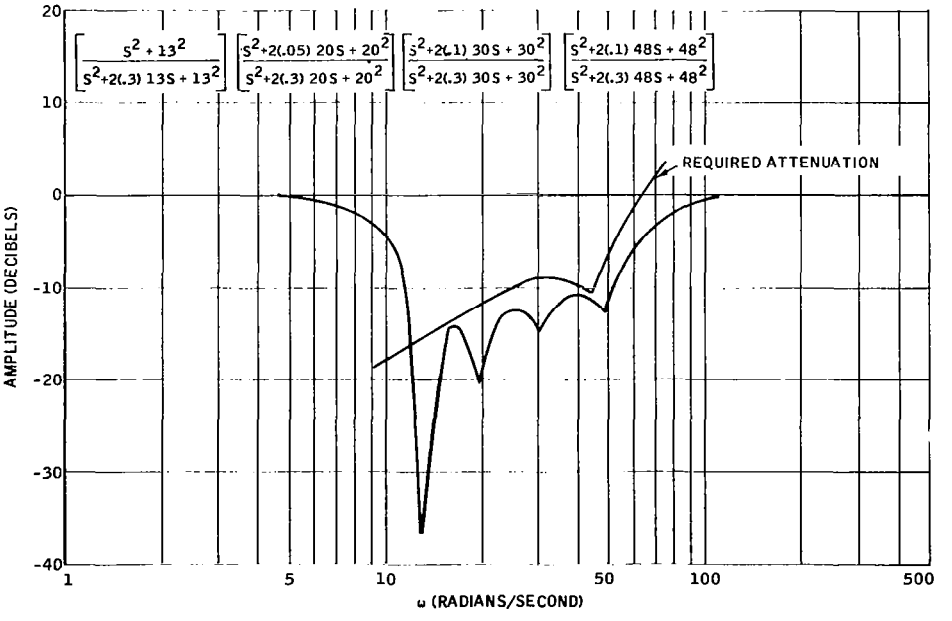

Figure 26. Notch Filter No. 3

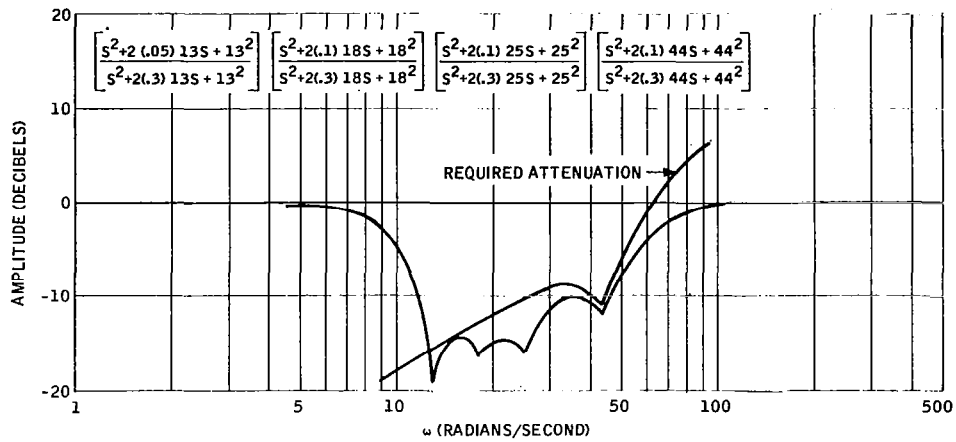

Figure 27. Notch Filter No. 4

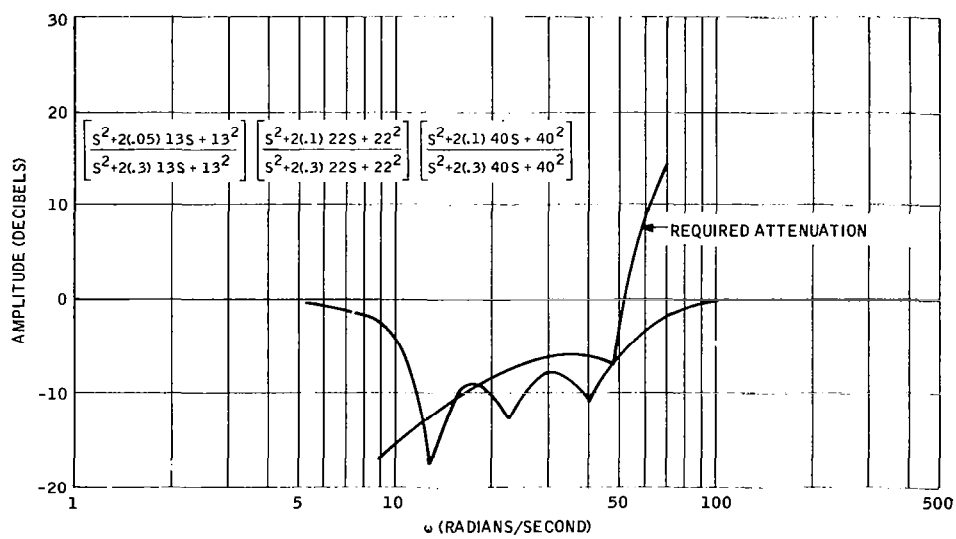

Figure 28. Notch Filter No. 5

$$\left(\frac{0.1S + 1}{0.02S + 1}\right)\left(\frac{S^2 + 2(0.01)\ 10\ S + 10^2}{S^2 + 2(0.3)\ 10S + 10^2}\right)\left(\frac{4^2}{S^2 + 2(0.7)\ 4S + 4^2}\right)$$

This filter, with other modifications to the controller, resulted in a rigid body frequency response which showed 46 db attenuation from the third mode frequency on out (see Figures E-5 through E-8). This filter was selected on the basis of its relative simplicity, increased tolerance to third mode slope variations, and because the damping on the second bending mode could be met without difficulty.

Rate Sensor Feedback Compensation

The addition of the forward loop filter made it necessary to add a compensation network to the rate feedback. A hi-passed rate signal was added to the primary rate feedback. This signal was used to place the first and second mode bending zeros in locations to assure the damping on the first and second modes. For this purpose the hi-passed rate signal was subtracted from the primary rate feedback. This feedback provided the required phase lag and signal amplification to meet the damping requirements.

As a result of these modifications the control system took the form shown in Figure 29. This system met the performance requirements at the four flight conditions.

DEFINITION OF DATA REQUIRED

For the control system defined by Figure 29 the only portions of the system requiring regulation by an identification process were the forward loop gain and the rate feedbacks.

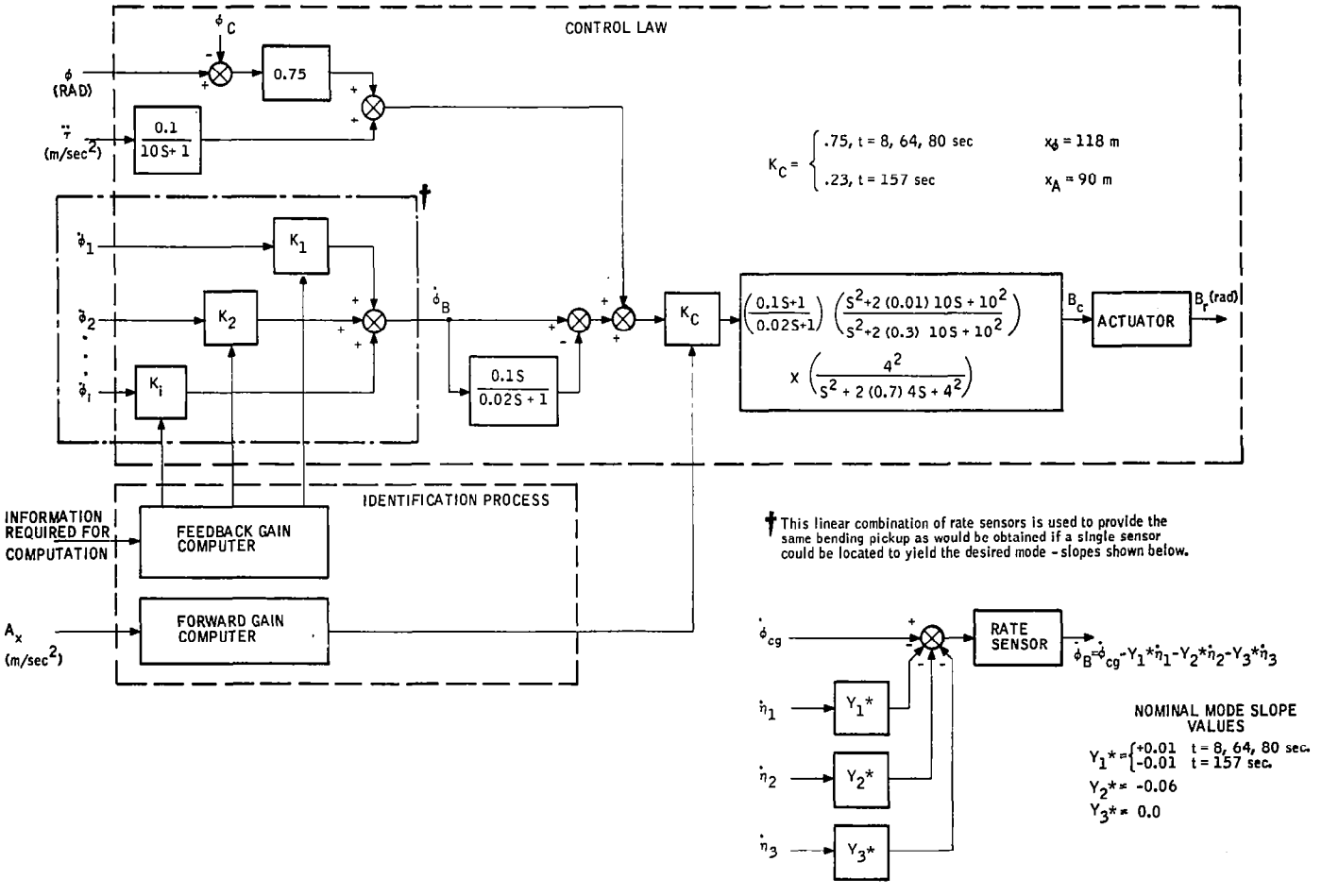

Figure 29. Nominal Flight Control System for Synthesis Study

A means for scheduling the forward loop gain, K_c, was developed based on the use of axial acceleration. One condition imposed on the system design was that parameter scheduling with time would not be permitted. Time is a natural parameter for scheduling parameters on a missile but such scheduling cannot accommodate unpredictable changes in the vehicle configuration or its environment.

Analysis of the system showed that K_c was almost completely dependent on the control effectiveness, C_2. If C_2 were a constant then K_c could have been a constant. It was then assumed if the parameter C_2 could be measured in some manner then it could be used to regulate the gain, K_c. C_2 is defined by the following relation:

$$C_2 = \frac{\ell_{cg} R'}{I_{xx}}$$

The only parameter which significantly affects a change in C_2 is the fuel consumption. Fuel consumption affects the center of gravity shift (which would change ℓ_{cg}), the vehicle inertia, I_{xx} and also the thrust, R'. The only other factor affecting C_2 would be the thrust gain with altitude. But this would be of only secondary significance. Thus, if one could measure the fuel consumption then the change in the control effectiveness could be determined. However, measurement of fuel consumption would tie the system to another subsystem (i. e. fuel measurement) which would be undesirable from a reliability standpoint. This factor has precluded the use of air data in many applications.

A simpler solution was to measure axial acceleration. Even though it is also a function of thrust gain with altitude and aerodynamic drag, axial acceleration does provide a relative measure of fuel consumption. The axial acceleration can be easily measured by an accelerometer which can be made as an integral part of the control system. Thus, the objection of depending on another subsystem is overcome.

Figure 30 illustrates the correspondence between the axial acceleration and the control effectiveness, C_2. The control effectiveness has been multiplied by 36.7 to match the scales of the two curves at the zero second condition. The control gain, K_c, has only two discrete values. As a consequence, it need be switched only once during the flight. Since only four conditions were analyzed it was not possible to establish exactly when the gain should be switched. However, it would be switched from a value of 0.75 to a value of 0.23 when the sensed axial acceleration exceeded a predetermined value. While the curves do not match exactly it is felt that the correspondence is close enough considering the gain is to be switched only once.

This is an open loop gain schedule. However, the system should, nevertheless, be tolerant to a wide variation of parameters. The control gain is sensitive to primarily, engine characteristics (i.e. burn rate, etc.), which account for variations in vehicle mass, and only secondarily to the external environment.

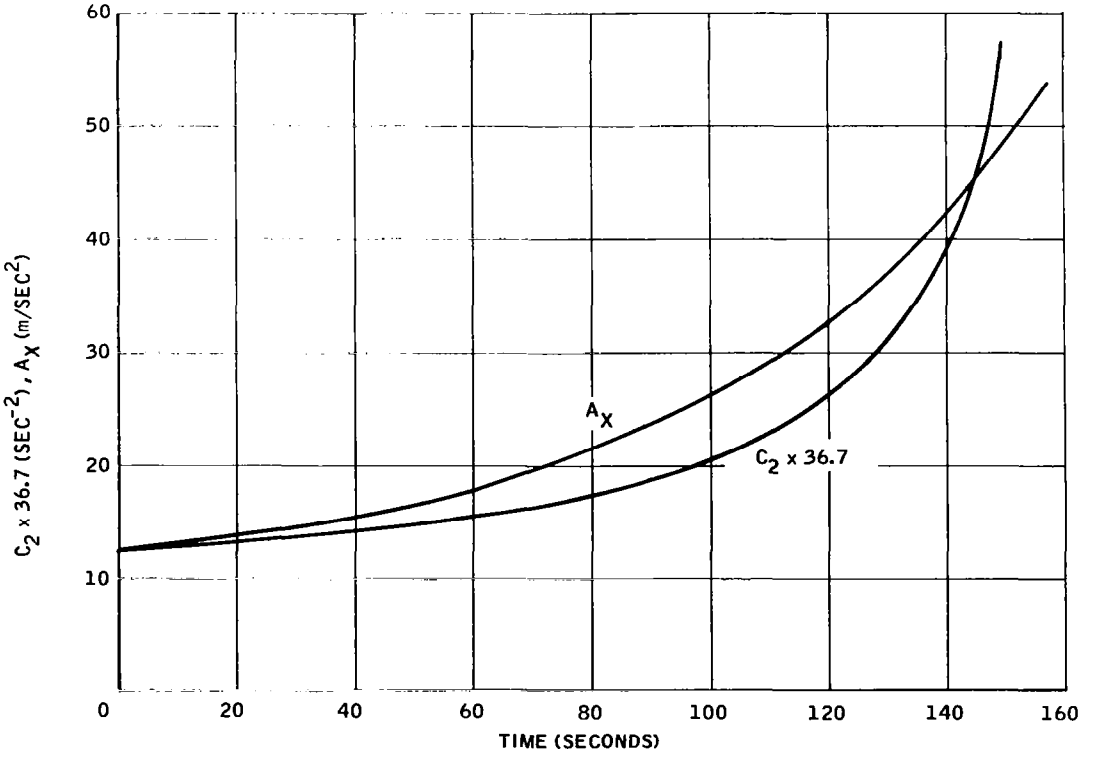

Figure 30. Correspondence of Axial Accel (A_x) to Control Effectiveness ($36.7C_2$).

The rate feedback consists of a combination of rigid body rate and bending rate signals (see Figure 29). The relative phase and amplitude of these signals is defined by a set of mode slopes (Y_1^*, Y_2^*, Y_3^*) as shown below for three bending modes:

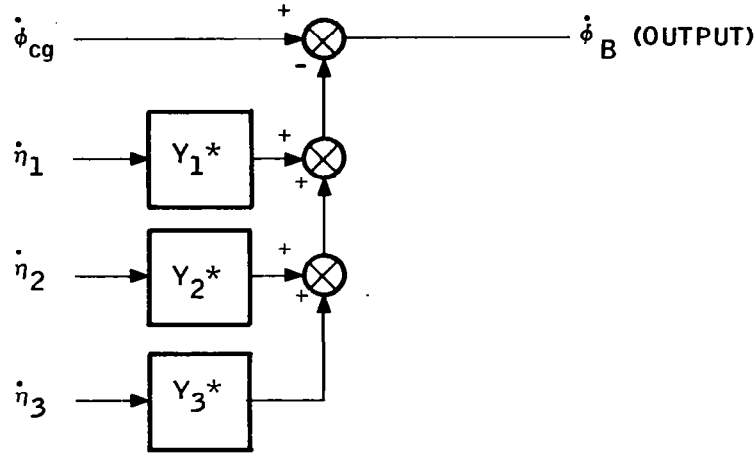

Ranges of Y_1^*, Y_2^*, Y_3^* were determined. The range of slopes were defined according to the damping requirements on the 1st and 2nd modes, gain stability on the third mode and a 6db system gain margin. Plots of the allowable mode slopes are shown in Figures 3-6 of Section 2. These plots were obtained on the analog computer. Figures D-21 through D-31, and E-25 through E-35 show root locus and frequency responses obtained from a digital computer for various values of the third mode slope. There was a slight discrepancy between these digital results and the analog results with regard to the maximum allowable positive value of the 3rd mode slope. The analog results indicate that a positive 3rd mode slope of approximately 0.1 could be tolerated (i.e. a 6db gain margin still existed) while the digital showed there was essentially no gain margin. The digital results indicated a maximum allowable positive slope somewhere between + 0.05 and + 0.1. The most probable reason for this discrepancy is that the vehicle dynamics were slightly different between the two simulations. The critical gain occurs at a frequency where the amplitude curve (on a frequency response plot) is changing rapidly with frequency. Thus any small charge in the dynamics could alter the result. However, these plots still provide a good measure of the range of allowable mode slopes.

It was observed that the range of allowable mode slopes is very restricted at the burnout condition. In fact the major problem area in the design of the system was to meet the damping requirement on the second mode while trying to gain stabilize the fourth mode and maximize the tolerance on the third mode slope. There was a persistant tradeoff between higher frequency attenuation at the earlier flight times and second mode damping at burnout.

A simpler and more tolerant system could have been realized if the damping requirement had been reduced on the second mode. There was no real basis for 0.05 damping on the second mode. The results of the study suggest that in future efforts consideration be given to reducing this requirement. A damping requirement of 0.01 - 0.02 would be more practical although it would be wise to first establish a basis for the requirement.

If 0.05 damping were desired the system might be simplified by relaxing the 46db gain stability requirement on the 4th and higher modes. Again some realistic basis should be established for defining the gain stability constraint.

PERFORMANCE EVALUATION

A set of nominal rate sensor slopes were defined for the purpose of evaluating the control system performance. The nominal slopes were defined to be:

$$Y_1'(X_\phi^\cdot) = \begin{cases} +\,0.01 & t = 8, 64, 80 \\ -\,0.01 & t = 157 \end{cases}$$

$$Y_2'(X_\phi^\cdot) = -\,0.06$$

$$Y_3'(X_\phi^\cdot) = 0$$

The following variations in vehicle parameters were analyzed:

1. ±20 percent variation in C_1 and C_2
2. ±20 percent variation in accelerometer bending mode deflections
3. ±20 percent variation in bending mode slopes at the attitude sensor location.
4. ±20 percent variation in bending mode frequencies

Analog computer traces showing responses of the nominal system to attitude commands and wind disturbances for a nominal vehicle and for the above variations are shown in Appendix C. Corresponding root locus plots are shown in Appendix D and frequency response plots in Appendix E. Some of the root locus and frequency response plots for the above variations are not shown. The reason was since either no change from the plots of the nominal system was observed or else the effect of the variation would be apparent from the plots of the nominal system.

These performance results show that acceptable performance was obtained for most all the variations. The only parameter variation which resulted in unacceptable performance was a 20 percent reduction in the bending mode frequencies. This reduction caused the 2nd mode to be only neutrally stable at the launch condition.

Other factors such as sensor dynamics and actuator non-linearities were not analyzed per se. The only sensor dynamics which could attribute any gain or phase characteristics at significant frequencies would be the accelerometer dynamics. These dynamics would attribute about ten degrees phase lag on the 2nd bending mode pickup on the accelerometer. This was not considered significant.

The actuator non-linearities considered were rate and deflection limits. Examination of actuator rates and deflections during a wind disturbance showed these limits would not have been exceeded. These rates and deflection limits would, however, limit the size of the attitude command possible, assuming a step input. However, since command inputs are usually of the order of one degree or less and are in the form of a ramp rather than a step, it was concluded these limits would not be exceeded.

SECTION 6
MULTIPLE BLENDER STUDY

The fundamental gyro blender approach to the control of a single bending mode of a very flexible booster has been studied and its advantages and limitations defined (see Ref. 2). An extension of this concept to control of two or more bending modes involves the use of additional rate sensors and blending circuits. In this study, the 1st and 2nd bending modes were to be actively controlled using three rate sensors and the multiple rate gyro blender concepts. Use of three rate sensors establishes three equations for the three unknown factors: rigid body rate and 1st and 2nd bending mode rates. The multiple blender implicitly identifies the relative content of each of the rate sensors and blends them to provide a desired combination of these three signals.

The primary purpose of the blender study was to determine the feasibility of combining blenders. Thus, only a minimum amount of time was spent to define functions not directly affecting the blender operation. For example, a fourth order filter was defined to simulate the gain and phase characteristics of a forward loop filter at the 1st and 2nd mode frequencies. Normally, the filter would have to provide gain stability for the 4th and higher bending modes. This, however, was not necessary to evaluate the operation of the multiple blender.

GENERAL BLENDER CONCEPT

The single rate gyro blender combines the outputs of two rate sensors to form an artificial mode slope for the first bending mode. This artificial mode slope is a linear combination of the first bending mode slopes at the two rate sensor stations. To do this the outputs of the two rate sensors, one placed aft and the other forward

of a given bending mode antinode, are each attenuated and then summed as shown in Figure 31. The attenuators are adaptively adjusted until the opposing first bending mode signals (opposing because of opposite signs on the mode slopes) from each sensor are made equal and, therefore, cancel each other. The logic can also be biased to provide only partial cancellation of the mode.

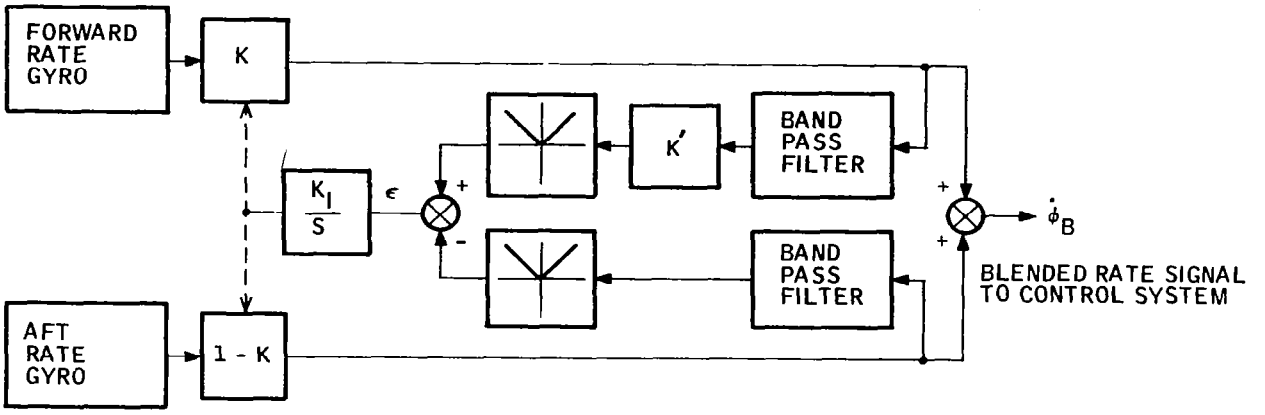

Figure 31. Single Blender Logic

If one gyro signal is attenuated by a factor K and the other by 1-K, it can be seen that signals common to both channels (rigid body in this case) will not be affected in any way by this attenuation-summing procedure.

To isolate the given bending mode signals from other signals (e.g., rigid body and other bending modes) the outputs of K and (1-K) elements are put through bandpass amplifiers with center frequencies equal to the given bending mode frequency (see Figure 31). The comparison of magnitude only is ensured by the use of absolute value circuits following the bandpass filters. The error signal (ϵ) resulting from the subtraction of these two bending signal magnitudes is integrated, and its output is used to set the variable attenuators. (See Figure 31.)

CANDIDATE MULTIPLE BLENDER CONFIGURATIONS

In combining the individual gyro blenders to form an integrated multiple blender, using three rate sensors instead of two, various configurations of individual blenders were considered. The evaluation of each of these configurations must be based on the analysis of the output signal of the multiple blender. Consider the output of the ith rate gyro:

$$\dot{\phi} = \dot{\phi}_{cg} - Y_1'(X_{si})\,\dot{\eta}_1 - Y_2'(X_{si})\,\dot{\eta}_2 - (\text{Higher Frequency Terms})$$

The higher frequency bending mode terms are neglected for the present because those modes are to be controlled by means other than the multiple blender (e.g., high frequency filtering to provide gain stabilization).

The multiple blender output will have the following similar form:

$$\dot{\phi}_B = \dot{\phi}_{cg} - Y_1^*\,\dot{\eta}_1 - Y_2^*\,\dot{\eta}_2 - (\text{Higher Frequency Terms})$$

Where the effective mode slopes, Y_1^* and Y_2^* are linear combinations of the actual mode slopes and whose values are dependent upon the multiple blender configuration employed. It should be emphasized that an individual blender can generate only one effective bending mode slope, Y_i^*, because it is sensitive to only one of the bending frequencies. As would be expected, independent control of the effective mode slopes, Y_1^* and Y_2^*, is necessary for the independent control of the first two structural bending modes.

One of the multiple blender configuration considered is shown in block diagram form in Figure 32.

This configuration was discarded because it could not control two separate bending modes. This fact becomes apparent if one considers the signal path from the

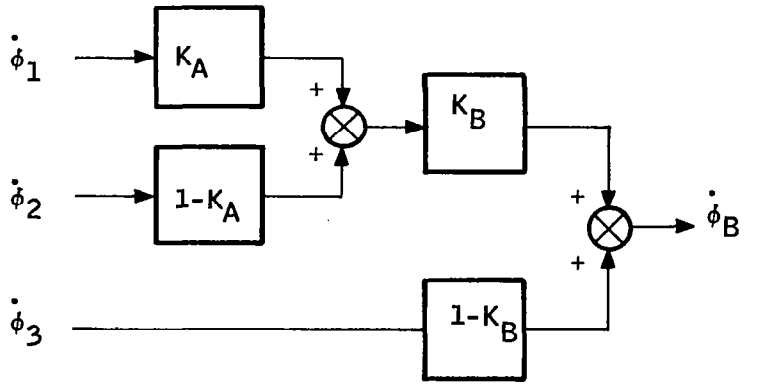

Figure 32. First Candidate Multiple Blender Configuration

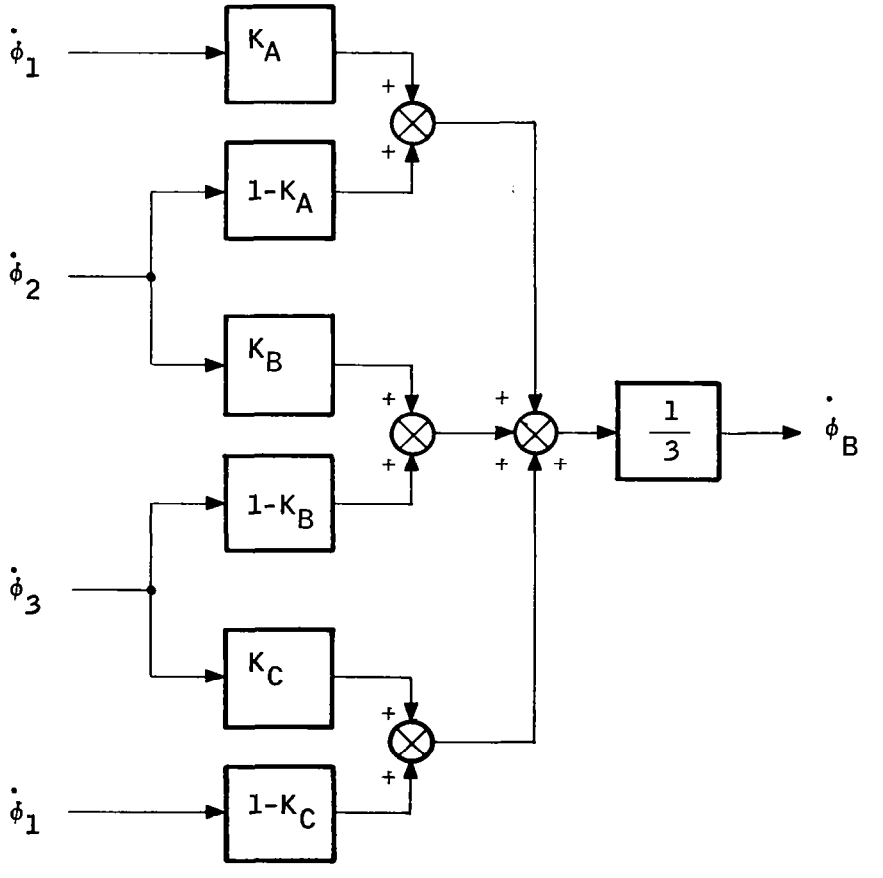

Figure 33. Second Candidate Multiple Blender Configuration

third rate gyro, $\dot{\phi}_3$, to the output, $\dot{\phi}_B$. Since the third rate gyro signal passes through only one attenuation factor $(1-K_B)$, only one of its bending mode slopes will be controlled. Thus, the output signal will contain one uncontrolled bending mode.

A second multiple blender configuration considered is shown in Figure 33.

This blender configuration contains the same basic problem area as the previously discussed blender, namely that two bending modes cannot be simultaneously controlled. The output signal, $\dot{\phi}_B$, of this blender is the sum of three individual blender outputs, each of which contains one uncontrolled bending mode slope. This configuration must then be likewise discarded.

The multiple blender configuration which was used in the study is shown in Figure 34.

The three rate sensor signals are combined in a linear fashion using a pyramid of three adaptive blenders. Blenders one and two are sensitive to only the first mode bending content of the three rate sensors. K_A and K_B (see Figure 34) are adjusted to provide an effective first mode slope, Y_1^*, and the outputs of the first and second blenders. In fact, it was desirable that the first and second blenders establish the same effective first mode slope, Y_1^*, at their outputs. By so doing, the third blender, which operates on only the second mode, could not alter the effective first mode slope, Y_1^*. As indicated, the third blender is sensitive to only the second bending mode signal occuring at the output of blenders one and two. Thus, the third blender will provide the effective second mode slope at its output without affecting the desired magnitude of the effective first mode slope as established by the first two blenders. Further, the third blender will automatically compensate for changes in the position (i. e., value of the attenuation K) of the first two blenders. This type of operation should assure maximum compatibility among the blenders so that no unstable combination can result. An unstable combination would be one wherein one blender would force another blender to move in such a manner as to force the first blender to move to a more undesirable location, etc.

DEFINITION OF SINGLE BLENDER LOGIC

Completion of the definition of the multiple blender configuration leads to further consideration of the individual blender adaptive logic to be used. Critical analysis of the adaptive logic network (as shown in Figure 31) indicates a severe restriction on the range of allowable blender positions. Assume that the inputs to a single blender from two rate gyros, located at X_F and X_A are the following:

$$\dot{\phi}(x_F) = \dot{\phi}_{cg} - Y_1'(x_F)\,\dot{\eta}_1 - Y_2'(x_F)\,\dot{\eta}_2$$

$$\dot{\phi}(x_A) = \dot{\phi}_{cg} - Y_1'(x_A)\,\dot{\eta}_1 - Y_2'(x_A)\,\dot{\eta}_2$$

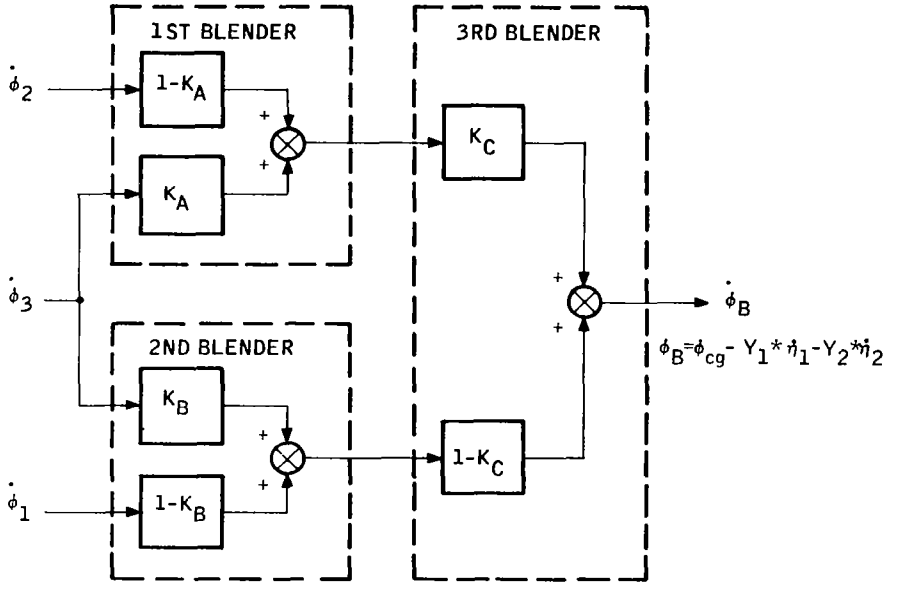

Figure 34. Conf. of Multiple Blender Used in Multiple Blender Study

Assume also that this blender operates at the first mode frequency so that only the first bending mode terms will be passed through the filters. Since the integration drives the error signal, ϵ, to zero, we can write the following steady-state equation: (see Figure 31)

$$|Y_1'(x_F)\ K\ | - |Y_1'(x_A)(1-K)\ | = \epsilon = 0$$

Rearranging this equation to provide the ratio of effective mode slopes, which determines the blender position, yields:

$$\frac{|K|}{|1-K|} = \frac{|Y_1'(x_A)|}{|Y_1'(x_b)|}$$

A plot of $\frac{|K|}{|1-K|}$ versus K appears in Figure 35. Examination of this curve reveals that the domain of K must be restricted to be $0 \leq K < 1$ for the following reasons. First, it is necessary to be able to accommodate a wide range of values of mode slope ratios, or equivalently of $\frac{|K|}{|1-K|}$. Secondly, proper operation of a multiple blender configuration can only be insured for a single valued curve of the mode slope ratio. Thirdly, note also that for negative values of K and positive values greater than one, the slope of the curve tends to be zero. If operation were attempted in this range of K, a very small change in mode slope ratio would result in an infinitely large change in blender position. This is most undesirable for proper blender operation. These three factors all restrict the blender to operate in the range $0 \leq K < 1$ if a satisfactory multiple blender operation is to be obtained.

The complexity of the single blender logic had to be increased for use in a multiple blender configuration. The basic reason was that the order of the bandpass filters had to be increased. The purpose of these filters is to pass a given bending mode signal and to reject the rigid body signal and other bending

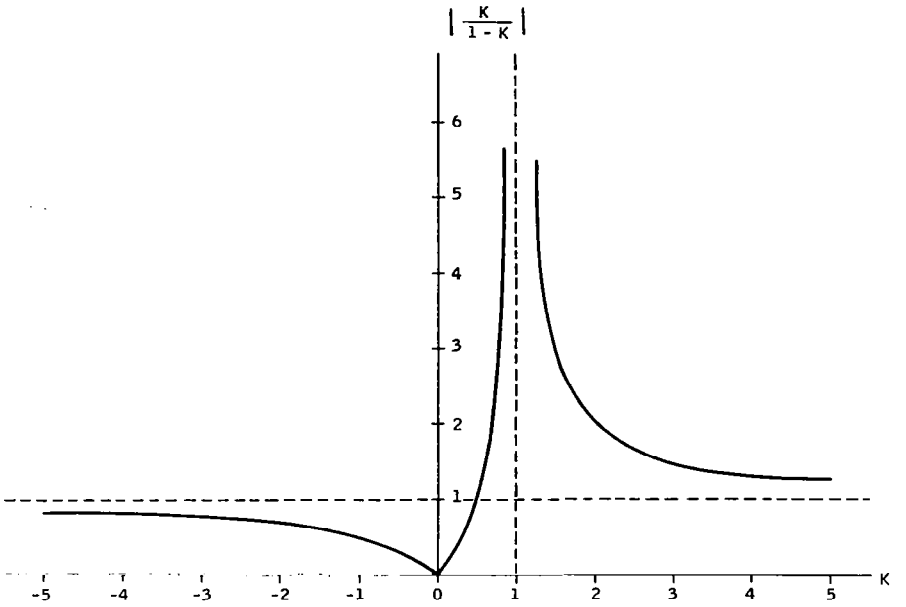

Figure 35. $\left| \frac{K}{1-K} \right|$ vs. K

mode signals from the blender logic. The requirement on the filters was more stringent for the multiple blender for two reasons: First, it was important that each blender attain its proper position to assure a unified operation. Second, since two modes were to be controlled, at least two large bending signals would be present. Thus, if one logic, operating on only one of these bending signals, is to function properly, the bandpass filters must adequately separate the two signals.

Frequency response characteristics of the filters that were used are shown in Figures 36 and 37 for the first and second mode blenders respectively. Both of these filters are of seventh order.

Although the operation of the blender depends largely on the quality of the bandpass filters, it is to some extent futile to design extremely sharp filters. A filter merely attenuates one signal relative to another. Thus, if the blender moves to drive the amplitude of the controlled bending mode signal to zero, the other signals at the output of the bandpasses will appear large in amplitude relative to the controlled mode. Further, to achieve improved filter characteristics, increased filter complexity is required. As was indicated earlier

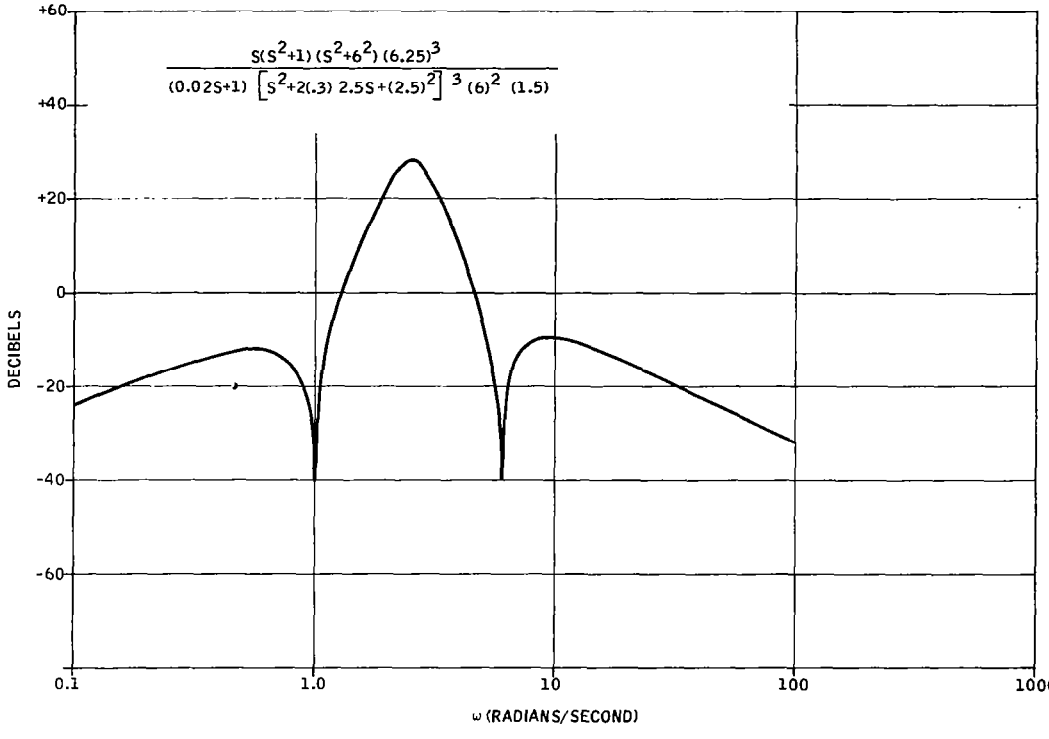

Figure 36. First-Mode Bandpass Filter

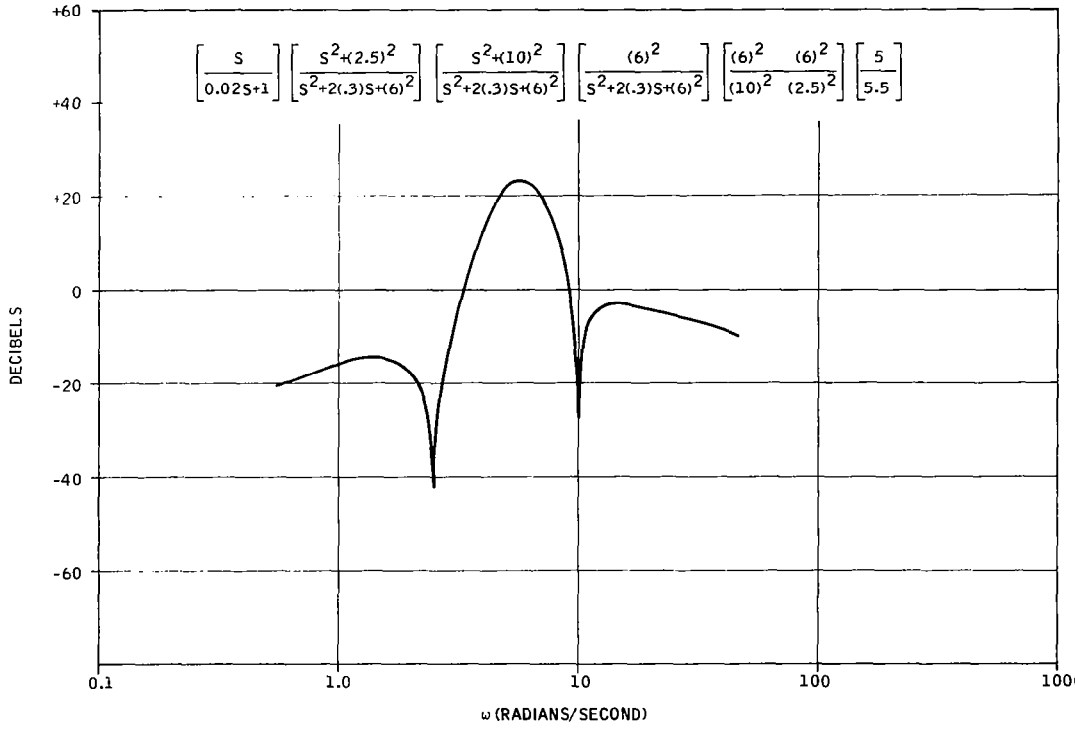

Figure 37. Second-Mode Bandpass Filter

the two bandpass filters in each logic must track rather closely (i.e., within 10 percent) to assure proper operation. This tracking problem becomes difficult to overcome as the complexity of the filter is increased. Analog computer analysis indicated that the integration rate on each of the three blenders could be the same. There was no apparent problem requiring a separation of bandwidth among the blender logics. The basic problem was to make each blender respond fast enough to drive it to a steady state position before the bending mode input signal decreased to zero. On the other hand, the gain could not be raised so high as to result in a poorly damped blender. An integration rate of 0.05 units/unit error on all blenders was selected as a good compromise. This value was not critical.

DEFINITION OF MODIFICATIONS TO RIGID BODY CONTROL SYSTEM

The rigid body control law from which the control law was developed for the flexible vehicle is the following:

$$B_c = 2.5 \left[\frac{S + .5}{S}\right] \left[\frac{.75}{.5S+1} (\phi - \phi_c) + \dot{\phi} + \frac{.4}{10S+1} \ddot{\tau}\right]$$

where $X_\phi = 118$ meters and $x_A = 90$ meters. The only parameters not specified as a result of the rigid body analysis were the number and location of rate sensors. Modifications had to be made to this control law for the multiple blender study for two reasons:

(1) to provide the necessary compensation for the bending modes not considered in the rigid body analysis.

(2) to compensate for design restrictions imposed by the multiple blender logic.

Forward Loop Compensation

The proportional-plus-integral term was removed for the multiple blender system because of the undesirable phase lag it contributed at the rigid body and first mode frequencies.

A fourth order notch filter was included in the control law to simulate the gain and phase characteristics at the 1st and 2nd mode frequencies of a filter which would provide gain stabilization of the fourth and higher modes. No attempt was made to complete the design of this filter to provide further attenuation required at frequencies in the neighborhood of the actuator dynamics. This effort was not considered imperative for the evaluation of the multiple blender concept. The following is a transfer function of the simplified filter used in the analysis:

$$H(s) = \left(\frac{S^2 + 13^2}{S^2 + 2(.3)\,13S + 13^2}\right)\left(\frac{S^2 + 16^2}{S^2 + 2(.3)\,16S + 16^2}\right)$$

This filter was designed to provide a system crossover frequency between the second and third mode frequencies (see the discussion of forward loop compensation for the synthesis study, pages 48 to 63).

Acceleration Feedback Compensation

The accelerometer feedback gain was reduced from 0.4 to 0.1 for the reasons described in the synthesis study (see page 53). With the accelerometer placed at body station 90 meters, the accelerometer picked up a large destabilizing second mode deflection. In order to compensate for this large destabilizing second mode pickup it would be necessary to generate a large effective 2nd mode slope with the blender. The other alternative would be to relocate the accelerometer. It was found that for the possible rate sensor locations and

the constraint that the blender positions all be between 0 and +1 that a sufficiently large effective 2nd mode slope (namely $Y_2^* = +.08$) could not be obtained and still maintain stability on the other modes. Thus, the only alternative left was to relocate the accelerometer.

It was found that moving the accelerometer back to station 60 meters resulted in improved bending pickups as evidenced in Table 1. Several stations were examined but 60 meters appeared to provide the best overall improvement.

Table 1. Comparison of Bending Mode Deflections for Accelerometer Locations of 60 and 90 Meters

Mode Deflection / Flight Time	Y_1 $X_A = 90$	Y_2 $X_A = 90$	Y_3 $X_A = 90$	Y_1 $X_A = 60$	Y_2 $X_A = 60$	Y_3 $X_A = 60$
8	-.24	1.75	-.22	-.69	-.009	.88
64	-.43	1.43	-.13	-.79	-.23	.70
80	-.56	1.31	.11	-.80	-.30	-.36

Moving the accelerometer back to station 60 meters improved the bending pickup but it degraded the rigid body response to attitude commands. To compensate, a term $l \ddot{\phi}_3$ ($l' = 30$ meters) was added to the accelerometer signal. This resulted in an accelerometer signal with the rigid body portion equivalent to that for an accelerometer located at station 90 meters. Of course, the net bending pickup on the sum of the $l \ddot{\varphi}_3$ terms and the accelerometer signal had to be modified. Resultant effective bending terms sensed by the accelerometer located at 60m, are shown in Table 2.

Table 2. Effective Accelerometer Bending Pickups

Flight Time	$Y_1(60) + 1'\ddot{\phi}_3$	$Y_2(60) + 1'\ddot{\phi}_3$	$Y_3(60) + 1'\ddot{\phi}_3$
8 sec	-.005	-.258	-1.58
64 sec	-.035	-.301	- .68
80 sec	-.025	-.30	- .65
157 sec	+.389	+.160	- .346

Rate Sensor Location

Three rate sensors are required to independently regulate the mode slopes on the first two bending modes. The location of these sensors was determined by the blender logic constraints and the magnitude of the mode slopes required to assure phase stability (as determined from an analysis of the attitude and accelerometer feedbacks). After re-locating the accelerometer, effective mode slopes of approximately -.01 and +.01 on the first and second modes respectively, were required on the output of the blender. These slopes (determined by computer analysis) are within the design range of the blenders and can be attained by biasing one of the input bandpass filters.

Three rate sensor locations were defined to obtain the desired mode slopes and yet satisfy the constraint on the blender position. To do this required that one sensor be placed where the second mode slope was positive. The only possible location was in the range 118 meters to 122 meters (see Figure B-1). Station 118 meters was selected. Since the first mode slope at 118 meters was large and negative (i.e., approximately -.115 as opposed to the required value of -.01) it was essential to place a sensor where there would be a large positive

slope on the first mode. This was essential in order to assure satisfactory 1st mode blender operation. If this was not done the blender would for practical purposes, completely favor the one gyro in order to reduce the effect of the large magnitude of slope occurring at station 118 meters. For this purpose a sensor (i.e., $\dot{\phi}_3$) was located at body station 46 meters. The first mode slope has its largest positive value at this station. At station 46 meters, the second mode slope was nearly zero. Thus, to effectively reduce the large positive 2nd mode slope occurring on the sensor located at 118 meters it was necessary to locate the third sensor where the 2nd mode slope was negative. Further, since the third mode slope was negative at the other two sensor locations, it was desirable to pick a station for the third sensor which would have a large positive value for the third mode slope. This was essential to achieve phase stabilization on the third mode. Thus, the remaining sensor, $\dot{\phi}_2$, was located at station 90 meters. As shown in Figures 7 and 8, the sensor placed at 118 meters was summed with the sensor placed at 46 meters in blender No. 1 because the first mode had opposite slopes at these two stations. Correspondingly the sensor at 46 meters was summed with the sensor at 90 meters in blender No. 2.

With these modifications to the rigid body controller the basic system took the following form:

$$\beta_c = K_s \left[\frac{.75}{.5S+1} (\phi - \phi_c) + \dot{\phi}\beta + \frac{.1}{10S+1} \left(\ddot{\tau} + \frac{1's}{.02S+1} \dot{\phi}_3 \right) \right] \left[\left(\frac{S^2 + 13^2}{S^2 + 2(.3)\,13S + 13^2} \right) \left(\frac{S^2 + 16^2}{S^2 + 2(.3)\,16S + 16^2} \right) \right]$$

where X_ϕ = 118 meters, X_A = 60 meters, 1' = 30 meters, $X_{\dot{\phi}_1}$ = 118 meters, $X_{\dot{\phi}_2}$ = 90 meters, $X_{\dot{\phi}_3}$ = 46 meters and

$$K_s = \begin{cases} 1.0, & t = 8,\ 64,\ 80 \text{ seconds} \\ .5, & t = 157 \text{ seconds} \end{cases}$$

PERFORMANCE EVALUATION

Performance of the multiple blender system at four flight times is demonstrated by means of the information presented in the following Figures:

a)	Root Locus Diagrams	Figures D-32 through D-35
b)	Frequency Response Characteristics	Figures C-11 through C-14
c)	Analog Computer Traces of Time Domain Response	Figures E-36 through E-39

The points on the root loci which correspond to the closed loop pole locations at the nominal operating gain are enclosed by a small square. For the Multiple Blender Study the nominal operating gain is 1.0 for the first three flight times of 8 seconds, 64 seconds, and 80 seconds, and 0.5 for the burnout condition at 157 seconds. For the root locus analysis, the blender positions, K_A, K_B, and K_C, were fixed at their calculated steady state values.

These steady-state blender positions were calculated by considering the total output signal from the multiple blender configuration as shown in Figure 34. The blender output is seen to be:

$$\dot{\phi}_B = \dot{\phi}_1 \left[(1-K_C)(1-K_B)\right] + \dot{\phi}_2 \left[K_C(1-K_A)\right] + \dot{\phi}_3 \left[K_C K_A + K_B(1-K_C)\right] \quad (1)$$

which can be written as

$$\dot{\phi}_B = K_1 \dot{\phi}_1 + K_2 \dot{\phi}_3 + K_3 \dot{\phi}_3 \quad (2)$$

where $K_1 = \left[(1-K_C)(1-K_B)\right]$

$K_2 = \left[K_C(1-K_A)\right]$

$K_3 = \left[K_C K_A + K_B(1-K_C)\right]$

Substituting the individual rate gyro outputs into equation (2) we have:

$$\dot{\phi}_B = K_1 [\dot{\phi}_{cg} - Y_1'(X_{s1})\,\dot{\eta}_1 - Y_2'(X_{s1})\,\dot{\eta}_2]$$
$$+ K_2 [\dot{\phi}_{cg} - Y_1'(X_{s2})\,\dot{\eta}_1 - Y_2'(X_{s2})\,\dot{\eta}_2]$$
$$+ K_3 [\dot{\phi}_{cg} - Y_1'(X_{s3})\,\dot{\eta}_1 - Y_2'(X_{s3})\,\dot{\eta}_3] \qquad (3)$$

The above equation expressed in terms of the ideal mode slopes becomes:

$$\dot{\phi}_B = \dot{\phi}_{cg} - Y_1^*\,\dot{\eta}_1 - Y_2^*\,\dot{\eta}_2 \qquad (4)$$

Equating equations (3) and (4) we obtain:

$$Y_1^* = K_1 Y_1'(X_{s1}) + K_2 Y_1'(X_{s2}) + K_3 Y_1'(X_{s3})$$

$$Y_2^* = K_1 Y_2'(X_{s1}) + K_2 Y_2'(X_{s2}) + K_3 Y_2'(X_{s3}) \qquad (5)$$

$$1 = K_1 + K_2 + K_3$$

The values of the ideal first and second mode slopes, Y_1^* and Y_2^*, were determined earlier by assuming a single rate sensor feedback defined by equation (4). The ideal mode slope values of $Y_1^* = -.01$ and $Y_2^* = +.01$ thus determined were substituted into equation (5) and with the help of the relationships defined for equation (2) the steady-state blender positions shown in Table 3 were determined.

Table 3. Steady-State Blender Positions for Ideal Mode Slopes of $Y_1^* = -.01$ and $Y_2^* = +.01$

Blender Position \ Flight Time	t = 8	t = 64	t = 80	t = 157
K_A	.479	.448	.434	.21
K_B	.753	.748	.743	.608
K_C	.344	.349	.397	.40

To obtain these positions the blender bandpass filters had to be biased by the gain factors K_1', K_2', K_3'. By so doing, the blender was forced to favor one gyro over the other to establish the desired mode slope. If this were not done, then the blender would attempt to cancel the mode. Average values of these constants were defined to be: $K_1' = 1.88$; $K_2' = 1.52$; $K_3' = 2.28$.

Examinations of the root locus diagrams shows that the system has at least a 6 db upper and lower gain margin for each of the flight conditions. The root locus diagrams also reveal that another performance requirement is met at all flight conditions, namely that the frequency of the rigid body response is at least 0.5 rad/sec.

Performance requirements for the Multiple Blender Study include a requirement for a phase margin of at least thirty degrees for each phase stabilized bending mode. Phase margin is defined to be the number of degrees of change in phase angle at the bending mode frequency occurring at the nominal operating gain required to cause that bending mode to go unstable. The phase margin was specified as a number of degrees of phase lag or phase lead, whichever was less to cause instability of the given mode. Thus the maximum possible phase margin would be 90° (lead or lag).

The phase margin of each bending mode for the four nominal flight conditions appears below in Table 4.

Table 4. Phase Margin of First three Structural Bending Modes

Bending Mode / Flight Time	1st Mode	2nd Mode	3rd Mode
8 sec.	62^{o} lead	13^{o} lag	11^{o} lead
64 sec.	81^{o} lead	71^{o} lag	12^{o} lead
80 sec.	88^{o} lead	46^{o} lag	17^{o} lead
157 sec.	85^{o} lag	17^{o} lag	---

No phase margin is given for the 3rd mode at t = 157 seconds because at this flight time the third mode is gain stable and phase margin is thus undefined.

From Table 4 it is apparent that the requirement on phase margin is not met for the third bending mode at the first three flight times, nor for the second bending mode at the first and last flight times. This marginal performance could be improved by using a more realistic forward loop high frequency filter.

Performance of the multiple blender in the time domain is demonstrated in the analog traces shown in Figures C-11 through C-14. System response is demonstrated for attitude commands at all four flight times and for model wind inputs and step changes in angle of attack, αgust, at the 64 second and 80 second flight times. The blender positions are indicated by K_A, K_B, and K_C in the three uppermost analog traces. Initial values of the blender positions are listed with each figure.

Adaptive multiple blender performance may be most easily observed on Run #3 at t=64 seconds. For this run the initial blender positions were all set at 0.5. When the system receives an attitude command, the blenders drive towards the steady state positions calculated to provide the desired damping of the first two modes. These calculated steady state blender positions for t = 64 are $K_A(0) = .45$, $K_B(0) = .75$, and $K_C(0) = .35$.

For the other runs shown, the initial blender positions were set at the steady state positions calculated for each flight condition to yield the desired bending mode damping ratios. It is apparent from these runs that the blenders never seem to achieve fixed steady state positions, but rather drift towards one direction whenever a command is input to the system.

This undesirable blender drift is partially a result of using non-ideal bandpass filters in the blender logic. Even though the unwanted signals, such as rigid body rate, are attenuated by the filters, they are evidently large enough to drive the blenders away from their ideal positions. This problem is particularly serious when the blender position is such that the given bending mode amplitude approaches zero. In addition, it was difficult for the blenders to reach a final value because of an apparent lack of information. In other words, the bending signal would die out before the blenders could be properly positioned. However, it is expected that in actual flight the bending modes would be excited sufficiently to ensure proper blender operation.

EVALUATION OF MULTIPLE BLENDER SYSTEM FEASIBILITY

The basic objective of this study was to investigate the feasibility of multiple blending based on the use of the single blender logic as defined in Reference 2. On the basis of the results obtained during this investigation, it appears that the concept of multiple blending is a feasible one.

An arrangement of three single adaptive blenders has been operated which has simultaneously provided control of two structural bending modes. The combining of individual blenders resulted in integrated operation in that the individual blenders aided, rather than opposed, each other.

It was concluded that the performance of the final multiple blender system investigated was degraded by the problem areas encountered. These problem areas lay primarily within the particular adaptive logic used rather than in the multiple blender concept. A serious limitation of the present blender logic is the requirement of the blender gains to lie between 0 and +1. This limitation, in turn, requires a more accurate knowledge of mode slopes than was desired as a design objective.

Another problem area of the multiple blender was the contamination of the logic signals by rigid body rate and consequent degradation of performance. This problem occurs when the blender correctly drives the bending signal towards zero, resulting in a small signal-to-noise ratio of the signal entering the blender logic. An additional objection to the present blender and adaptive logic is the overall complexity. Each blender has two adaptively adjusted gains, K and (1-K), and two seventh order bandpass filters which must be closely matched. Also included in each logic network are two absolute value circuits (rectifiers), and an integrator.

An additional factor affecting the feasibility of the multiple blender system investigated is the stricter component tolerance requirements which result from the increased system complexity. As is true in the single blender logic, the band pass filters in the multiple blender logics must have closely matched frequency response characteristics in order to function correctly. However, the increased complexity of the individual filters defined for the multiple blender system results in stricter component tolerances than were necesssary for the single blender configuration.

Upon consideration of the problem areas encountered with the adaptive logic used in the multiple blender system, it was concluded that a new blender logic was needed which would be free from some or all of the limitations previously discussed. It was felt that this new adoptive logic should have the following properties:

- Extended range of blender positions beyond 0 to +1.
- Reduced complexity, particularly as regards the bandpass filters.
- Reduced contamination of the blender logic by the rigid body rate.

If a logic can be developed which will have the above properties, it should result in desirable multiple blender performance.

DEVELOPMENT OF NEW BLENDER LOGICS

Design objectives for the investigation of new blender logics were the following:

- Reduced contamination of blender logic by rigid body rate signals
- Extended range of allowable blender positions beyond the range 0 to +1
- Reduced overall complexity

Experience with the nominal multiple blender system has shown that many of the problem areas connected with it are a result of using two parallel signal paths within the logic. The block diagram of Figure 38 makes these parallel logic paths apparent.

One of the problem areas of the nominal blender system which is due to the use of parallel logic paths is the restriction on allowable blender positions to lie between 0 and +1. The blender position restriction (discussed under the section entitled "Definition of Single Blender Logic") results from subtracting the two logic signals after they have been separately rectified. Another problem area of

of the nominal blender logic is the difficulty in obtaining two filters with closely matched frequency response characteristics for the two parallel logic paths.

Consideration of the problem areas encountered with the type of adaptive logic used in the nominal blender system indicates a need for a new adaptive logic with a single signal path. In order to define an adaptive logic which would have a single signal path, a different blender configuration was necessary. A candidate blender configuration which would allow the use of a single signal path in the adaptive logic is shown in Figure 39.

It is easily demonstrated that the new blender configuration provides the same type of blended rate signal to the control system as the nominal blender configuration. The blended rate signals of two configurations are shown to be identical as follows:

- Nominal blender configuration: $\dot{\phi}_B = K\,\dot{\phi}_{G1} + (1-K)\,\dot{\phi}_{G2}$
- New blender configuration: $\dot{\phi}_B = \dot{\phi}_{G2} - K(\dot{\phi}_{G2} - \dot{\phi}_{G1}) = K\,\dot{\phi}_{G1} + (1-K)\,\dot{\phi}_{G2}$

A basic difference in the new blender configuration from the nominal blender configuration is that the difference of the two rate gyro signals is taken before the logic operations are performed. Utilizing the difference of two rate gyro outputs for the input signal to the logic results in the following improvements in the performance and mechanization of the blender system:

- Contamination of the blender logic by rigid body rate signals is reduced because the rigid body rate is subtracted out before the logic operations.
- Logic complexity is reduced; first because the single signal path eliminates the need for one filter and rectifier, and secondly because the remaining filter need not separate rigid body rate from bending signals.

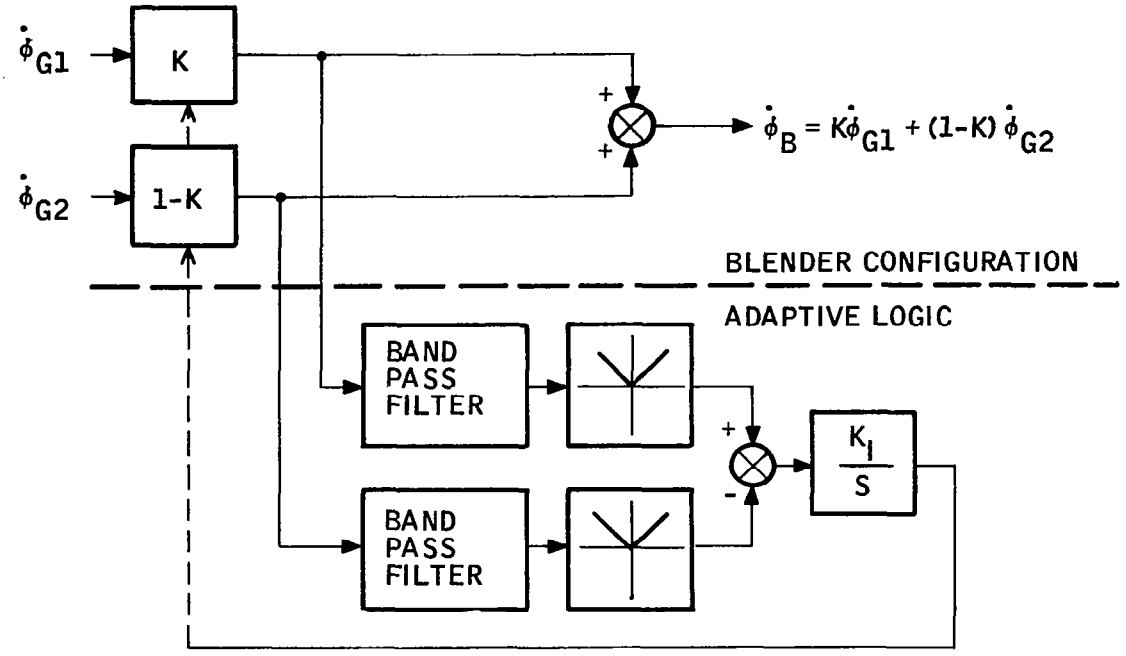

Figure 38. Nominal Blender Configuration and Adaptive Logic

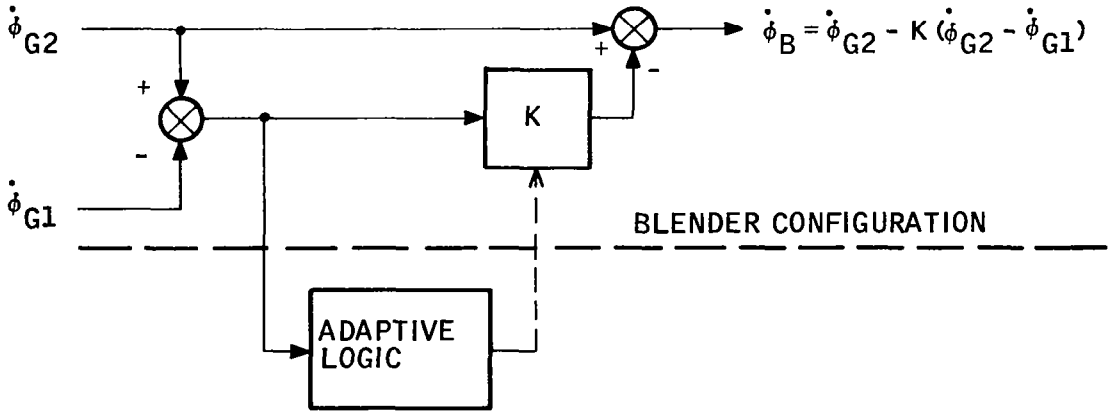

Figure 39. Blender Configuration Utilizing Difference of Rate Gyro Signals

- The complexity of the blender configuration is also reduced by eliminating one of the two multiplications (K and (1-K)) required for the nominal blender configuration.

With a blender configuration selected which would provide the difference of two rate gyro signals, it was necessary to develop an adaptive logic which would operate on the rate gyro difference signal to adjust the blender position, K. To interpret the significance of the rate gyro difference signal, assume that the two rate gyro outputs each contain one bending mode signal:

$$\dot{\phi}_{G1} = \dot{\phi}_{cg} - Y_1'(X_{s1})\,\dot{\eta}_1$$

$$\dot{\phi}_{G2} = \dot{\phi}_{cg} - Y_1'(X_{s2})\,\dot{\eta}_1$$

then

$$(\dot{\phi}_{G2} - \dot{\phi}_{G1}) = -(Y_1'(X_{s2}) - Y_1'(X_{s1})\,\dot{\eta}_1$$

Since the difference of the two rate gyro signals, $(\dot{\phi}_{G2} - \dot{\phi}_{G1})$ contains no rigid body rate, it is a measure of the bending signal amplitude. It is conceivable that if the time rate of change of the bending amplitude could be obtained, it could be used to drive the blender position so that the damping ratio of the bending signal would be controlled.

Further consideration of the techniques of using the derivative of bending amplitude to drive blender position reveals that before the derivative signal is used to drive the blender position, it must be compared to a reference signal. Failure to compare the derivative signal to a reference would be equivalent to comparing it to zero. This means that the system would assume steady-state performance when the derivative of the bending amplitude signal becomes zero, or equivalently when the bending amplitude becomes a constant. This would not be acceptable operation unless the bending amplitude were zero as well as a constant.

One common type of reference signal to use for comparison is a constant set point. A set point reference signal has the advantage of being very simple, but it has the disadvantage in that it feeds a constant error signal to the rest of the control system even when the error signal of interest, in this case the derivative of the bending amplitude, has gone to zero. It should be apparent at this point that the reference signal used for comparison with the derivative of the bending amplitude should have a finite value when the derived signal is finite, and should go to zero when the derived signal becomes zero. It then appears obvious that the bending amplitude signal could be conveniently used as the reference signal.

The bending amplitude signal used in the newly defined adaptive logic is a smoothed dc signal obtained from the difference of the rate gyro outputs by rectifying and filtering. Consider the case in which a stable bending mode receives a disturbance. The rectified bending amplitude signal may then be expressed as:

$$Y = Ae^{-\zeta wt}$$

If we compare the magnitude, Y, against its derivative as indicated accompanying diagram, we have:

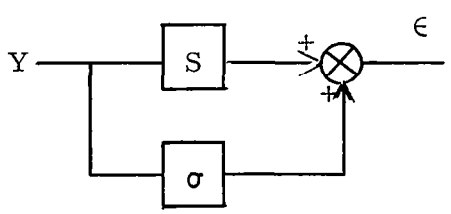

$$\epsilon = Y(\sigma + s)$$

$$= Ae^{-\zeta \omega t} \quad (\sigma - \zeta \omega)$$

If the error signal, ϵ, is driven to zero, we may write for steady-state operation:

$$\zeta = \frac{\sigma}{\omega}$$

The range of values of the bending mode frequency is small enough to consider frequency constant. The use of this type of blender logic will thus allow one to select the desired damping ratio for a given bending mode.

A suitable procedure for driving the error signal, ε, to zero is to feed this error signal into an integrator which sets the blender position K. A block diagram of the new blender configuration and general form of the new adaptive logic is shown in Figure 40.

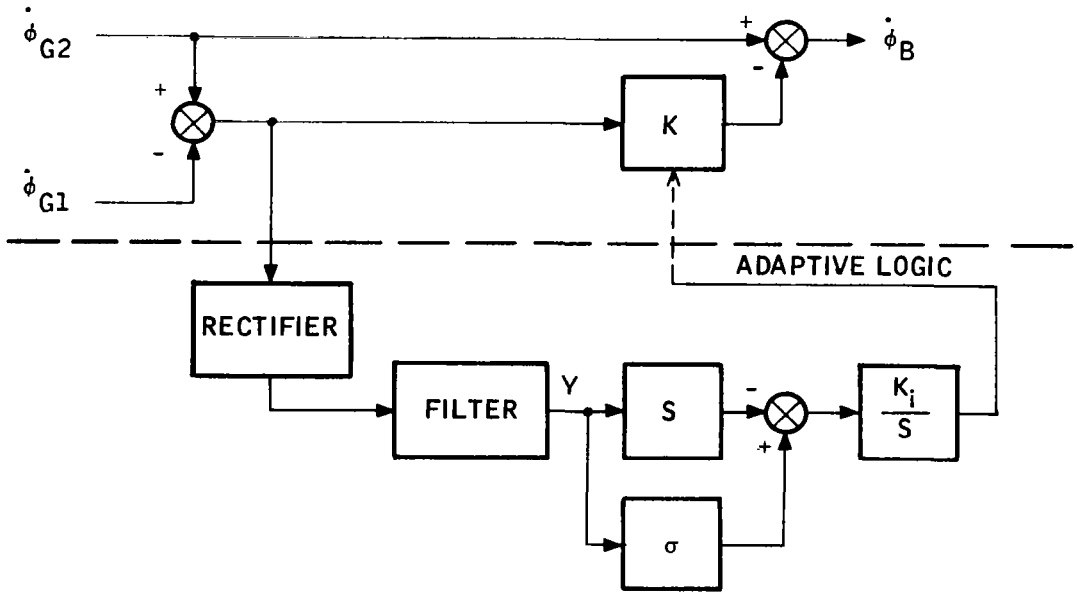

Figure 40. New Blender Conf. and General Form of Adaptive Logic

Preliminary investigation of the new adaptive logic indicated the following problem areas:

- The blender position does not assume its steady-state position during the time it takes the first bending disturbance to damp out. The result is that the system requires a few input disturbances in order for the blender to position itself for the desired damping ratio of the blending mode.

- The blender position is too sensitive to command inputs to the booster control system. Ideally, once the blender has attained its steady state position, it should remain fixed when the vehicle receives command inputs.

- A phase difference between the bending amplitude signal and its derivative was observed which seemed to cause difficulty in nulling the sum of the two signals. Although the significance of this phase difference was not thoroughly investigated, the amount of phase shift was found, as expected, to be less for a digital sample-and-hold mechanization of the derivative function than it was for a hi-pass mechanization.

It appears that the problem areas indicated lie within the mechanization of the logic rather than in the theory of operation, and thus are potentially solvable.

Various alternate mechanizations are possible with the new adaptive logic, some of which have been investigated. For reference purposes, a block diagram of the specific mechanization of the blender configuration and adaptive logic which was evaluated on the analog computer is shown in Figure 40. One of the functions which can be mechanized differently is the derivative function, denoted by an "S" in Figure 40. During the study, the derivative function was mechanized both with a digital sample-and-hold network and with an analog hi-pass circuit. Blender performance was similar for the two mechanizations. The hi-pass circuit has the advantage of being the simpler mechanization, but it also has the disadvantage of greater transmission of high frequency signals. The hi-pass derivative mechanization will result in a noisy output signal unless precautions are taken to carefully filter the incoming signal.

Another logic function which can be alternately mechanized, according to the mechanization used for the derivative function, is the ripple filter used to obtain a smooth bending amplitude signal. It was found that when the digital sample-and-hold network was used for the derivative function, only a single first-order

lag was necessary for the ripple filter. On the other hand, when the hi-pass circuit was used, it was necessary to use a first-order lag and a second-order notch filter with center frequency at the ripple frequency.

A third possible alternate mechanization in the new blender logic is the use of a feedback loop from the output of the integrator to the proportional gain σ. If this feedback loop is used, the gain σ becomes an adjustable gain rather than a constant. The reason that this feedback path is optional is that the integrator output already has a closed loop path through the vehicle back to the logic.

The feedback loop from the integrator output to the adjustable gain, σ, was added for the following reasons:

1) To speed up blender response to disturbances by avoiding the time response of the vehicle and sensors.

2) To eliminate integrator drift off due to small error signals by forcing the input signal to the integrator to be zero.

3) To cause the integrator output to be exactly σ, where $\sigma = \zeta\omega$, so that the integrator output is directly related to the damping ratio.

A final alternate mechanization possible with the new blender logic is the use of the discrete blender positioning function. This function converts the continuously variable integrator output into discrete values which, in turn, allow the blender to assume only corresponding discrete positions. This function was included to eliminate blender position drift due to small error signals fed into the integrator and to reduce blender position sensitivity to command inputs. If the integrator drift and system sensitivity to command inputs could be reduced by other means, the discrete blender positioning function could be eliminated.

Preliminary performance results of the new blender configuration and adaptive logic appear in the analog computer traces of Figures C-15 and C-16. Figure C-15 shows system operation for a desired damping ratio of 0.1 and Figure C-16 indicates the operation for a desired damping ratio of 0.2. As indicated previous, Figure 9 is a block diagram of the particular system evaluated. Only the first bending mode was included in the simulation.

Performance of the new blender system was evaluated as a function of the bending mode slopes at the first and second rate gyro locations, $Y_1'(X_{s1})$ and $Y_1'(X_{s2})$ respectively. Attention should be centered on the trace of the first bending mode signal, η_1, and in particular, on the damping ratio of any disturbance of this signal. For each run the initial blender position was zero, which is the position corresponding to the least stable operation of the bending mode. During each first disturbance then, the blender position changes rapidly to provide better damping of the bending signal. In either of the two figures of analog traces it can be seen that for latter disturbances, the damping ratio of the first bending mode appears to be nearly constant for the various combinations of mode slopes used.

If we compare Figures C-15 and C-16, it is apparen t that the traces of Figure C-16 do indeed have a higher damping ratio and those of Figure C-15 although the values of damping ratio may not be .2 and .1 as desired. Thus the system performs approximately as desired.

One other feature to be noted about the performance of the new blender is that the blender position is still quite sensitive to input commands. This is one of the problem areas which needs further study.

In summary, it is felt that the newly defined blender configuration and adaptive logic represent a feasible approach to an improved rate gyro blender. This system meets the design objectives and has some additional benefits as well.

Certain problem areas were indicated by preliminary investigation;but it is felt that these are not inherent in the theory of operation. Further detailed study is necessary to refine the mechanization and to evaluate the alternate design approaches indicated.

REFERENCES

1. "Model Vehicle #2 for Advanced Control Studies", George C. Marshall Space Flight Center.

2. "Advanced Control System for the Saturn V Configuration", MH Aero Report 1300-TR1, NASA Contract No. NAS 8-5069, 27 November 1963.

LITERATURE STUDY BIBLIOGRAPHY

The following is a list of articles and documents that were reviewed. The information contained in these publications covers several possible control schemes.

1. Andeen, Richard E., "Stabilizing Flexible Vehicles", Astronautics and Aeronautics, August, 1964.

2. Andeen, Richard E., "Self-Adaptive Autopilots", Space and Aeronautics, April, 1965.

3. Box, James L. and Davis, Jack C., "A Survey of Adaptive Methods for Bending Suppression in Large Boosters."

4. Freed, L.E., "A Method of Damping Missile Structural Bending Modes for Autopilot Design", Space Technology Laboratory, May 1959.

5. Hosenthien, Hans H., and Borelli, Michael T., "Self-Adaptive Tracking Filters", Presented to the Society of Automotive Engineers, July 1964.

6. Lewis, Robert C. and Carter, Thomas E., "A Dual Rate Gyro Approach to the Elastic Feedback Problem", George C. Marshall Space Flight Center, MTD- Aero-63-21, 4 March 1963.

7. Swaim, Robert L., "Elastic Mode Effects on Closed-Loop Stability of a Winged Booster," Air Force Flight Dynamics Laboratory Report, 1963.

8. Swaim, Robert L., "Active Control of Booster Elasticity", Air Force Flight Dynamics Laboratory, TDR No. FDL-TDR- 64, September, 1964.

9. "Standardized Space Guidance Study, Program Definition Phase 1A", Volume II, Annex H, Sperry Gyro SSD-TDR-64-131, May 1964 (Secret).

10. "Standardized Space Guidance System Phase 1A Study", TDR No. SSD-TDR-64-129, part 1, 28 May 1964 (Secret).

11. "Standardized Space Guidance System - Program Definition Studies - Phase 1A Final Report, Volume X, Annexes D, E, F, G, H, I, J, and K, SSD-TDR-64-130(X), May 1964.

APPENDIX A
NOMENCLATURE
DEFINITION OF SYMBOLS AND UNITS

Symbol	Definition	Unit
ϕ	Attitude angle.	rad
ν	Angle between reference and inertial velocity vector.	rad
α	Angle of attack.	rad
β	Control deflection angle.	rad
V	Velocity.	m/sec
V_w	Wind Velocity.	m/sec
Z	Direction normal to reference.	m.
z	Direction normal to vehicle centerline.	m.
X	Direction of the vehicle centerline.	m.
F	Total thrust of the vehicle booster.	kg
M	Total mass of the vehicle.	$kg\text{-}sec^2/m$
I_{xx}	Pitch plane moment of inertia about the CG.	$kg\text{-}m\text{-}sec^2$
X	Drag force.	kg
a_{LA}	Vehicle longitudinal acceleration.	m/sec^2
q	Dynamic pressure.	kg/m^2
R'	Thrust of control engines	kg

DEFINITION OF SYMBOLS AND UNITS (Continued)

Symbols	Definition	Unit
N'	Aerodynamic force	kg
C_1	Aerodynamic moment coefficient	$1/sec^2$
C_2	Control moment coefficient	$1/sec^2$
a_o	Displacement gain	Unitless
a_1	Rate gain	sec
b_o	Angle-of- Attack gain	Unitless
g_2	Accelerometer gain	sec^2
$\ell_A = X_A - X_{cg}$	Distance from vehicle CG to accelerometer	m
$1_{cp} = x_{cg} - x_{cp}$	Distance from vehicle CG to the CP	m
$1_{cg} = x_{cg} - x_\beta$	Distance from engine gimbal to vehicle CG	m
$1_E = x_\beta - x_E$	Distance from engine gimbal to engine mass CG	m
A	Cross sectional reference area	m^2
η_i	Generalized displacement of the i^{th} mode (usually denoted as "normal coordinates")	m
M_i	Generalized mass	$kg\text{-}sec^2/m$
M'_α	Bending moment due to a change in the angle of attack	$\frac{K_p - M}{rad}$
M'_β	Bending moment due to a deflection of the the engine gimbal	$\frac{K_p - M}{rad}$

DEFINITION OF SYMBOLS AND UNITS (Continued)

Symbol	Definition	Unit
M_x	Concentrated mass at Sta. X.	kg-sec^2/m
f_i	Bending frequency.	cps
ω_i	Bending frequency.	rad/sec
ζ_i	Bending Mode damping.	Unitless
$Y_i(X)$	Normalized* displacement at Sta	Unitless
$Y'_i(X)$	Normalized* slope $\frac{d}{dx}[Y_i(X)]$	1/m
$Y_i(X)\eta_i$	Displacement at Sta. X due to the i^{th} mode.	m
$Y'_i(X)\eta_i$	Angular displacement at Sta. X due to the i^{th} mode.	rad.
$Y'_i(X)\dot{\eta}_i$	Angular rate at Sta. X due to the i^{th} mode.	rad/sec
$Y'_i(X)\ddot{\eta}_i$	Angular acceleration at Sta. X due to the i^{th} mode.	rad/sec^2
V_i	Reference potential energy of the i^{th} mode.	kg-m
Q_i	Generalized force for the i^{th} mode.	kg
$W_{(x, t)}$	Force distribution over the length of the vehicle for all forces acting upon the vehicle.	kg/m

*The bending displacement is normalized to "+1" at the vehicle gimbal point. The slope is a function of the normalized displacement.

X_β = 2.54 M (gimbal point)

DEFINITION OF SYMBOLS AND UNITS (Continued)

Symbol	Definition	Unit
M_k	Mass	$kg\text{-}sec^2/m$
I_k	Moment of inertia.	$kg\text{-}sec^2\text{-}m$
$X_k - X_\beta$	Distance to the vehicle Sta X_k as measured from the vehicle gimbal point.	m
l_k	Distance between two vehicle stations.	m
ζ_k	Damping.	Unitless
ω_k	Angular frequency.	rad/sec

Subscripts "k":

CG	Center of gravity.
CP	Center of pressure.
LA	Longitudinal acceleration.
ϕ	Position gyro.
A	Accelerometer.
α	Angle of attack.
E	Engine.
IR	Instantaneous rotation.
R	Rigid body.
B	Bending body.
W	Wind.
i	i^{th} bending mode.
X	Vehicle Station.
β	Engine gimbal.
x	Denotes acceleration measured at accelerometer.
F	Denotes angular acceleration due to a deformation of the tail.

DEFINITION OF SYMBOLS AND UNITS (Continued)

Symbol	Definition	Unit
Superscripts:		
"."	Derivative w.r.t. time.	
*'	Denotes required effective mode slope.	

APPENDIX B
VEHICLE EQUATIONS AND DATA

This appendix contains the vehicle equations of motion and data as used in the study. The equations of motion and data were derived from Reference 1 entitled "Model Vehicle #2 for Advanced Control Studies".

I. VEHICLE EQUATIONS

A. Rotation of the Vehicle at Station x_{cg}

$$\ddot{\phi}_{cg} = \ddot{\phi}_R + \ddot{\phi}_{BF}$$

$$\ddot{\phi}_R = -C_1\alpha - C_2\beta_r$$

$$\ddot{\phi}_{B_F} = \frac{F(x_{cg}-x_E)}{I_{xx}} \sum_{i=1}^{3} Y'_i(x_\beta)\eta_i - \frac{F}{I_{xx}} \sum_{i=1}^{3} Y_i(x_\beta)\eta_i$$

B. Acceleration Normal to Vehicle Reference at Station x_{cg}

$$\ddot{z} = \ddot{z}_R + \ddot{z}_B$$

$$\ddot{z}_R = \left(\frac{F-x}{m}\right)\phi_{cg} + \frac{R'}{m}\beta_r + \frac{N'}{m}\alpha$$

$$\ddot{z}_B = -\sum_{i=1}^{3} \frac{F}{m} Y'_i(x_\beta)\eta_i$$

C. Acceleration Normal to the Vehicle Longitudinal Axis at the Sensor Location x_A.

$$\ddot{\tau} = \ddot{z}_{Rx} + \ddot{z}_{Bx}$$

$$\ddot{z}_{Rx} = \frac{R'}{m}\beta_r + \frac{N'}{m}\alpha + \ell_A\ddot{\phi}_R$$

$$\ddot{z}_{Bx} = \sum_{i=1}^{3} Y_i(x_A)\ddot{\eta}_i - \sum_{i=1}^{3} \frac{F}{m} Y'_i(x_\beta)\eta_i$$

D. Angular Relations

$$\alpha = \alpha_w + \phi_R - \frac{\dot{z}}{V}, \quad \alpha_w = \frac{V_w}{V}$$

$$\phi = \phi_{cg} + \phi_B = \phi_{cg} - \sum_{i=1}^{3} Y'_i(x_\phi)\eta_i$$

$$\dot{\phi} = \dot{\phi}_{cg} + \dot{\phi}_B = \dot{\phi}_{cg} - \sum_{i=1}^{3} Y'_i(x_\phi)\dot{\eta}_i$$

$$\ddot{\phi} = \ddot{\phi}_{cg} + \ddot{\phi}_B = \ddot{\phi}_{cg} - \sum_{i=1}^{3} Y'_i(x_\phi)\ddot{\eta}_i$$

$$\beta = \beta_r + \beta_B = \beta_r - \sum_{i=1}^{3} Y'_i(x_\beta)\eta_i$$

E. Bending Equations

$$\ddot{\eta}_i + 2\zeta_i\omega_i\dot{\eta}_i + \omega^2{}_i\,\eta_i = \sum_{i=1}^{3} \frac{Q_i}{M_i}$$

$$\sum_{i=1}^{3} Q_i = Q_{i_\beta} + Q_{i_N}$$

$$Q_{i\beta} = R' Y_i(x_\beta)\beta$$

$$Q_{iN} = \sum_n qA \left(\frac{\partial C_{z\alpha}}{\partial (x/D)} \Delta x_n Y_i(x_n)\right)\alpha$$

$$M_i = \int_0^L mx[Y_i(x)]^2 dx$$

F. Accelerometer Equation at Station x_A

$$A_a \left[\frac{s^2}{\omega_a^2} + \frac{2\zeta_a}{\omega_a} s + 1\right] = \ddot{z} - \left(\frac{F-x}{m}\right)\phi_{cg} + \ell_A \ddot{\phi}_R + \sum_{i=1}^{3} Y_i(x_a)\ddot{\eta}_i$$

G. Engine Gimbal - Actuator Dynamics

$$\frac{\beta_r}{\beta_c} = \frac{31130}{(s+14.64)(s^2+9.08s+2126)}$$

H. Additional Definitions

$R' = 1/2\ F$

$N' = C_{z\alpha} qA$

$A = \frac{\pi}{4} D^2$

$X = C_{D_O} qA$

$\ell_\alpha = x_{cg} - x_\alpha$

$$\alpha_T = \alpha_R - Y'_i(x_\alpha)\eta_i - \sum_i \frac{Y_i(x_\alpha)\dot{\eta}_i + \ell_\alpha \dot{\phi}_R}{V}$$

$$C_1 = \frac{N'}{I_{xx}} \ell_{cp}$$

$$C_2 = \frac{R'}{I_{xx}} \ell_{cg}$$

Bending Moment = $I = M'_\alpha \alpha + M'_\beta \beta$

First Bending Mode Geometry

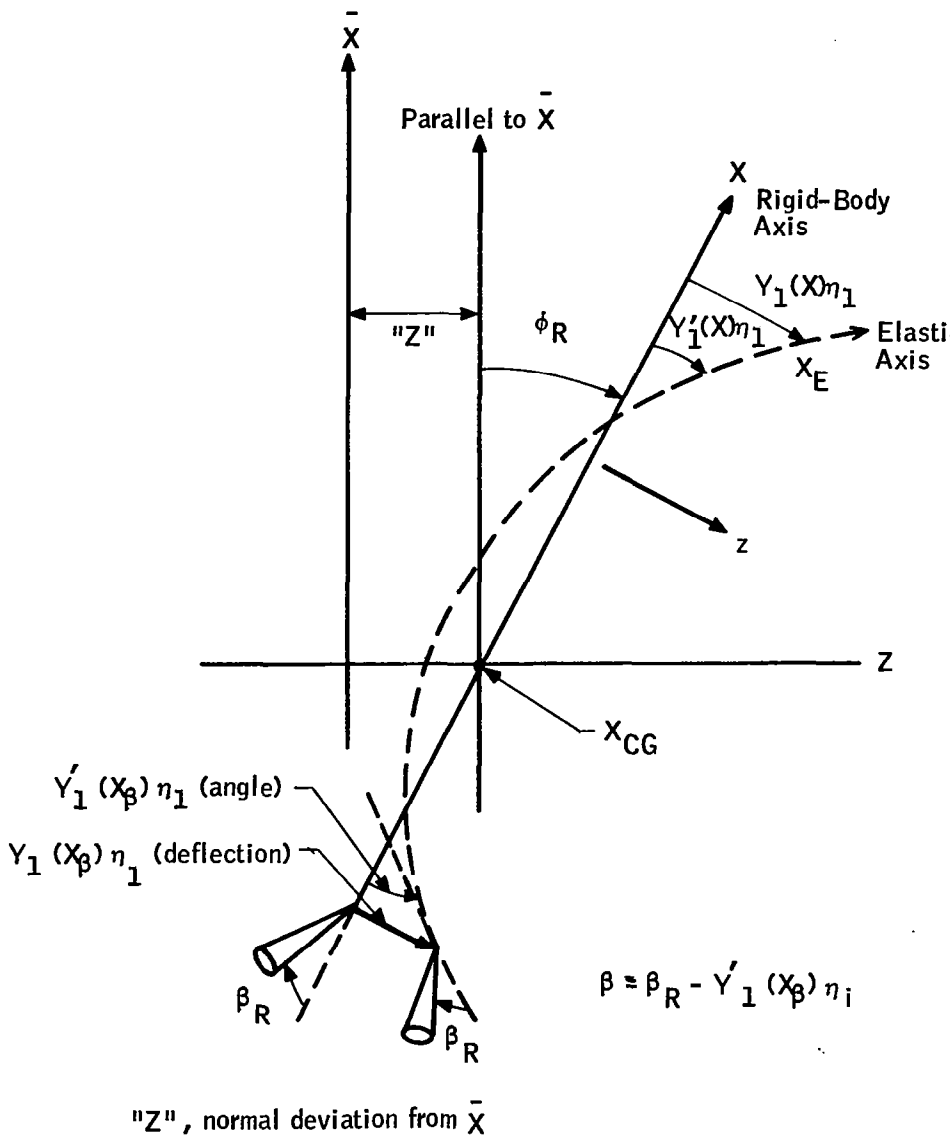

Figure B-A. First Bending Mode Geometry

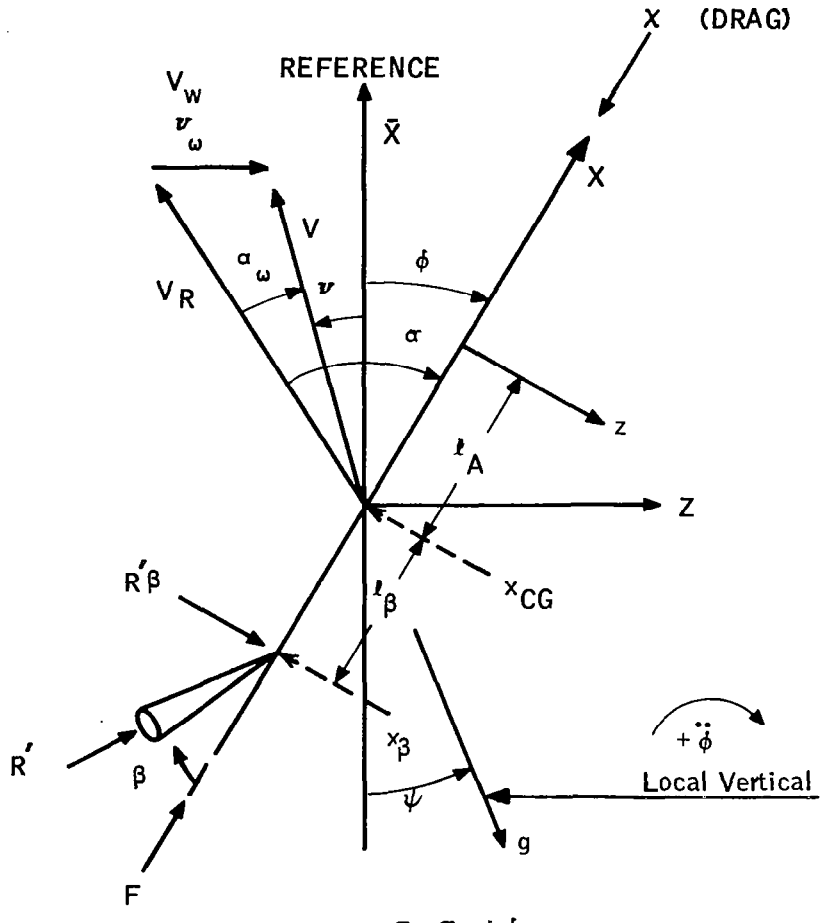

Figure B-B. Rigid Body Coordinate

Angle-of-Attack Meter Coordinate

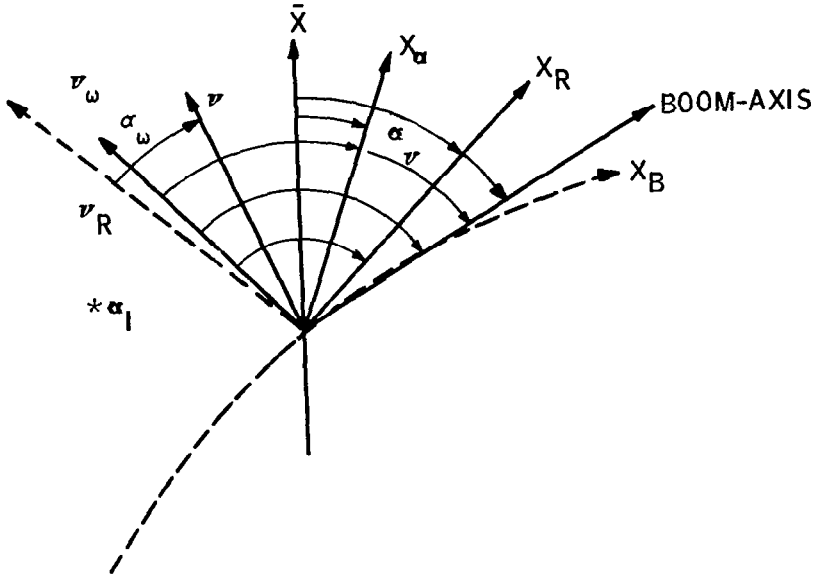

$$\phi_{\beta_{(X_\alpha)}} = -\Sigma Y_i' (X_\alpha)\, \eta_i$$

$$\alpha_I = \frac{\Sigma_i\, Y_i (X_\alpha)\, \eta_i + \ell_2 \dot{\phi}_a}{v}$$

* Induced wind angle due to bending and attitude motion.

Figure B-C. Angle-of-Attack Meter Coordinate

Table B-1. Vehicle Data for Flight Conditions Studied

Parameter	t = 8 sec	t = 64 sec	t = 80 sec	t = 157 sec	Units
h	0	7.5×10^3	$13. \times 10^3$	64×10^3	m
V	20.7	338.1	519.3	2520.5	m/sec
M	0.061	1.001	1.767	7.999	-
q	31	3205.	3841.	93.	kg/m^2
m	407813.8	297554.9	266051.2	116412.4	$\frac{kg\text{-}sec^2}{m}$
F	5234418.	5651545.	5819805.	6150420.	kg
$R' = 1/2\ F$	2617209.	2825772.	2909902.	3075210.	kg
x_{cg}	37.6	39.6	41.2	68.0	m
x_{cp}	47.3	39.2	53.3	62.3	m
x_β	2.54	2.54	2.54	2.54	m
I_{xx}	280×10^6	260×10^6	250×10^6	90×10^6	$kg\text{-}sec^2 m$
C_{D_0}	1.16	1.08	0.77	0.24	-
D	10	10	10	10	m
C_{z_α}	4.6	5.8	4.9	3.25	1/rad
$C_{P/D}$	4.7	3.9	5.3	6.2	calibers
$\ell_{cg} = x_{cg} - x_\beta$	35.06	37.06	38.66	65.46	m
qA	2433	252×10^3	302×10^3	7300	kg
$\ell_{cl} = x_{cg} - x_{cp}$	-9.7	+0.4	-12.1	+5.7	m
A	78.5	78.5	78.5	78.5	m^2
X	2320	2.72×10^5	2.33×10^5	1750	kg
N'	1.12×10^4	1.46×10^6	1.48×10^6	2.37×10^4	kg
C_1	-3.88×10^{-4}	$+22.4 \times 10^{-4}$	-7.16×10^{-2}	$+15.0 \times 10^{-4}$	$1/sec^2$
C_2	0.327	0.401	0.448	2.23	$1/sec^2$
$\left(\frac{F-X}{m}\right)$	12.87	18.10	21.0	52.8	m/sec^2
$\frac{R'}{m}$	6.41	9.50	10.9	26.5	m/sec^2
N'/m	0.0274	4.91	5.56	0.205	m/sec^2
R'/mV	0.310	0.0281	0.0211	0.0105	1/sec
N'/mV	0.00133	0.0145	0.0107	8.07×10^{-5}	1/sec
ω_1	2.17	2.28	2.31	2.92	rad/sec
ω_2	5.05	5.48	5.65	6.59	rad/sec
ω_3	8.8	8.94	9.16	11.7	
ω_4	12.3	12.4	12.5	24.9	rad/sec

Table B-1 (Cont'd)

$\frac{R'}{M_1} Y_1(x_\beta)$	13.7	15.9	17.0	172.	m/sec^2
$\frac{R'}{M_2} Y_2(x_\beta)$	16.7	23.6	25.2	105.	m/sec^2
$\frac{R'}{M_3} Y_3(x_\beta)$	15.7	23.2	29.6	18.	m/sec^2
$\Sigma \frac{\partial c_{z\alpha}}{\partial(x/D)} \Delta x_n Y_1(x_n)$		+2.033	+1.920		1/rad
$\Sigma \frac{\partial c_{z\alpha}}{\partial(x/D)} \Delta x_n Y_2(x_n)$		+1.193	+1.058		1/rad
$\Sigma \frac{\partial c_{z\alpha}}{\partial(x/D)} \Delta x_n Y_3(x_n)$		+2.778	+2.509		1/rad
$A_1 = qA\Sigma \frac{\partial c_{z\alpha}}{\partial(x/D)} \Delta x_n Y_1(x_n)$		5.12×10^5	5.80×10^5		kg/rad
$A_2 = qA\Sigma \frac{\partial c_{z\alpha}}{\partial(x/D)} \Delta x_n Y_2(x_n)$		3.01×10^5	3.19×10^5		kg/rad
$A_3 = qA\Sigma \frac{\partial c_{a\alpha}}{\partial(x/D)} \Delta x_n Y_3(x_n)$		7.9×10^5	7.57×10^5		kg/rad
$\frac{A_1}{M_1}$		2.89	3.40		$\frac{m}{sec^2} \frac{1}{rad}$
A_2/M_2		2.51	2.76		$\frac{m}{sec^2} \frac{1}{rad}$
A_3/M_3		5.76	7.73		$\frac{m}{sec^2} \frac{1}{rad}$
$\lvert\beta_{r_{max}}\rvert$	5	5	5	5	deg
$\dot{\beta}_{max}$	10	10	10	10	deg/sec

Table B-1 (Cont'd)

$\zeta_1, \zeta_2, \zeta_3, \zeta_4$	0.005	0.005	0.005	0.005	
M_{B_1}	190, 180.	177, 466.	170, 748.	17866.	$\frac{kg\text{-}sec^2}{m}$
M_{B_2}	156, 252.	119, 850.	115, 674.	29067.	$\frac{kg\text{-}sec^2}{m}$
M_{B_3}	165, 879.	121, 505.	98, 114.	169960.	$\frac{kg\text{-}sec^2}{m}$
M_{B_4}	423, 461.	676, 259.	565, 743.	203, 336.	$\frac{kg\text{-}sec^2}{m}$
Total Vehicle Length	144.86	144.86	144.86	144.86	m
$Y_1(x_\beta)$	1.0	1.0	1.0	1.0	-
$Y_2(x_\beta)$	1.0	1.0	1.0	1.0	-
$Y_3(x_\beta)$	1.0	1.0	1.0	1.0	-
$Y'_1(x_\beta)$	0.03472	0.03587	0.03563	0.0209	rad/m
$Y'_2(x_\beta)$	0.04399	0.04646	0.04727	0.03091	rad/m
$Y'_3(x_\beta)$	0.05192	0.05559	0.05660	0.04932	rad/m
$+\frac{F}{m} Y'_1(x_\beta)$	+0.425	+0.682	+0.779	+1.11	$1/sec^2$
$+\frac{F}{m} Y'_2(x_\beta)$	+0.540	+0.882	+1.03	+1.64	$1/sec^2$
$+\frac{F}{m} Y'_3(x_\beta)$	+0.637	+1.05	+1.24	+2.61	$1/sec^2$
$\frac{F \ell_{cg}}{I_{xx}} Y'_1(x_\beta) - \frac{F}{I_{xx}} Y_1(x_\beta)$	0.0039	0.0072	0.0110	0.0275	m/sec^2
$\frac{F \ell_{cg}}{I_{xx}} Y'_2(x_\beta) - \frac{F}{I_{xx}} Y_2(x_\beta)$	0.0100	0.0157	0.0211	0.0730	m/sec^2
$\frac{F \ell_{cg}}{I_{xx}} Y'_3(x_\beta) - \frac{F}{I_{xx}} Y_3(x_\beta)$	0.0151	0.0231	0.0298	0.155	m/sec^2

Table B-2. Bending Mode Frequency, Effective Mass and Damping Data

t (sec)	f_{B_1} (cps)	M_{B_1} (kg - sec^2/m)	f_{B_2} (cps)	M_{B_2} (kg - sec^2/m	f_{B_3} (cps)	M_{B_3} (kg - sec^2/m	f_{B_4} (cps)	M_{B_4} (kg - sec^2/m
0	0.3432	193188	0.8056	165516.2	1.3978	162154.5	1.9665	350110.7
10	0.3468	190179.6	0.8124	156252.3	1.3983	165879.3	1.9764	423460.6
20	0.3503	187663.4	0.8206	147492.4	1.3989	165517.7	1.9824	498270.4
30	0.3537	185474.8	0.8302	139430.6	1.4006	160882.0	1.9856	582366.3
40	0.3570	183447.2	0.8413	132266.6	1.4041	152473.5	1.9870	643847.6
50	0.3602	181332.2	0.8537	126158.6	1.4105	141015.6	1.9873	690353.0
60	0.3632	178807.2	0.8676	121270.6	1.4212	127235.5	1.9873	700359.1
70	0.3661	175455.7	0.8825	117722.5	1.4375	112894.8	1.9880	640126.6
80	0.3690	170748.1	0.8984	115674.3	1.4616	98114.7	1.9900	565743.8
90	0.3719	164030.3	0.9148	115194.1	1.4958	84381.6	1.9947	460784.2
100	0.3750	154477.3	0.9312	116055.5	1.5432	72794.8	2.0050	323332.1
110	0.3784	141217.7	0.9472	117700.5	1.6063	64581.8	2.0268	198745.3
120	0.3828	123324.7	0.9625	118416.8	1.6839	63649.8	2.0763	102021.2
130	0.3889	100064.3	0.9772	114087.9	1.7621	81053.7	2.1963	50113.5
140	0.3990	71417.6	0.9924	99897.4	1.8180	131216.5	2.4798	28619.2
150	0.4280	34467.2	1.0223	55256.9	1.8534	169695.1	3.2215	16001.4
157	0.4639	17866.5	1.0492	29067.6	1.8639	169960.9	3.9569	203335.9

$\zeta_{B_1} = 0.005$

$\zeta_{B_2} = 0.005 \qquad 0.0005 \leq \zeta_{B_i} \leq 0.025$

$\zeta_{B_3} = 0.005$

Subscripts

B_1 = 1st bending mode

B_2 = 2nd bending mode

B_3 = 3rd bending mode

B_4 = 4th bending mode

Table B-3. Bending Mode Shapes t = 8 sec

Location	Y_1	Y_1'	Y_2	Y_2'	Y_3	Y_3'	Y_4	Y_4'
-2.54 m	1.0	0.03472	1.0	0.04399	1.0	0.05192	1.0	0.06227
0	0.93051	0.03477	0.91173	0.04429	0.89073	0.05509	0.87366	0.06407
2	0.86092	0.03481	0.82290	0.04448	0.77883	0.05565	0.74412	0.06516
4	0.79122	0.03495	0.73350	0.04523	0.66734	0.05771	0.61158	0.06897
6	0.72105	0.03521	0.64171	0.04651	0.54838	0.06110	0.46728	0.07495
8	0.65041	0.03541	0.54769	0.04746	0.42376	0.06332	0.31358	0.07830
10	0.57944	0.03554	0.45218	0.04797	0.29607	0.06414	0.15614	0.07864
12	0.50830	0.03559	0.35611	0.04802	0.16822	0.06347	0.00115	0.07586
14	0.43715	0.03555	0.26045	0.04756	0.04323	0.06128	-0.14521	0.07003
16	0.36618	0.03540	0.16623	0.04657	-0.07582	0.05754	-0.27699	0.06133
18	0.29483	0.03614	0.07114	0.04934	-0.19279	0.06103	-0.39669	0.06010
20	0.22330	0.03537	-0.02399	0.04569	-0.30628	0.05226	-0.50347	0.04644
22	0.15345	0.03446	-0.11118	0.04139	-0.40088	0.04201	-0.58132	0.03080
24	0.08770	0.03245	-0.17975	0.03212	-0.45397	0.02081	-0.60239	0.00098
26	0.02332	0.03191	-0.24103	0.02910	-0.48693	0.01205	-0.58865	-0.01469
28	-0.03986	0.03126	-0.29589	0.02570	-0.50188	0.00286	-0.54399	-0.02982
30	-0.10167	0.03053	-0.34361	0.02197	-0.49826	-0.00648	-0.47032	-0.04359
32	-0.16190	0.02969	-0.38357	0.01796	-0.47609	-0.01565	-0.37107	-0.05529
34	-0.22037	0.02877	-0.41529	0.01373	-0.43598	-0.02436	-0.25102	-0.06431
36	-0.27692	0.02776	-0.43837	0.00934	-0.37914	-0.03235	-0.11598	-0.07021
38	-0.33136	0.02667	-0.45259	0.00487	-0.30727	-0.03935	0.02749	-0.07271
40	-0.38355	0.02551	-0.45784	0.00038	-0.22255	-0.04517	0.17247	-0.07172
42	-0.43336	0.02428	-0.45417	-0.00404	-0.12754	-0.04962	0.31204	-0.06734
44	-0.48065	0.02300	-0.44177	-0.00833	-0.02508	-0.05260	0.43970	-0.05987
46	-0.52537	0.02135	-0.41433	-0.01865	-0.10569	-0.07371	0.57304	-0.06833
48	-0.56559	0.01887	-0.37055	-0.02506	0.25506	-0.07536	0.70013	-0.05846

*All stations should be advanced 2.54 meters.

Table B-3 (Cont'd). Bending Mode Shapes t = 8 sec

Location	Y_1	Y_1'	Y_2	Y_2'	Y_3	Y_3'	Y_4	Y_4'
50	-0.60080	0.01627	-0.31479	-0.02748	0.40433	-0.06909	0.80405	-0.04079
52	-0.63124	0.01416	-0.25121	-0.03405	0.54101	-0.06734	0.87451	-0.02940
54	-0.65740	0.01200	-0.17882	-0.03828	0.67253	-0.06394	0.92036	-0.01618
56	-0.67889	0.00943	-0.09796	-0.04255	0.78961	-0.05186	0.92287	0.01613
58	-0.69508	0.00676	-0.00909	-0.04620	0.87801	-0.03626	0.85505	0.05139
60	-0.70594	0.00411	0.08634	-0.04911	0.93381	-0.01939	0.71961	0.08338
62	-0.71179	0.00181	0.18751	-0.05191	0.96248	-0.01045	0.53351	0.10009
64	-0.71324	-0.00035	0.29367	-0.05419	0.97626	-0.00335	0.32174	0.11133
66	-0.71044	-0.00245	0.40397	-0.05604	0.97599	0.00358	0.08975	0.12030
68	-0.70348	-0.00450	0.51757	-0.05749	0.96210	0.01027	-0.15788	0.12696
70	-0.69247	-0.00649	0.63366	-0.05854	0.93511	0.01667	-0.41652	0.13131
72	-0.67754	-0.00843	0.75145	-0.05919	0.89567	0.02271	-0.68154	0.13335
74	-0.65879	-0.01031	0.87015	-0.05945	0.84451	0.02838	-0.94837	0.13313
76	-0.63636	-0.01212	0.98897	-0.05934	0.78245	0.03361	-1.21255	0.13071
78	-0.60681	-0.01756	1.11928	-0.06823	0.69091	0.05617	-1.52925	0.17145
80	-0.56725	-0.02196	1.25431	-0.06670	0.56819	0.06630	-1.86036	0.15952
82	-0.51992	-0.02546	1.38111	-0.06029	0.43273	0.06959	-2.14251	0.12315
84	-0.46488	-0.02968	1.49590	-0.05440	0.28820	0.07506	-2.35507	0.08886
86	-0.40073	-0.03461	1.59804	-0.04745	0.13195	0.08133	-2.49430	0.04837
88	-0.32584	-0.04033	1.68320	-0.03762	-0.03808	0.08869	-2.52788	-0.01563
90	-0.23961	-0.04585	1.74792	-0.02701	-0.22105	0.09384	-2.43080	-0.08123
92	-0.14266	-0.05103	1.79169	-0.01732	-0.41202	0.09729	-2.21126	-0.13297
94	-0.03571	-0.05587	1.81788	-0.00888	-0.60851	0.09913	-1.90795	-0.16955
96	0.08062	-0.06041	1.82721	-0.00046	-0.80735	0.09944	-1.53668	-0.20087
98	0.20571	-0.06464	1.81977	0.00789	-1.0051	0.09804	-1.10831	-0.22661
100	0.33896	-0.06856	1.79574	0.01612	-1.19841	0.09502	-0.63423	-0.24655

Table B-3 (Cont'd). Bending Mode Shapes t = 8 sec

Location	Y_1	Y_1'	Y_2	Y_2'	Y_3	Y_3'	Y_4	Y_4'
102	0.47974	-0.07217	1.75540	0.02419	-1.38413	0.09046	-0.12622	-0.26052
104	0.62745	-0.07549	1.69912	0.03205	-1.55925	0.08445	0.40369	-0.26844
106	0.78237	-0.08207	1.62626	0.04407	-1.72346	0.08693	0.95708	-0.32508
108	0.95410	-0.08954	1.51795	0.06401	-1.87461	0.06404	1.59895	-0.31474
110	1.13999	-0.09623	1.37096	0.08284	-1.97808	0.03898	2.20616	-0.29011
112	1.33844	-0.10210	1.18720	0.10078	-2.02858	0.01110	2.74907	-0.25049
114	1.54764	-0.10671	0.96766	0.11953	-2.01575	-0.02990	3.18324	-0.16437
116	1.76455	-0.11036	0.70960	0.13746	-1.90451	-0.07571	3.38495	-0.05427
118	1.98908	-0.11408	0.42023	0.15163	-1.72251	-0.10592	3.42703	0.01202
120	2.22062	-0.11742	0.10385	0.16462	-1.48193	-0.13450	3.33742	0.07755
122	2.45882	-0.12087	-0.23871	0.17831	-1.18288	-0.16551	3.11088	0.15175
124	2.70495	-0.12546	-0.61273	0.19675	-0.81216	-0.20830	2.71077	0.25798
126	2.96020	-0.12960	-1.02558	0.21535	-0.34495	-0.25742	2.05303	0.39694
128	3.22250	-0.13253	-1.47094	0.22931	0.21072	-0.29666	1.13749	0.51488
130	3.48961	-0.13444	-1.93990	0.23902	0.83467	-0.32570	0.01130	0.60702
132	3.75978	-0.13571	-2.42475	0.24565	1.50719	-0.34595	-1.2719	0.67263
134	4.03209	-0.13652	-2.92065	0.24982	2.21314	-0.35880	-2.6627	0.71452
136	4.30549	-0.13681	-3.42235	0.25153	2.93744	-0.36447	-4.11461	0.73413
138	4.57904	-0.13665	-3.92527	0.25096	3.66657	-0.36335	-5.58489	0.73201
140	4.85209	-0.13643	-4.42601	0.24995	4.39006	-0.36060	-7.03953	0.72392
142	5.12473	-0.13619	-4.92478	0.24870	5.10789	-0.35682	-8.47666	0.71176

Table B-3 (Cont'd). Bending Mode Shapes t = 60 sec

Location	Y_1	Y_1'	Y_2	Y_2'	Y_3	Y_3'	Y_4	Y_4'
-2.54 m	1.0	0.03587	1.0	0.04646	1.0	0.05559	1.0	0.06335
0	0.92820	0.03593	0.90674	0.04681	0.88791	0.05651	0.87147	0.06518
2	0.85629	0.03597	0.81285	0.04703	0.77415	0.05709	0.73968	0.06629
4	0.78425	0.03613	0.71829	0.04788	0.65876	0.05919	0.60484	0.07015
6	0.71169	0.03642	0.62103	0.04933	0.53677	0.06263	0.45813	0.07617
8	0.63862	0.03664	0.52126	0.05037	0.40909	0.06485	0.30200	0.07949
10	0.56518	0.03678	0.41988	0.05091	0.27838	0.06562	0.14228	0.07972
12	0.49156	0.03682	0.31799	0.05087	0.14768	0.06480	-0.01470	0.07678
14	0.41812	0.03660	0.21730	0.04973	0.02071	0.06201	-0.16344	0.07177
16	0.34522	0.03629	0.11934	0.04818	-0.09980	0.05837	-0.30093	0.06552
18	0.27235	0.03674	0.02170	0.05022	-0.21910	0.06256	-0.43542	0.07146
20	0.19962	0.03597	-0.07503	0.04642	-0.33566	0.05379	-0.56397	0.05677
22	0.12854	0.03509	-0.16356	0.04199	-0.43332	0.04352	-0.66093	0.03945
24	0.06106	0.03336	-0.23403	0.03303	-0.48891	0.02189	-0.68688	0.00154
26	-0.00516	0.03284	-0.29691	0.02980	-0.52368	0.01279	-0.67181	-0.01662
28	-0.07025	0.03224	-0.35299	0.02622	-0.53976	0.00326	-0.62072	-0.03432
30	-0.13405	0.03155	-0.40159	0.02234	-0.53664	-0.00637	-0.53552	-0.05061
32	-0.19638	0.03077	-0.44219	0.01823	-0.51445	-0.01576	-0.41986	-0.06464
34	-0.25708	0.02992	-0.47442	0.01398	-0.47397	-0.02461	-0.27902	-0.07570
36	-0.31599	0.02899	-0.49806	0.00966	-0.41659	-0.03261	-0.11951	-0.08324
38	-0.37308	0.02811	-0.51388	0.00635	-0.34596	-0.03753	0.05090	-0.08672
40	-0.42843	0.02723	-0.52362	0.00340	-0.26716	-0.04115	0.22607	-0.08819
42	-0.48198	0.02631	-0.52755	0.00054	-0.18185	-0.04405	0.40249	-0.08796
44	-0.53364	0.02535	-0.52584	-0.00224	-0.09147	-0.04622	0.57673	-0.08602

Table B-3 (Cont'd). Bending Mode Shapes t = 60 sec

Location	Y_1	Y_1'	Y_2	Y_2'	Y_3	Y_3'	Y_4	Y_4'
46	-0.58390	0.02444	-0.51496	-0.00881	0.02254	-0.06410	0.78867	-0.11557
48	-0.63057	0.02221	-0.49172	-0.01440	0.15254	-0.06565	1.00886	-0.10407
50	-0.67263	0.01968	-0.45769	-0.01902	0.28279	-0.06054	1.19947	-0.07746
52	-0.71002	0.01770	-0.41533	-0.02331	0.40273	-0.05920	1.33922	-0.06179
54	-0.74337	0.01564	-0.36453	-0.02746	0.51863	-0.05648	1.44417	-0.04267
56	-0.77211	0.01303	-0.30452	-0.03264	0.62284	-0.04668	1.48300	0.00804
58	-0.79540	0.01026	-0.23425	-0.03754	0.70362	-0.03384	1.40985	0.06483
60	-0.81316	0.00749	-0.15484	-0.04177	0.75740	-0.01980	1.22659	0.11752
62	-0.82575	0.00519	-0.06767	-0.04515	0.78860	-0.01236	0.96041	0.14430
64	-0.83393	0.00301	0.02542	-0.04787	0.80737	-0.00642	0.65327	0.16232
66	-0.83783	0.00089	0.12355	-0.05020	0.81436	-0.00060	0.31345	0.17697
68	-0.83751	-0.00119	0.22594	-0.05213	0.80987	0.00506	-0.05224	0.18817
70	-0.83309	-0.00323	0.33179	-0.05366	0.79428	0.01049	-0.43684	0.19588
72	-0.82464	-0.00521	0.44033	-0.05481	0.76809	0.01566	-0.83338	0.20011
74	-0.81228	-0.00714	0.55076	-0.05557	0.73185	0.02053	-1.23493	0.20090
76	-0.79611	-0.00902	0.66234	-0.05595	0.68621	0.02506	-1.63466	0.19832
78	-0.77288	-0.01442	0.78680	-0.06594	0.61598	0.04387	-2.11829	0.26332
80	-0.73945	-0.01899	0.91841	-0.06556	0.51919	0.05272	-2.62962	0.24728
82	-0.69780	-0.02275	1.04399	-0.06024	0.41080	0.05603	-3.06905	0.19348
84	-0.64792	-0.02723	1.15988	-0.05558	0.29370	0.06119	-3.40650	0.14316
86	-0.58836	-0.03248	1.26579	-0.05007	0.16555	0.06711	-3.63630	0.08367
88	-0.51730	-0.03861	1.35799	-0.04203	0.02421	0.07424	-3.71041	-0.01085
90	-0.43408	-0.04456	1.43328	-0.03314	-0.12991	0.07950	-3.59110	-0.10822
92	-0.33933	-0.05012	1.49091	-0.02500	-0.29248	0.08299	-3.28971	-0.18514

Table B-3 (Cont'd). Bending Mode Shapes t = 60 sec

Location	Y_1	Y_1'	Y_2	Y_2'	Y_3	Y_3'	Y_4	Y_4'
94	-0.23386	-0.05530	1.53386	-0.01794	-0.46100	0.08529	-2.86394	-0.23948
96	-0.11834	-0.06016	1.56260	-0.01079	-0.63258	0.08605	-2.33703	-0.28620
98	0.00657	-0.06470	1.57699	-0.00360	-0.80418	0.08532	-1.72471	-0.32482
100	0.14024	-0.06892	1.57700	0.00358	-0.97285	0.08313	-1.04356	-0.35499
102	0.28203	-0.07282	1.56270	0.01071	-1.13576	0.07957	-0.31075	-0.37644
104	0.43129	-0.07639	1.53424	0.01774	-1.29023	0.07471	0.45611	-0.38903
106	0.58833	-0.08345	1.49104	0.02787	-1.43602	0.07765	1.25945	-0.47346
108	0.76345	-0.09155	1.41690	0.04608	-1.57237	0.05853	2.19675	-0.46078
110	0.95393	-0.09880	1.30728	0.06345	-1.66870	0.03740	3.08796	-0.42694
112	1.15808	-0.10521	1.16355	0.08018	-1.72021	0.01372	3.88932	-0.37100
114	1.37396	-0.11029	0.98604	0.09830	-1.71762	-0.02157	4.53561	-0.24715
116	1.59846	-0.11436	0.77057	0.11594	-1.62994	-0.06118	4.84607	-0.08792
118	1.83138	-0.11846	0.52480	0.12957	-1.48127	-0.08718	4.92607	-0.00773
120	2.07200	-0.12213	0.25302	0.14209	-1.28214	-0.11181	4.81579	0.10250
122	2.31997	-0.12593	-0.04402	0.15532	-1.03260	-0.13856	4.50730	0.21002
124	2.57666	-0.13099	-0.37149	0.17318	-0.72120	-0.17553	3.94713	0.36423
126	2.84344	-0.13557	-0.73681	0.19143	-0.32626	-0.21814	3.01188	0.56699
128	3.11804	-0.13883	-1.13415	0.20523	0.14551	-0.25226	1.70004	0.73947
130	3.39798	-0.14096	-1.55488	0.21489	0.67669	-0.27755	0.07981	0.87451
132	3.68134	-0.14238	-1.99146	0.22149	1.2502	-0.29520	-1.77063	0.97073
134	3.96710	-0.14328	-2.43903	0.22566	1.85286	-0.30641	-3.77888	1.03219
136	4.25407	-0.14361	-2.89243	0.22738	2.47153	-0.31136	-5.87687	1.06100
138	4.54121	-0.14344	-3.34708	0.22684	3.09443	-0.31040	-8.00192	1.05797
140	4.82780	-0.14319	-3.79960	0.22584	3.71244	-0.30801	-10.10414	1.04614
142	5.11394	-0.14292	-4.25016	0.22460	4.32554	-0.30472	-12.18073	1.02832

Table B-3 (Cont'd). Bending Mode Shapes t = 80 sec

Location	Y_1	Y_1'	Y_2	Y_2'	Y_3	Y_3'	Y_4	Y_4'
-2.54 m	1.0	0.03563	1.0	0.04727	1.0	0.05660	1.0	0.06362
0	0.92869	0.03569	0.90509	0.04764	0.88583	0.05758	0.87095	0.06544
2	0.85725	0.03573	0.80950	0.04788	0.76990	0.05818	0.73864	0.06654
4	0.78569	0.03590	0.71321	0.04878	0.65226	0.06038	0.60333	0.07037
6	0.71359	0.03619	0.61403	0.05033	0.52773	0.06397	0.45623	0.07634
8	0.64096	0.03642	0.51220	0.051428	0.39729	0.06625	0.29982	0.07961
10	0.56795	0.03657	0.40870	0.05197	0.26381	0.06695	0.13990	0.07977
12	0.49493	0.03643	0.30541	0.05118	0.13163	0.06498	-0.01645	0.07625
14	0.42230	0.03619	0.20423	0.04995	0.00446	0.06207	-0.16423	0.07133
16	0.35020	0.03590	0.10583	0.04839	-0.11612	0.05840	-0.30095	0.06519
18	0.27818	0.03626	0.00796	0.05016	-0.23514	0.06215	-0.43455	0.07078
20	0.20636	0.03554	-0.08870	0.04641	-0.35094	0.05346	-0.56208	0.05644
22	0.13608	0.03472	-0.17730	0.04208	-0.44804	0.04330	-0.64878	0.03952
24	0.06905	0.03317	-0.24862	0.03349	-0.50418	0.02215	-0.68654	0.00267
26	0.00317	0.03270	-0.31244	0.03026	-0.53929	0.01288	-0.67400	-0.01522
28	-0.06168	0.03214	-0.36944	0.02669	-0.55543	0.00324	-0.62599	-0.03265
30	-0.12534	0.03150	-0.41899	0.02283	-0.55221	-0.00643	-0.54436	-0.04869
32	-0.18764	0.03079	-0.46063	0.01878	-0.52993	-0.01577	-0.43279	-0.06248
34	-0.24844	0.03002	-0.49416	0.01495	-0.48992	-0.02353	-0.29691	-0.07223
36	-0.30776	0.02929	-0.52120	0.01210	-0.43829	-0.02800	-0.14774	-0.07670
38	-0.36556	0.02851	-0.54258	0.00929	-0.37832	-0.37832	-0.00882	-0.07962
40	-0.42176	0.02768	-0.55838	0.00652	-0.31121	-0.03513	0.16969	-0.08101
42	-0.47627	0.02682	-0.56867	0.00379	-0.23820	-0.03779	0.33177	-0.08084
44	-0.52900	0.02591	-0.57356	0.00111	-0.16048	-0.03983	0.49199	-0.07914

Table B-3 (Cont'd). Bending Mode Shapes t = 80 sec

Location	Y_1	Y_1'	Y_2	Y_2'	Y_3	Y_3'	Y_4	Y_4'
46	-0.58057	0.02518	-0.57065	-0.00443	-0.06234	-0.05526	0.68639	-0.10592
48	-0.62880	0.02303	-0.55620	-0.01001	0.05015	-0.05702	0.88844	-0.09562
50	-0.67258	0.02055	-0.53078	-0.01504	0.16377	-0.05317	1.06395	-0.07167
52	-0.71176	0.01863	-0.49622	-0.01950	0.26953	-0.05242	1.19367	-0.05759
54	-0.74704	0.01662	-0.45282	-0.02389	0.37264	-0.05051	1.29210	-0.04040
56	-0.77778	0.01403	-0.39924	-0.02985	0.46701	-0.04300	1.33109	0.00517
58	-0.80310	0.01128	-0.33364	-0.03566	0.54309	-0.03284	1.26940	0.05629
60	-0.82290	0.00852	-0.25705	-0.04082	0.59754	-0.02146	1.10849	0.10381
62	-0.83757	0.00623	-0.17121	-0.04471	0.63371	-0.01549	0.87274	0.12800
64	-0.84787	0.00409	-0.07861	-0.04783	0.65986	-0.01067	0.59997	0.14430
66	-0.85393	0.00198	0.01983	-0.05054	0.67642	-0.00590	0.29760	0.15759
68	-0.85583	-0.00008	0.12327	-0.05283	0.68350	-0.00120	-0.02828	0.16779
70	-0.85363	-0.00210	0.23087	-0.05471	0.68132	0.00336	-0.37143	0.17487
72	-0.84744	-0.00408	0.34181	-0.05617	0.67018	0.00775	-0.72561	0.17882
74	-0.83736	-0.00600	0.45525	-0.05721	0.64045	0.01194	-1.08458	0.17968
76	-0.82348	-0.00787	0.57039	-0.05786	0.62257	0.01590	-1.44224	0.17752
78	-0.80264	-0.01319	0.70000	-0.06906	0.57488	0.03104	-1.87573	0.23626
80	-0.77166	-0.01776	0.83839	-0.06921	0.50475	0.03892	-2.33486	0.22220
82	-0.73244	-0.02155	0.97139	-0.06402	0.42347	0.04265	-2.73004	0.17419
84	-0.68494	-0.02606	1.09510	-0.05962	0.33302	0.04791	-3.03430	0.12935
86	-0.62770	-0.03133	1.20939	-0.05441	0.23130	0.05398	-3.24263	0.07633
88	-0.55890	-0.03751	1.31055	-0.04666	0.11574	0.06161	-3.31212	-0.00799
90	-0.47783	-0.04351	1.39530	-0.03796	-0.01385	0.06767	-3.20899	-0.09493
92	-0.38513	-0.04911	1.46270	-0.02997	-0.15363	0.07192	-2.94327	-0.16361

Table B-3 (Cont'd). Bending Mode Shapes t = 80 sec

Location	Y_1	Y_1'	Y_2	Y_2'	Y_3	Y_3'	Y_4	Y_4'
94	-0.28164	-0.05433	1.51575	-0.02306	-0.30064	0.07486	-2.56652	-0.21212
96	-0.16803	0.05923	1.55482	-0.01599	-0.45211	0.07638	-2.09945	-0.25385
98	-0.04495	-0.06380	1.57966	-0.00884	-0.60522	0.07651	-1.55606	-0.28839
100	0.08697	-0.06806	1.59013	-0.00163	-0.75723	0.07529	-0.95108	-0.31539
102	0.22707	-0.07199	1.58619	0.00557	-0.90550	0.07278	-0.29982	-0.33464
104	0.37471	-0.07560	1.56788	0.01272	-1.04751	0.06905	0.38205	-0.34600
106	0.53020	-0.08271	1.53464	0.02269	-1.18311	0.07299	1.09672	-0.42140
108	0.73093	-0.09089	1.47034	0.04143	-1.31345	0.05716	1.93131	-0.41047
110	0.89320	-0.09823	1.36944	0.05939	-1.41034	0.03933	2.72556	-0.38067
112	1.09628	-0.10472	1.23315	0.07681	-1.46905	0.01901	3.44045	-0.33117
114	1.31126	-0.10988	1.06147	0.09601	-1.48083	-0.01204	4.01787	-0.22122
116	1.53502	-0.11403	0.84921	0.11487	-1.41705	-0.04725	4.29693	-0.07974
118	1.76733	-0.11818	0.60480	0.12927	-1.29939	-0.07015	4.37131	0.00520
120	2.00746	-0.12191	0.33288	0.14253	-1.13723	-0.09189	4.27669	0.08937
122	2.25505	-0.12577	0.03420	0.15654	-0.93050	-0.11559	4.00599	0.18490
124	2.51150	-0.13091	-0.29672	0.17549	-0.66896	-0.14838	3.51170	0.32192
126	2.77820	-0.13557	-0.66796	0.19499	-0.33290	-0.18655	2.68403	0.50219
128	3.05285	-0.13888	-1.07344	0.20977	0.07211	-0.21725	1.52149	0.65557
130	3.33294	-0.14106	-1.50403	0.22016	0.53069	-0.24010	0.08470	0.77567
132	3.61652	-0.14251	-1.95169	0.22728	1.02756	-0.25607	-1.55685	0.86125
134	3.90255	-0.14342	-2.41118	0.23177	1.55078	-0.26621	-3.33877	0.81591
136	4.18980	-0.14376	-2.87695	0.23363	2.08852	-0.27072	-5.20052	0.94156
138	4.47723	-0.14358	-3.34409	0.23305	2.63014	-0.26988	-7.08634	0.93886
140	4.76411	-0.14333	-3.80895	0.23199	3.16740	-0.26773	-8.95187	0.92835
142	5.05052	-0.14306	-4.27173	0.23065	3.70022	-0.26476	-10.79460	0.91249

Table B-3 (Cont'd). Bending Mode Shapes t = 157 sec

Location	Y_1	Y'_1	Y_2	Y'_2	Y_3	Y'_3	Y_4	Y'_4
-2.54 m	1.0	0.02090	1.0	0.03091	1.0	0.04932	1.0	0.10303
0	0.95810	0.02100	0.93768	0.03143	0.89977	0.05093	0.78675	0.11012
2	0.91601	0.02107	0.87438	0.03178	0.79662	0.05195	0.56162	0.11380
4	0.87386	0.02108	0.81076	0.03183	0.69260	0.05204	0.33419	0.11342
6	0.83169	0.02108	0.74710	0.03181	0.58863	0.05189	0.10887	0.11169
8	0.78954	0.02107	0.68356	0.03172	0.48521	0.05149	0.11163	0.10859
10	0.74744	0.02103	0.62031	0.03150	0.38292	0.05074	-0.32470	0.10436
12	0.70544	0.02097	0.55760	0.03118	0.28246	0.04968	-0.52844	0.09922
14	0.66358	0.02089	0.49563	0.03078	0.18436	0.04836	-0.72095	0.09314
16	0.62190	0.02079	0.43455	0.03029	0.08911	0.04683	-0.90040	0.08617
18	0.58028	0.02087	0.37381	0.03061	-0.00474	0.04742	-1.06985	0.08389
20	0.53877	0.02064	0.31370	0.02948	-0.09620	0.04397	-1.22398	0.07005
22	0.49774	0.02039	0.25600	0.02820	-0.18034	0.04011	-1.34929	0.05503
24	0.45766	0.01993	0.20293	0.02601	-0.25154	0.03409	-1.43712	0.03908
26	0.41795	0.01978	0.15162	0.02528	-0.31758	0.03192	-1.50749	0.03123
28	0.37854	0.01962	0.10185	0.02448	-0.37910	0.02958	-1.56187	0.02310
30	0.33948	0.01944	0.05374	0.02361	-0.43576	0.02705	-1.59974	0.01475
32	0.30078	0.01925	0.00745	0.02267	-0.48719	0.02436	-1.62077	0.00626
34	0.26249	0.01904	-0.03688	0.02166	-0.53306	0.02149	-1.62476	-0.00228
36	0.22463	0.01882	-0.07912	0.02057	-0.57304	0.01846	-1.61169	-0.01079
38	0.18723	0.01858	-0.11913	0.01942	-0.60681	0.01528	-1.58168	-0.01919
40	0.15034	0.01832	-0.15676	0.01820	-0.63407	0.01196	-1.53513	-0.02733
42	0.11396	0.01805	-0.19187	0.01690	-0.65453	0.00849	-1.47253	-0.03523
44	0.07815	0.01776	-0.22433	0.01554	-0.66793	0.00489	-1.39445	-0.04280

Table B-3 (Cont'd). Bending Mode Shapes t = 157 sec

Location	Y_1	Y_1'	Y_2	Y_2'	Y_3	Y_3'	Y_4	Y_4'
46	0.04266	0.01757	-0.25511	0.01450	-0.67565	0.00118	-1.28929	-0.06224
48	0.00820	0.01688	-0.28092	0.01128	-0.65974	-0.00712	-1.15026	-0.07663
50	-0.02482	0.01606	-0.30002	0.00752	-0.64677	-0.01635	-0.98400	-0.08690
52	-0.05631	0.01543	-0.31216	0.00460	-0.60679	-0.02368	-0.79970	-0.09733
54	-0.08651	0.01477	-0.31833	0.00155	-0.55178	-0.03136	-0.59471	-0.10748
56	-0.11527	0.01397	-0.31678	-0.00334	-0.47353	-0.04786	-0.33768	-0.15142
58	-0.14235	0.01309	-0.30491	-0.00851	-0.36145	-0.06374	-0.00838	-0.17231
60	-0.16762	0.01218	-0.28291	-0.01344	-0.22105	-0.07605	0.32648	-0.15699
62	-0.19117	0.01139	-0.25236	-0.01681	-0.06123	-0.08269	0.62850	-0.14658
64	-0.21320	0.01064	-0.21597	-0.01955	0.10838	-0.08669	0.91093	-0.13515
66	-0.23372	0.00988	-0.17436	-0.02203	0.28455	-0.08925	1.16617	-0.11945
68	-0.25273	0.00913	-0.12804	-0.02425	0.46438	-0.09035	1.38620	-0.10006
70	-0.27023	0.00838	-0.07754	-0.02620	0.64501	-0.09006	1.56447	-0.07787
72	-0.28624	0.00763	-0.02341	-0.02788	0.82368	-0.08840	1.69625	-0.05354
74	-0.30075	0.00689	0.03381	-0.02929	0.99772	-0.08544	1.77815	-0.02818
76	-0.31379	0.00615	0.09356	-0.03042	1.16460	-0.08125	1.80850	-0.00224
78	-0.32451	0.00438	0.16521	-0.03959	1.35141	-0.09689	1.73897	0.07291
80	-0.33143	0.00255	0.24622	-0.04131	1.53273	-0.08426	1.55266	0.11177
82	-0.33486	0.00085	0.32664	-0.03930	1.67567	-0.05902	1.31181	0.13062
84	-0.33463	-0.00112	0.40397	-0.03803	1.76924	-0.03412	1.02646	0.15483
86	-0.33017	-0.00341	0.47861	-0.03650	1.80955	-0.00483	0.69163	0.18123
88	-0.32061	-0.00617	0.54891	-0.03376	1.77486	0.04004	0.28505	0.22417
90	-0.30555	-0.00888	0.61305	-0.03026	1.64964	0.08483	-0.18733	0.24372
92	-0.28522	-0.01140	0.66998	-0.02696	1.44148	0.11995	-0.67512	0.24446

Table B-3 (Cont'd). Bending Mode Shapes t = 157 sec

Location	Y_1	Y_1'	Y_2	Y_2'	Y_3	Y_3'	Y_4	Y_4'
94	-0.26008	-0.01372	0.72111	-0.02412	1.17593	0.14497	-1.16119	0.23999
96	-0.23043	-0.01592	0.76629	-0.02102	0.86442	0.16589	-1.62815	0.22545
98	-0.19651	-0.01798	0.80501	-0.01767	0.51531	0.18254	-2.0567	0.20177
100	-0.15859	-0.01992	0.83682	-0.01411	0.13728	0.19480	-2.42979	0.17018
102	-0.11693	-0.02172	0.86135	-0.01039	-0.26084	0.20262	-2.73304	0.13221
104	-0.07180	-0.02339	0.87828	-0.00653	-0.67015	0.20599	-2.95548	0.08965
106	-0.02306	-0.02657	0.88733	-0.00232	-1.09156	0.24404	-3.08855	0.03932
108	0.03398	-0.03041	0.88103	0.00855	-1.56725	0.23028	-3.04568	-0.07765
110	0.09833	-0.03388	0.85322	0.01928	-2.00580	0.20657	-2.78684	-0.18053
112	0.16926	-0.03698	0.80389	0.03006	-2.38621	0.17219	-2.32724	-0.27808
114	0.24596	-0.03958	0.73195	0.04304	-2.67609	0.10309	-1.64366	-0.44312
116	0.32727	-0.04175	0.63132	0.05636	-2.78319	0.01691	-0.57074	-0.59148
118	0.41289	-0.04382	0.50880	0.06600	-2.76438	-0.03549	0.64991	-0.62230
120	0.50240	-0.04567	0.36778	0.07494	-2.64198	-0.08681	1.89667	-0.62053
122	0.59563	-0.04760	0.20865	0.08446	-2.41283	-0.14440	3.10335	-0.57681
124	0.69329	-0.05018	0.02758	0.09741	-2.04934	-0.22620	4.16101	-0.44971
126	0.79614	-0.05256	-0.18151	0.11119	-1.49018	-0.33065	4.72448	-0.10309
128	0.90308	-0.05428	-0.41499	0.12181	-0.73832	-0.41831	4.54584	0.28345
130	1.01285	-0.05542	-0.66665	0.12939	0.16941	-0.48616	3.60289	0.65240
132	1.12447	-0.05618	-0.93084	0.13462	1.19234	-0.53428	1.99085	0.93754
134	1.23736	-0.05666	-1.20371	0.13792	2.29430	-0.56497	-0.08568	1.12589
136	1.35090	-0.05684	-1.48122	0.13932	3.44087	-0.57919	-2.45320	1.22801
138	1.46455	-0.05676	-1.75983	0.13894	4.60056	-0.57745	-4.93591	1.23725
140	1.57791	-0.05663	-2.03683	0.13819	5.74856	-0.57142	-7.38051	1.21093
142	1.69104	-0.05648	-2.31232	0.13721	6.88342	-0.56249	-9.75634	1.15772

POSSIBLE SENSOR LOCATIONS

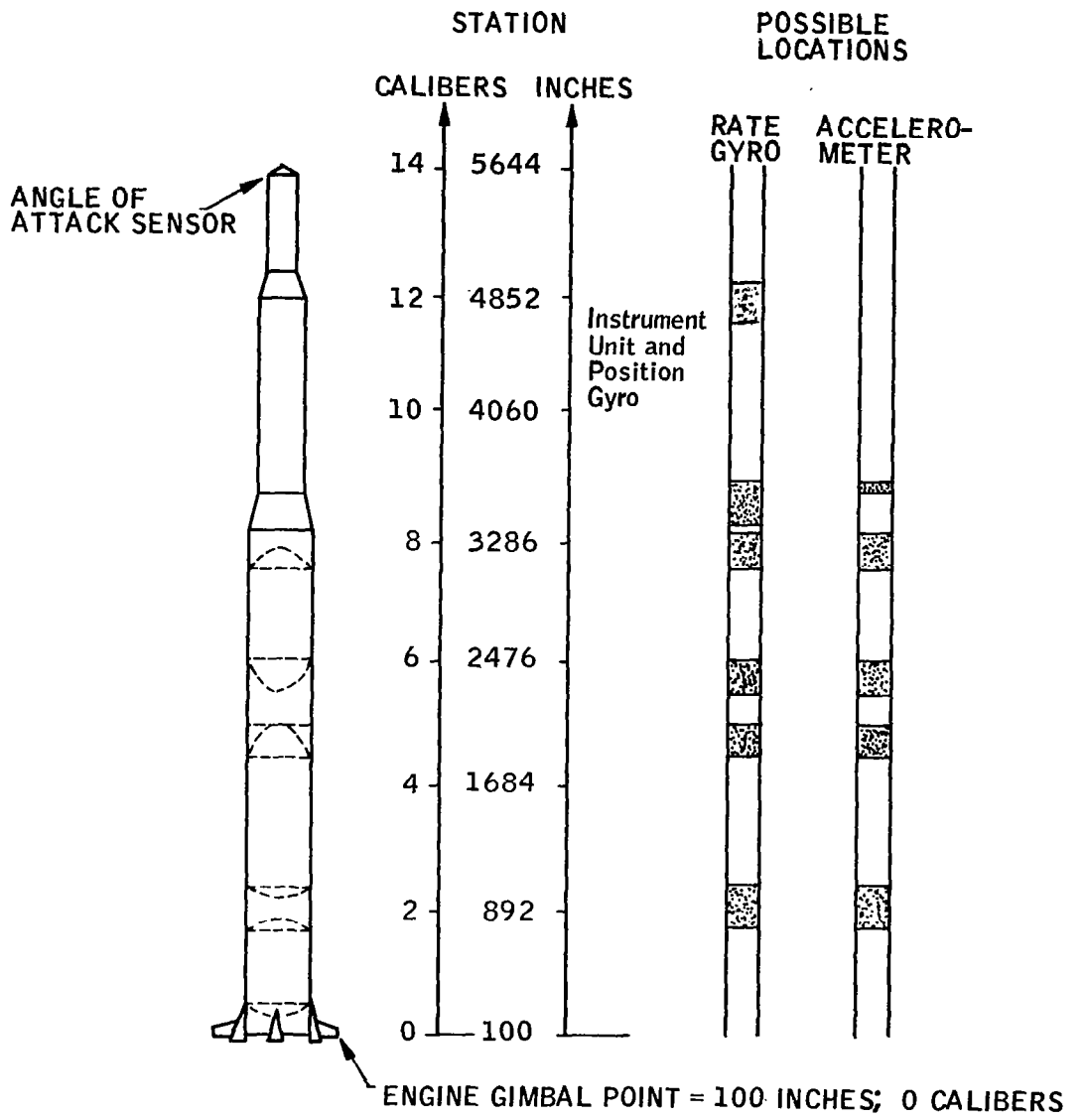

Figure B-D Possible Sensor Locations

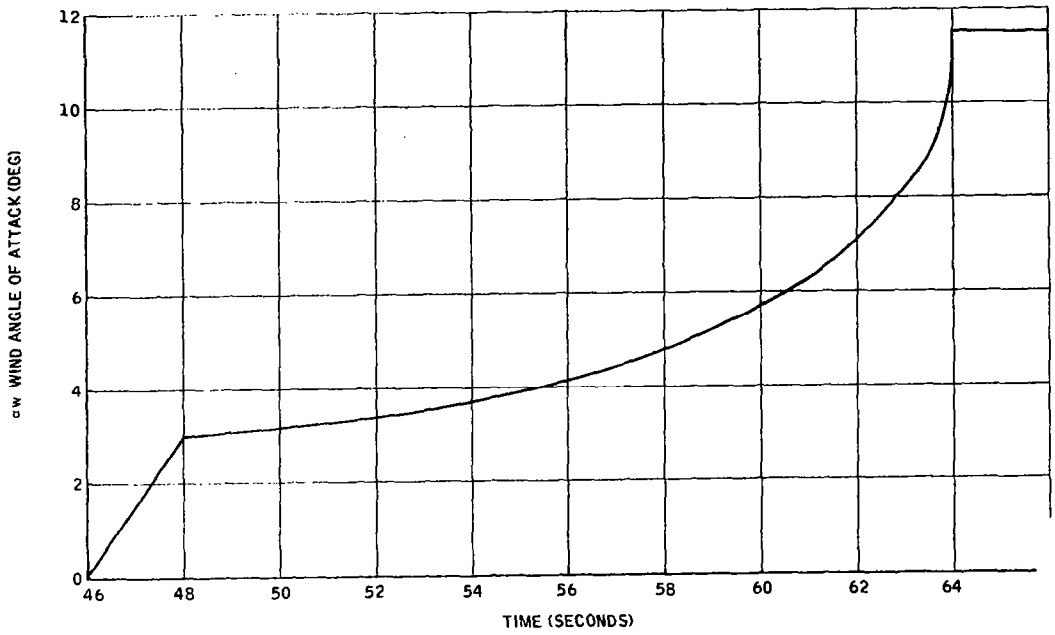

Figure B-E. Wind Model for t = 64 Seconds Condition

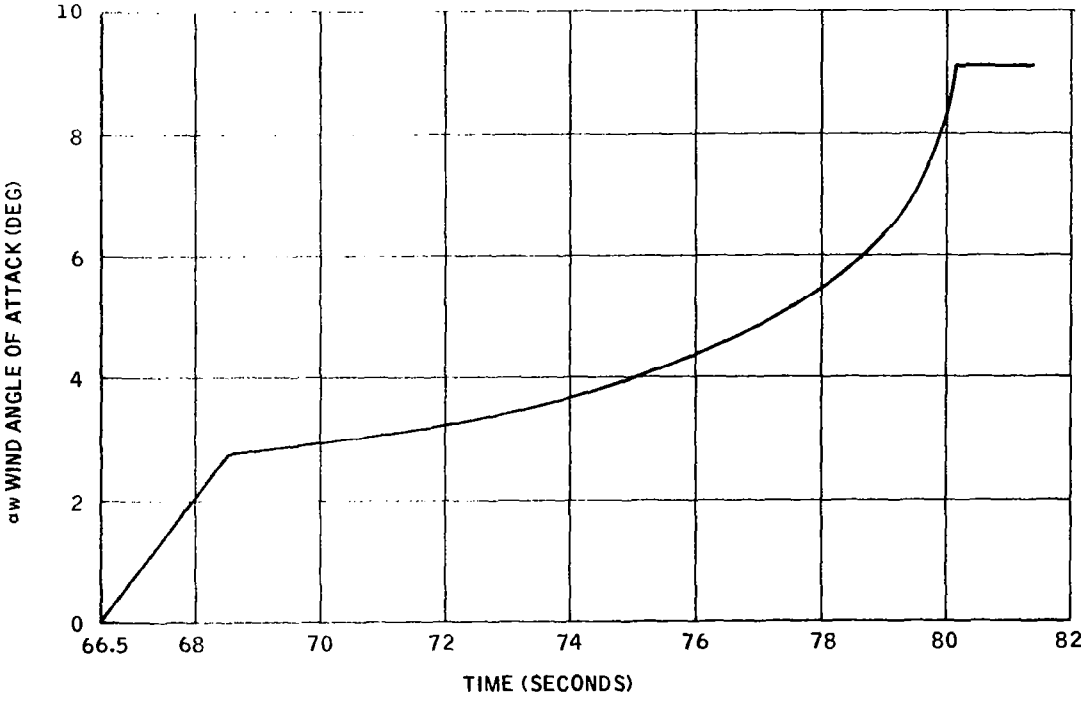

Figure B-F. Wind Model for t = 80 Seconds Condition

APPENDIX C
ANALOG COMPUTER TRACES

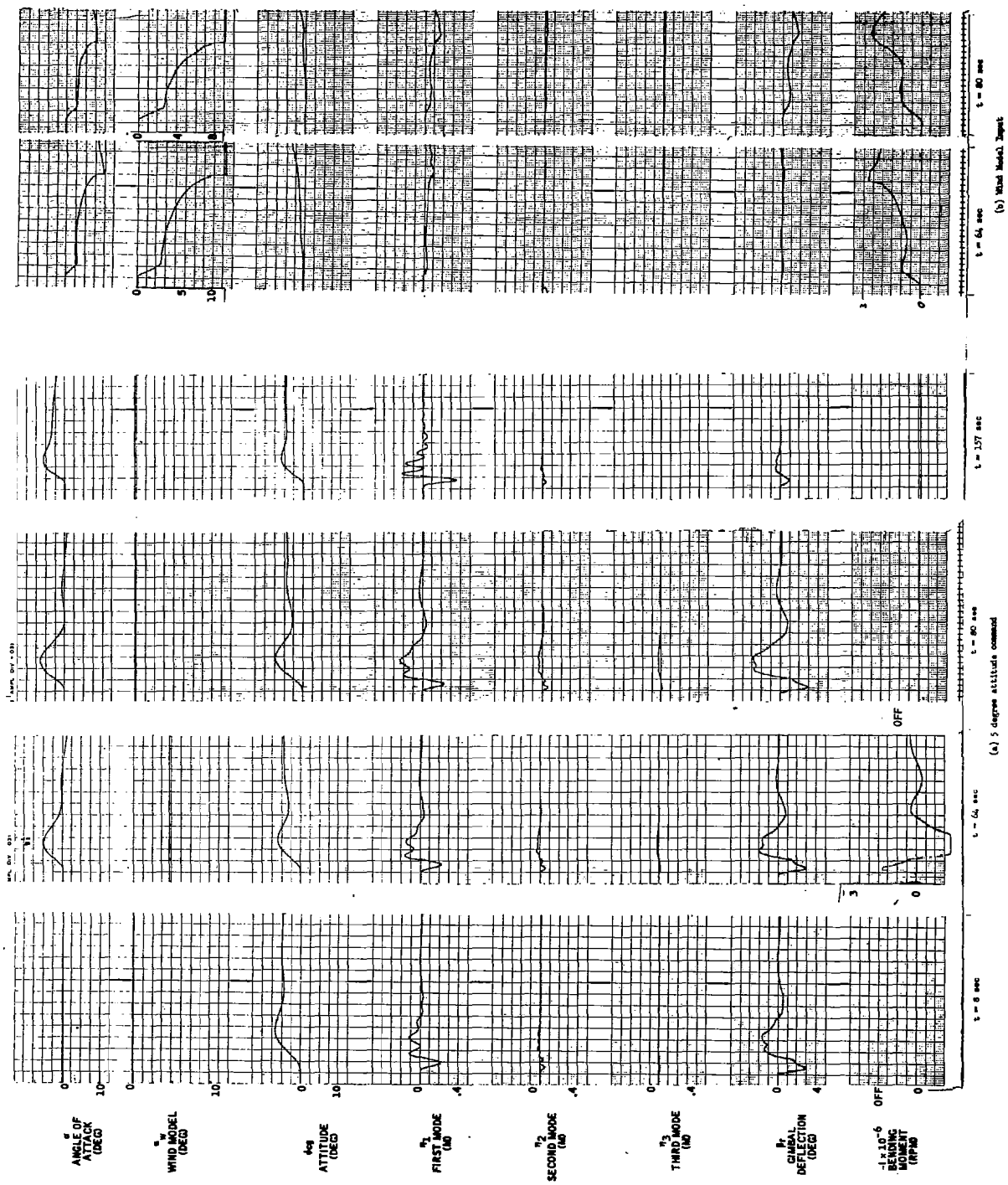

Figure C-1. Nominal System Response to Attitude Commands and Wind Disturbances

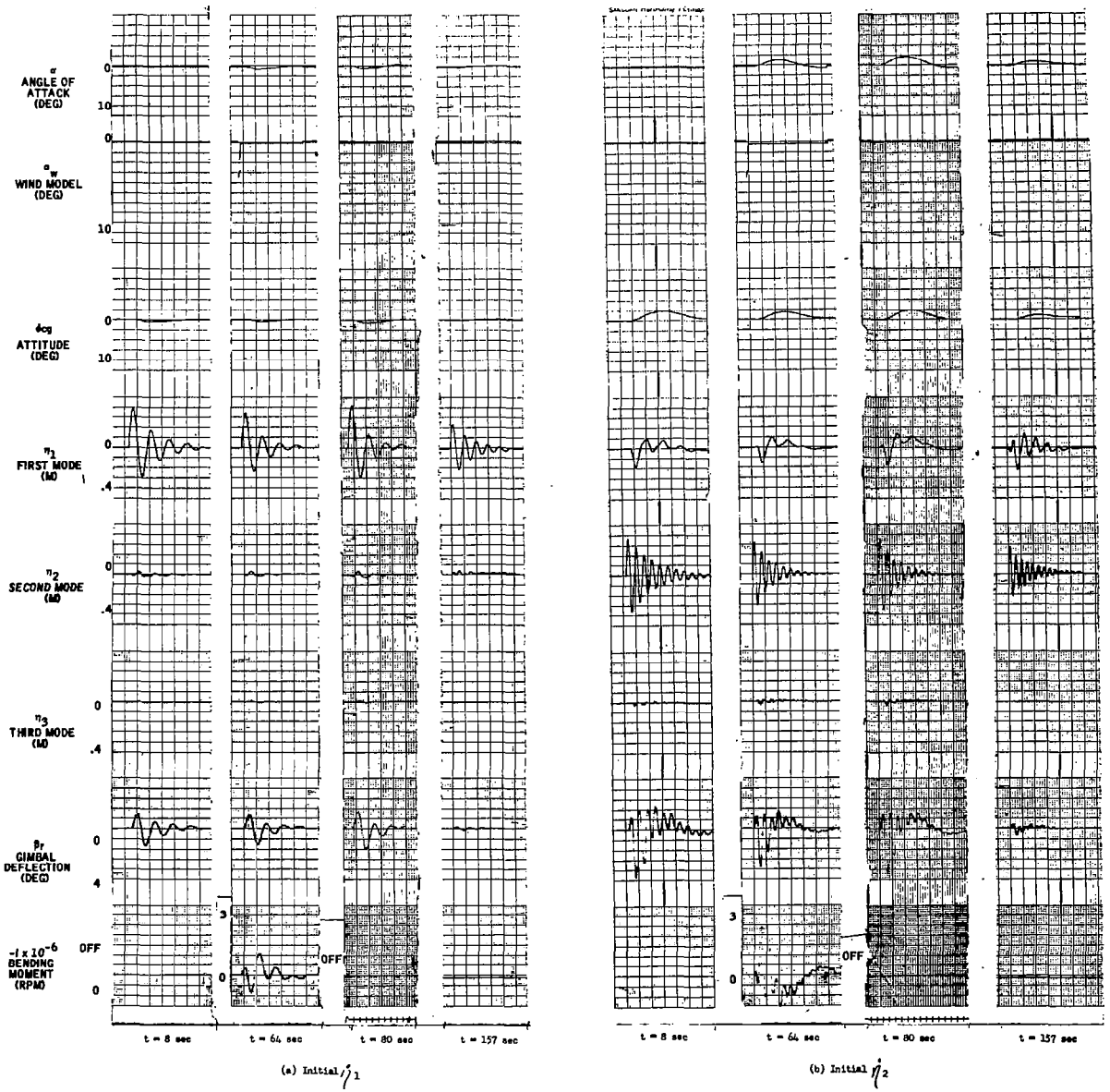

Figure C-2. Nominal System Response to Initial Bending Mode Rate Inputs

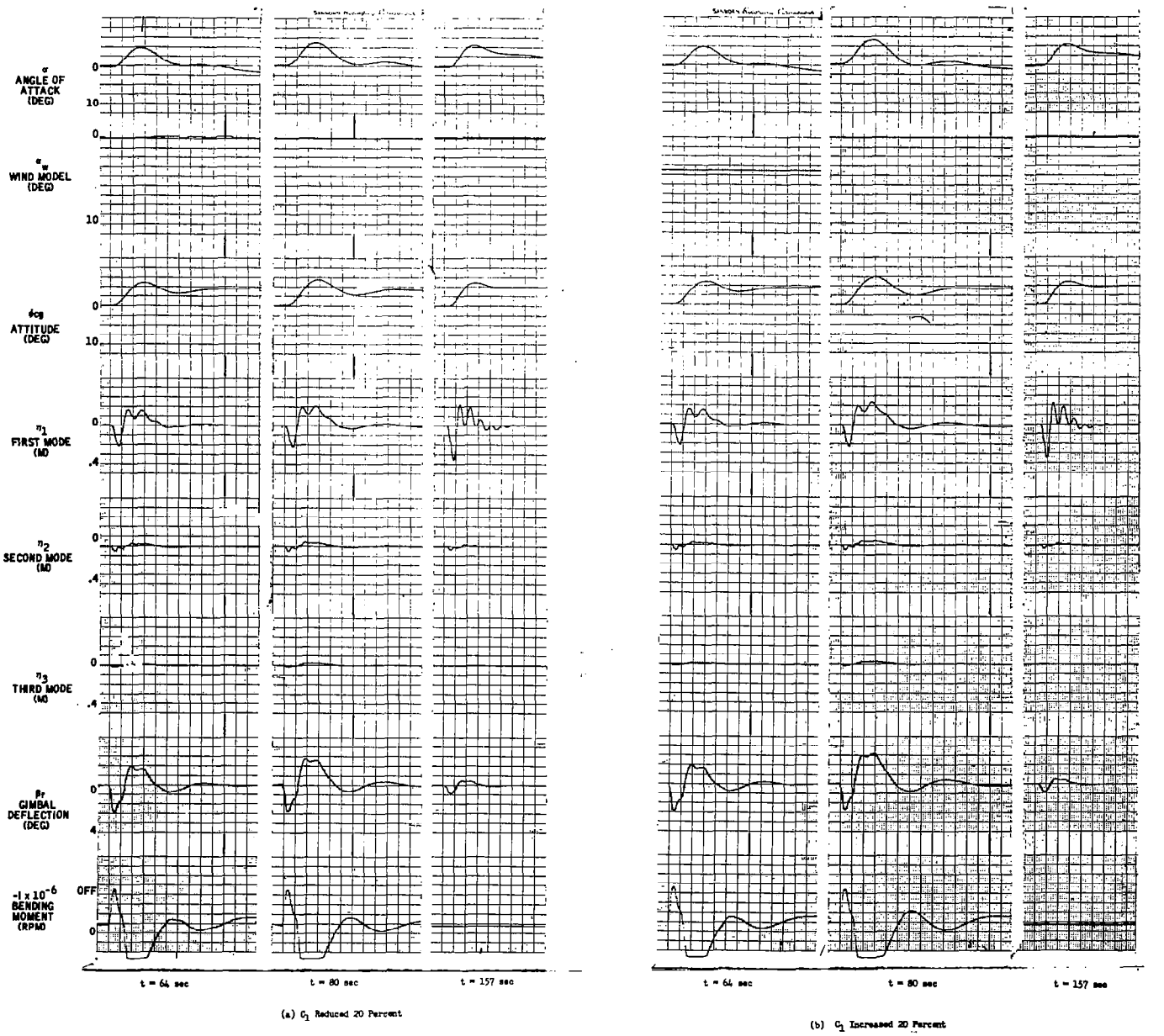

Figure C-3. Nominal System, ± 20 percent Variation in C_1, Attitude Command Response

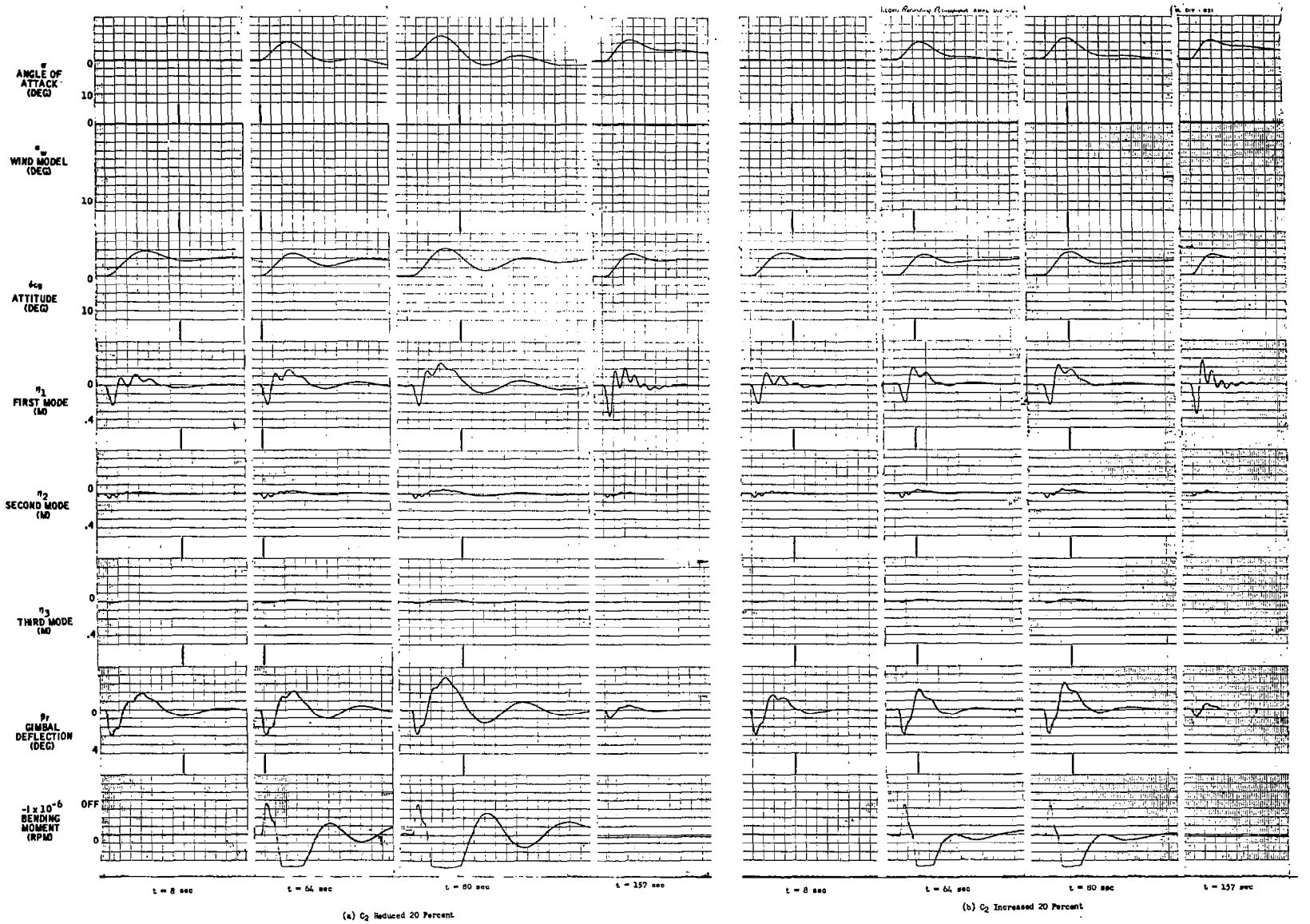

Figure C-4. Nominal System, ± 20 percent Variation in Control Effectiveness, C_2, Attitude Command Response

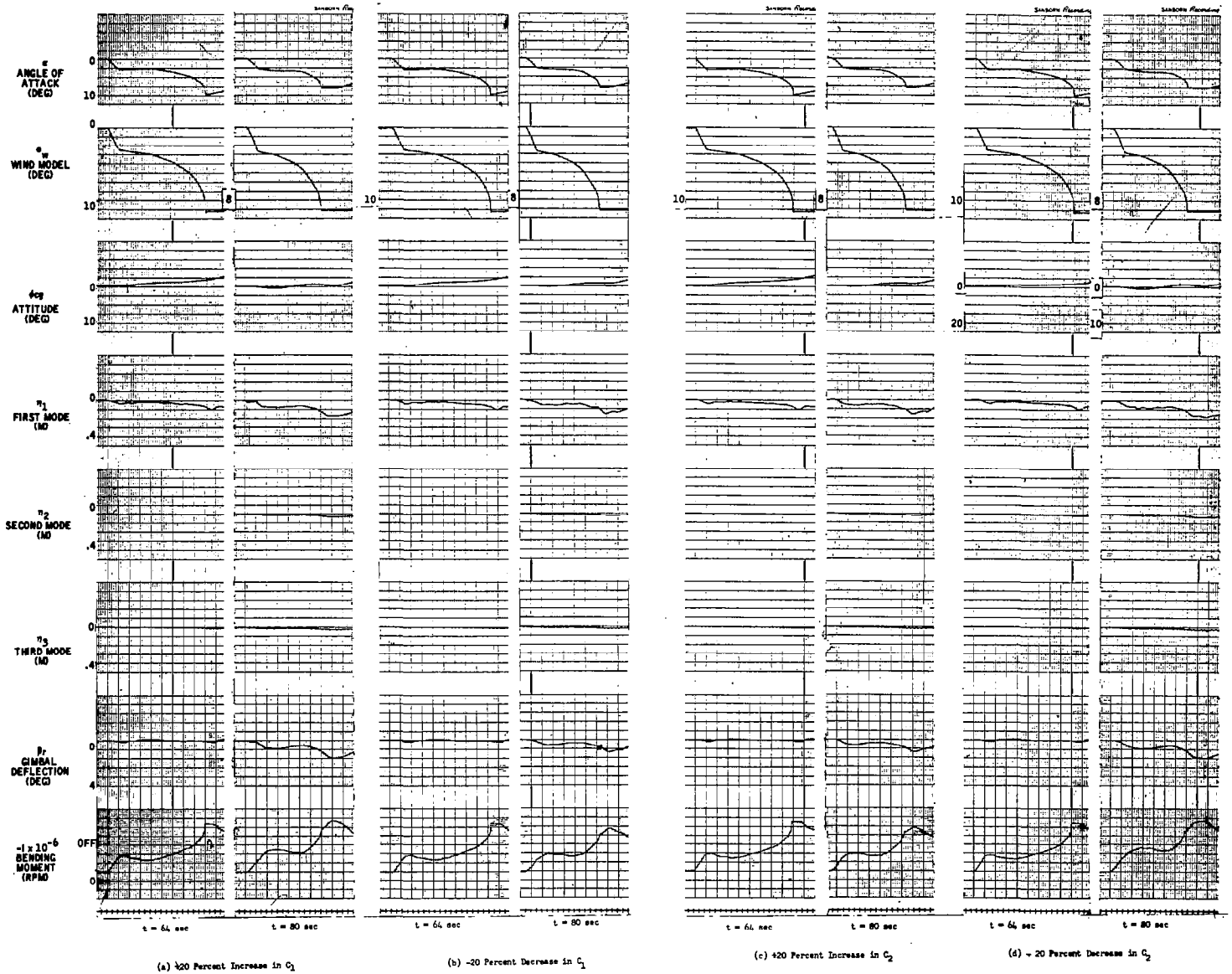

Figure C-5. Nominal System, ± 20 percent Variation in C_1 and ± 20 percent Variation in C_2, Model Wind Input

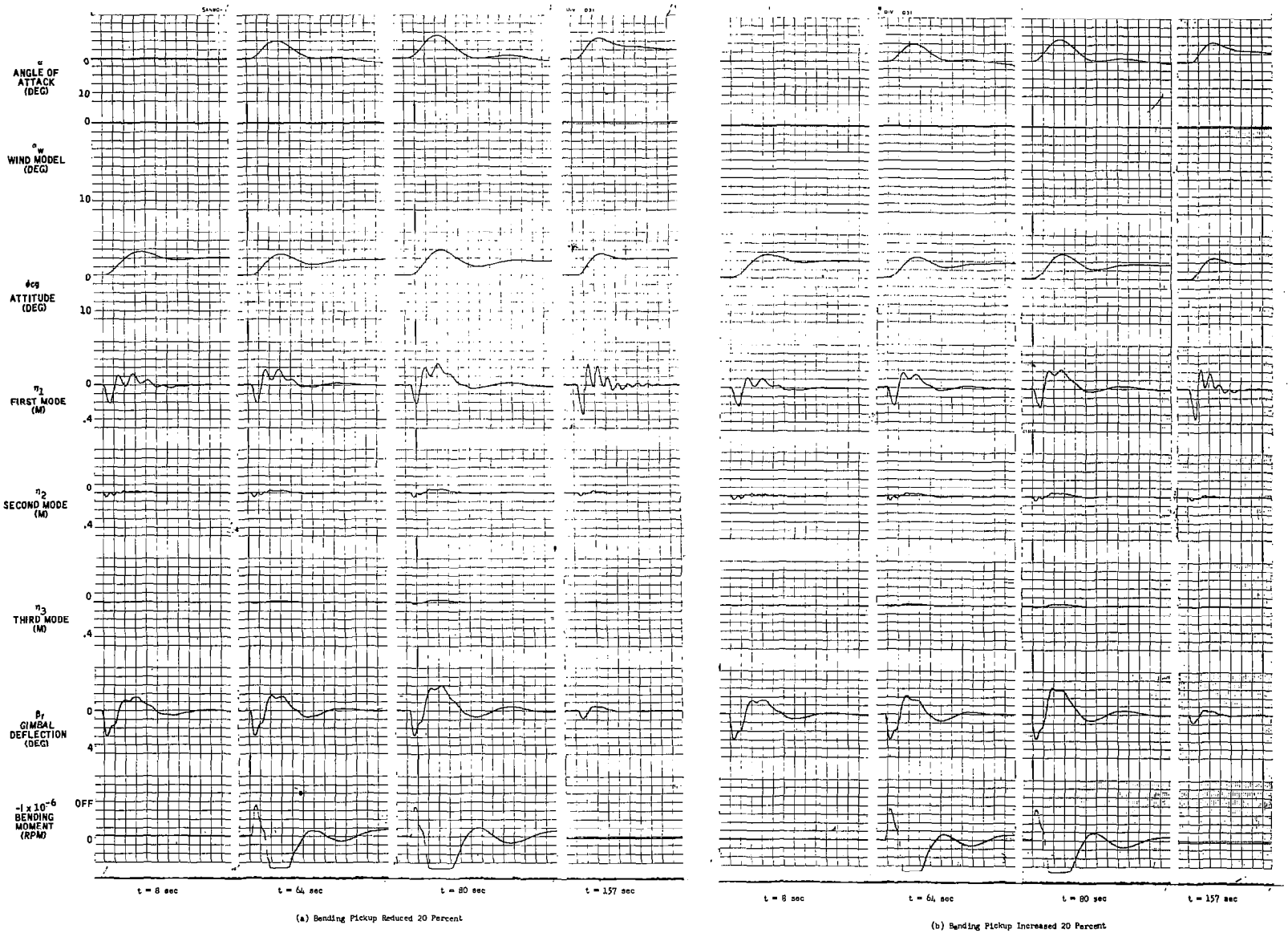

Figure C-6. Nominal System, ± 20 percent Variation in Attitude Sensor Bending Pickup, Attitude Command Response

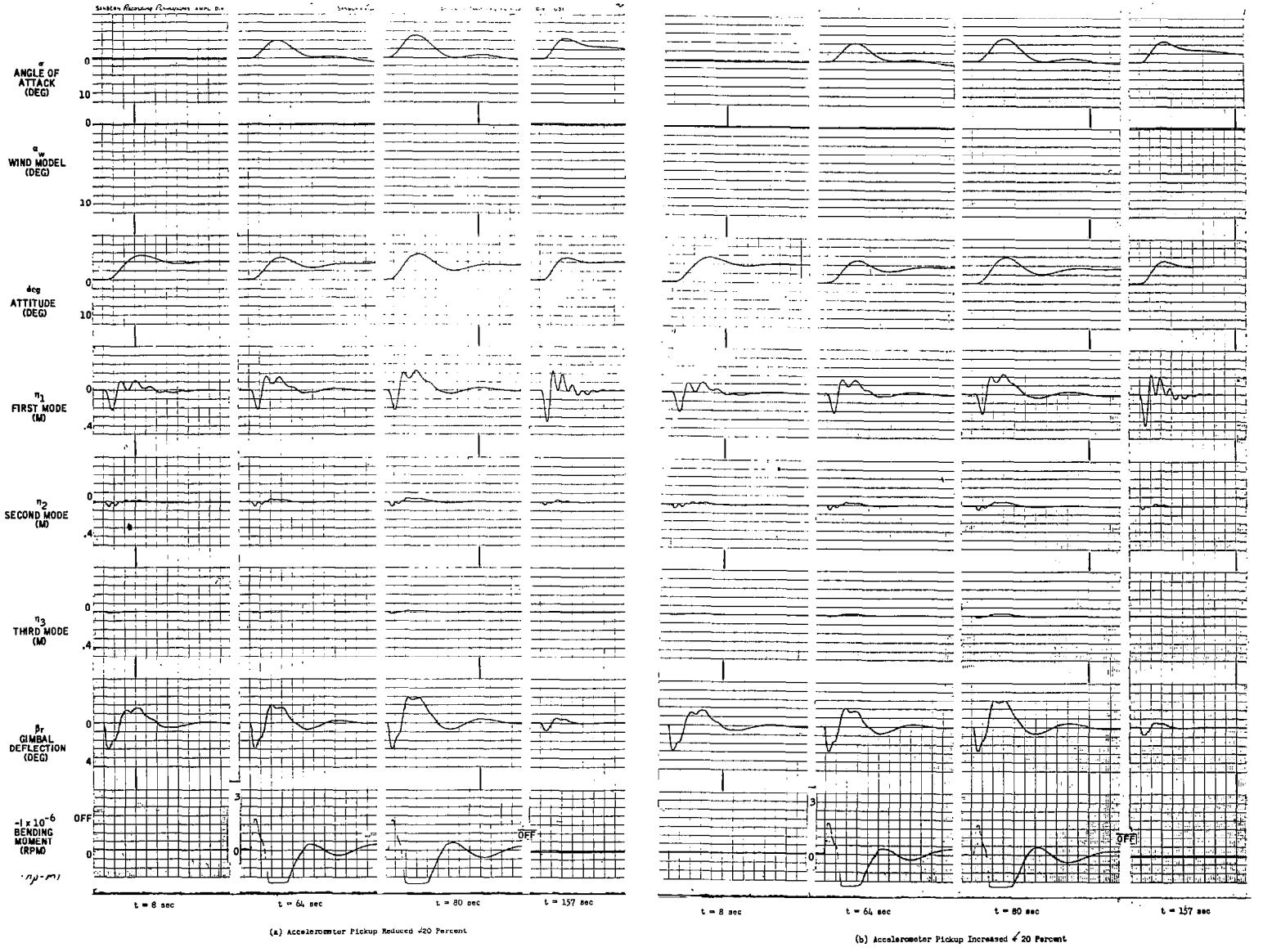

Figure C-7. Nominal System, ± 20 percent Variation in Accelerometer Bending Pickup, Attitude Command Response

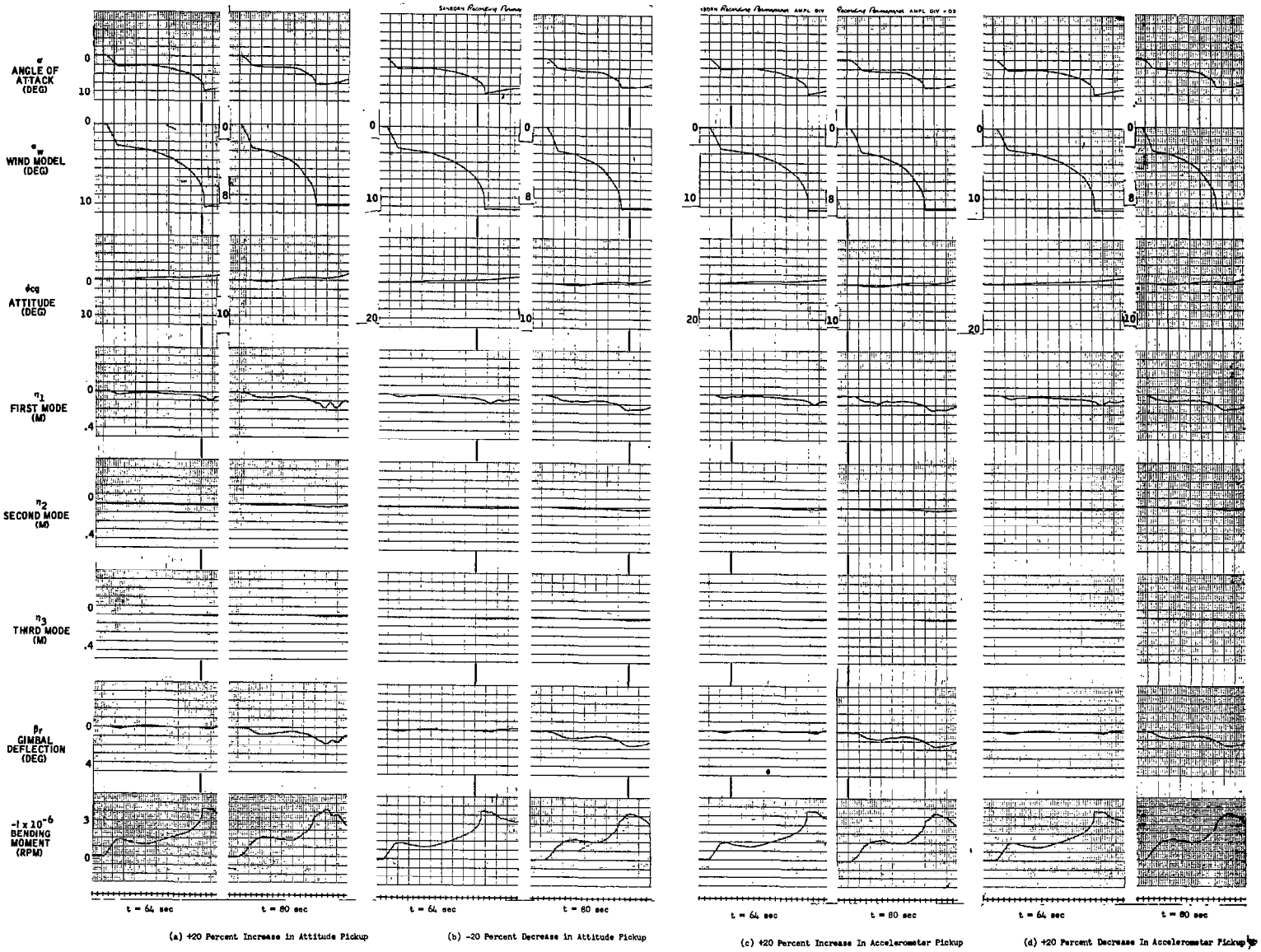

Figure C-8. Nominal System, ± 20 percent Variation in Attitude Sensor Bending Pickup and ± 20 percent Variation in Accelerometer Bending Pickup, Model Wind Input

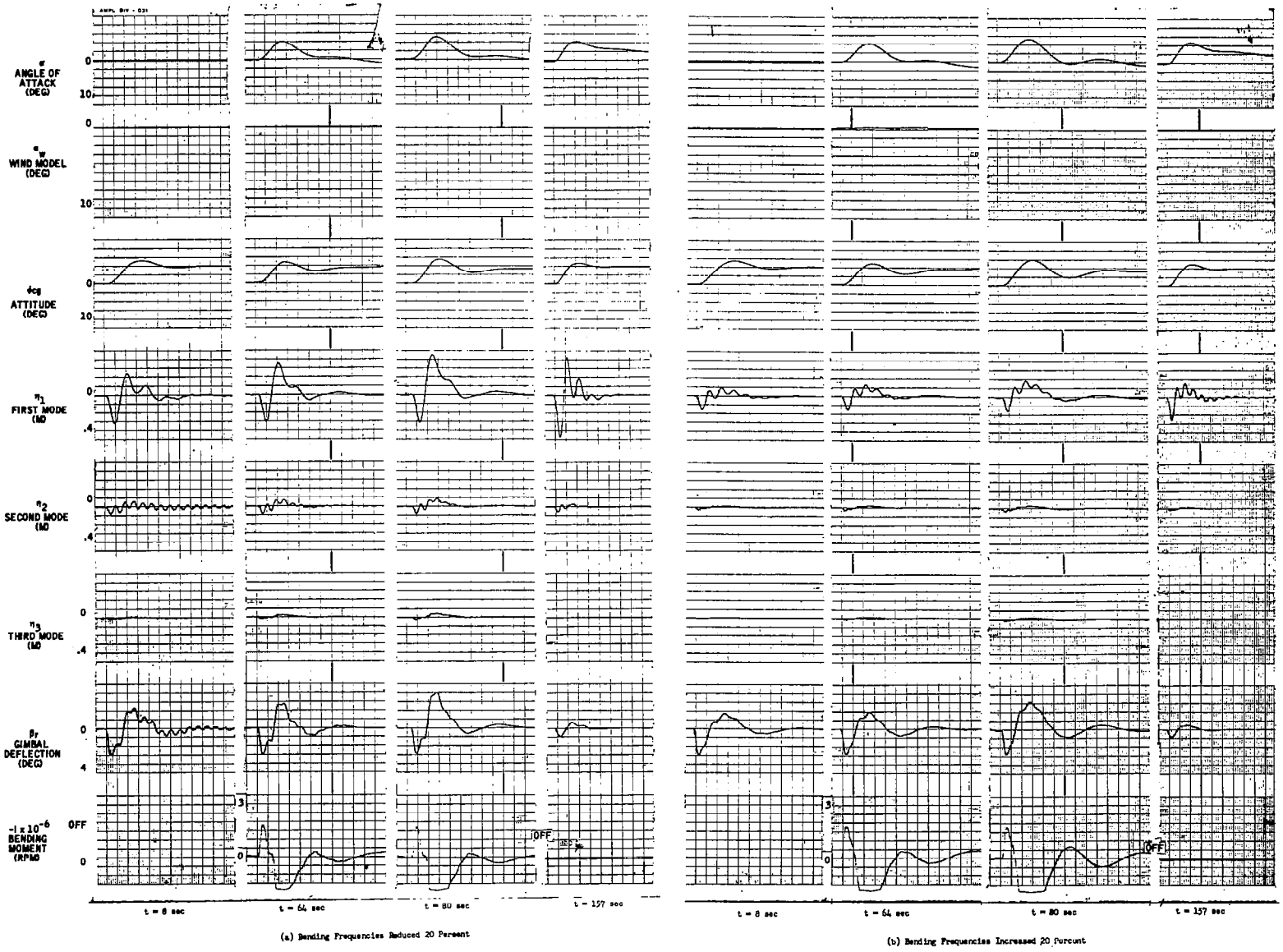

Figure C-9. Nominal System, ± 20 percent Variation in Bending Frequencies, Attitude Command Response

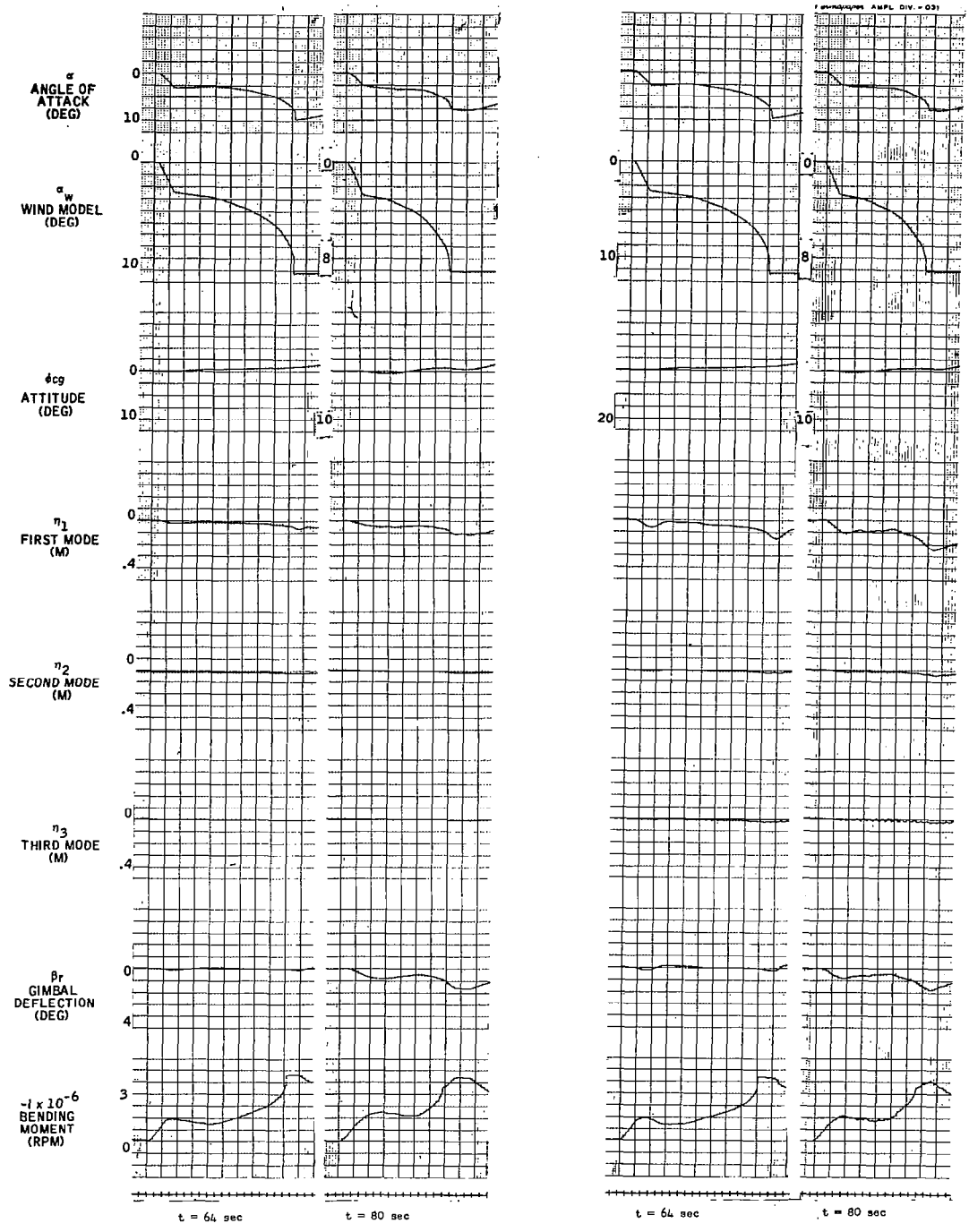

(a) 20 Percent Increase

(b) 20 Percent Decrease

Figure C-10. Nominal System, ± 20 percent Variation in Bending Frequencies, Model Wind Input

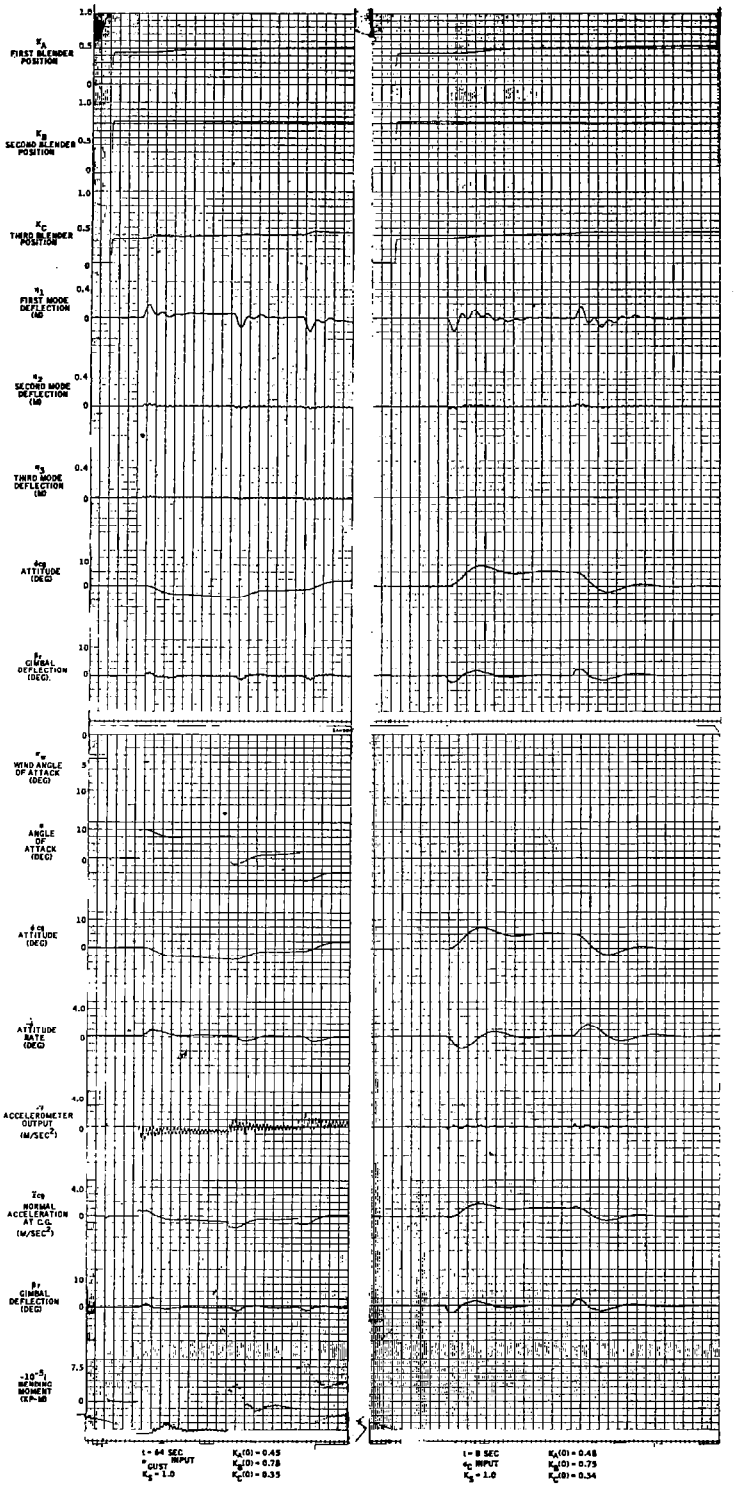

Figure C-11. Performance of Nominal Multiple Blender System (1)

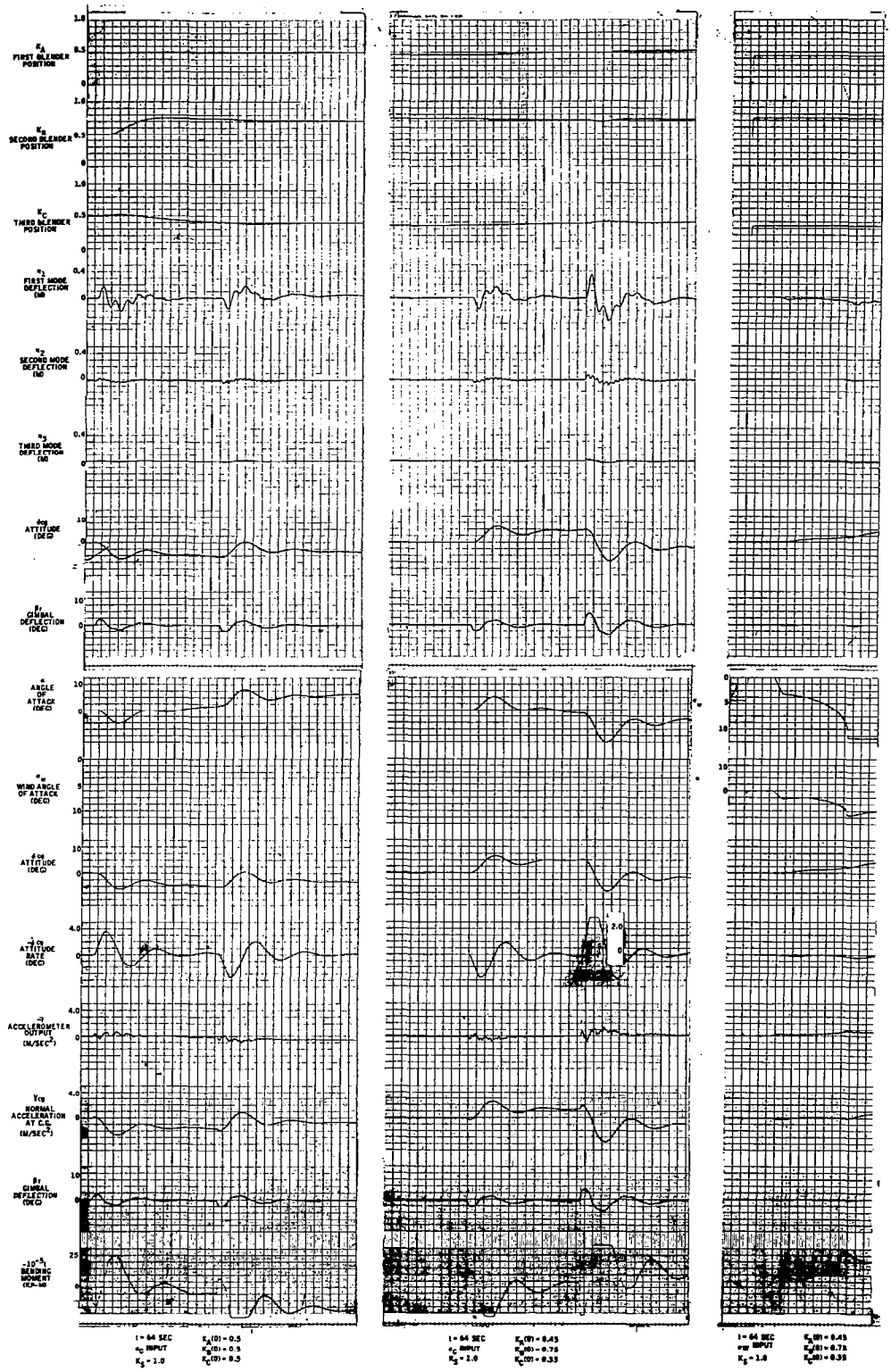

Figure C-12. Performance of Nominal Multiple Blender System (2)

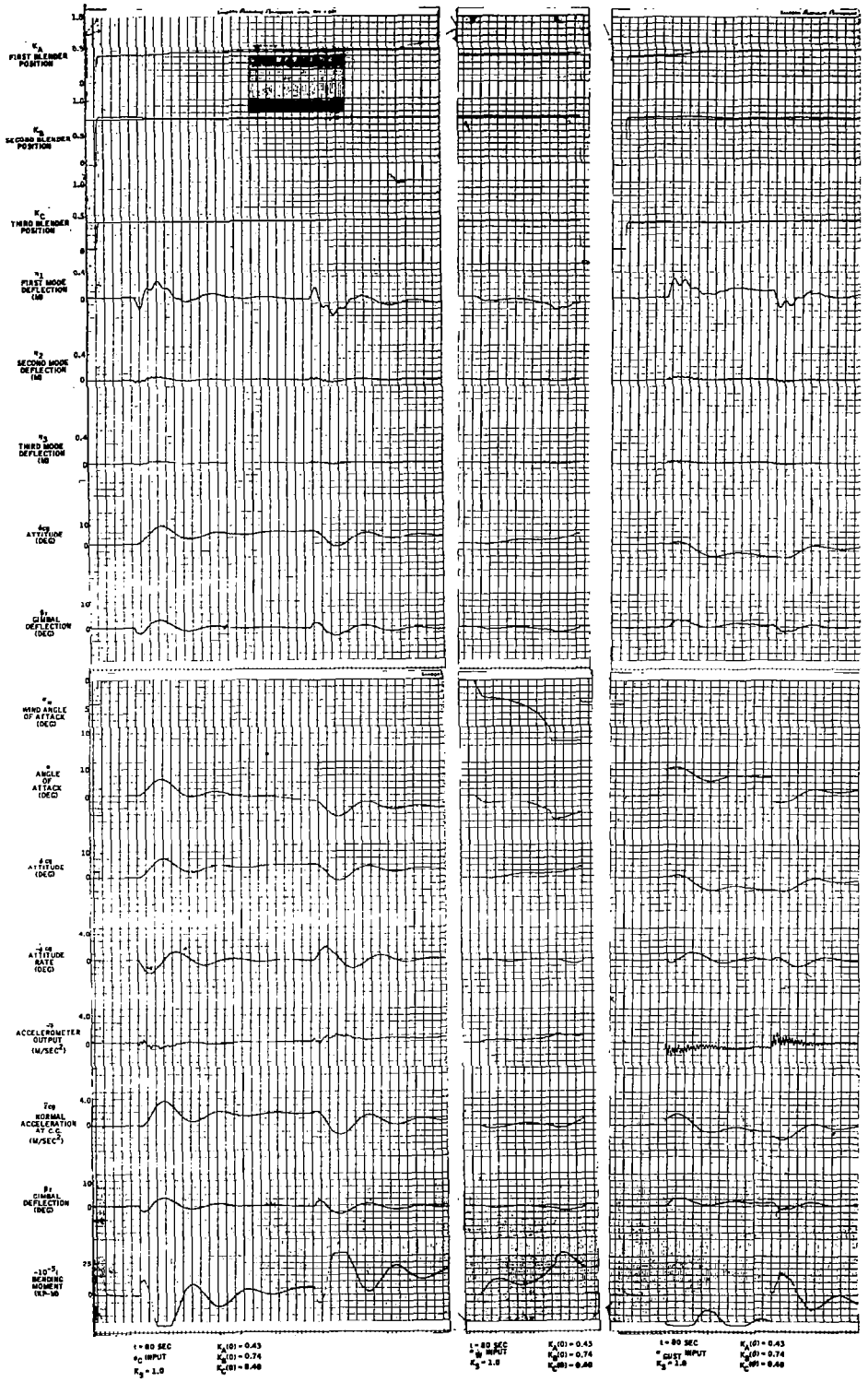

Figure C-13. Performance of Nominal Multiple Blender System (3)

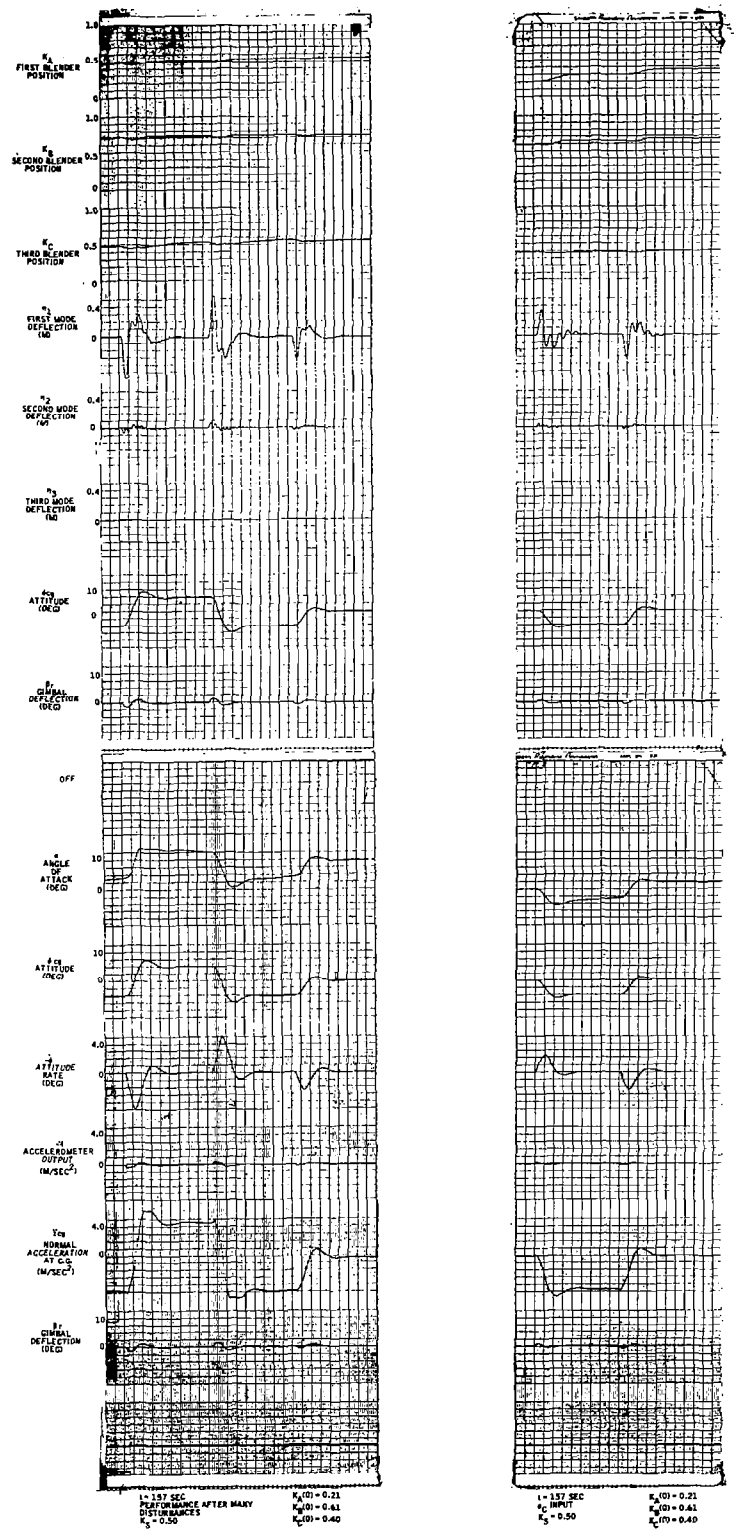

Figure C-14. Performance of Nominal Multiple Blender System (4)

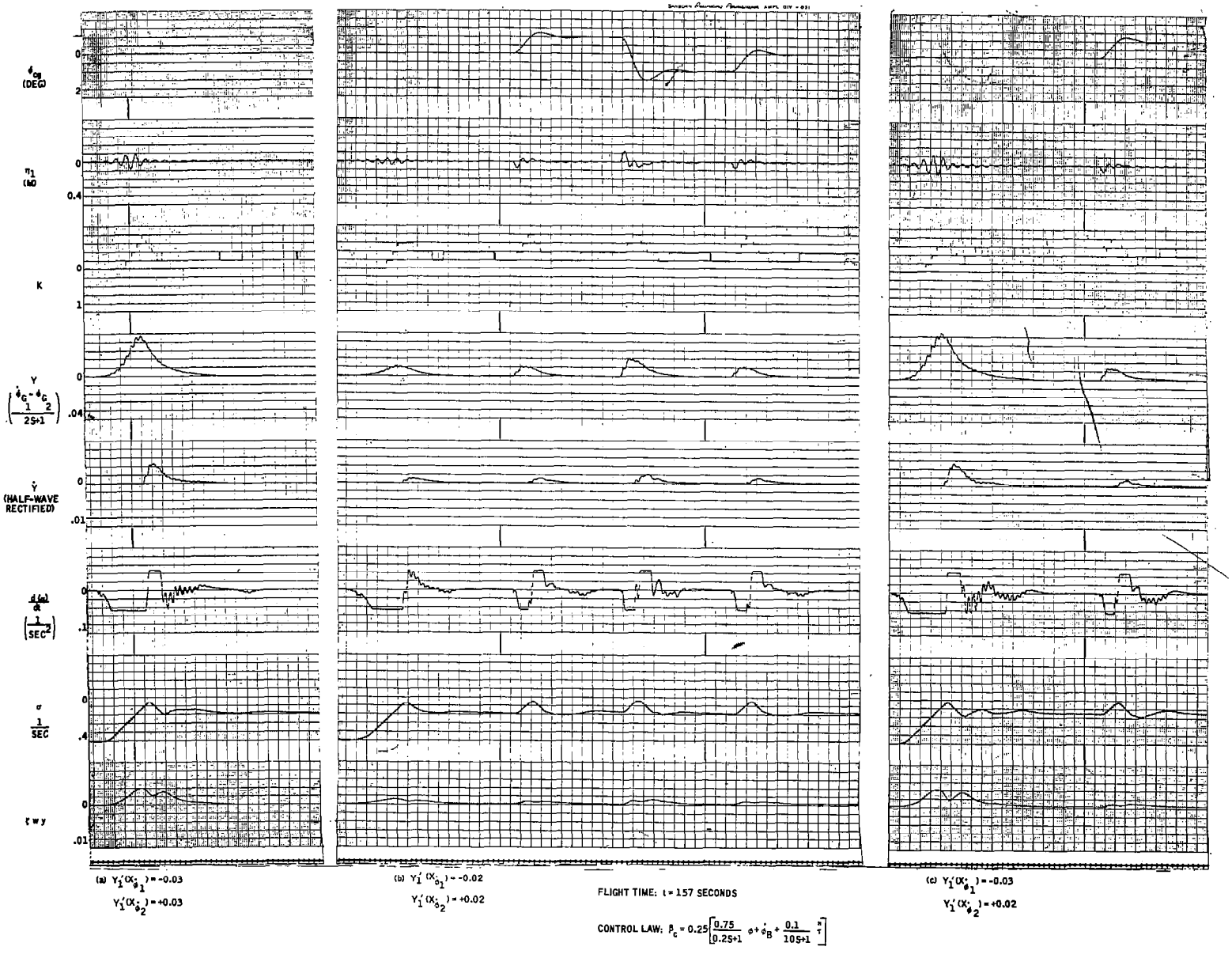

Figure C-15. Performance of New Adaptive Blender for Desired First-Mode Damping of 0.1

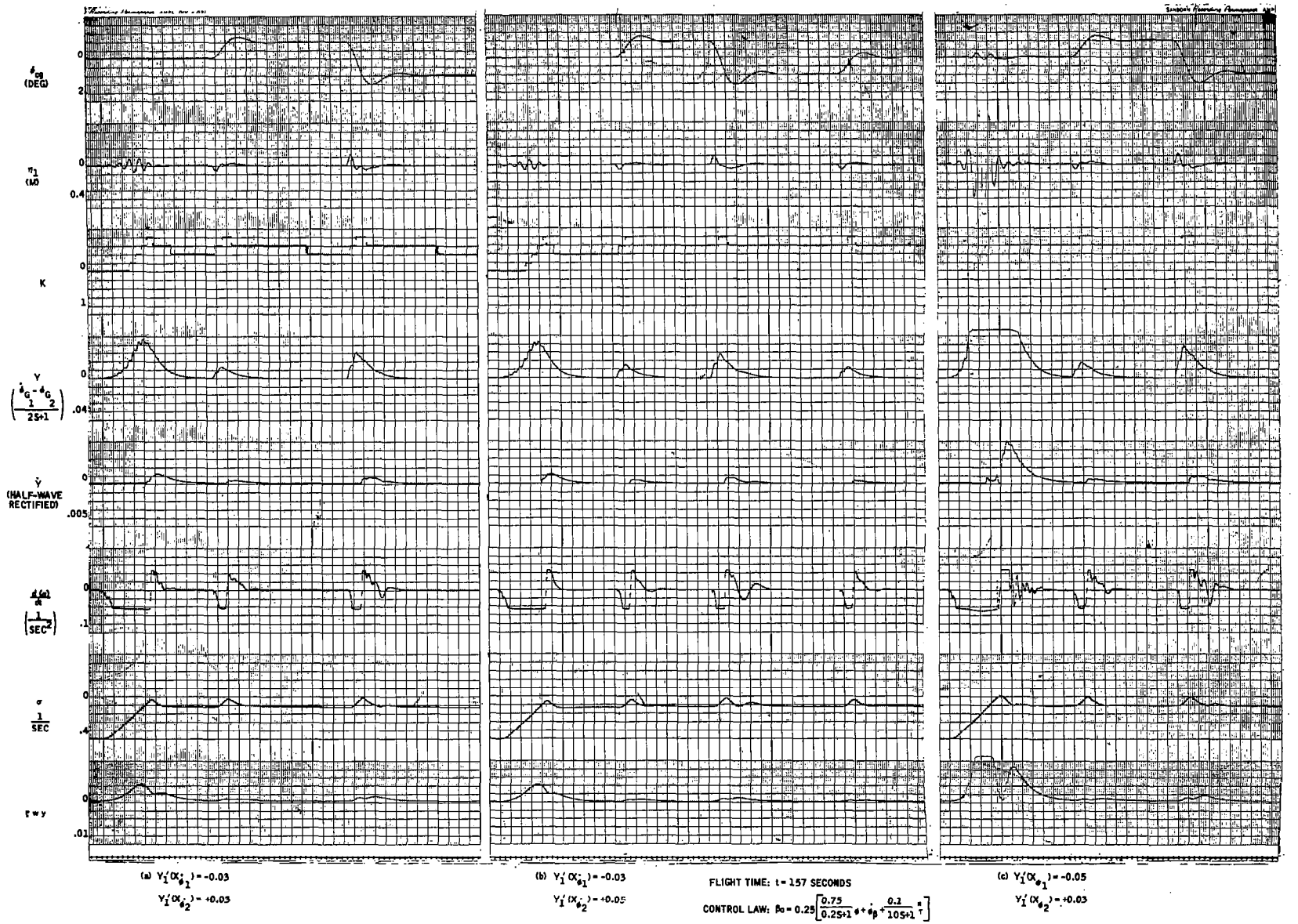

Figure C-16. Performance of New Adaptive Blender for Desired First-Mode Damping of 0.2

APPENDIX D
ROOT LOCUS PLOTS

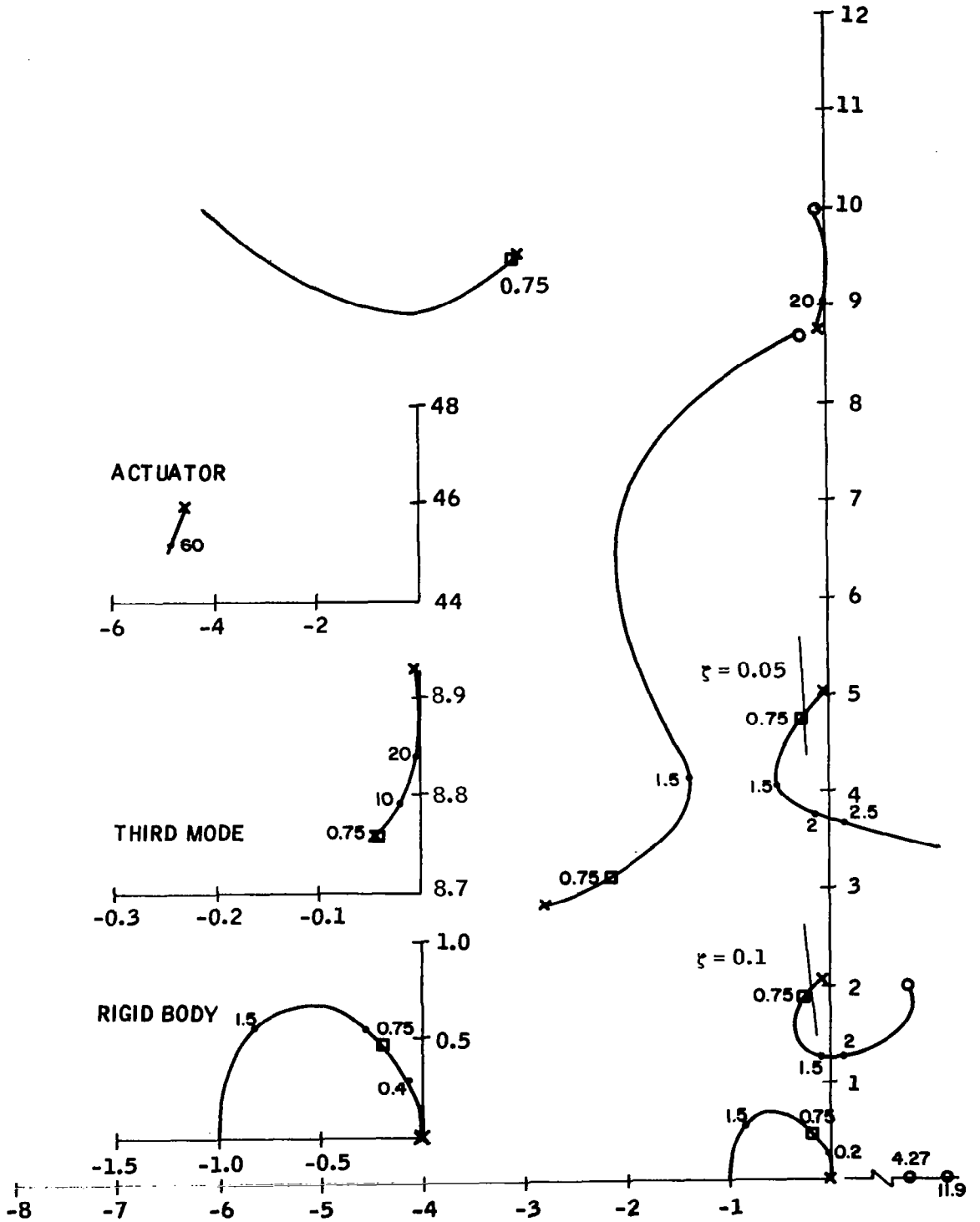

Figure D-1. t = 8 seconds, Nominal System, Y'_1 = +0.001, Y'_2, = -0.06, Y'_3 = 0

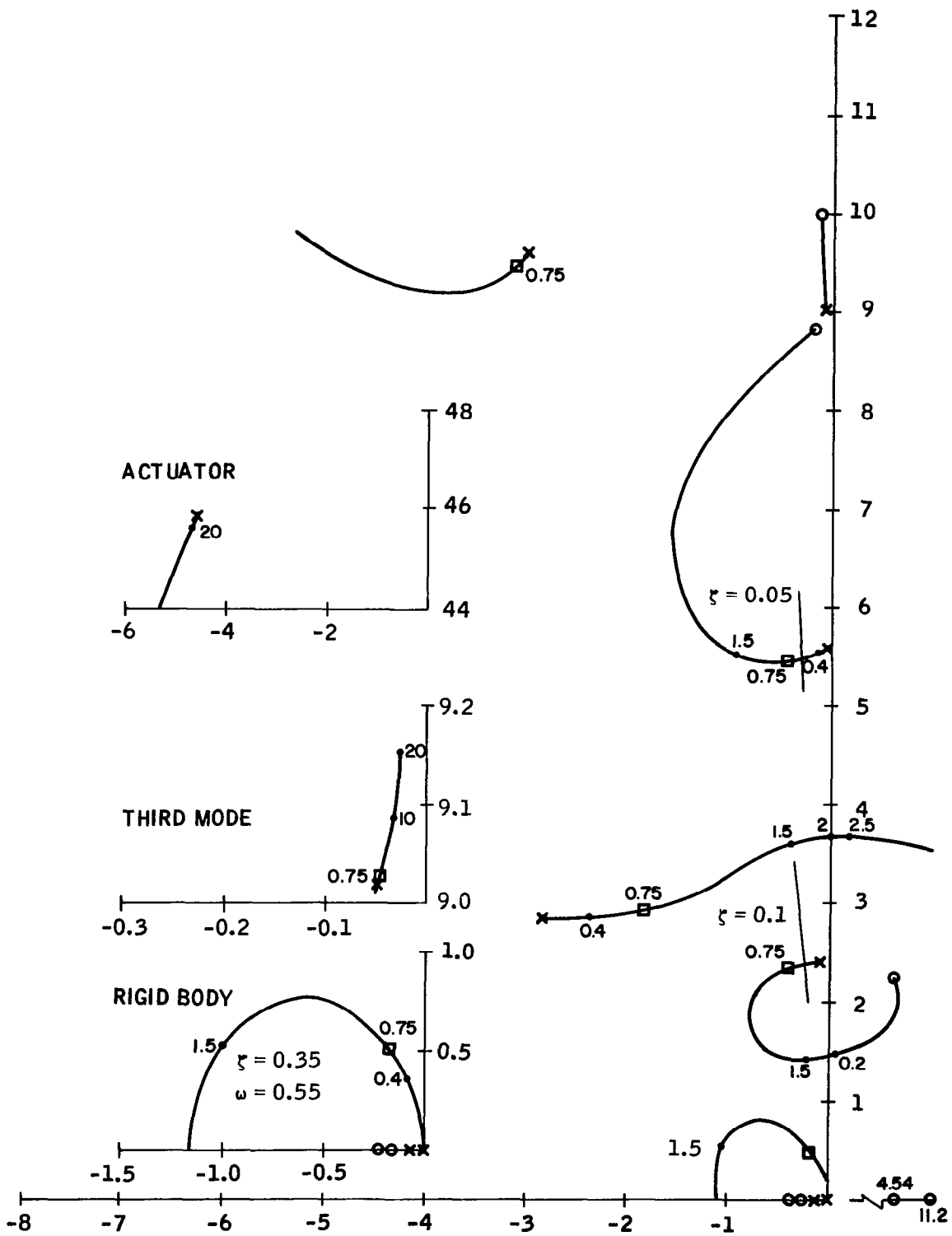

Figure D-2. t = 64 seconds, Nominal System, $Y'_1 = +0.01$, $Y'_2 = -0.06$, $Y'_3 = 0$

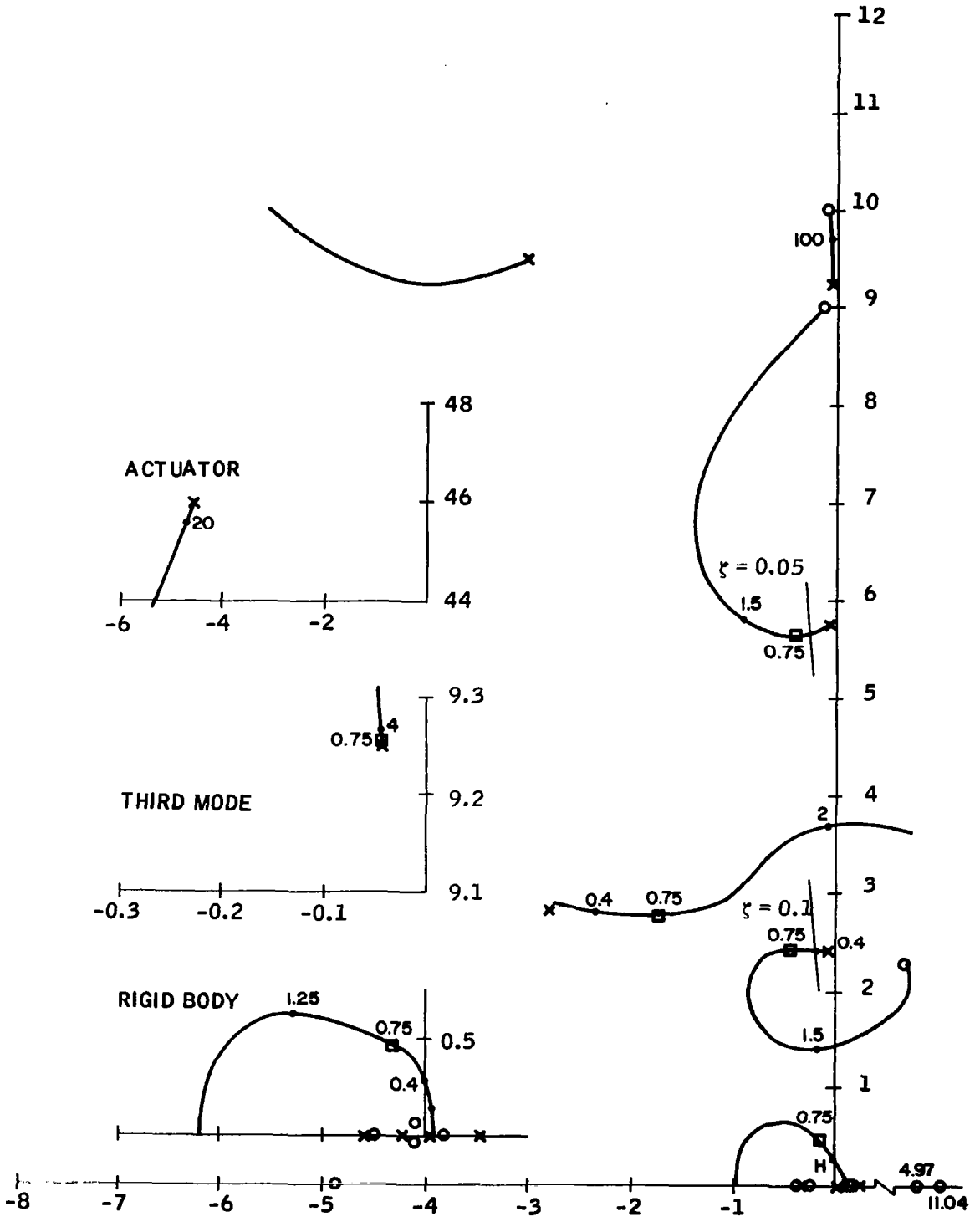

Figure D-3. t = 80 seconds, Nominal System, $Y'_1 = +0.01$, $Y'_2 = -0.06$, $Y'_3 = 0$

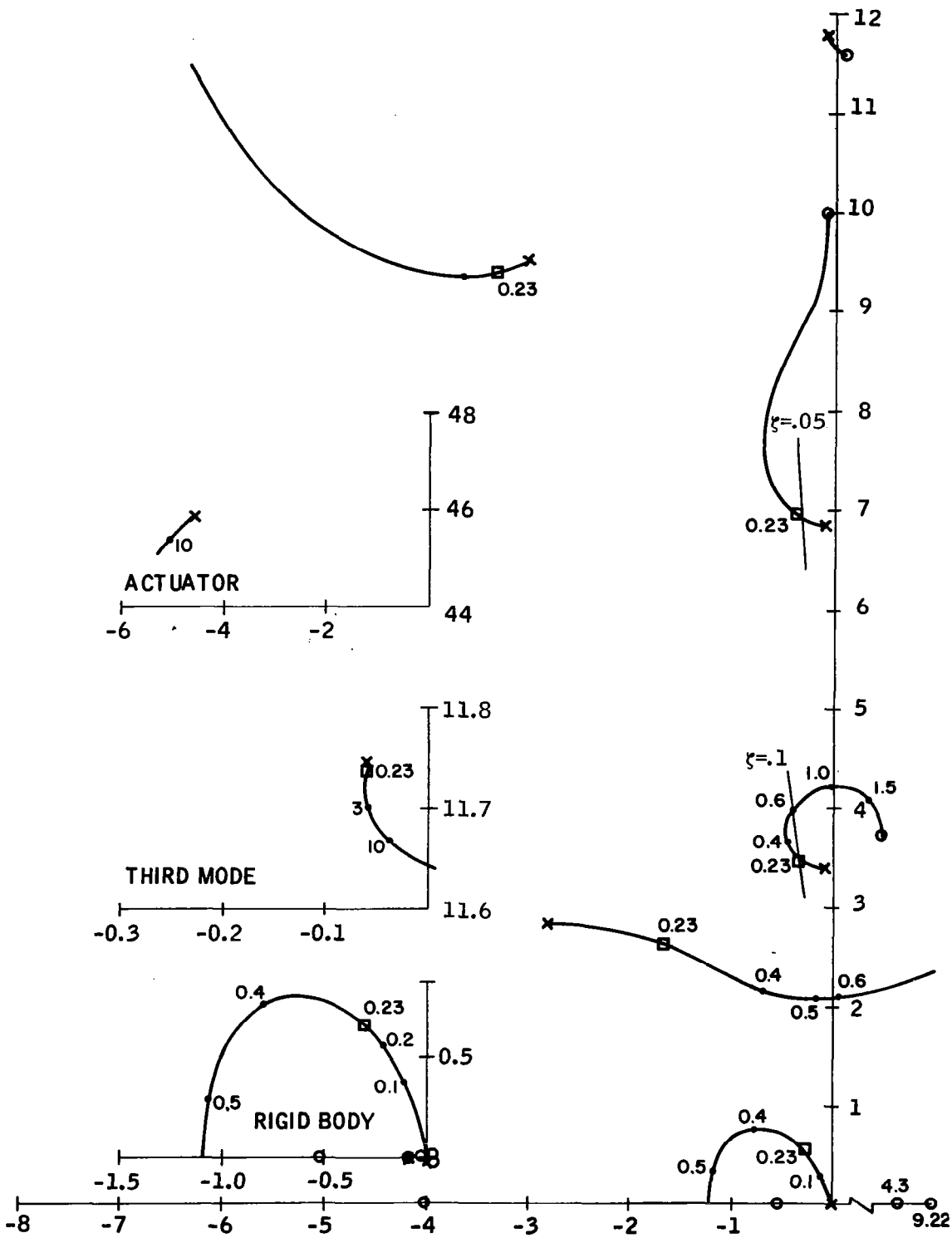

Figure D-4. t = 157 seconds, Nominal System, $Y'_1 = -0.01$, $Y'_2 = -0.06$, $Y'_3 = 0$

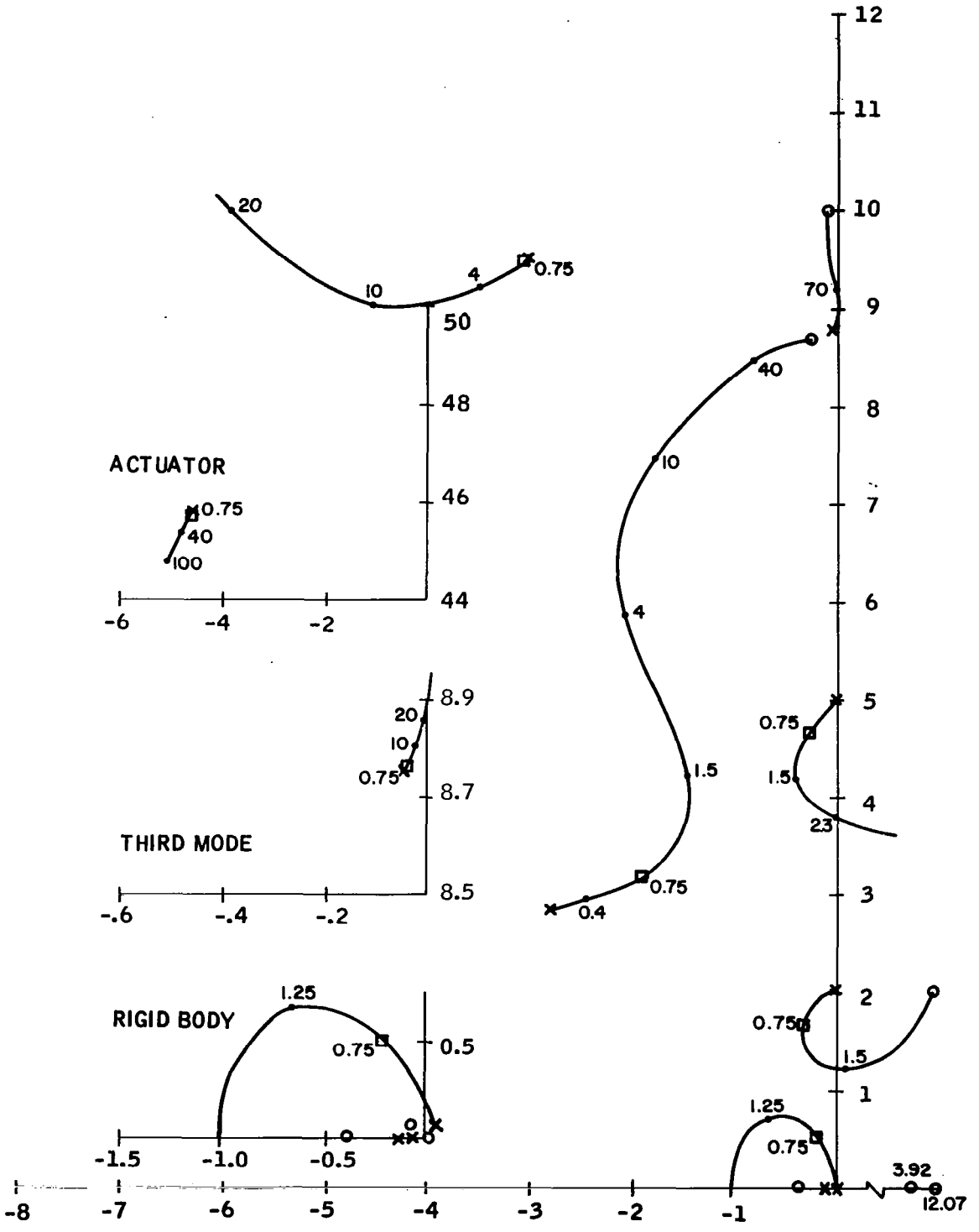

Figure D-5. t = 8 seconds, Nominal System, +20 percent Variation in Attitude Sensor Bending Pickup

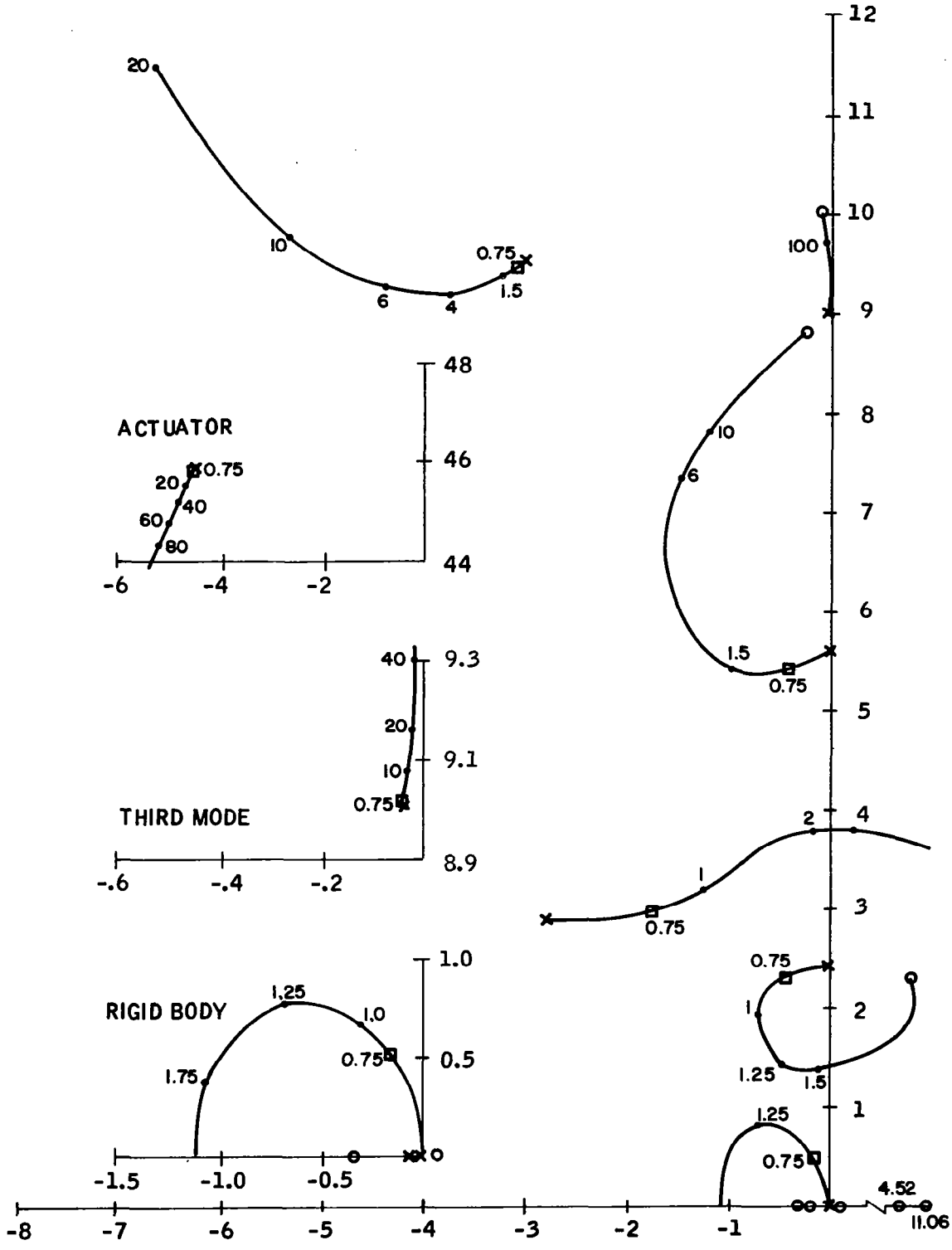

Figure D-6. t = 64 seconds, Nominal System, +20 percent Variation in Attitude Sensor Bending Pickup

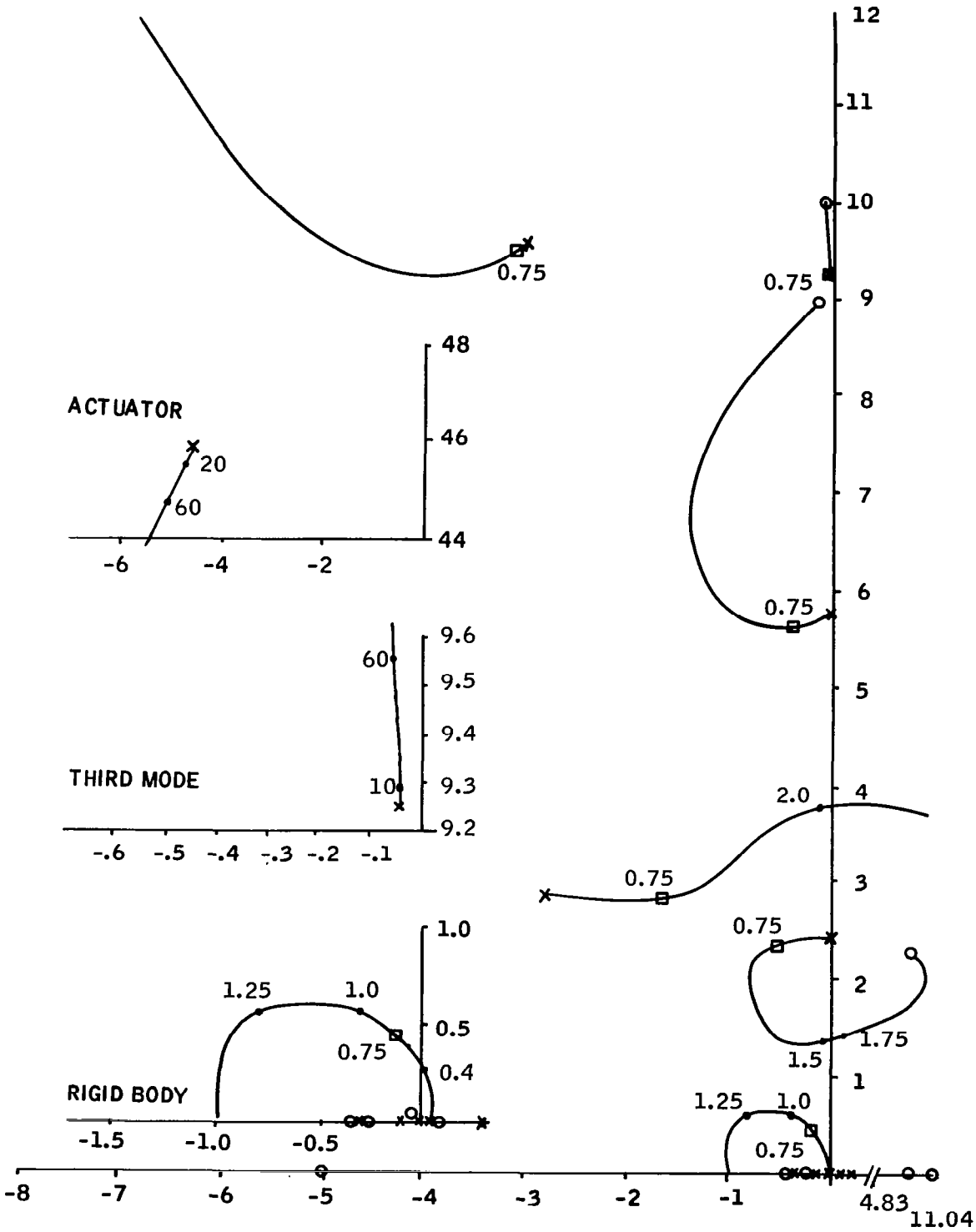

Figure D-7. t = 80 seconds, Nominal System, +20 percent Variation in Attitude Sensor Bending Pickup

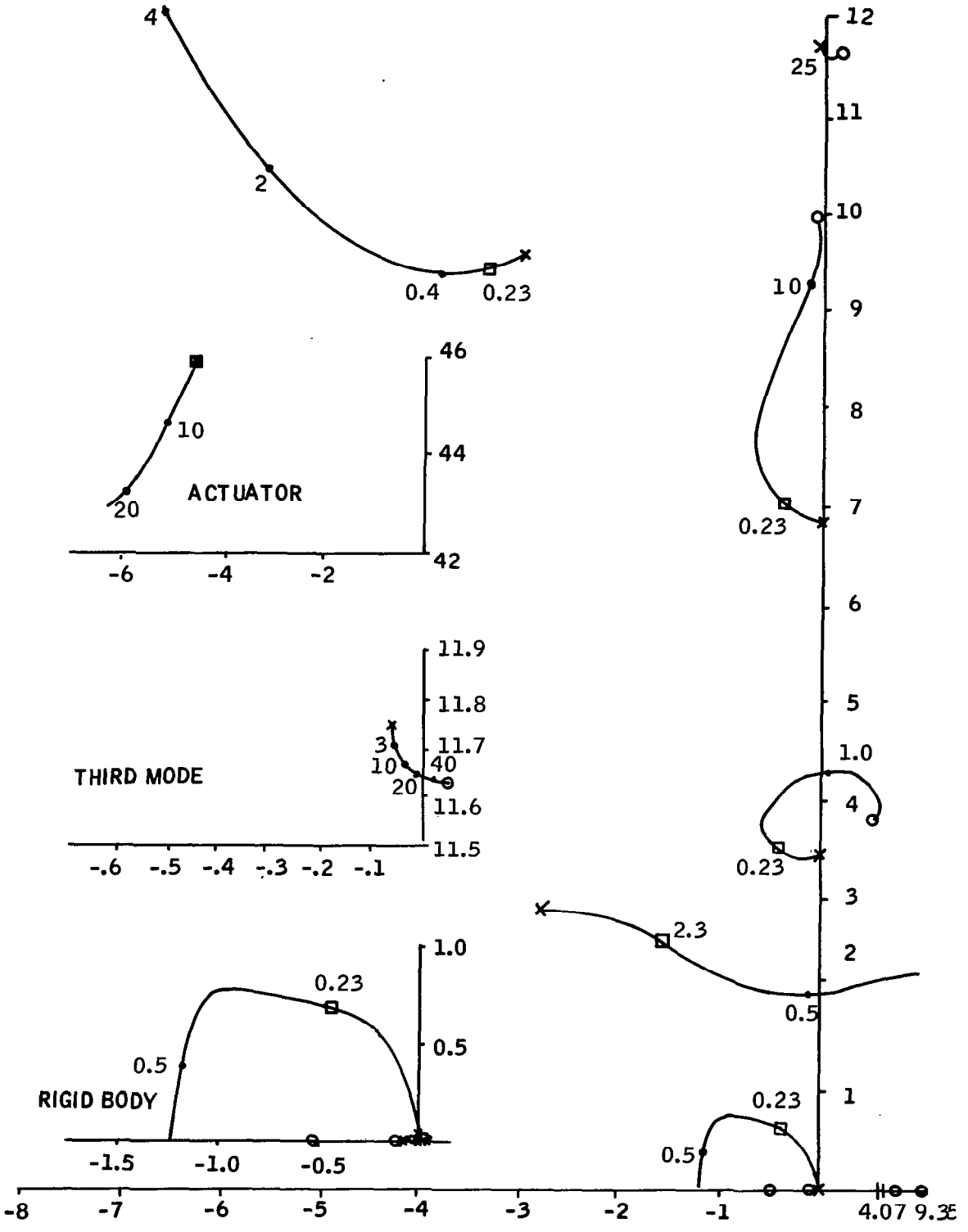

Figure D-8. t = 157 seconds, Nominal System, +20 percent Variation in Attitude Sensor Bending Pickup

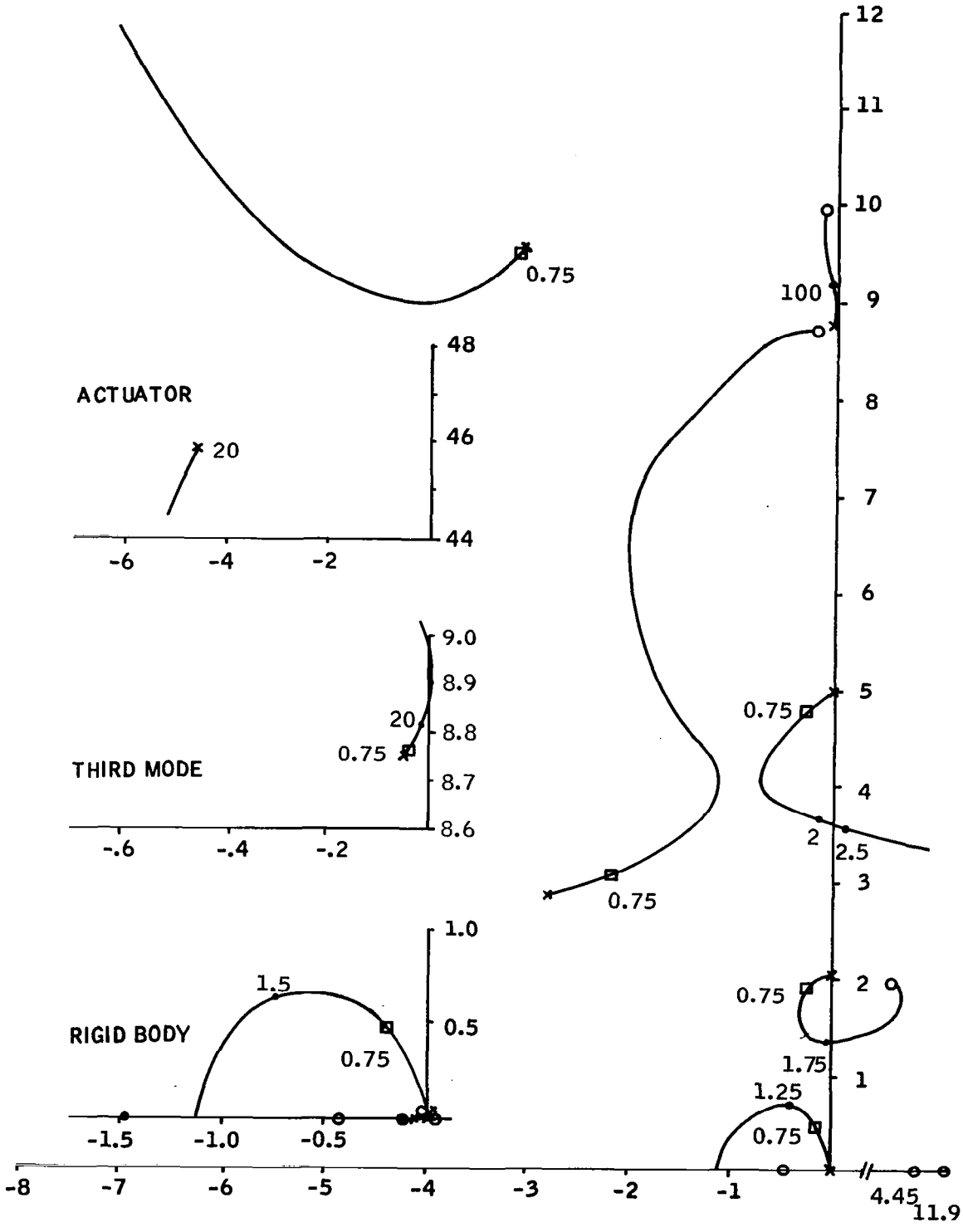

Figure D-9. t = 8 seconds, Nominal System, -20 percent Variation in Attitude Sensor Bending Pickup

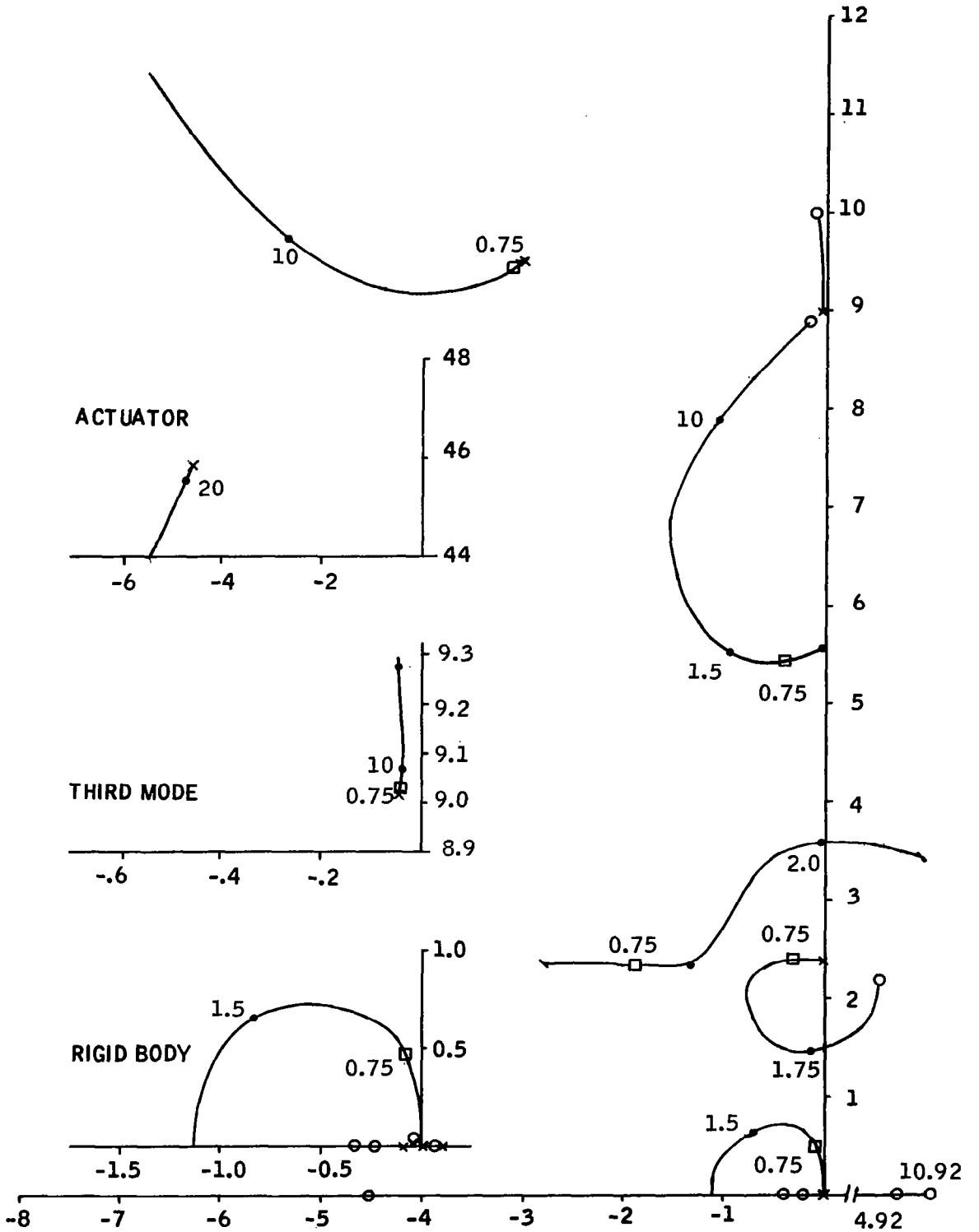

Figure D-10. t = 64 seconds, Nominal System, -20 percent Variation in Attitude Sensor Bending Pickup

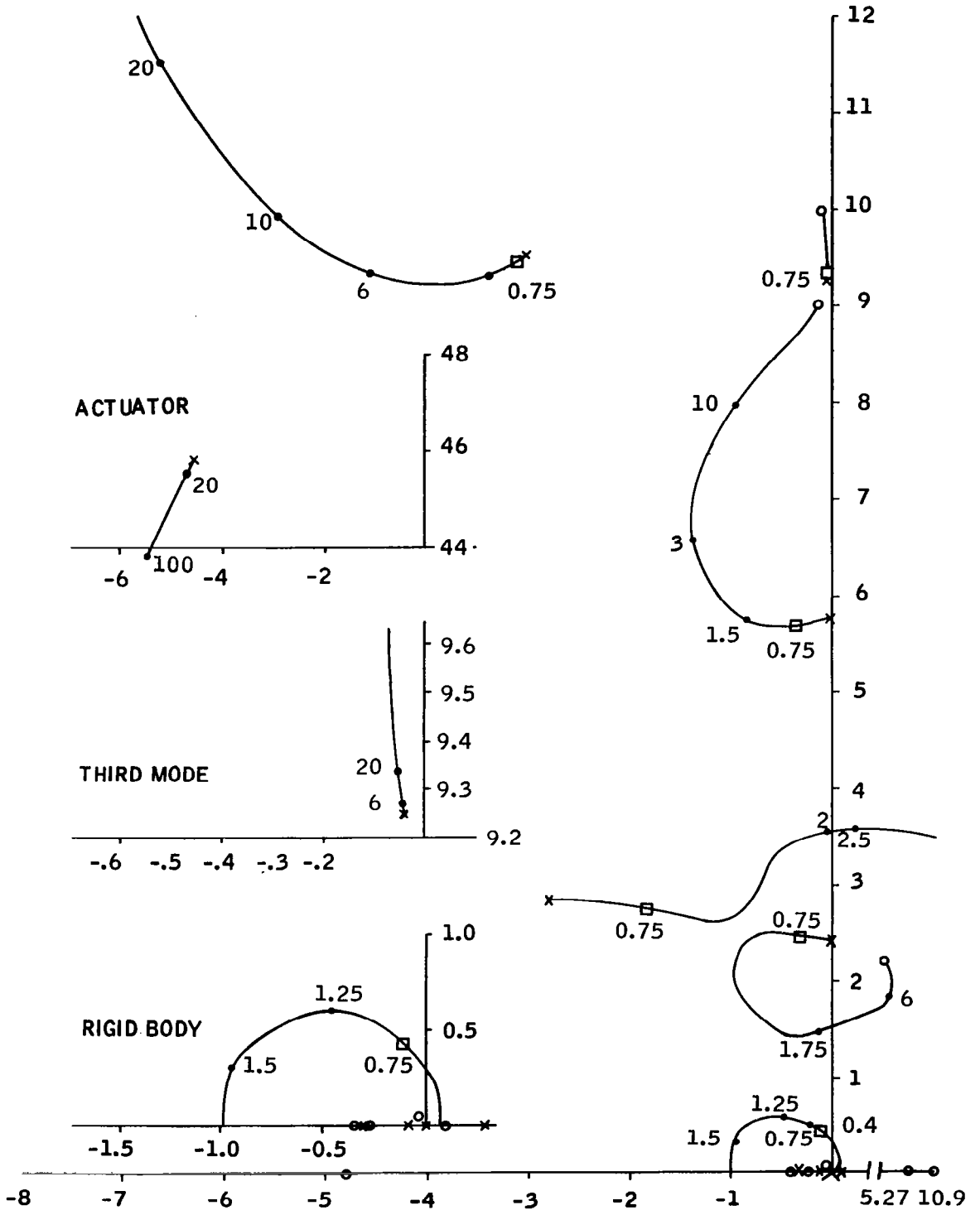

Figure D-11. t = 80 seconds, Nominal System, -20 percent Variation in Attitude Sensor Bending Pickup

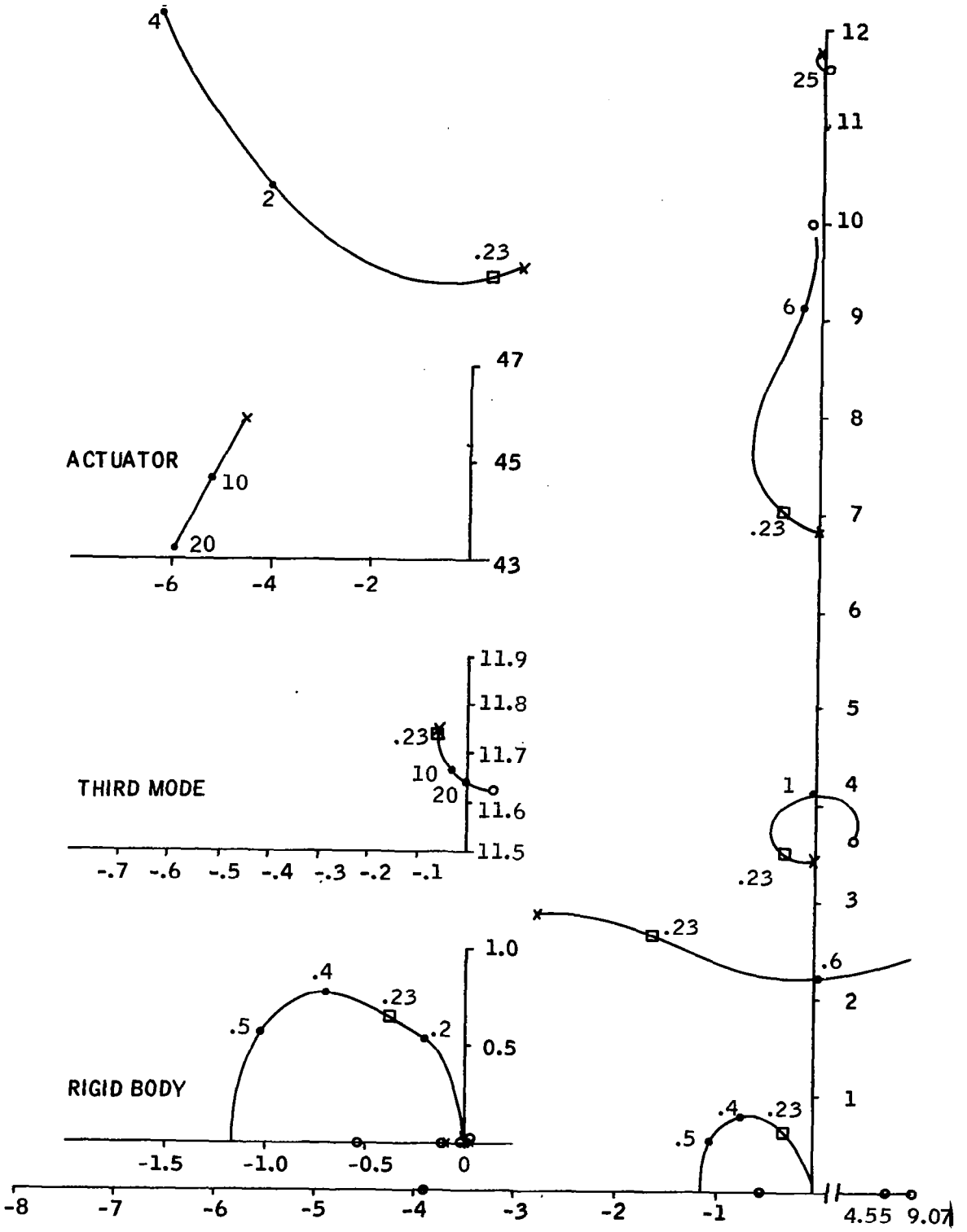

Figure D-12. t = 157 seconds, Nominal System, -20 percent Variation in Attitude Sensor Bending Pickup

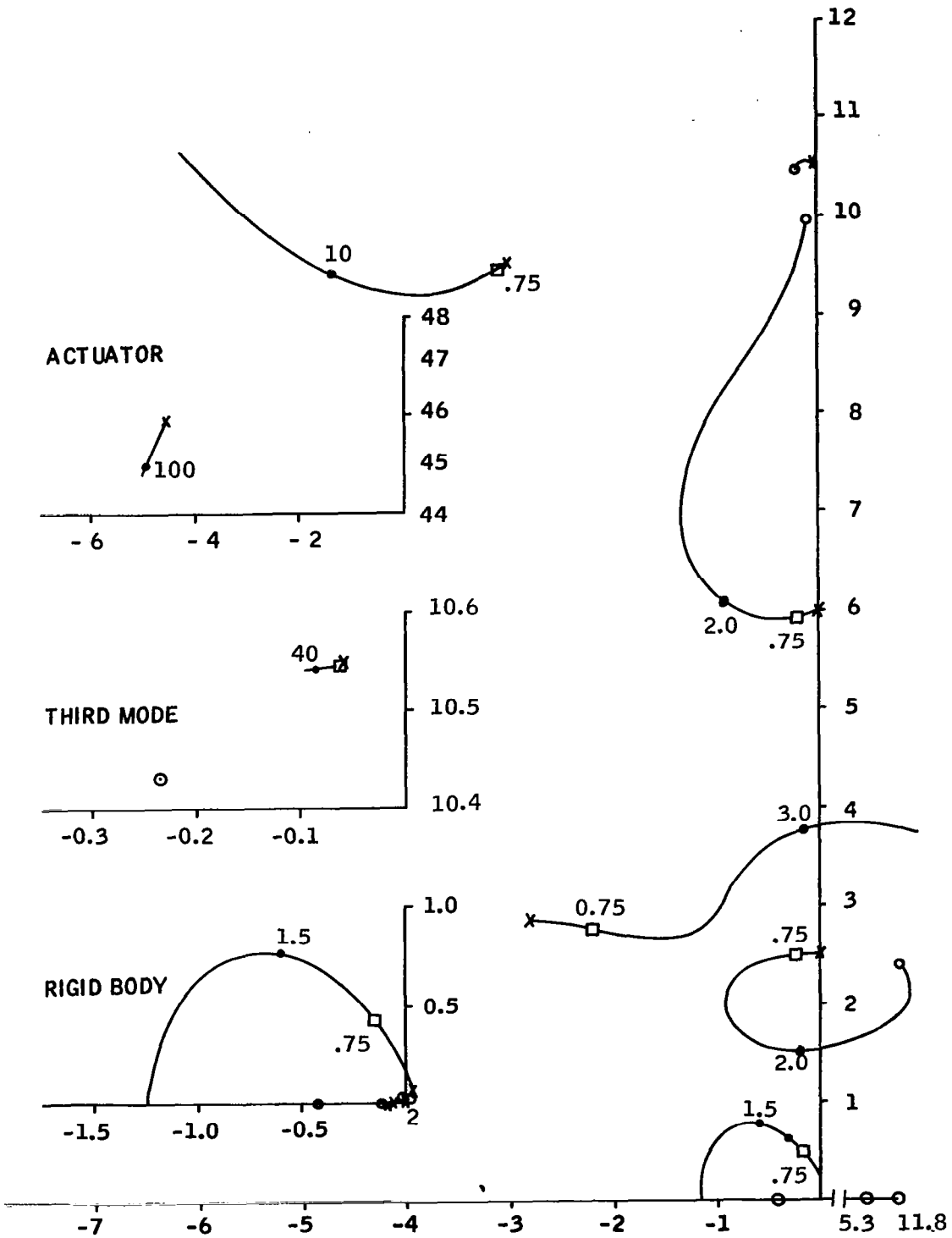

Figure D-13. t = 8 seconds, Nominal System, +20 percent Variation in Bending Frequencies

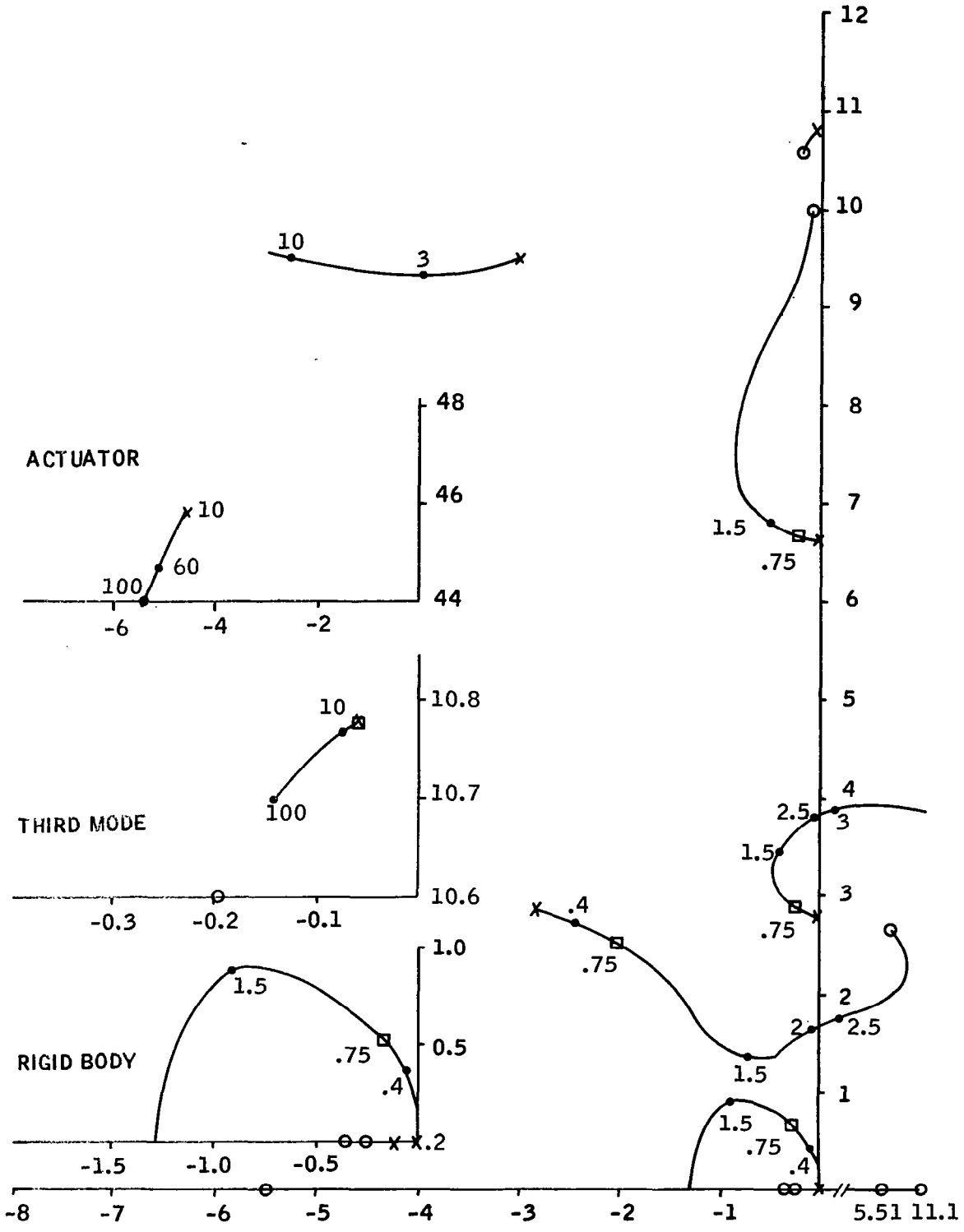

Figure D-14. t = 64 seconds, Nominal System, +20 percent Variation in Bending Frequencies

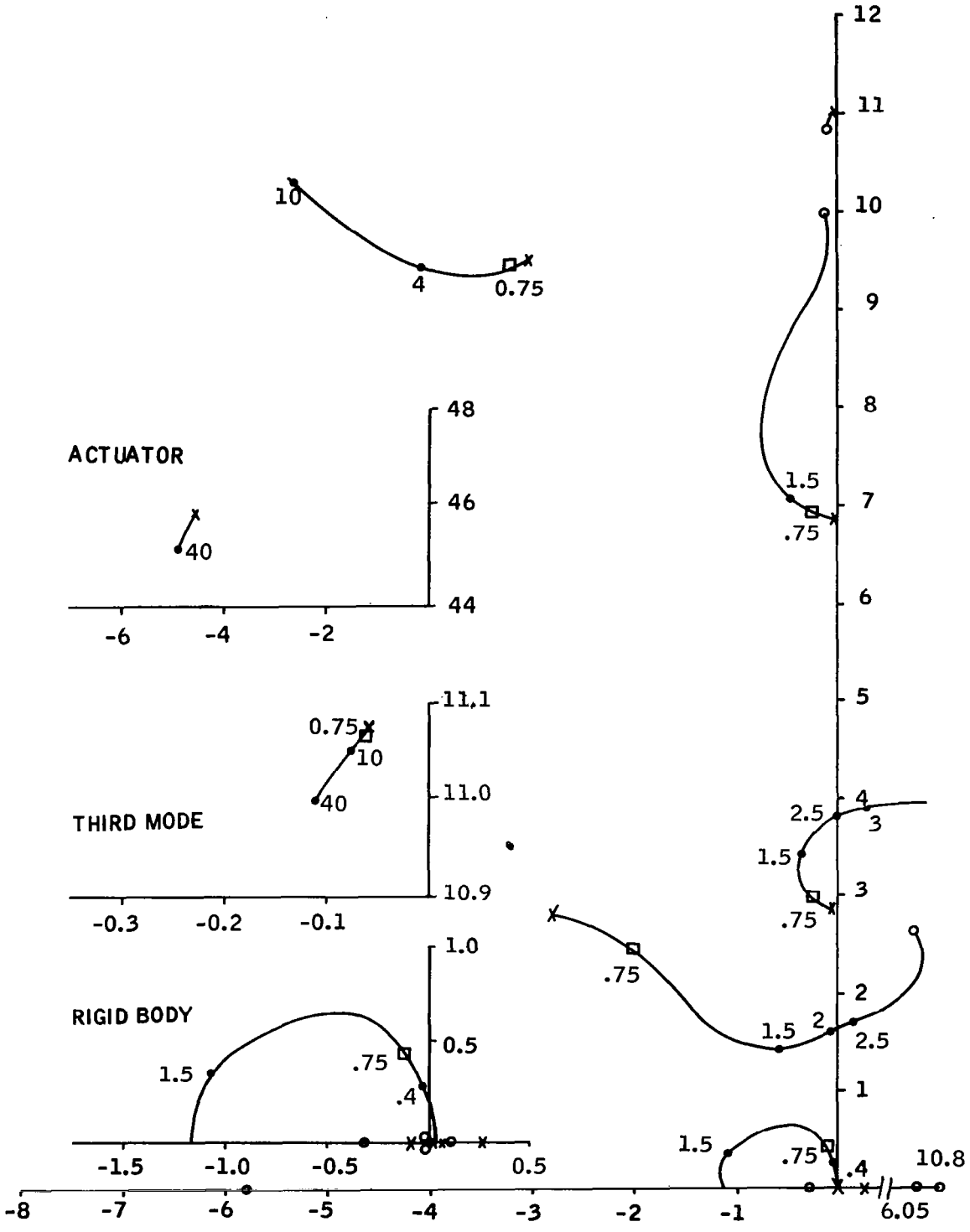

Figure D-15. t = 80 seconds, Nominal System, +20 percent Variation in Bending Frequencies

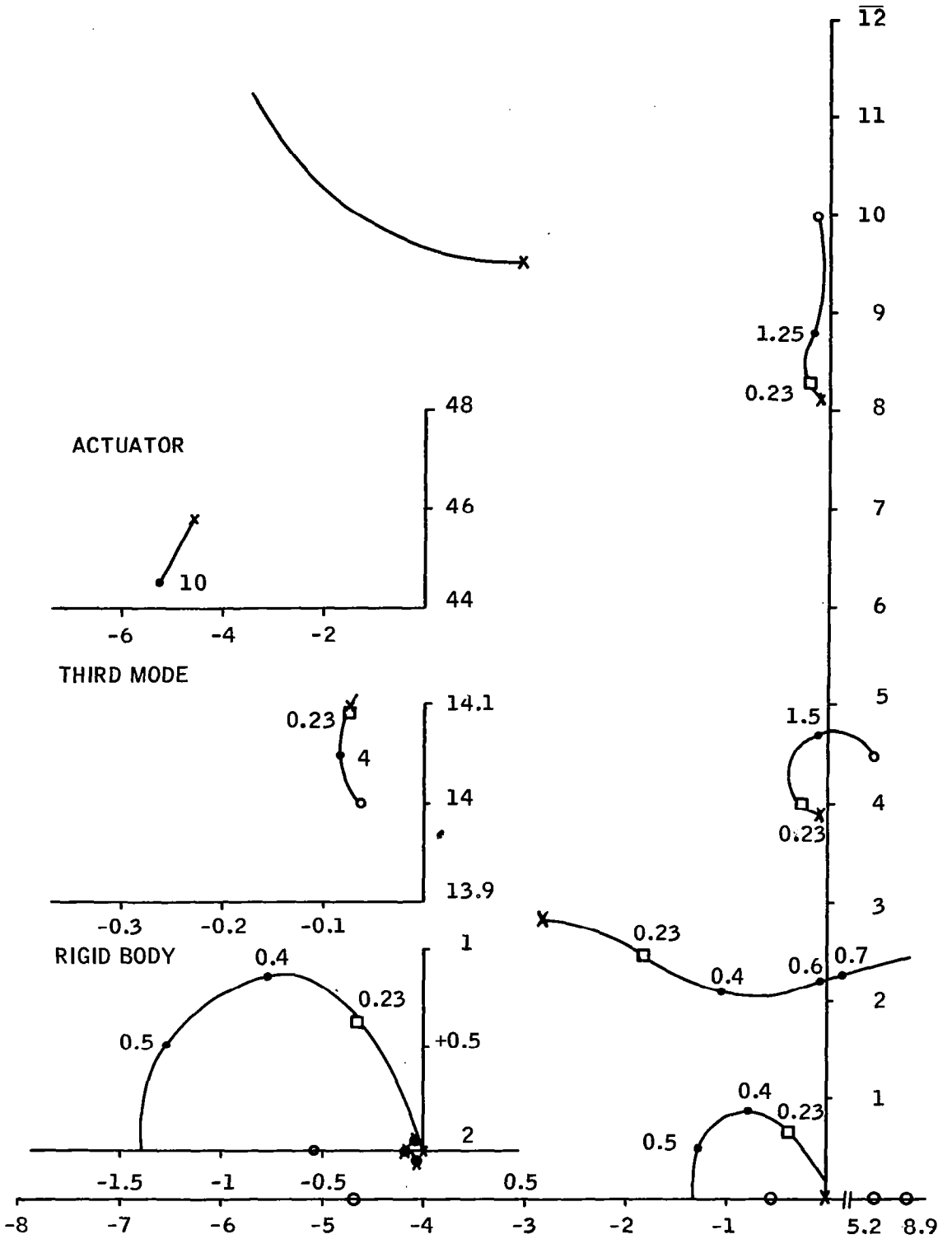

Figure D-16. t = 157 seconds, Nominal System, +20 percent Variation in Bending Frequencies

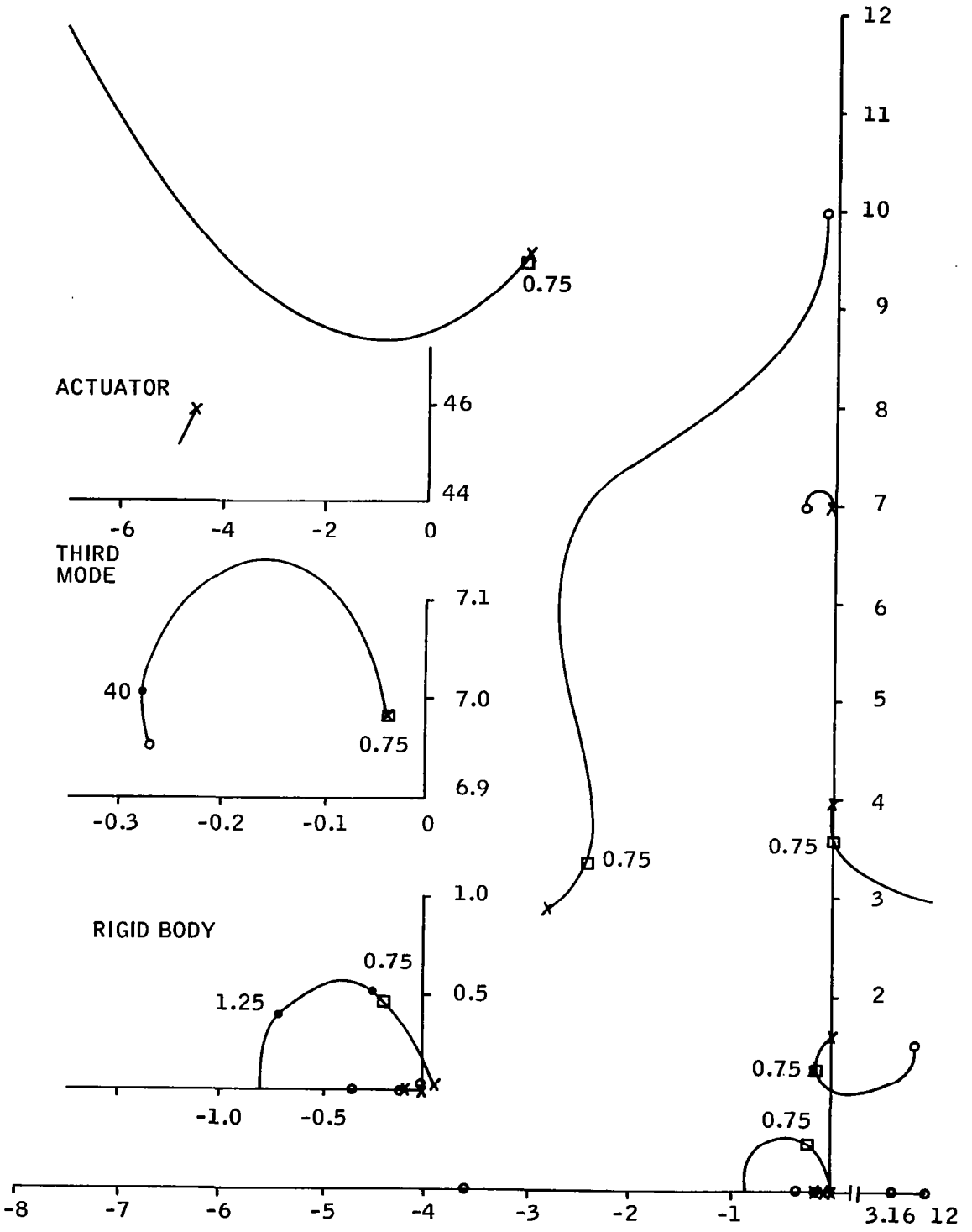

Figure D-17. t = 8 seconds, Nominal System, -20 percent Variation in Bending Frequencies

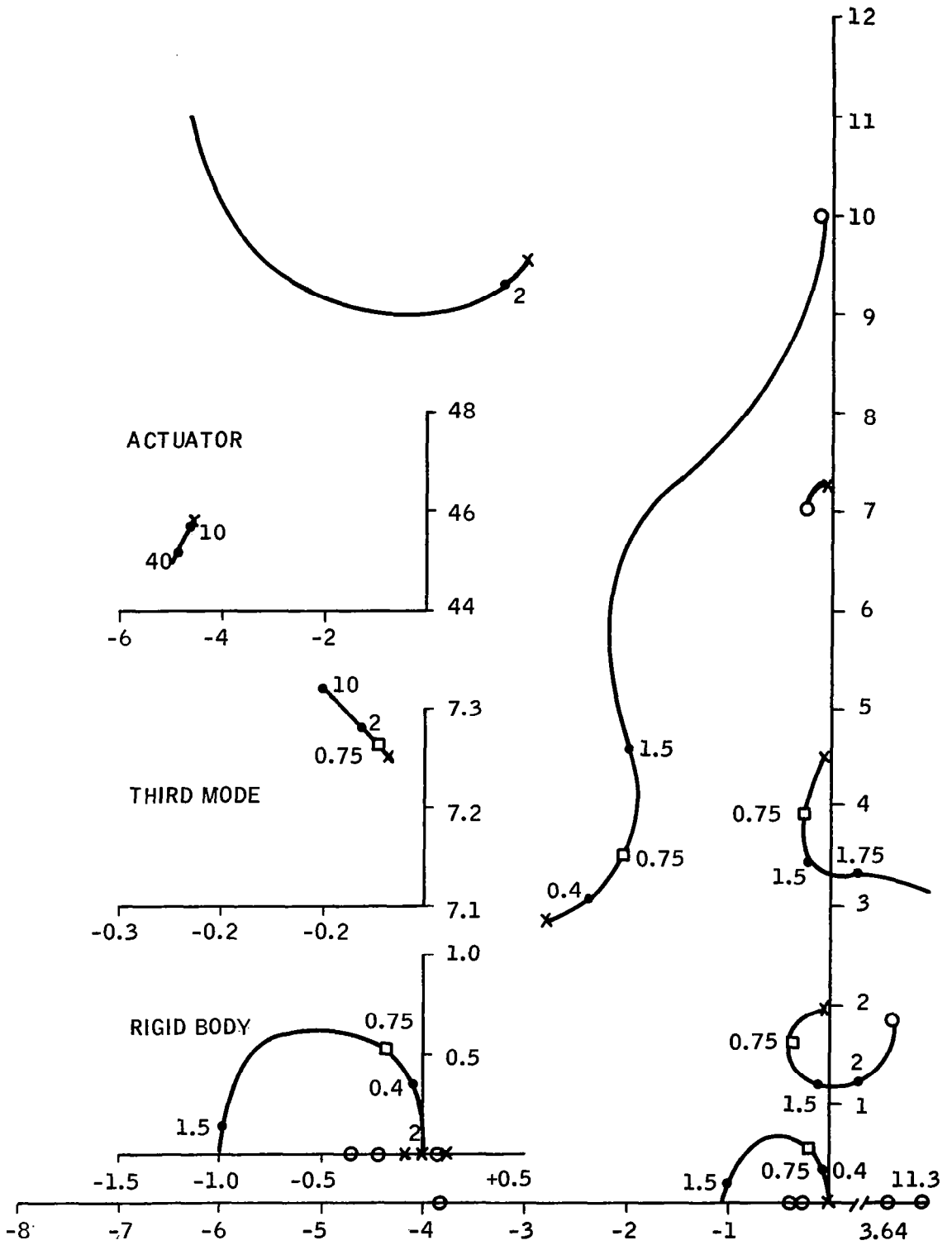

Figure D-18. t = 64 seconds, Nominal System, -20 percent Variation in Bending Frequencies

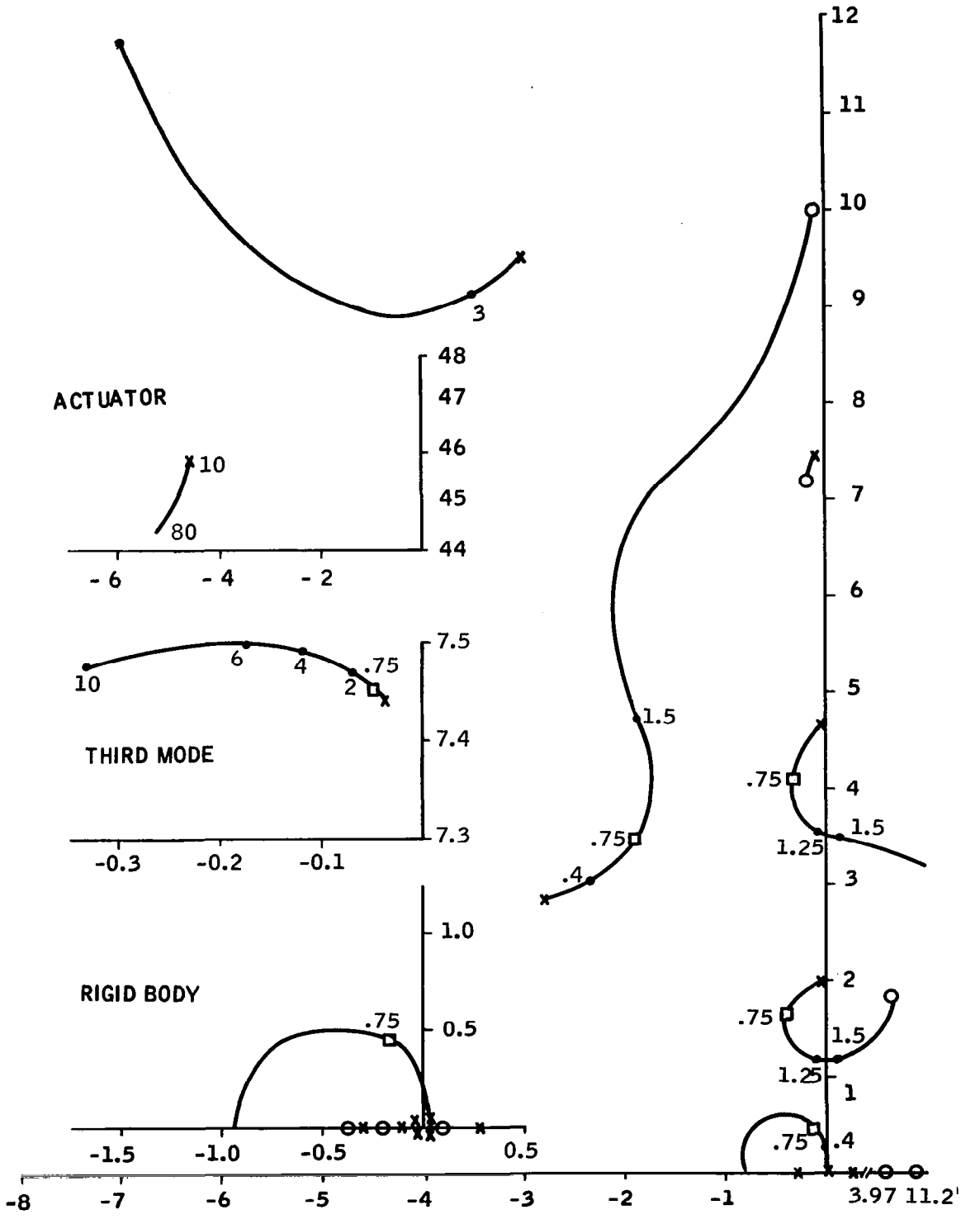

Figure D-19. t = 80 seconds, Nominal System, -20 percent Variation in Bending Frequencies

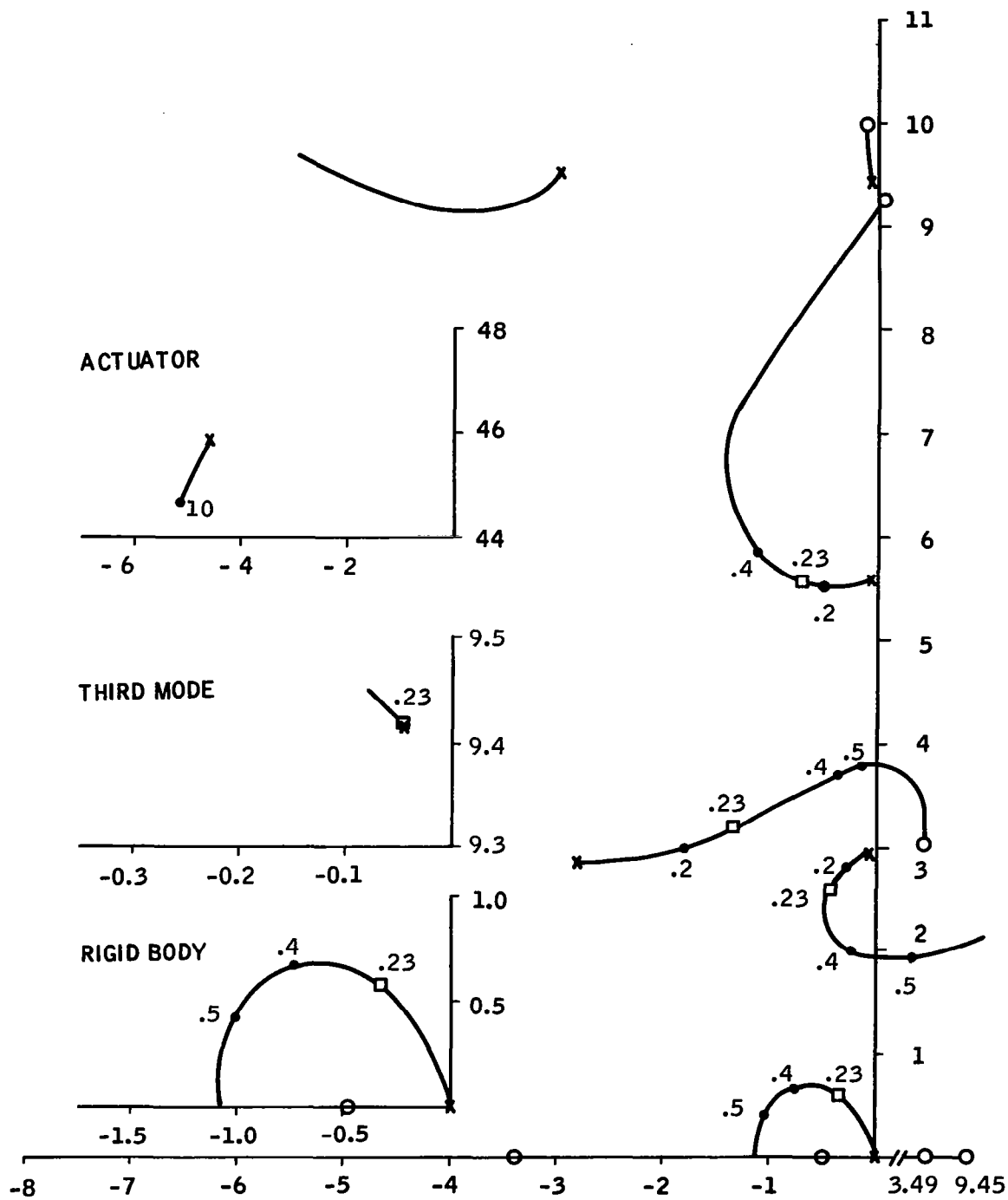

Figure D-20. t = 157 seconds, Nominal System, -20 percent Variation in Bending Frequencies

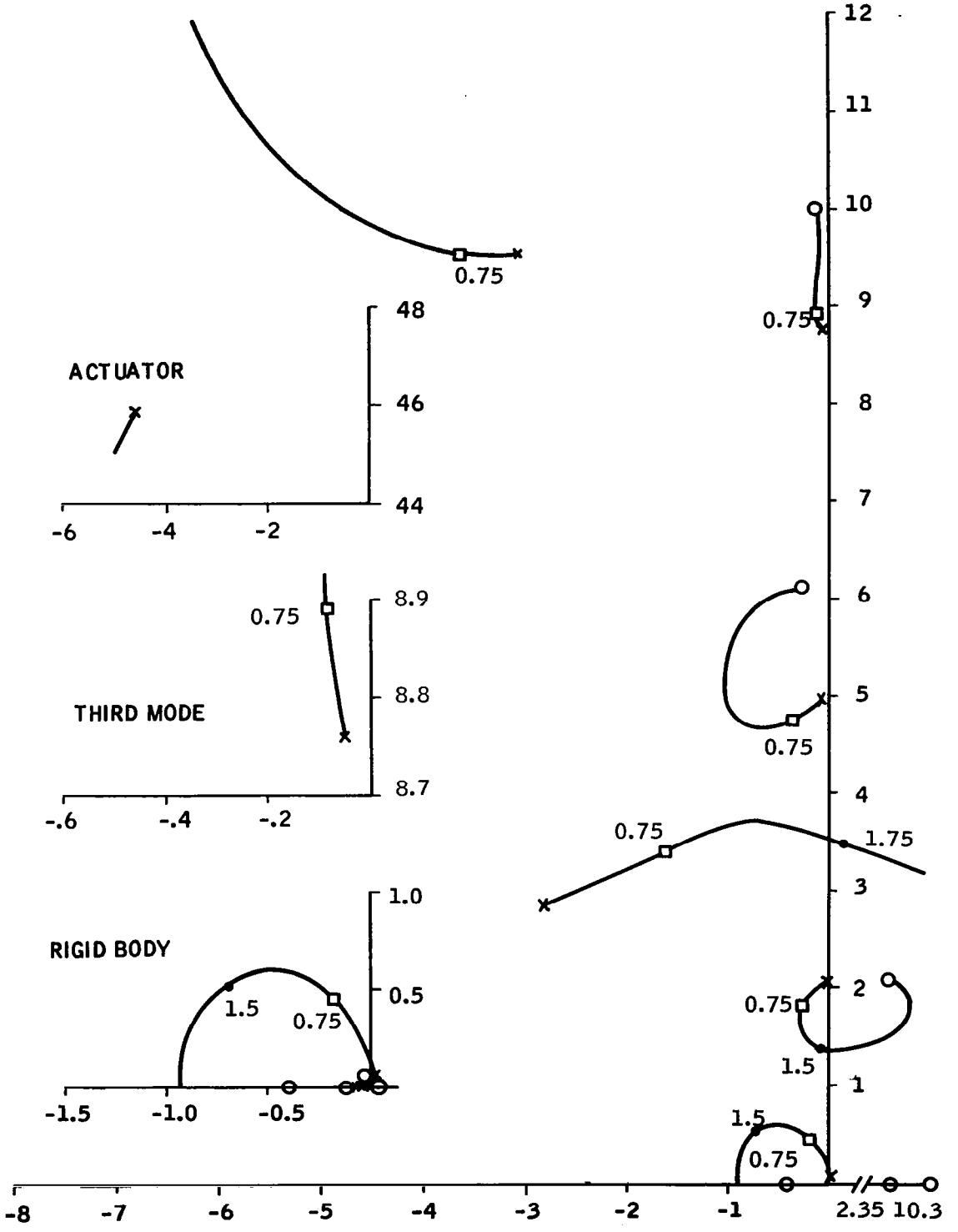

Figure D-21. t = 8 seconds, Nominal System, $Y'_1 = +0.01$, $Y'_2 = -0.06$, $Y'_3 = -0.2$

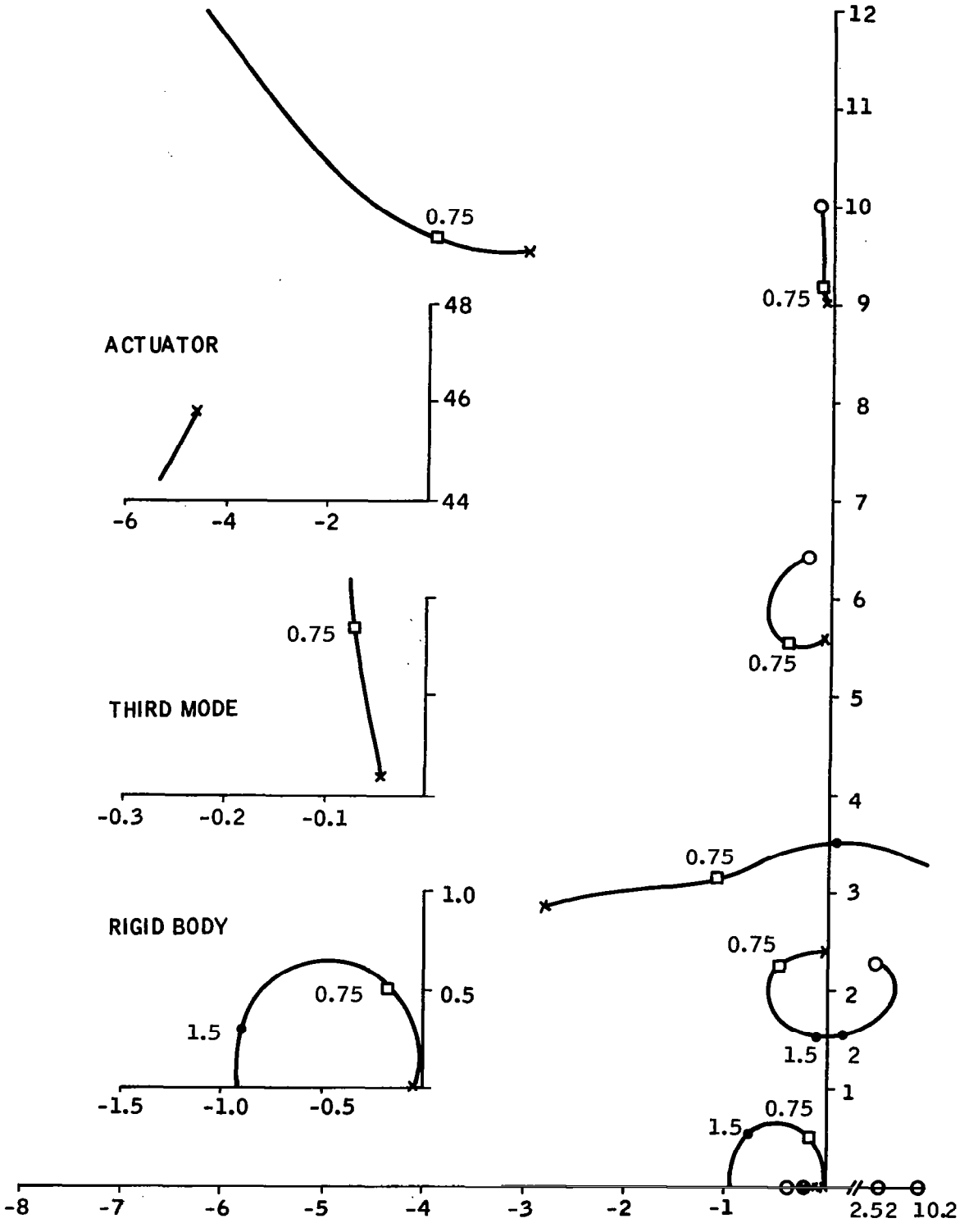

Figure D-22. t = 64 seconds, Nominal System, $Y'_1 = +0.01$, $Y'_2 = -0.06$, $Y'_3 = -0.2$

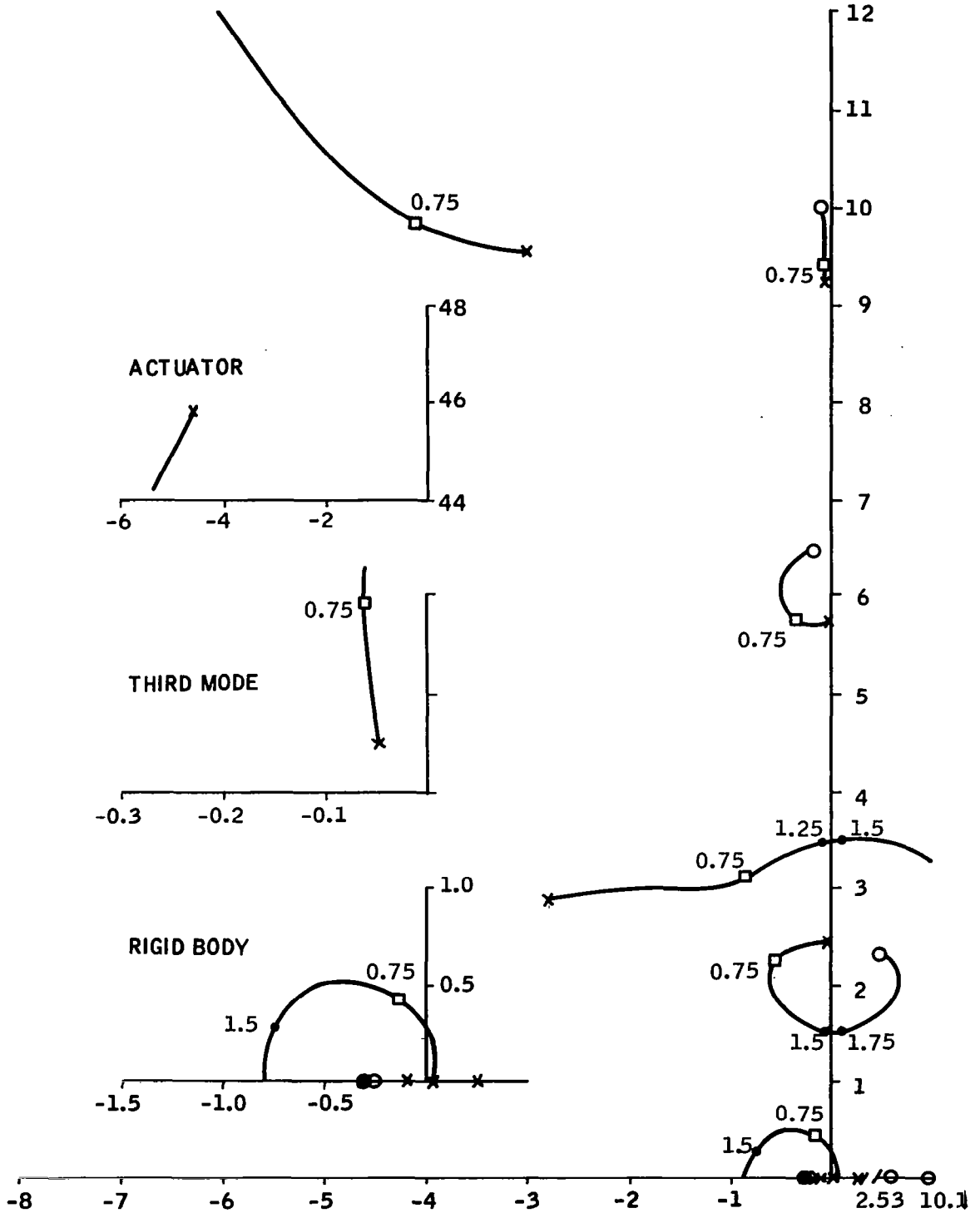

Figure D-23. t = 80 seconds, Nominal System, $Y'_1 = +0.01$, $Y'_2 = -0.06$, $Y'_3 = -0.2$

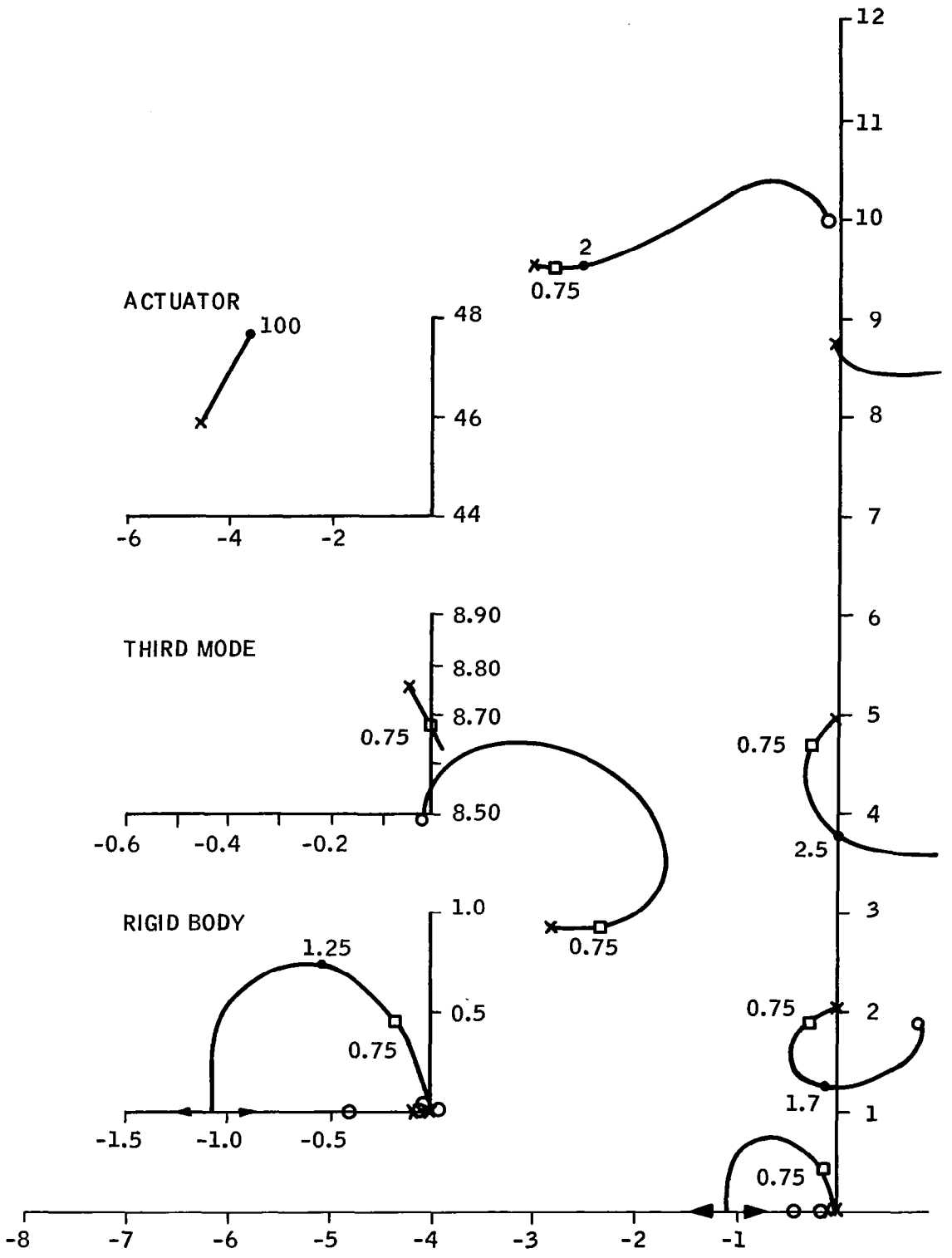

Figure D-24. $t = 8$ seconds, Nominal System, $Y'_1 = +0.01$, $Y'_2 = -0.06$, $Y'_3 = +0.1$

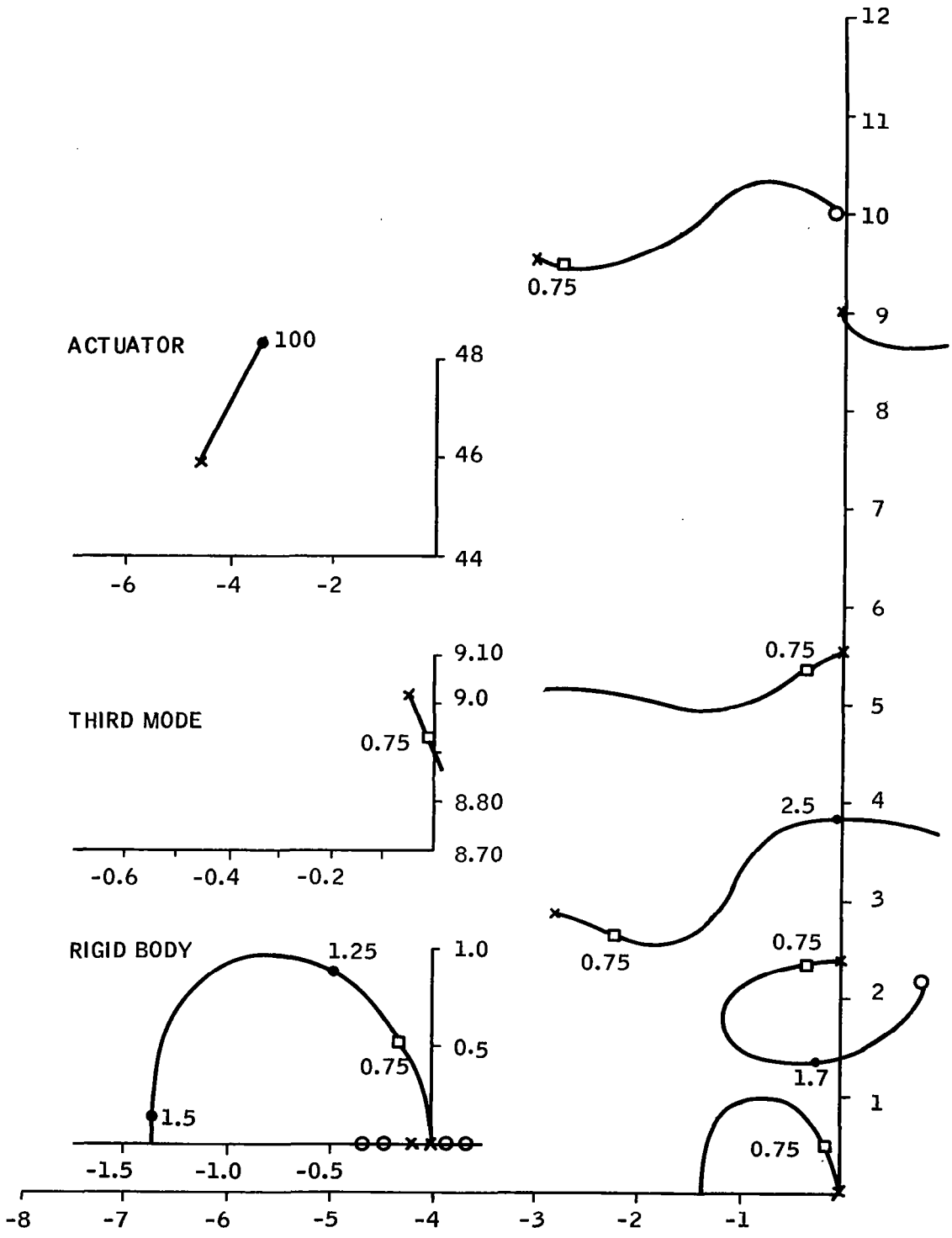

Figure D-25. t = 64 seconds, Nominal System, $Y'_1 = +0.01$, $Y'_2 = -0.06$, $Y'_3 = +0.1$

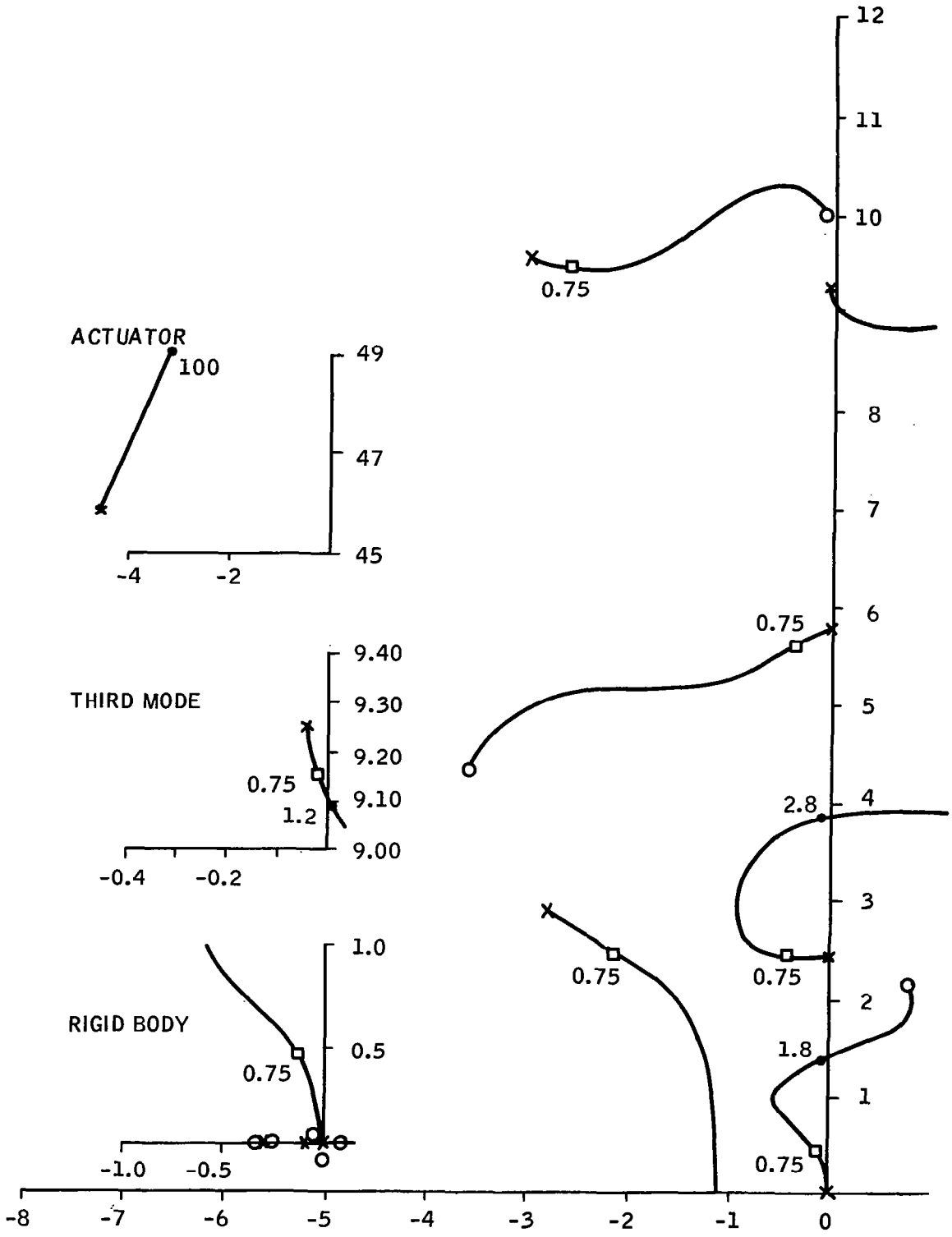

Figure D-26. t = 80 seconds, Nominal System, $Y'_1 = +0.01$, $Y'_2 = -0.06$, $Y'_3 = +0.1$

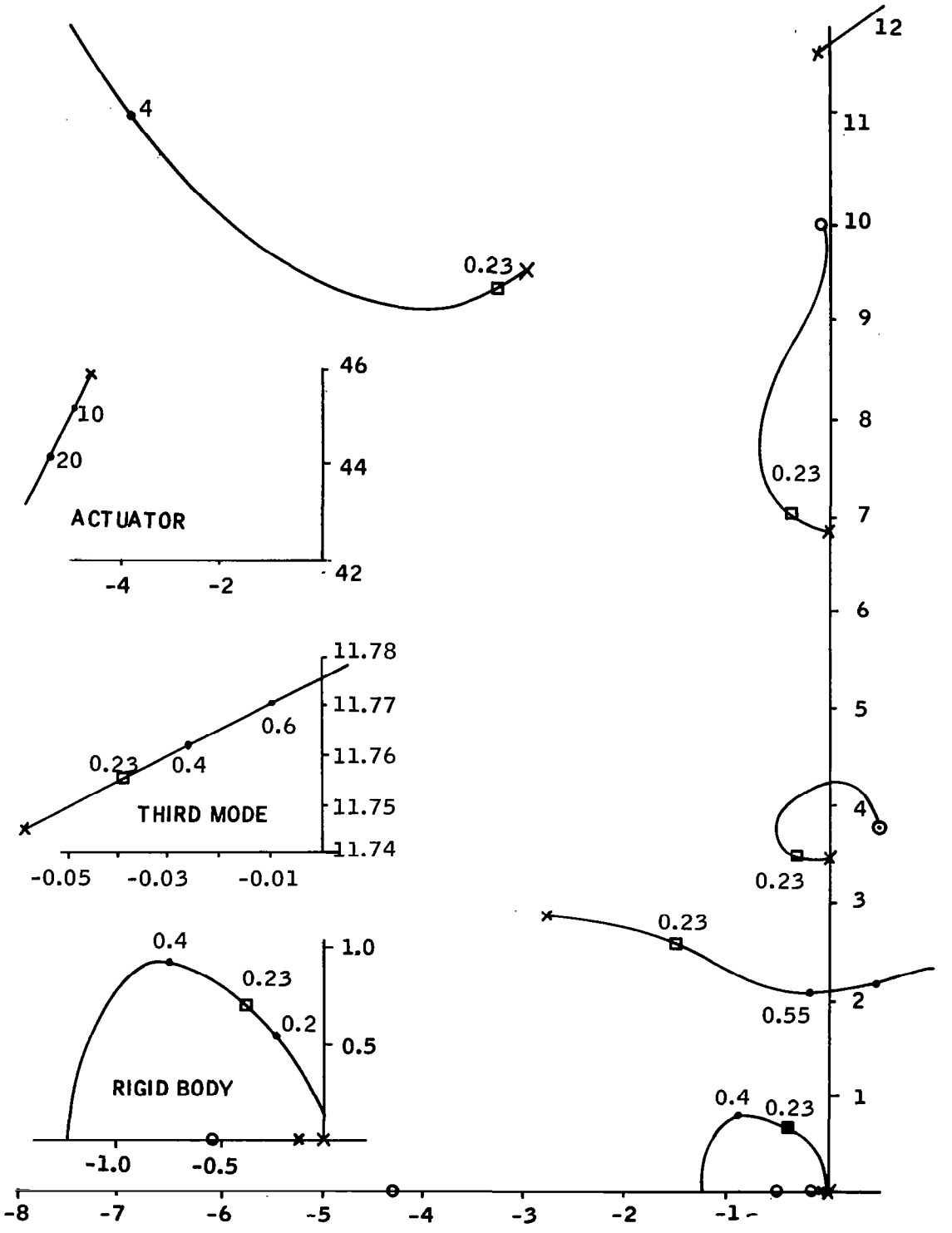

Figure D-27. t = 157 seconds, Nominal System, $Y'_1 = -0.01$, $Y'_2 = -0.06$, $Y'_3 = +0.1$

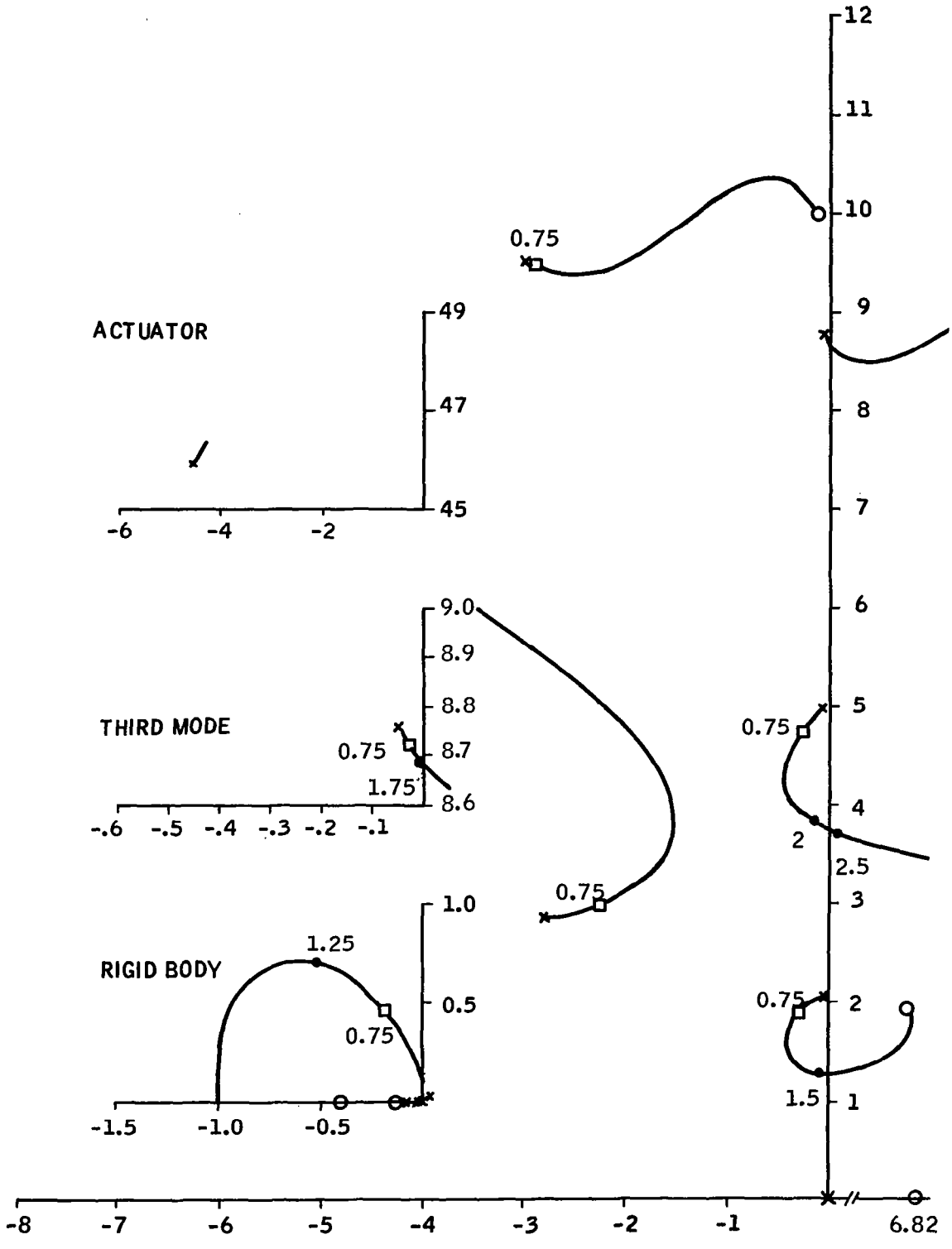

Figure D-28. t = 8 seconds, Nominal System, $Y'_1 = +0.01$, $Y'_2 = -0.06$, $Y'_3 = +0.05$

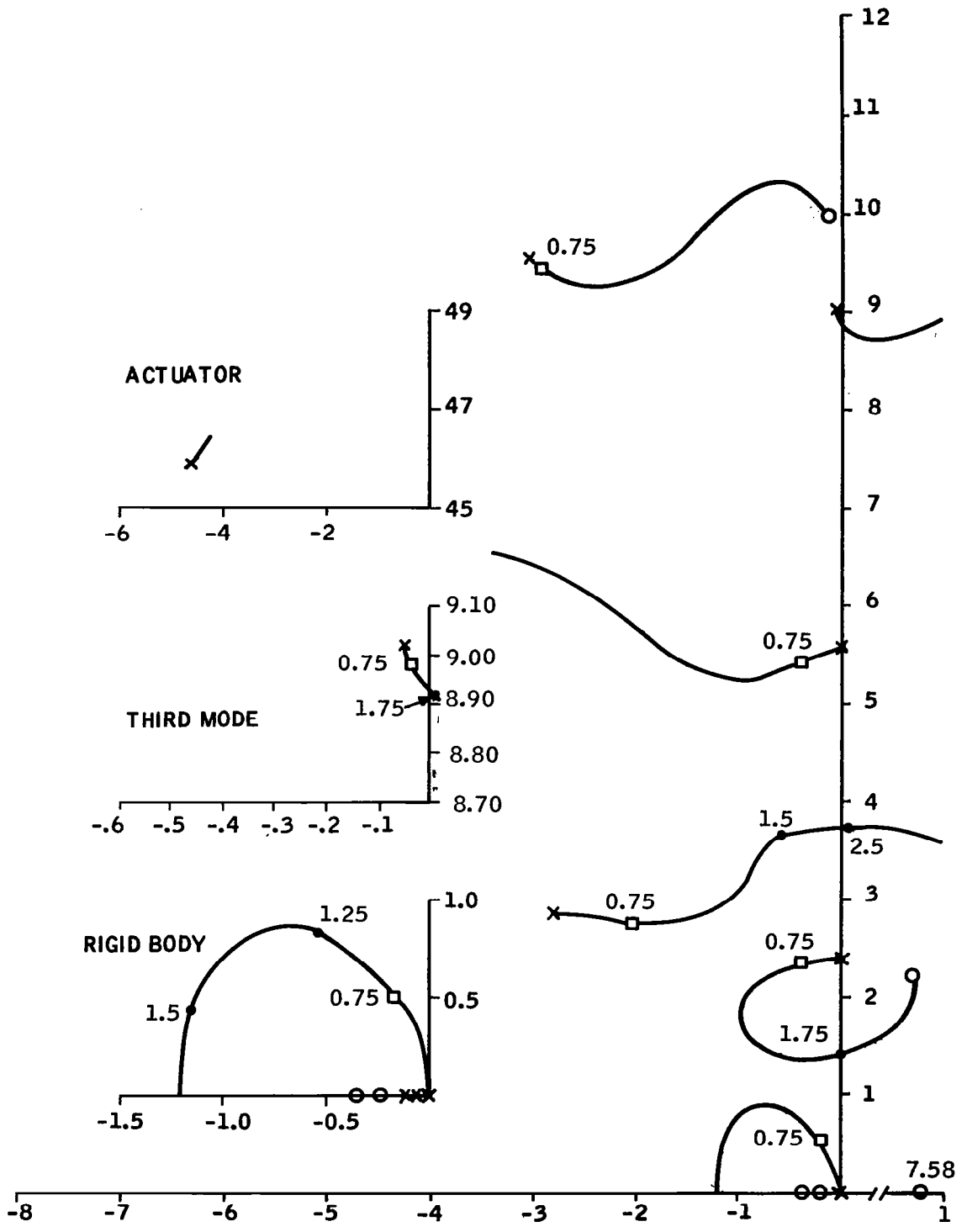

Figure D-29. $t = 64$ seconds, Nominal System, $Y'_1 = +0.01$, $Y'_2 = -0.06$, $Y'_3 = +0.05$

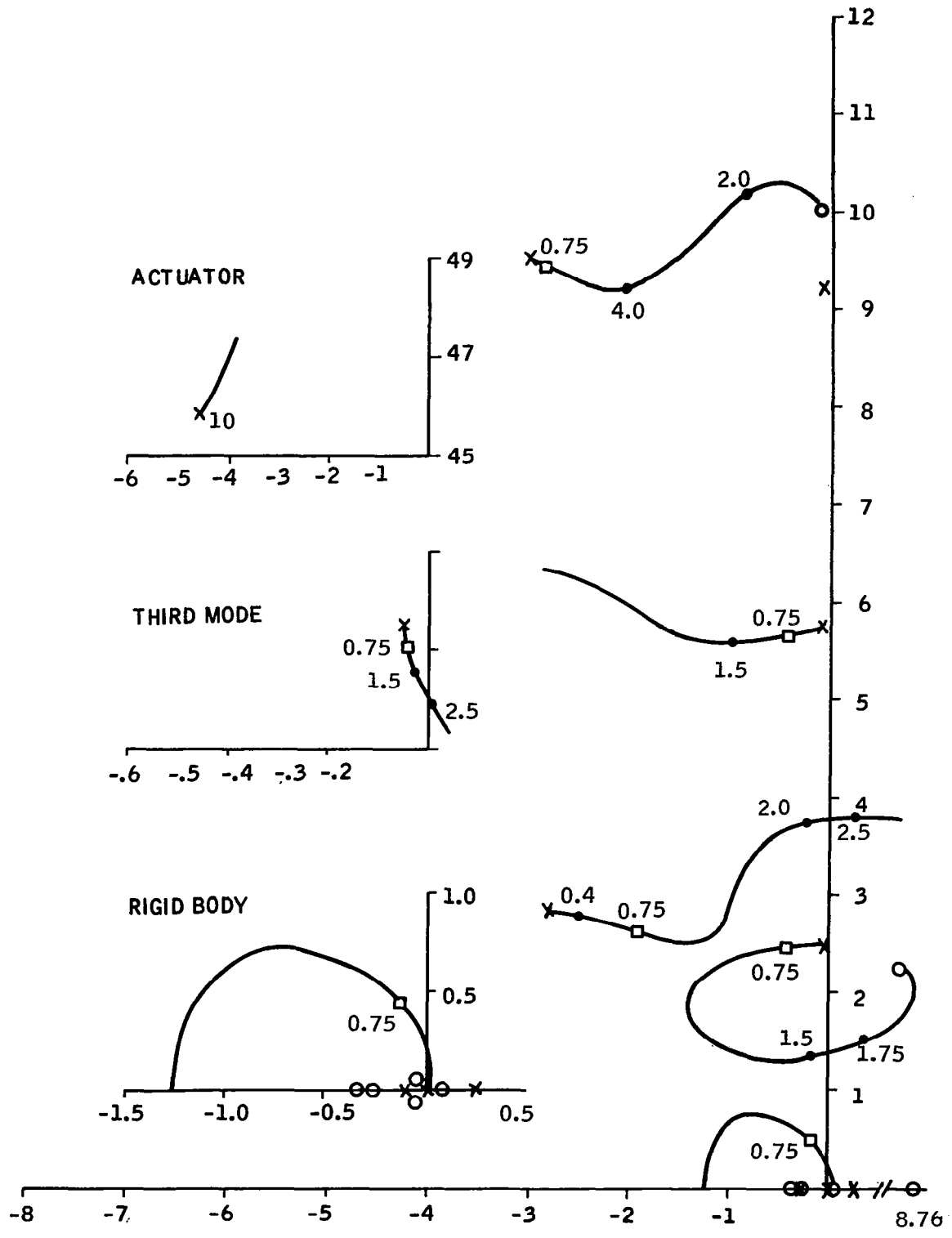

Figure D-30. $t = 80$ seconds, Nominal System, $Y'_1 = +0.01$, $Y'_2 = -0.06$, $Y'_3 = +0.05$

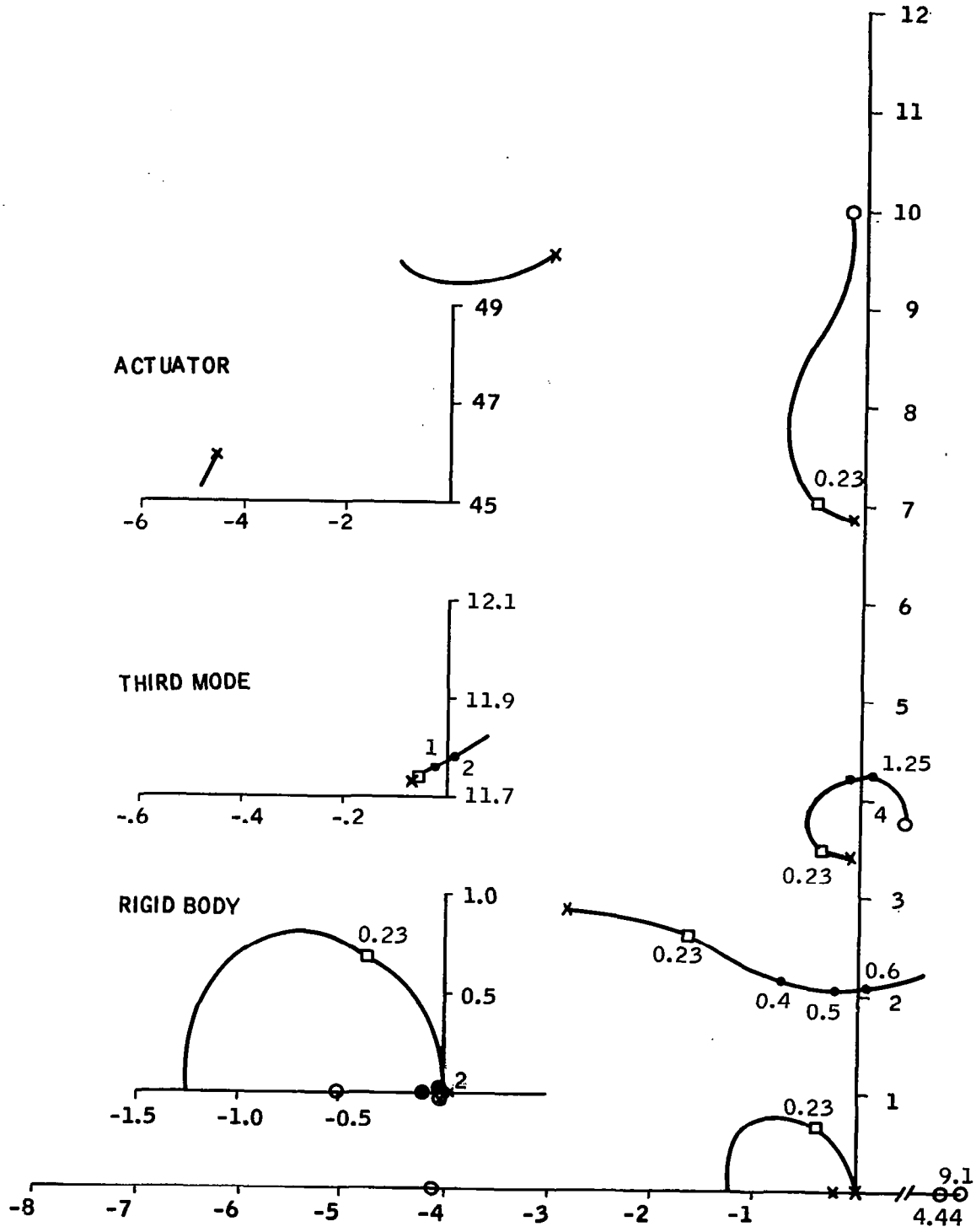

Figure D-31. t = 157 seconds, Nominal System, $Y'_1 = +0.01$ $Y'_2 = -0.06$, $Y'_3 = +0.05$

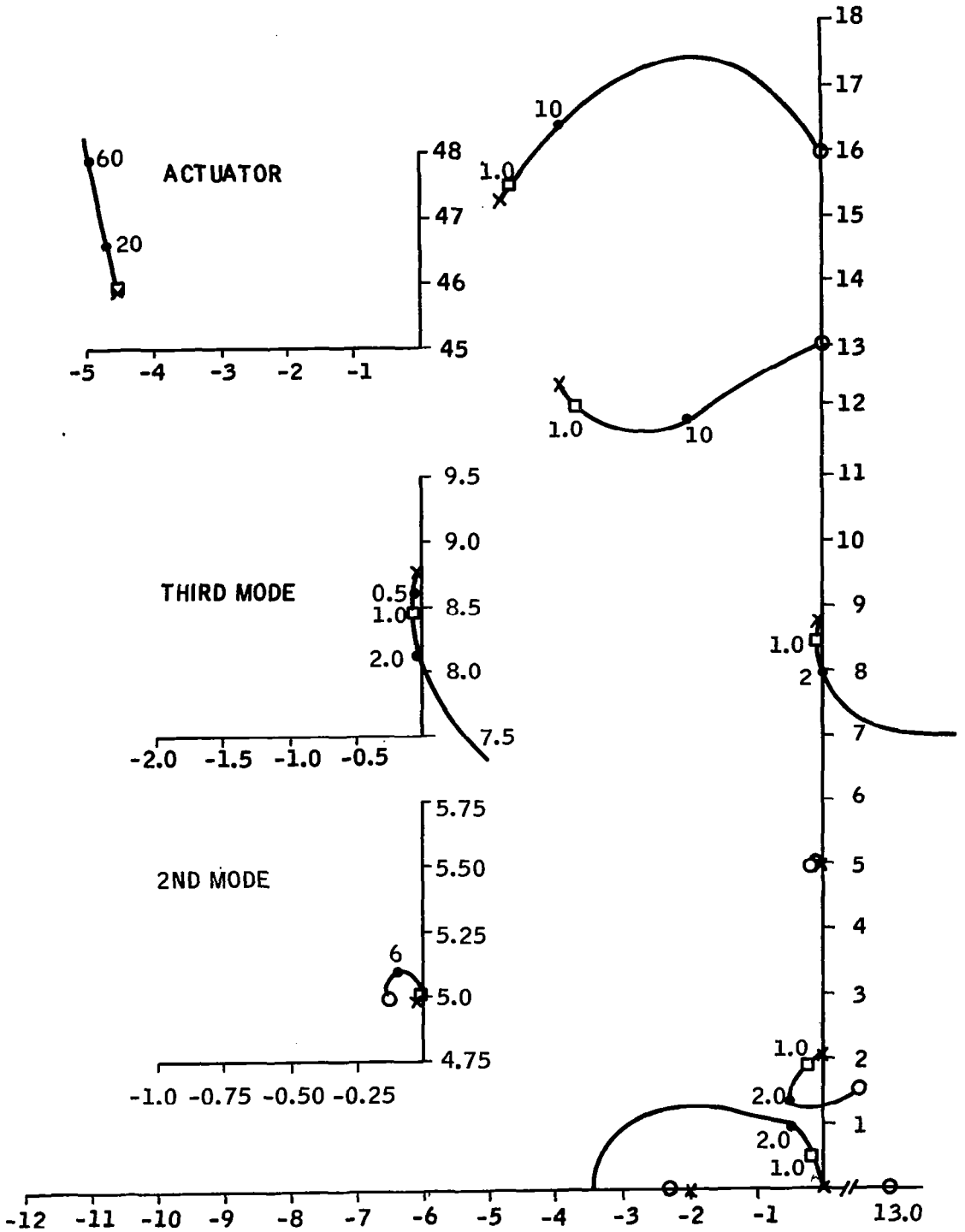

Figure D-32. t = 8 seconds, Nominal Multiple Blender System, $K_A = 0.479$, $K_B = 0.753$, $K_C = 0.344$

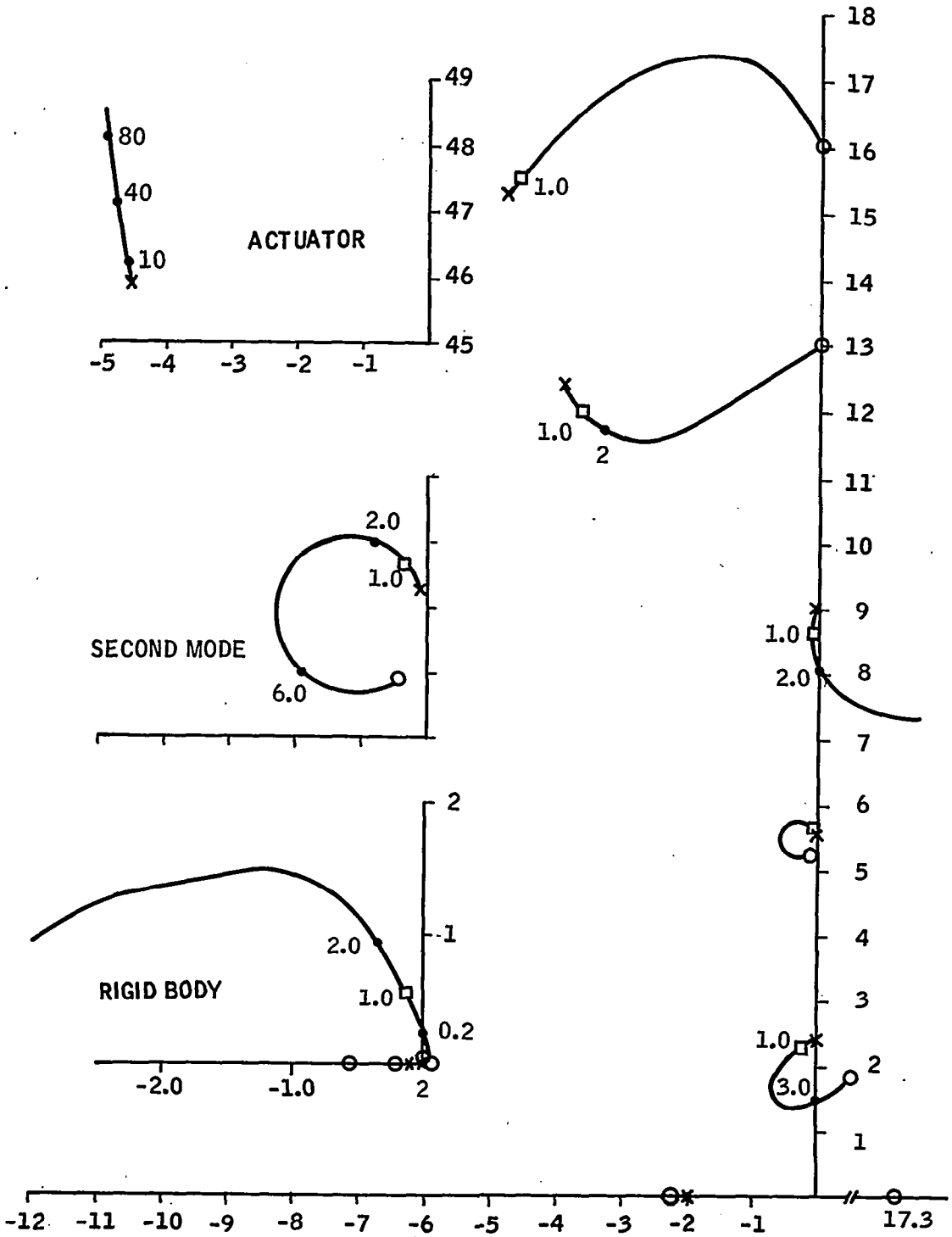

Figure D-33. t = 64 seconds, Nominal Multiple Blender System, $K_A = 0.448$, $K_B = 0.748$, $K_C = 0.349$

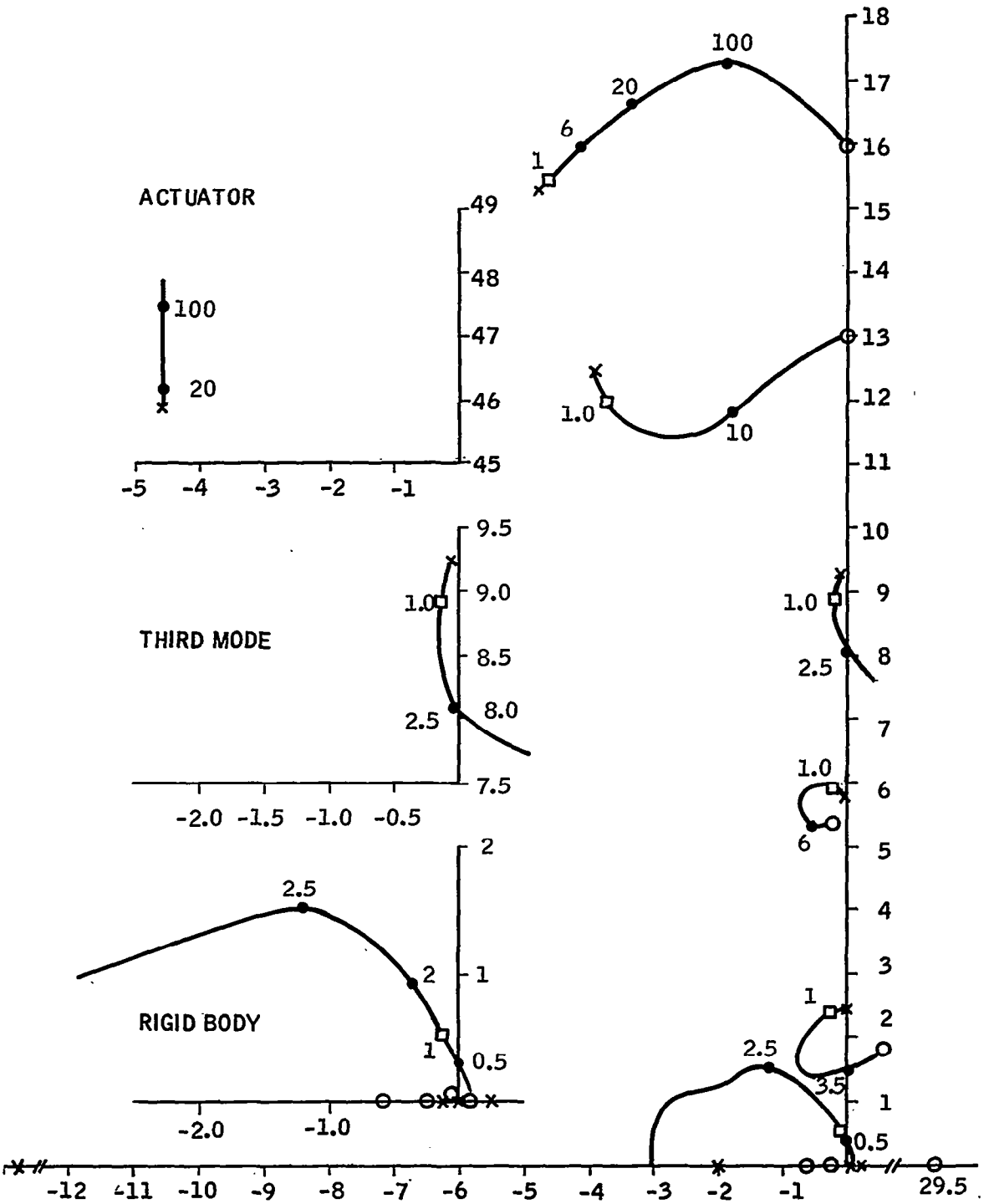

Figure D-34. t = 80 seconds, Nominal Multiple Blender System, $K_A = 0.434$, $K_B = 0.743$, $K_C = 0.397$

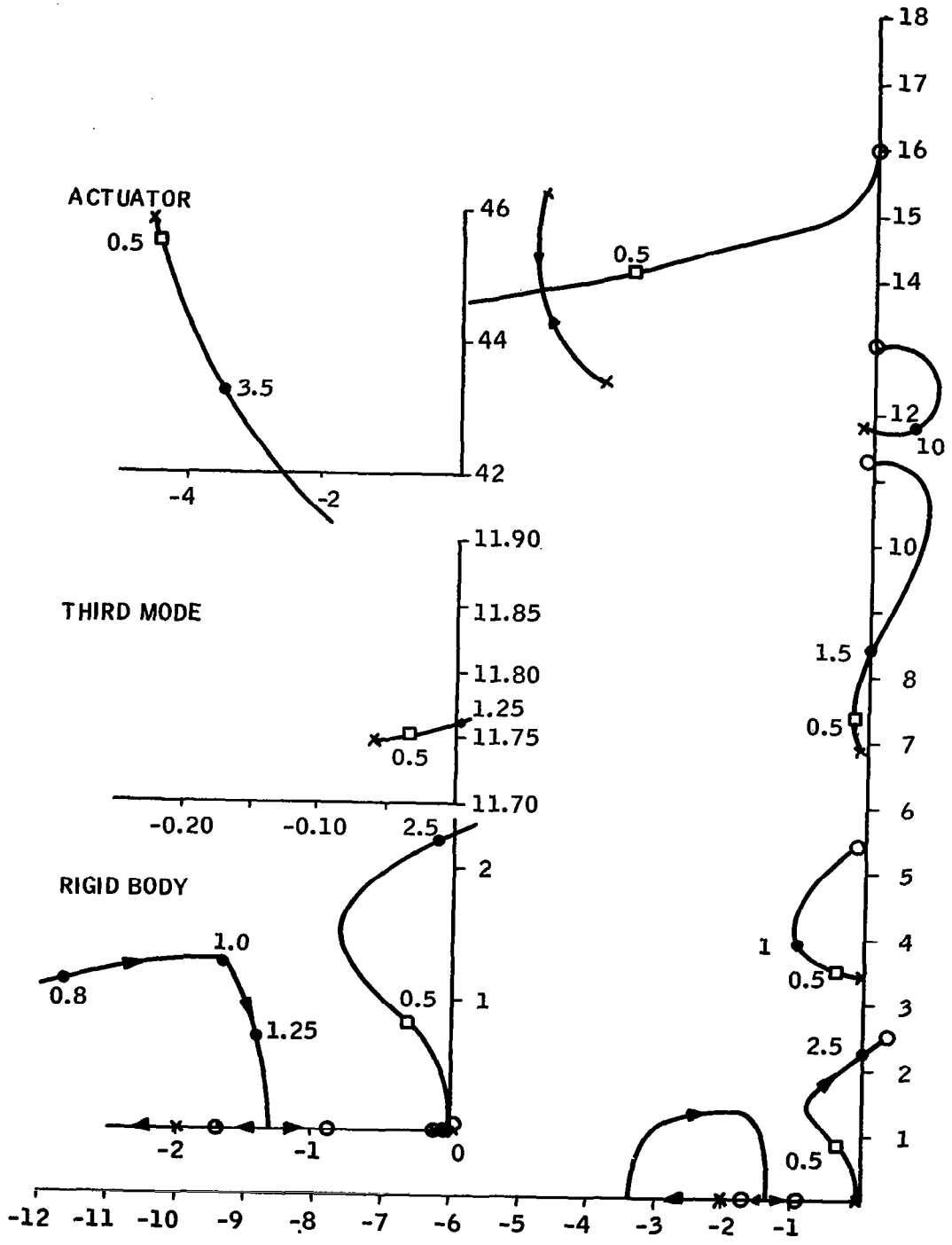

Figure D-35. t = 157 seconds, Nominal Multiple Blender System, $K_A = 0.210$, $K_B = 0.608$, $K_C = 0.40$

APPENDIX E
FREQUENCY RESPONSE PLOTS

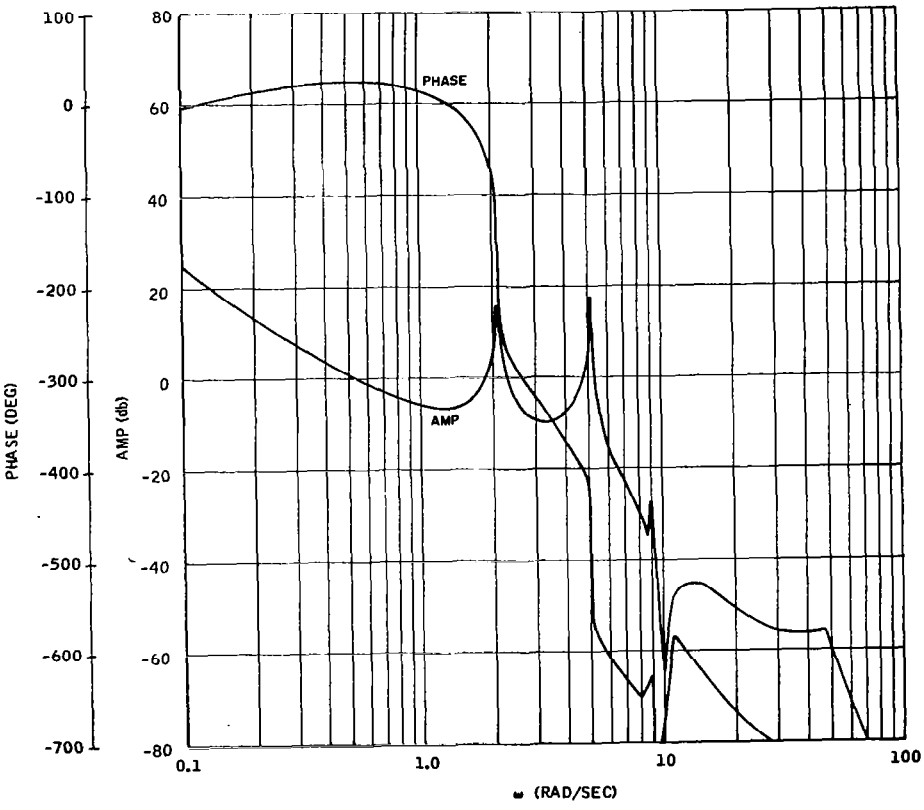

Figure E-1. $t = 8$ seconds, Nominal System, $Y'_1 = +0.01$, $Y'_2 = -0.06$, $Y'_3 = 0$

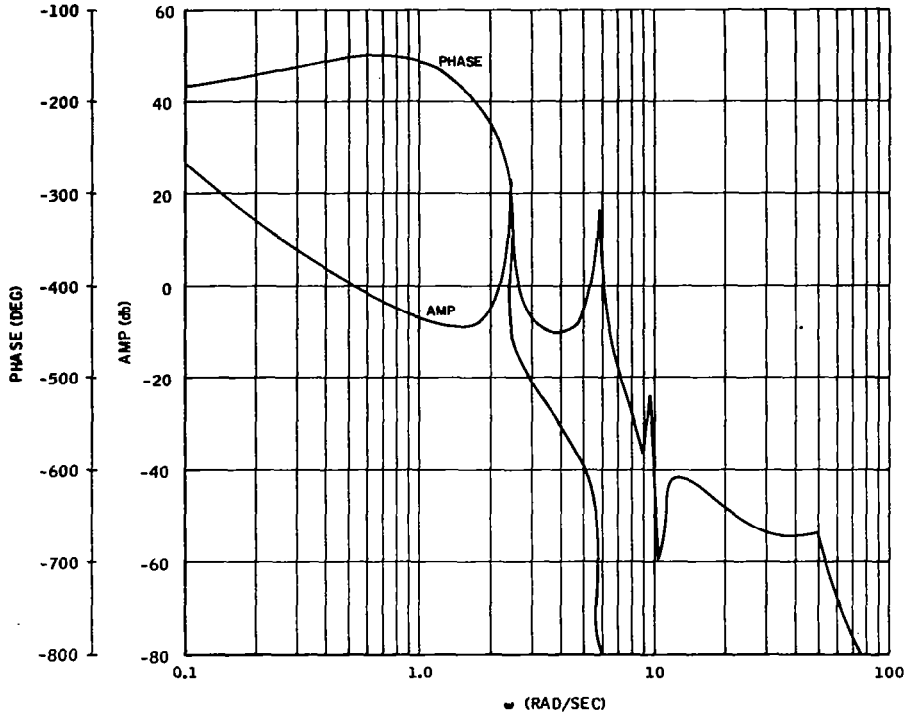

Figure E-2. t = 64 seconds, Nominal System, $Y'_1 = +0.01$, $Y'_2 = -0.06$, $Y'_3 = 0$

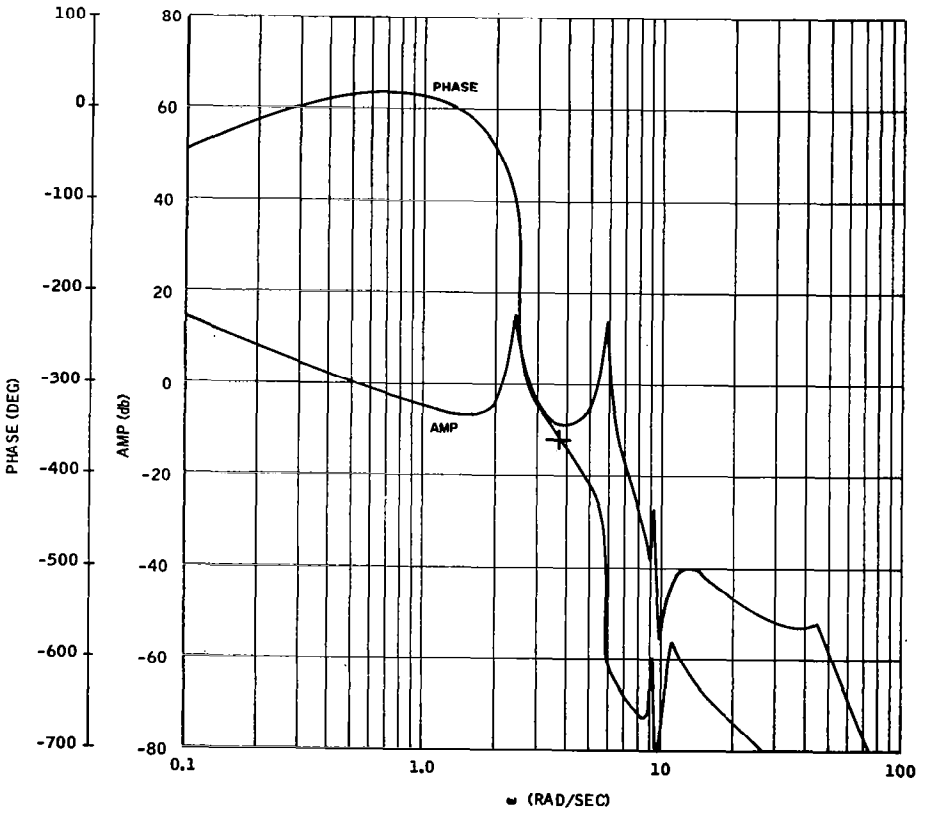

Figure E-3. t = 80 seconds, Nominal System, $Y'_1 = +0.01$, $Y'_2 = -0.06$, $Y'_3 = 0$

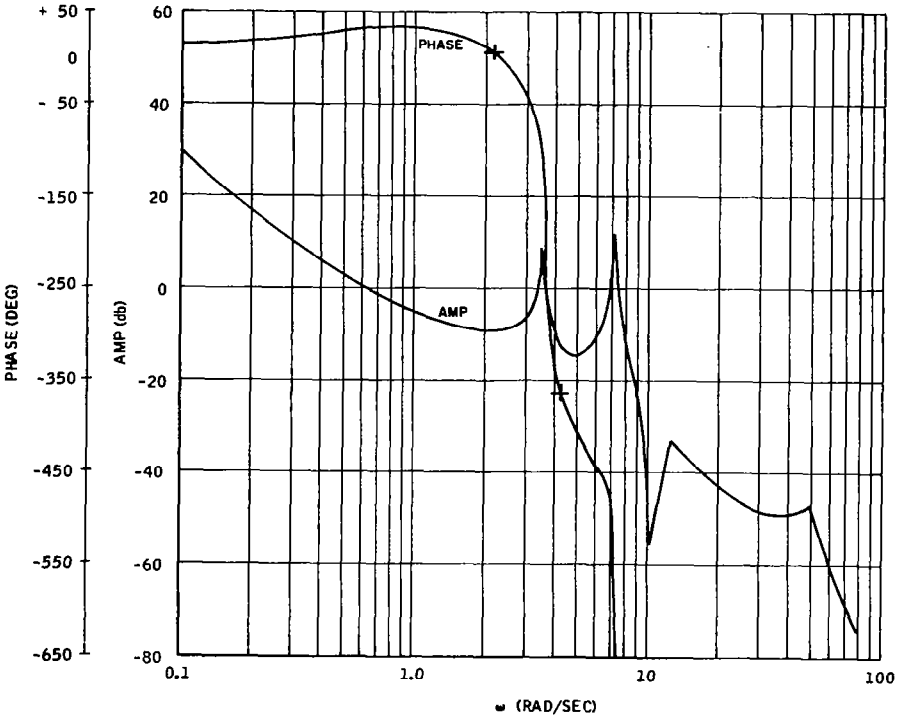

Figure E-4. t = 157 seconds, Nominal System, $Y'_1 = -0.01$, $Y'_2 = -0.06$, $Y'_3 = 0$

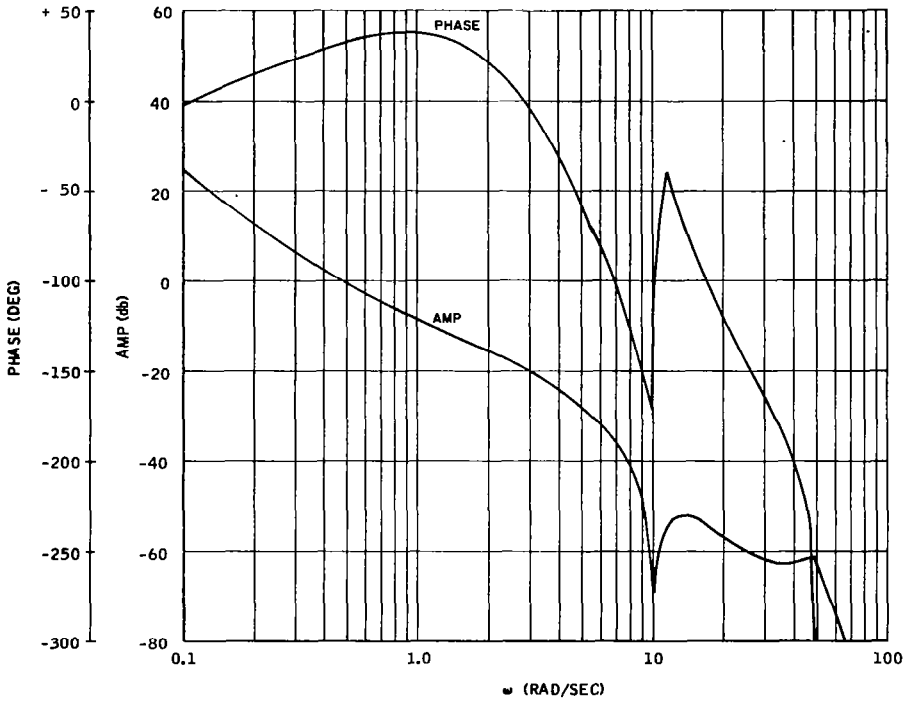

Figure E-5. t = 8 seconds, Nominal System, $Y'_1 = -0.01$, $Y'_2 = -0.06$, $Y'_3 = 0$, Rigid Vehicle

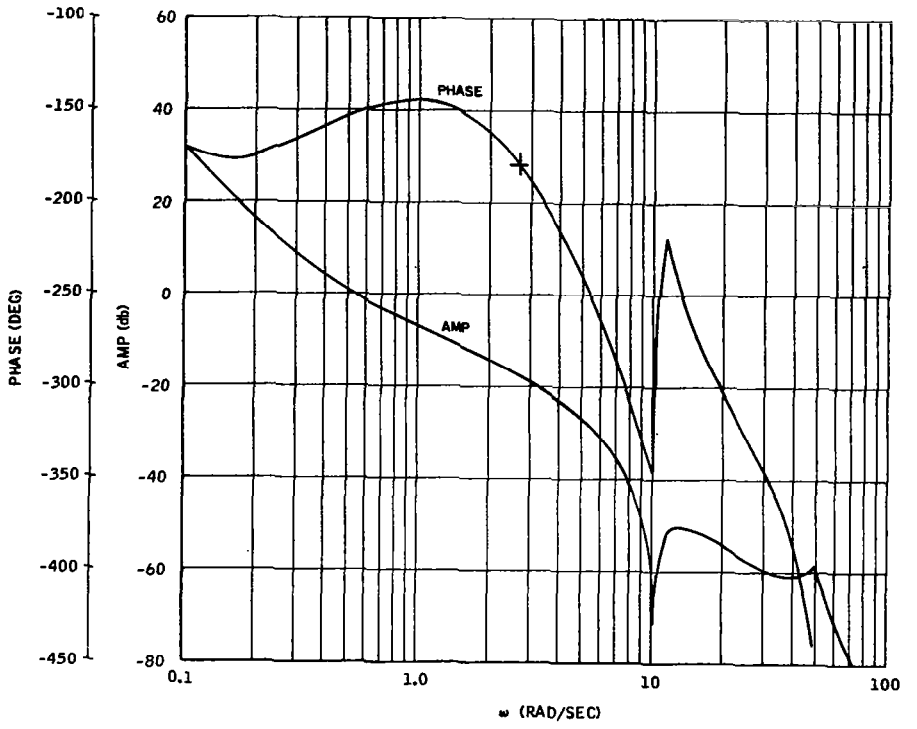

Figure E-6. t = 64 seconds, Nominal System, $Y'_1 = -0.01$, $Y'_2 = -0.06$, $Y'_3 = 0$, Rigid Vehicle

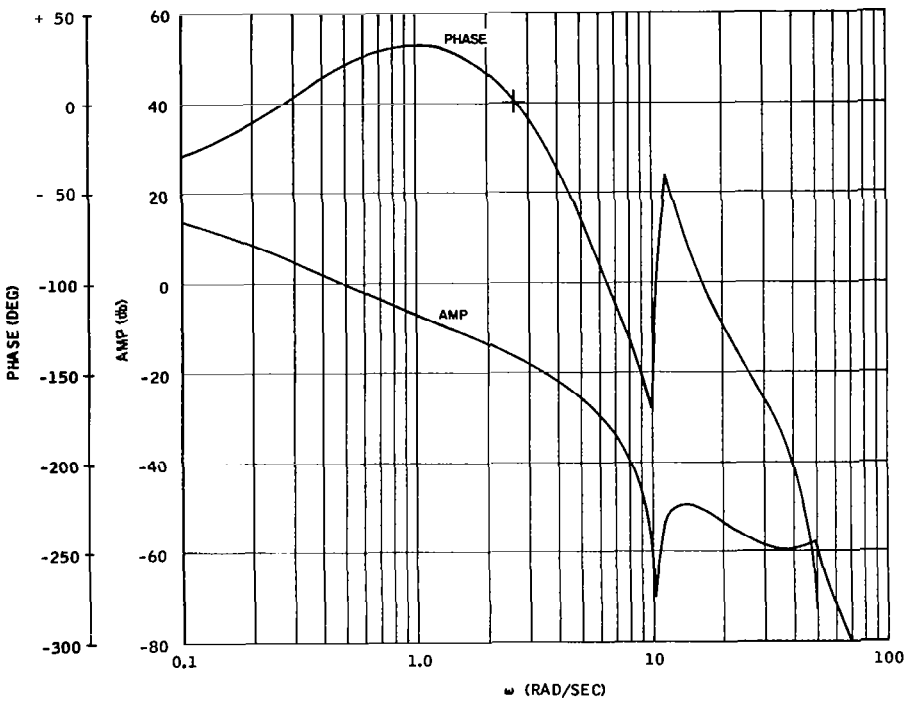

Figure E-7. t = 80 seconds, Nominal System, $Y'_1 = -0.01$, $Y'_2 = -0.06$, $Y'_3 = 0$, Rigid Vehicle

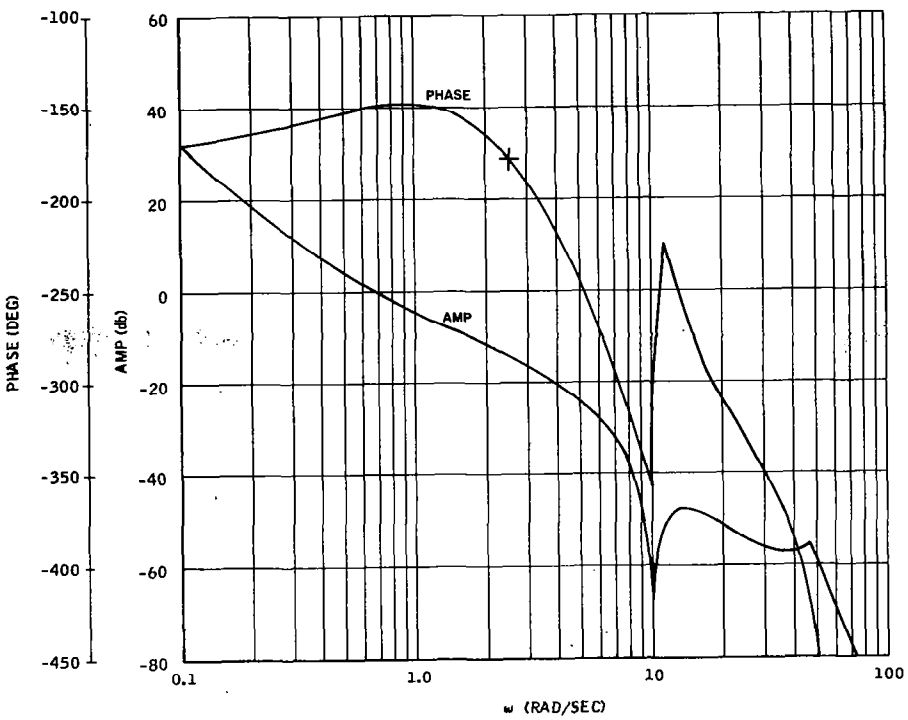

Figure E-8. t = 157 seconds, Nominal System, $Y'_1 = -0.01$, $Y'_2 = -0.06$, $Y'_3 = 0$, Rigid Vehicle

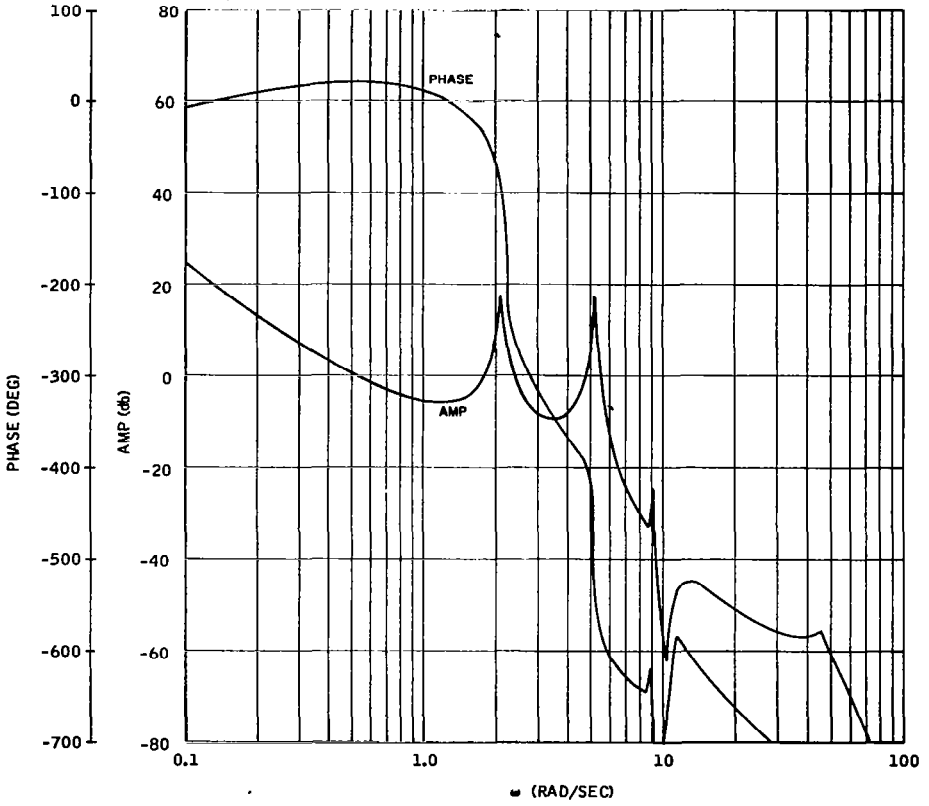

Figure E-9. t = 8 seconds, Nominal System, +20 percent Variation in Attitude Sensor Bending Pickup

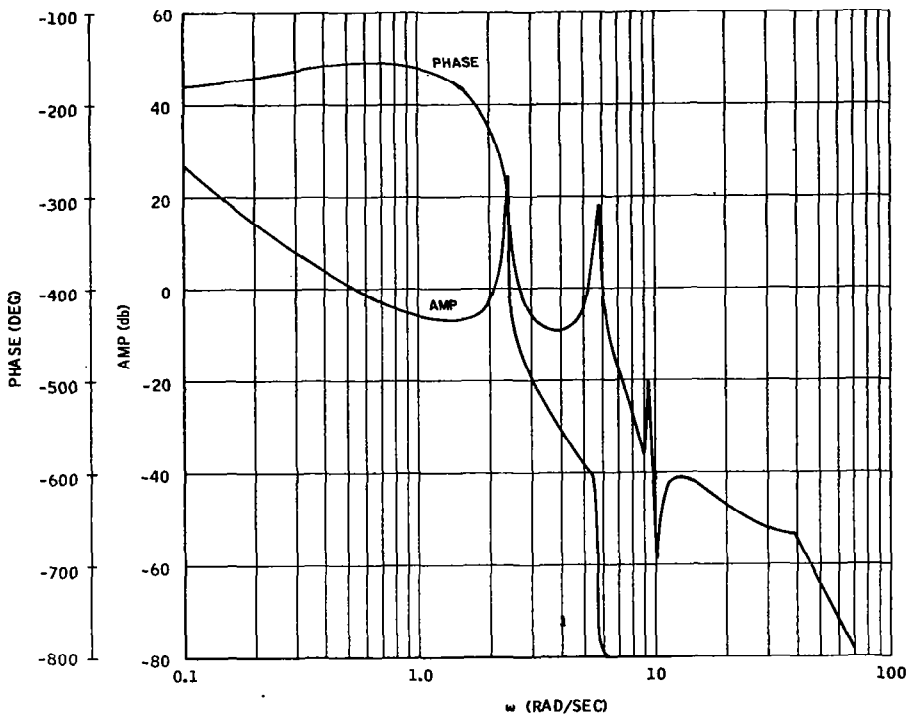

Figure E-10. t = 64 seconds, Nominal System, +20 percent Variation in Attitude Sensor Bending Pickup

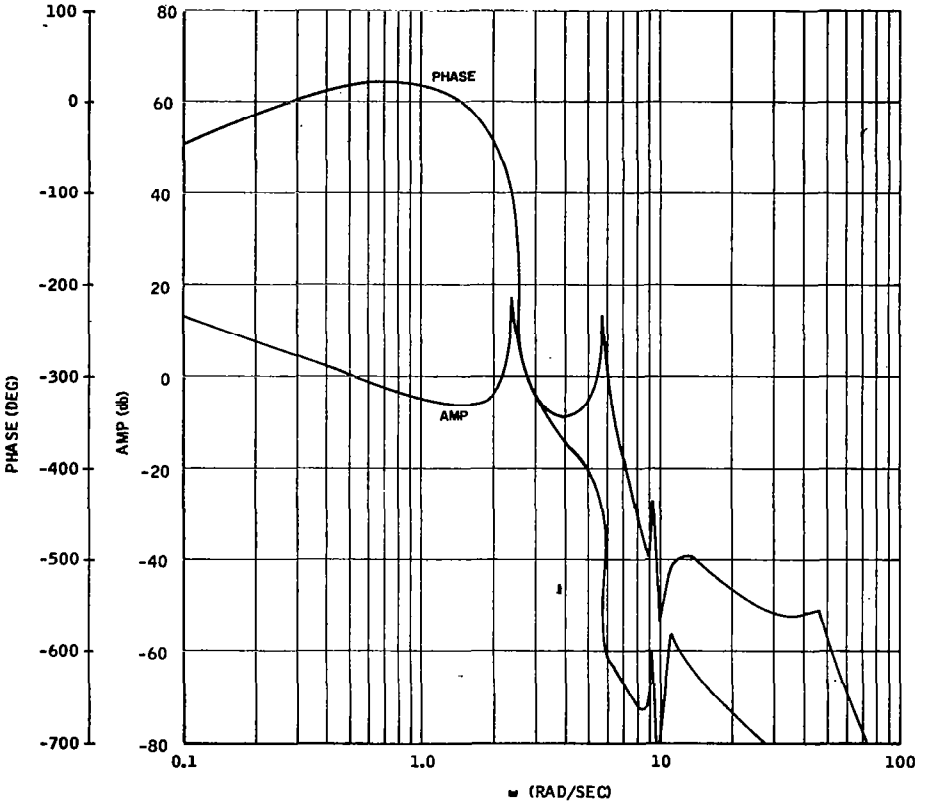

Figure E-11. t = 80 seconds, Nominal System, +20 percent Variation in Attitude Sensor Bending Pickup

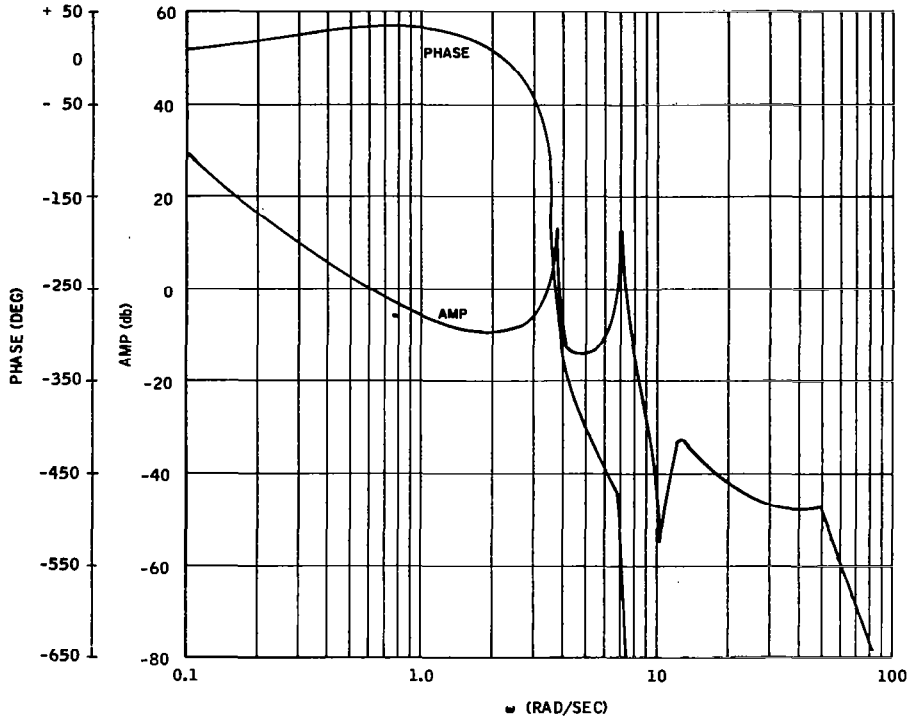

Figure E-12. t = 157 seconds, Nominal System, +20 percent Variation in Attitude Sensor Bending Pickup

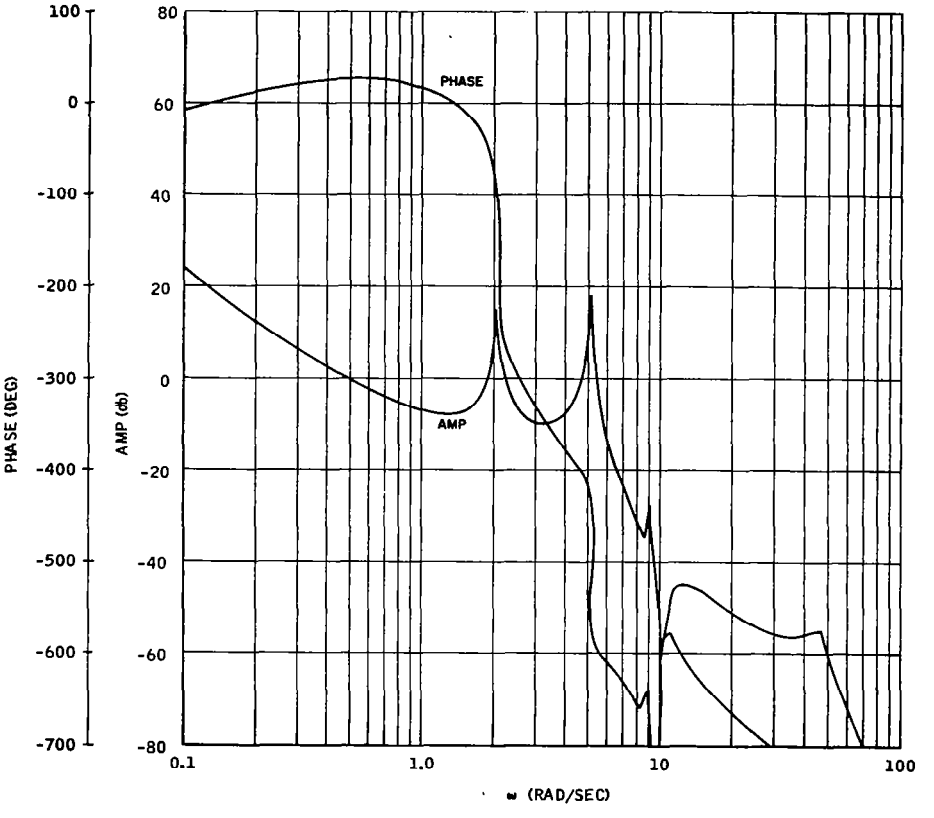

Figure E-13. t = 8 seconds, Nominal System, -20 percent Variation in Attitude Sensor Bending Pickup

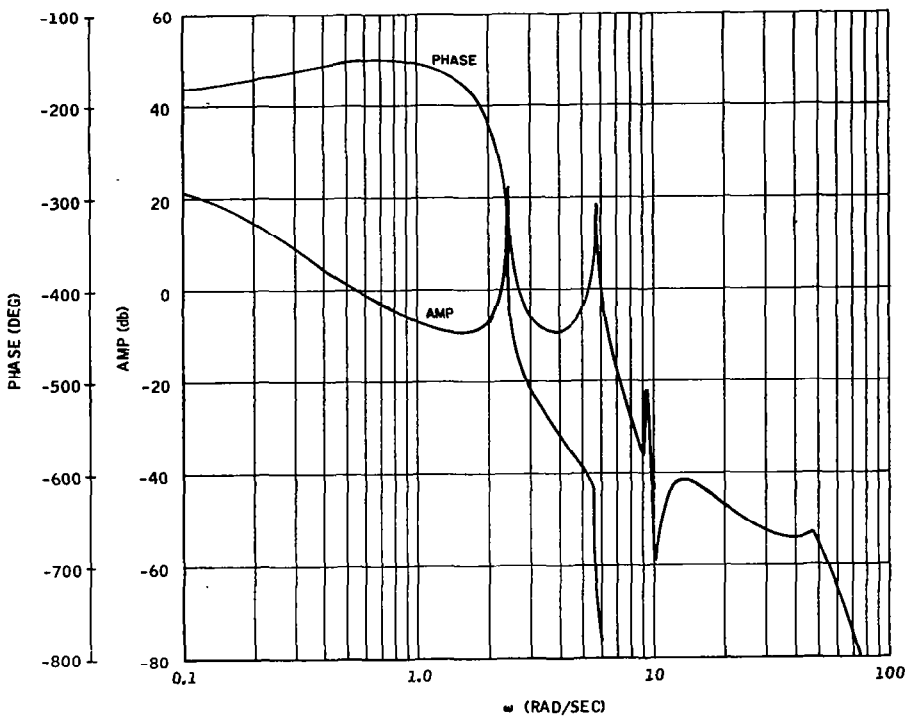

Figure E-14. t = 64 seconds, Nominal System, -20 percent Variation in Attitude Sensor Bending Pickup

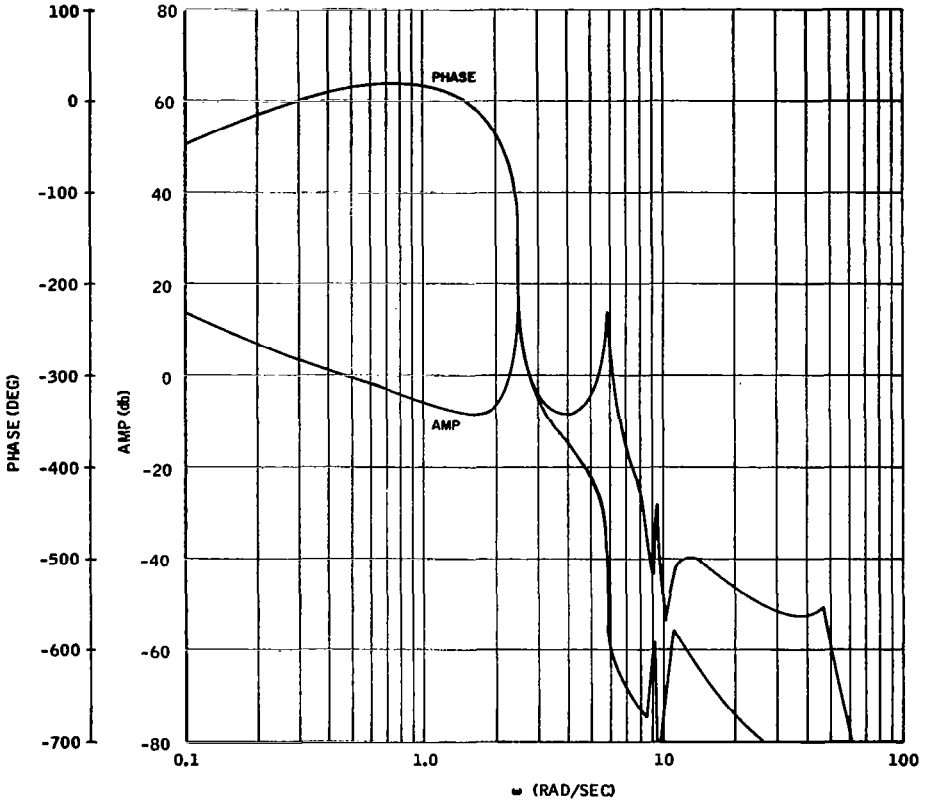

Figure E-15. t = 80 seconds, Nominal System, -20 percent Variation in Attitude Sensor Bending Pickup

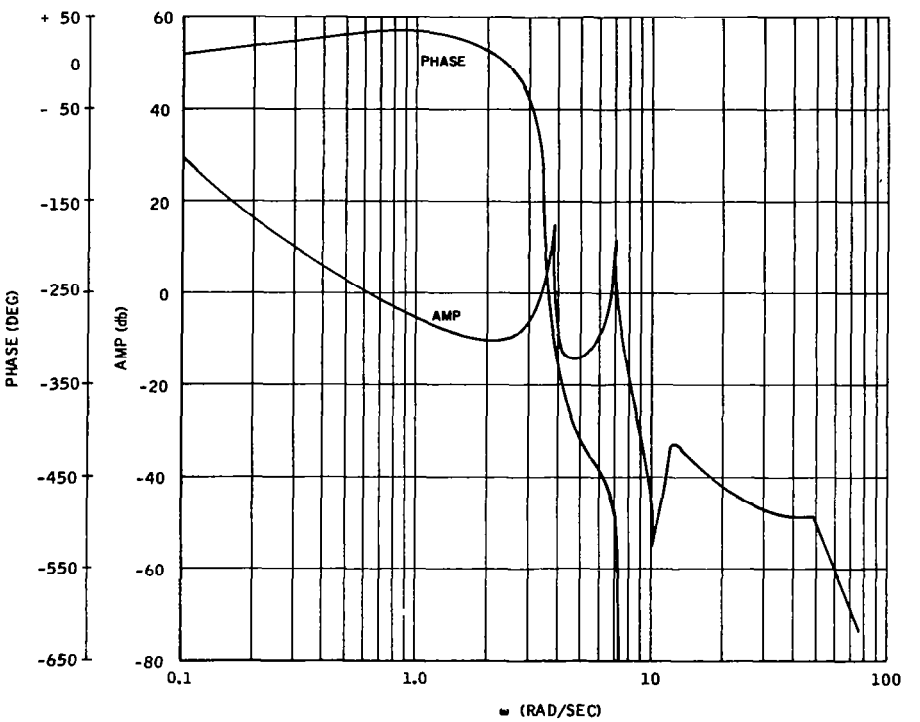

Figure E-16. t = 157 seconds, Nominal System, -20 percent Variation in Attitude Sensor Bending Pickup

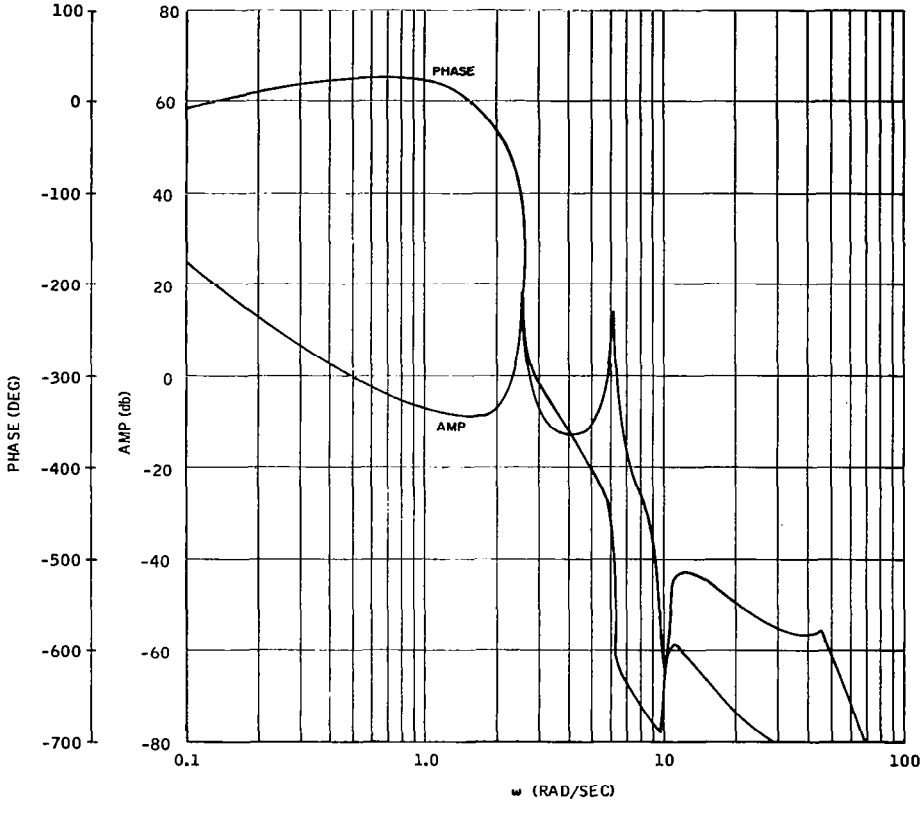

Figure E-17. t = 8 seconds, Nominal System, +20 percent Variation in Bending Frequencies

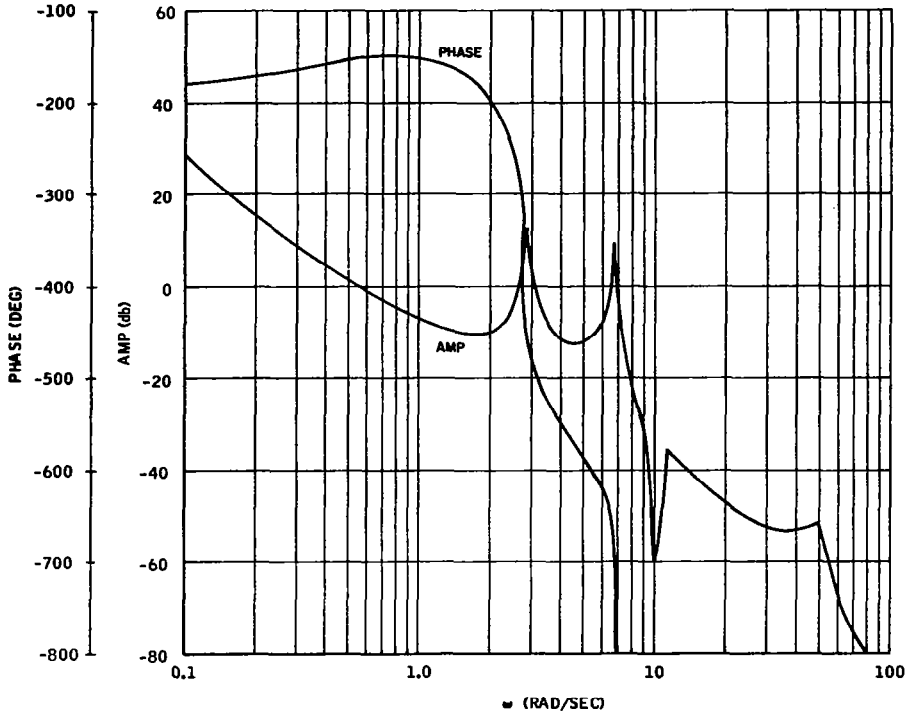

Figure E-18. t = 64 seconds, Nominal System, +20 percent Variation in Bending Frequencies

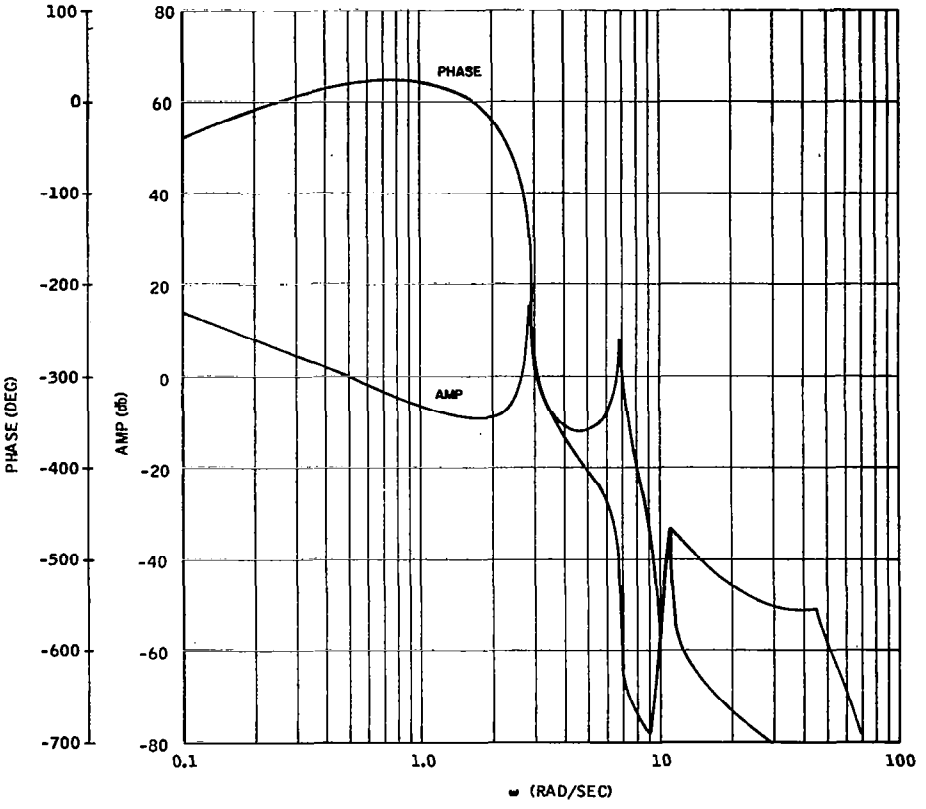

Figure E-19. t = 80 seconds, Nominal System, +20 percent Variation in Bending Frequencies

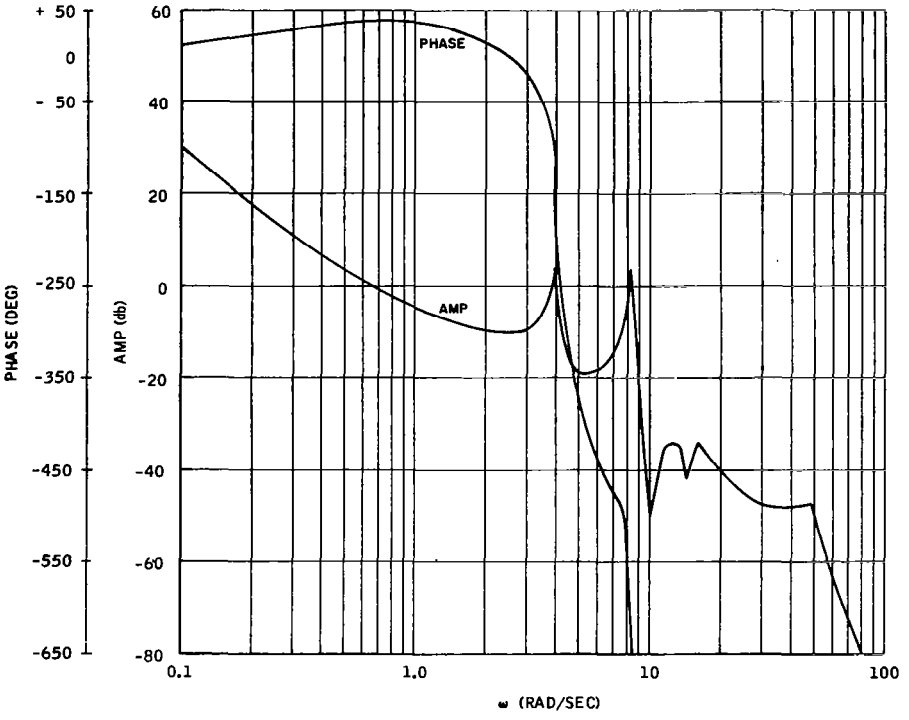

Figure E-20. t = 157 seconds, Nominal System, +20 percent Variation in Bending Frequencies

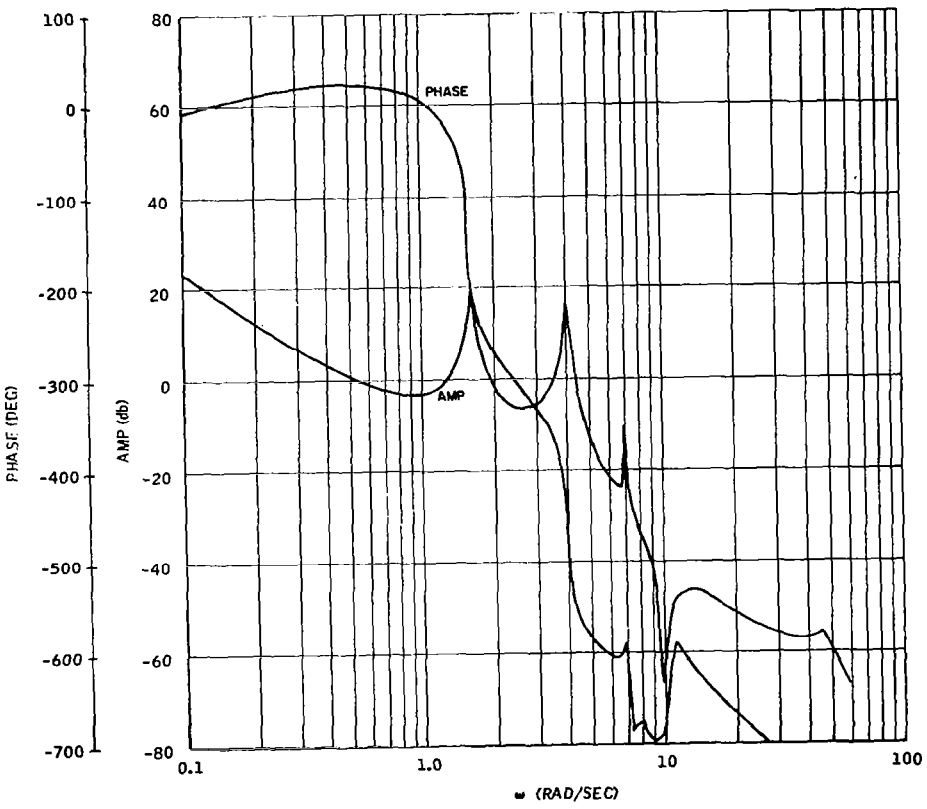

Figure E-21. t = 8 seconds, Nominal System, -20 percent Variation in Bending Frequencies

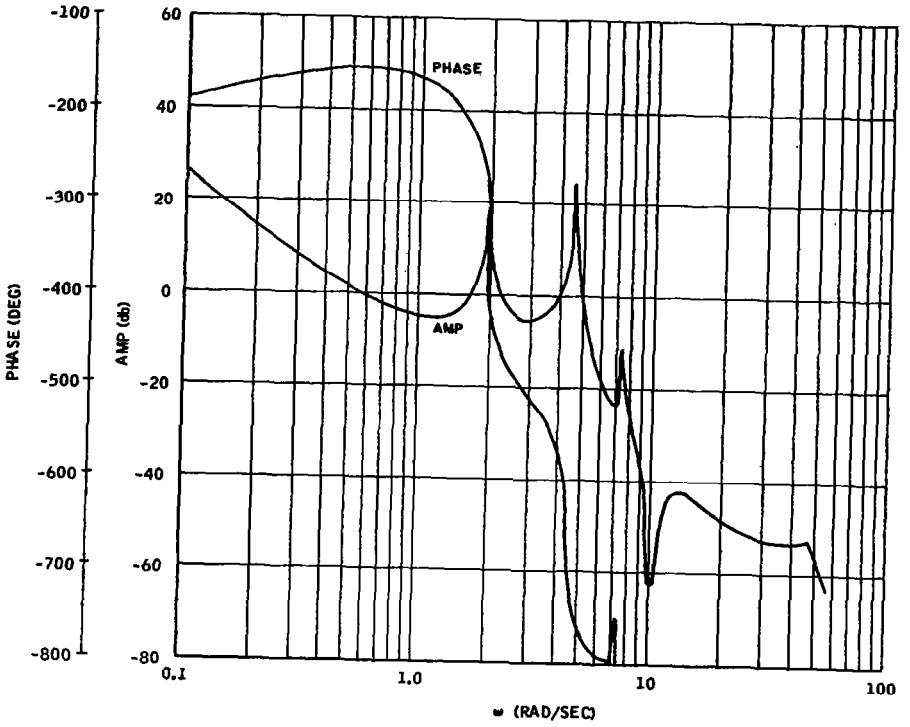

Figure E-22. t = 64 seconds, Nominal System, -20 percent Variation in Bending Frequencies

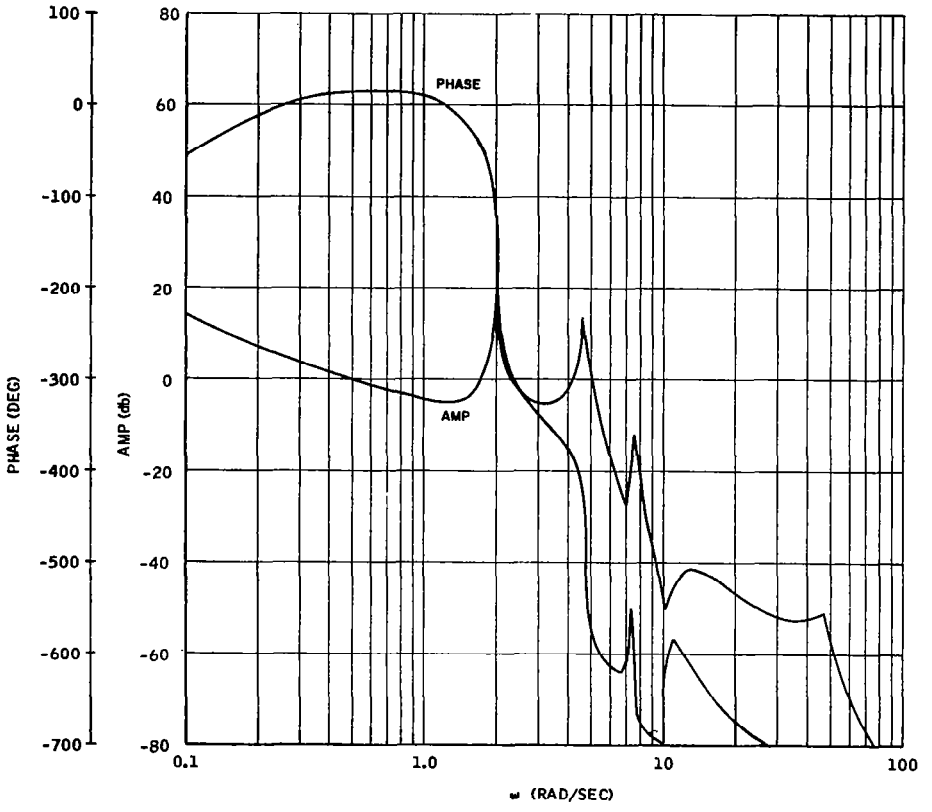

Figure E-23. t = 80 seconds, Nominal System, -20 percent Variation in Bending Frequencies

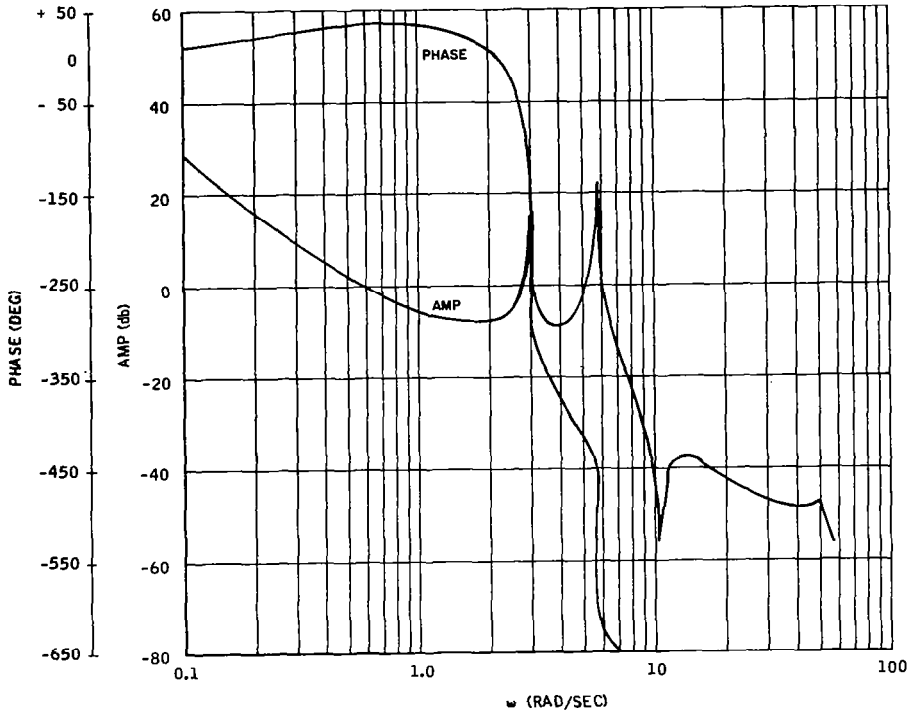

Figure E-24. t = 157 seconds, Nominal System, -20 percent Variation in Bending Frequencies

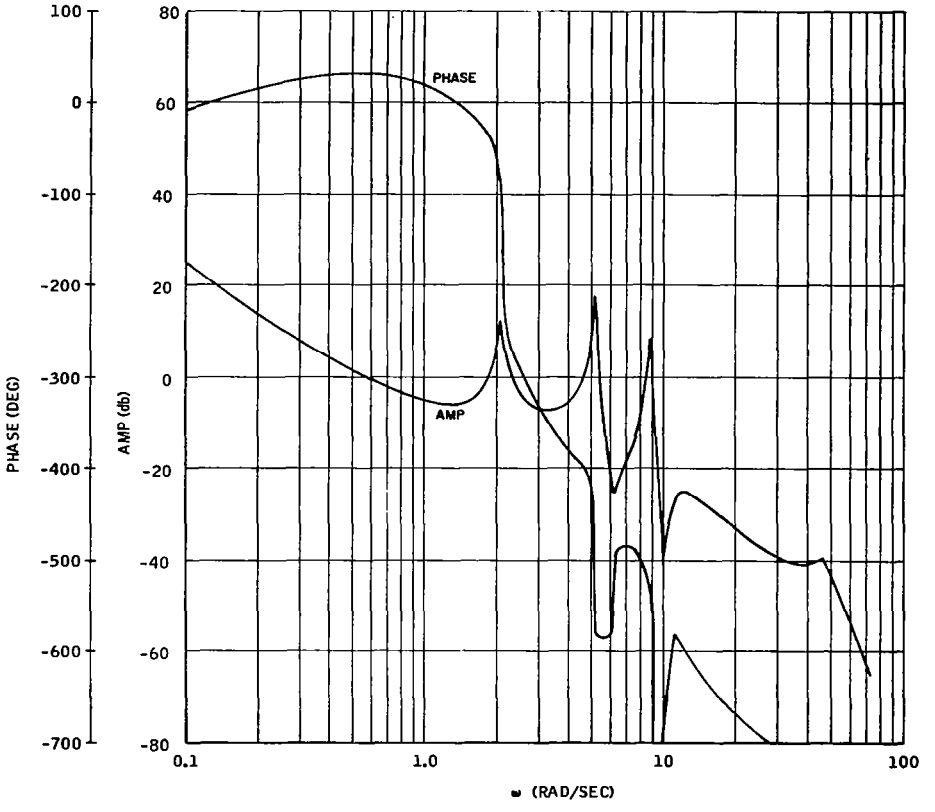

Figure E-25. t = 8 seconds, Nominal System, $Y'_1 = +0.01$, $Y'_2 = -0.06$, $Y'_3 = -0.2$

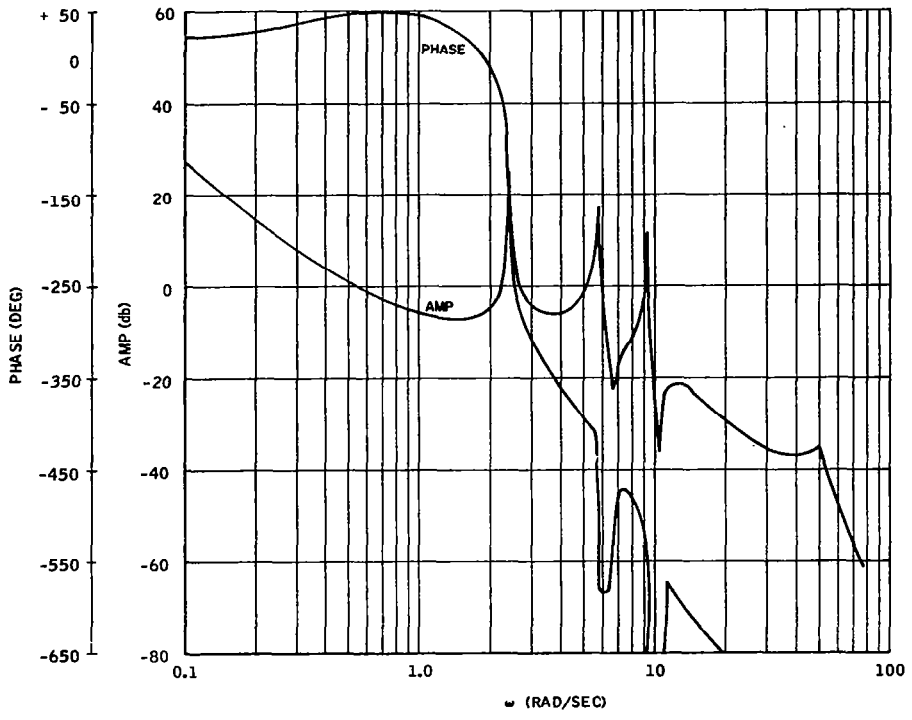

Figure E-26. t = 64 seconds, Nominal System, $Y'_1 = +0.01$, $Y'_2 = -0.06$, $Y'_3 = -0.2$

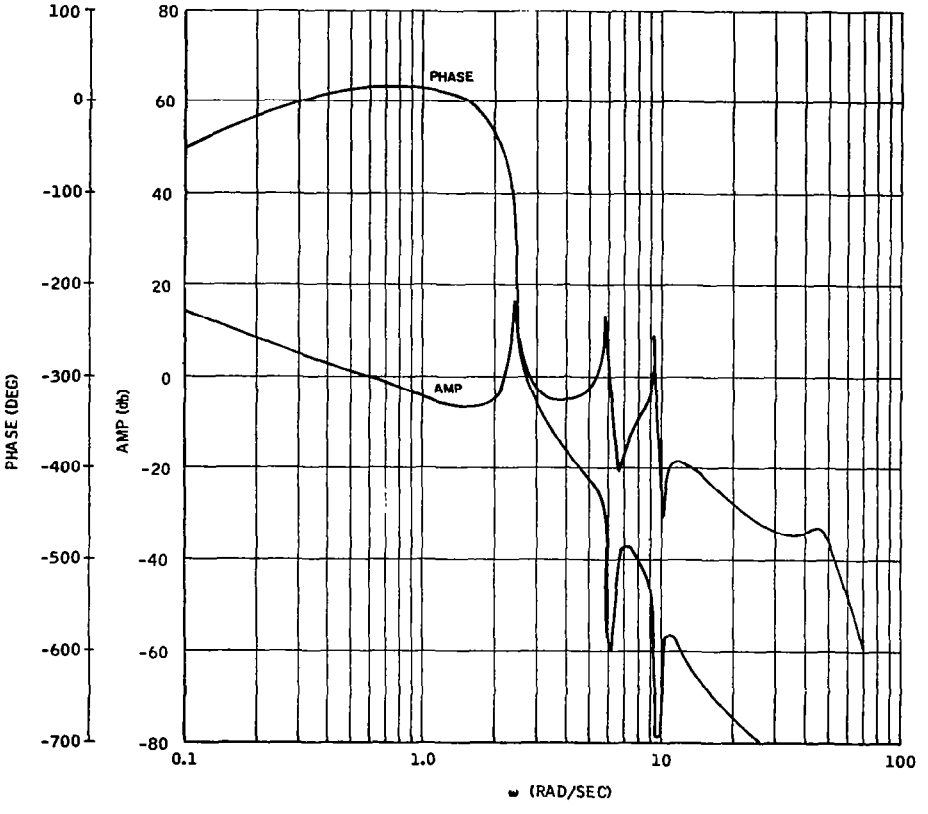

Figure E-27. t = 80 seconds, Nominal System, $Y'_1 = +0.01$, $Y'_2 = -0.06$, $Y'_3 = -0.2$

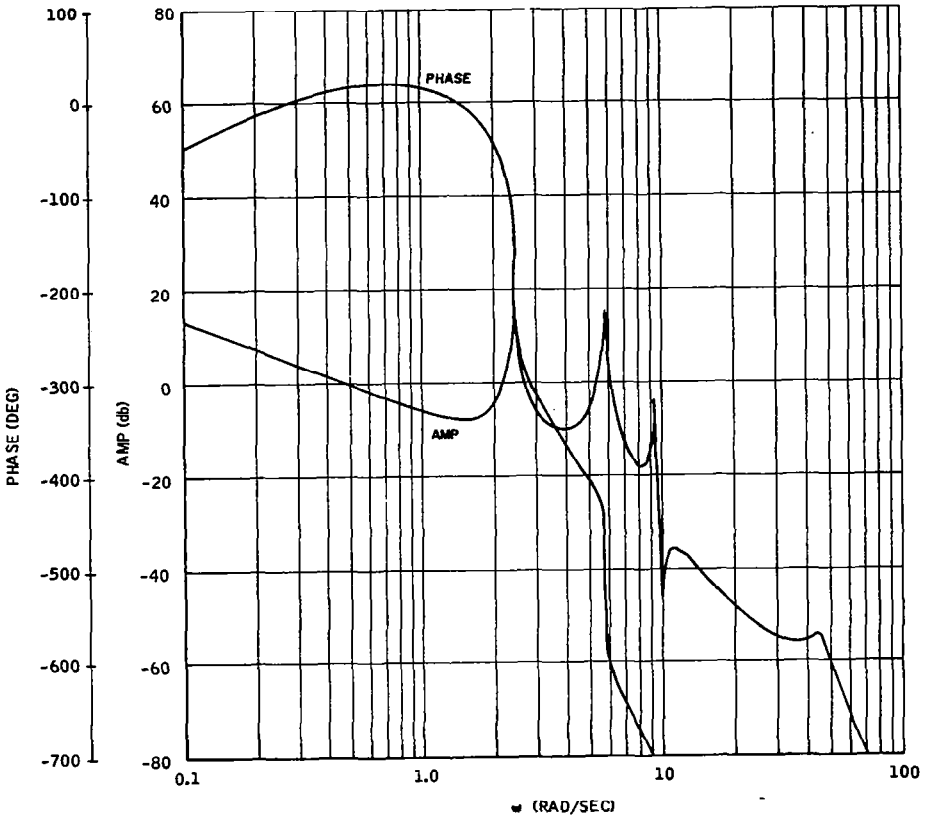

Figure E-28. t = 8 seconds, Nominal System, $Y'_1 = +0.01$, $Y'_2 = -0.06$, $Y'_3 = +0.1$

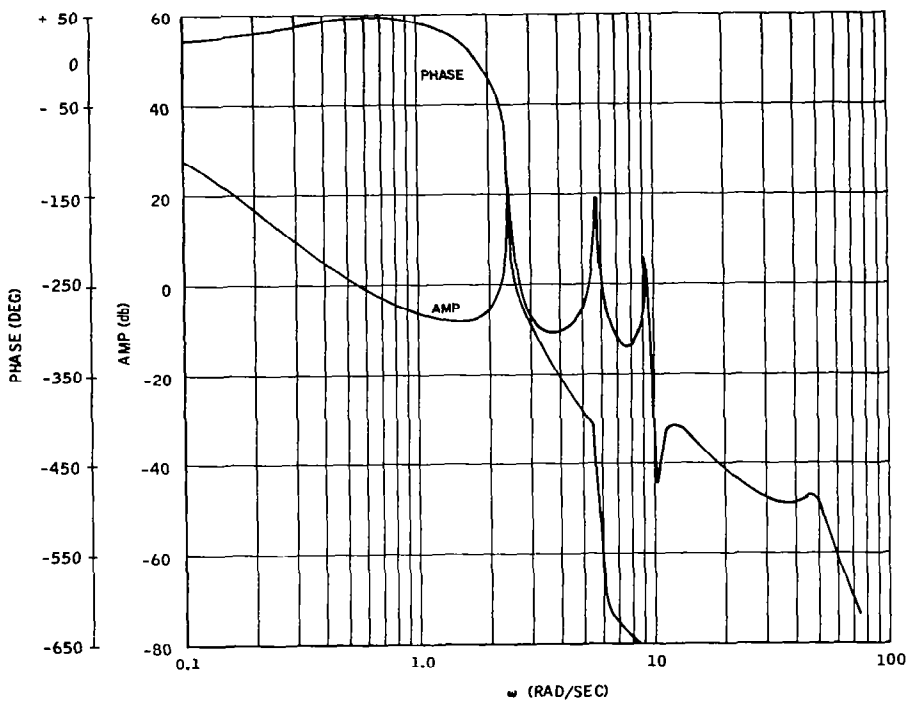

Figure E-29. t = 64 seconds, Nominal System, $Y'_1 = +0.01$, $Y'_2 = -0.06$, $Y'_3 = +0.1$

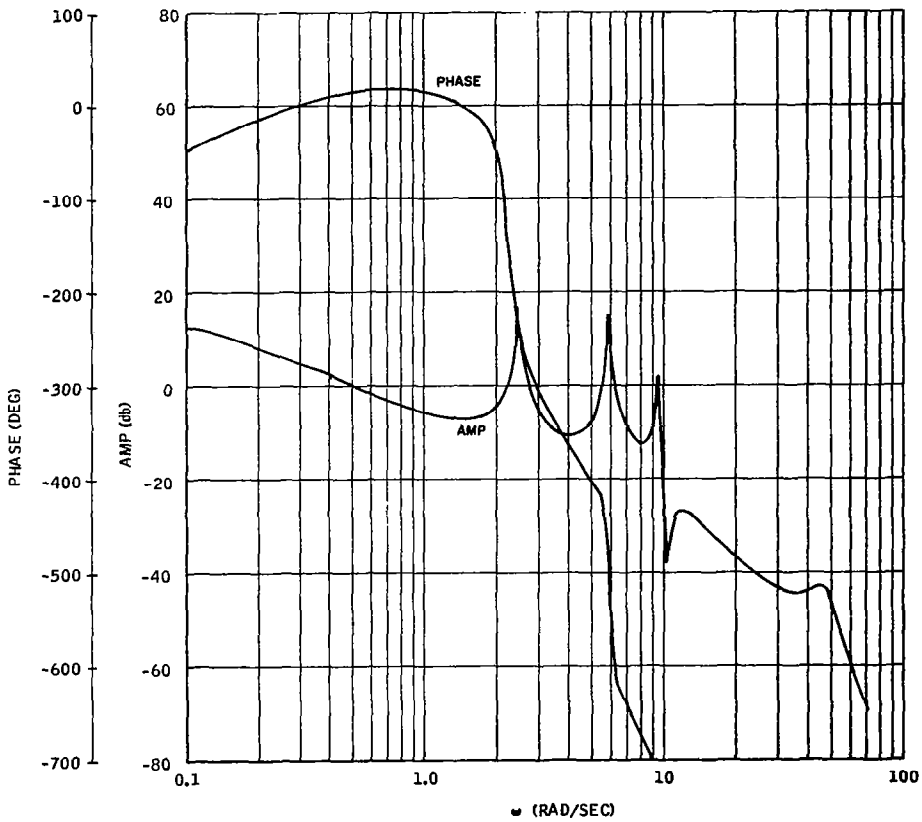

Figure E-30. t = 80 seconds, Nominal System, Y'_1 = +0.01, Y'_2 = -0.06, Y'_3 = +0.1

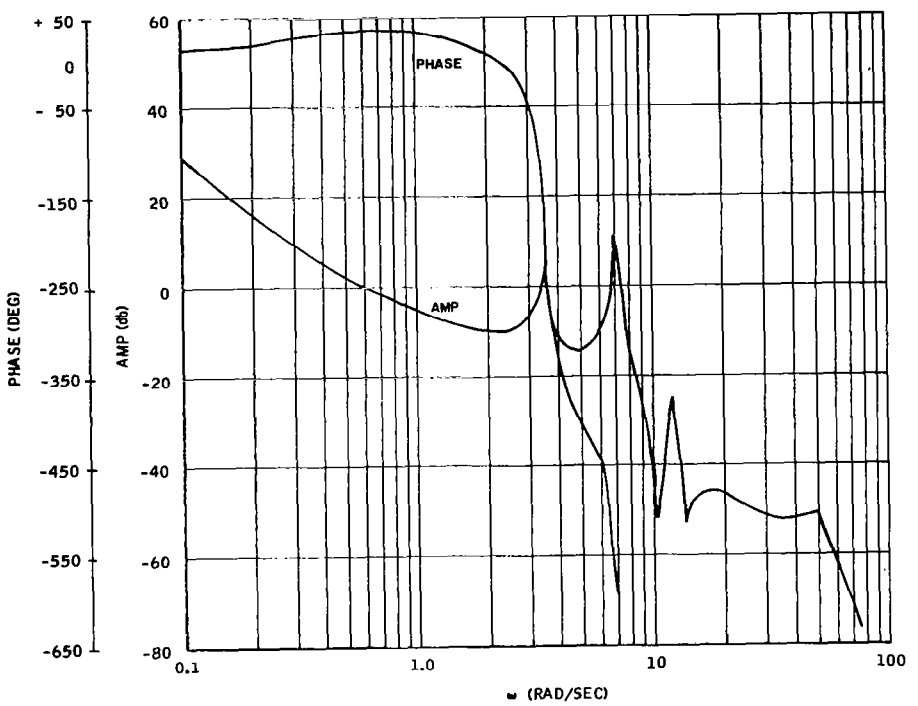

Figure E-31. t = 157 seconds, Nominal System, $Y'_1 = +0.01$, $Y'_2 = -0.06$, $Y'_3 = +0.1$

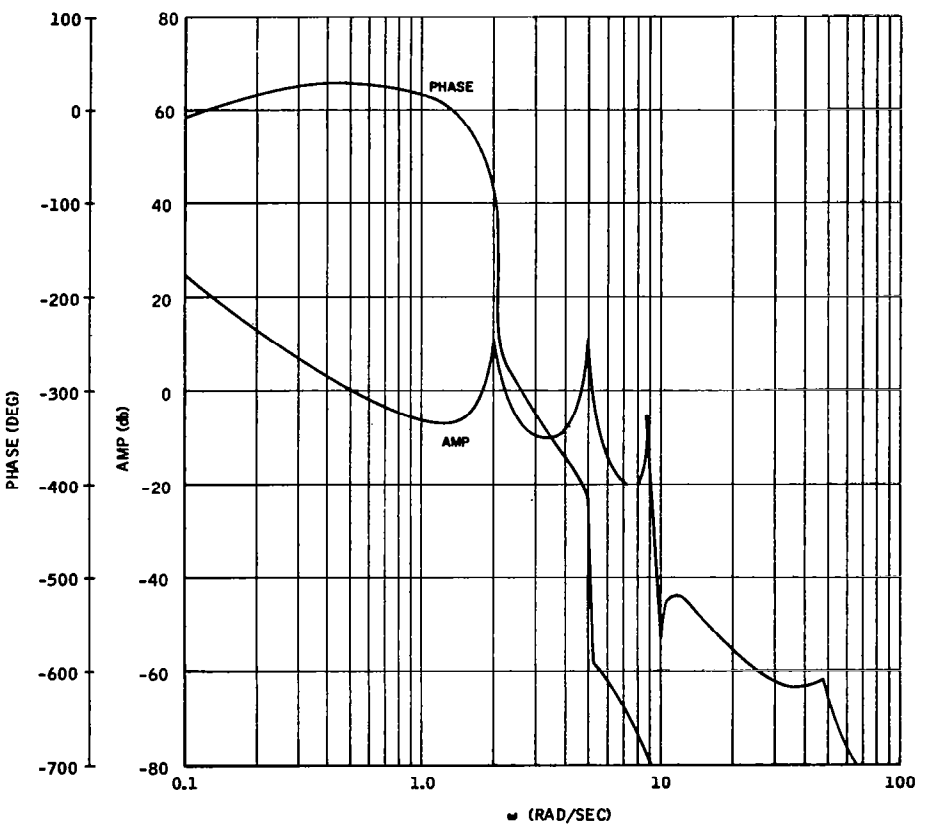

Figure E-32. t = 8 seconds, Nominal System, $Y'_1 = +0.01$, $Y'_2 = -0.06$, $Y'_3 = +0.05$

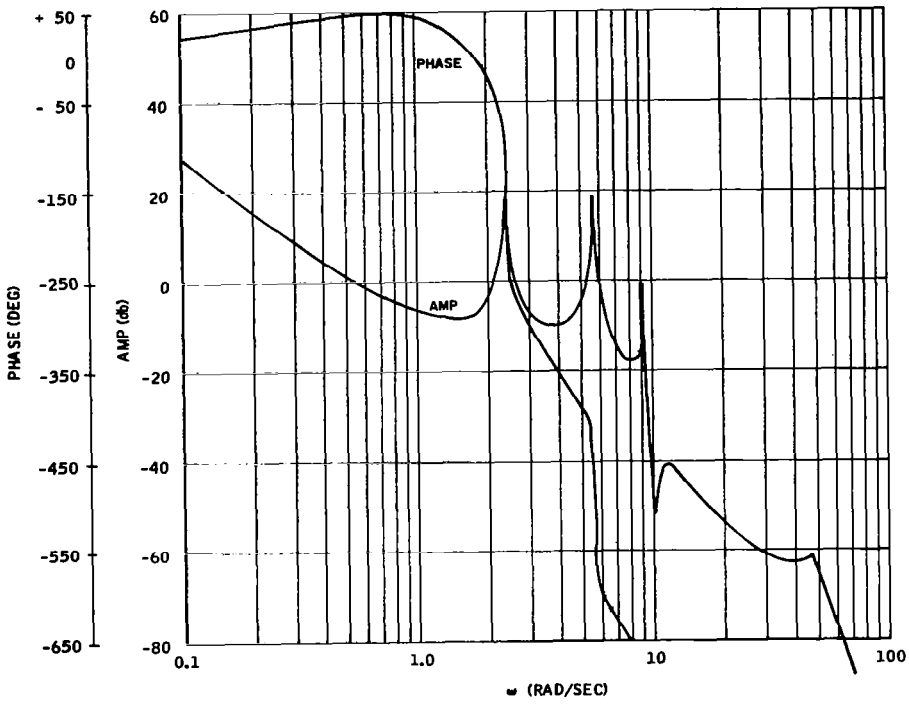

Figure E-33. t = 64 seconds, Nominal System, Y'_1 = +0.01, Y'_2 = -0.06, Y'_3 = +0.05

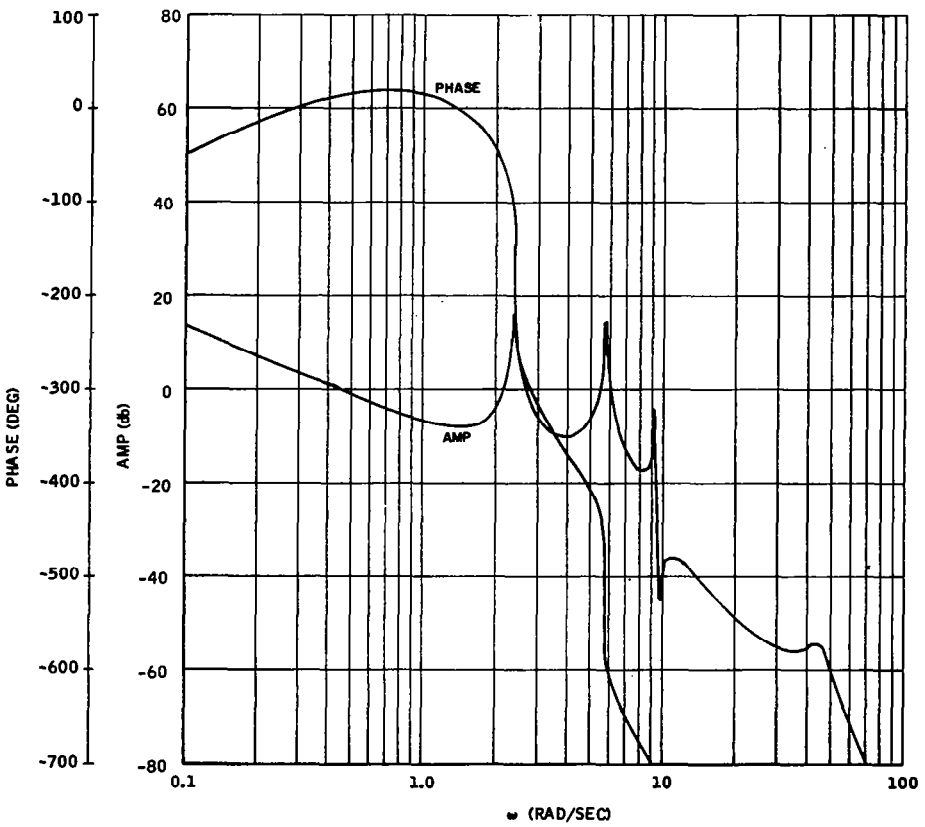

Figure E-34. t = 80 seconds, Nominal System, $Y'_1 = +0.01$, $Y'_2 = -0.06$, $Y'_3 = +0.05$

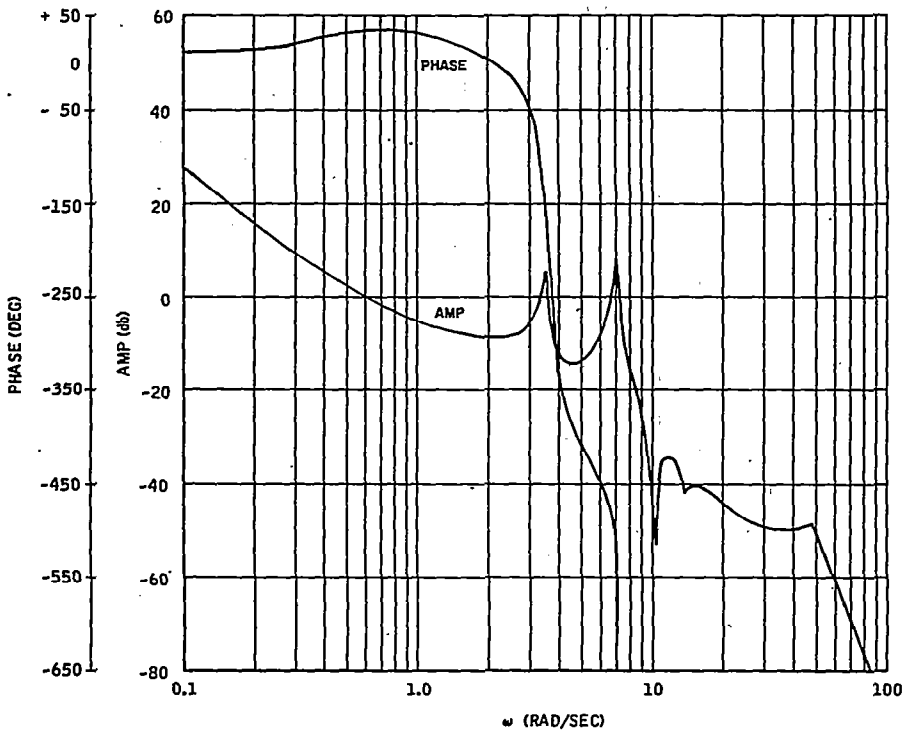

Figure E-35. t = 157 seconds, Nominal System, $Y'_1 = +0.01$, $Y'_2 = -0.06$, $Y'_3 = +0.05$

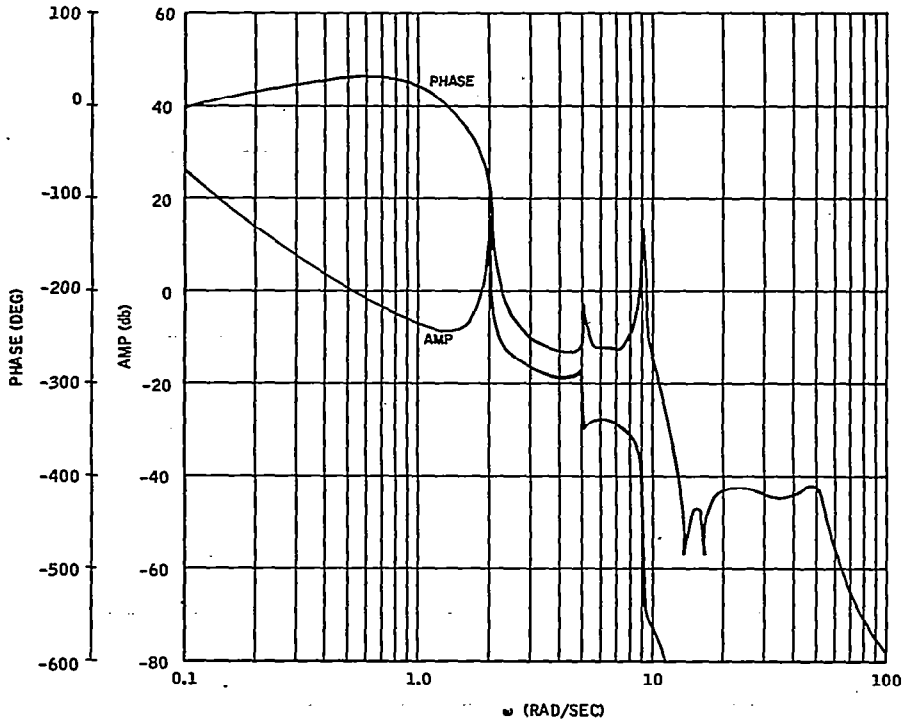

Figure E-36. t = 8 seconds, Nominal Multiple Blender System, $K_A = 0.479$, $K_B = 0.753$, $K_C = 0.349$

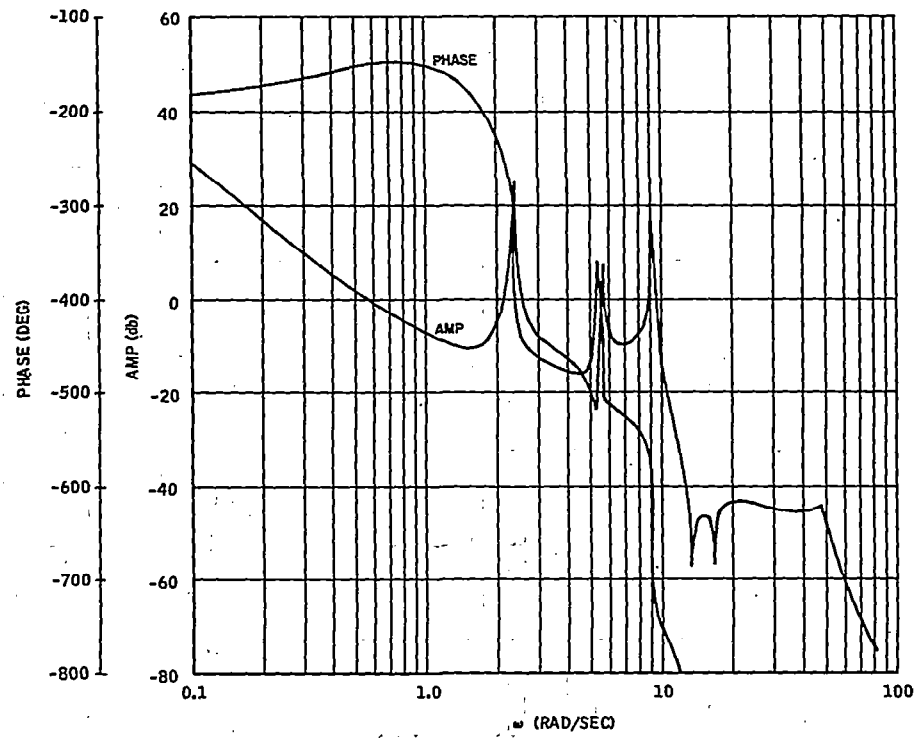

Figure E-37. t = 64 seconds, Nominal Multiple Blender System, $K_A = 0.479$, $K_B = 0.753$, $K_C = 0.349$

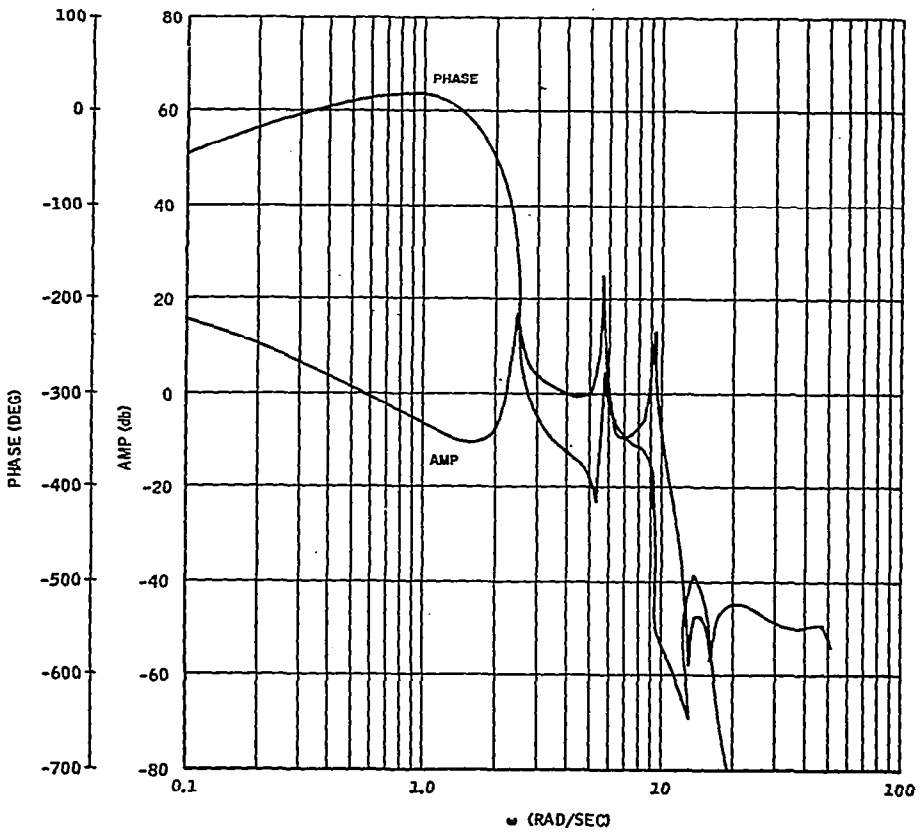

Figure E-38. t = 80 seconds, Nominal Multiple Blender System, $K_A = 0.434$, $K_B = 0.743$, $K_C = 0.397$

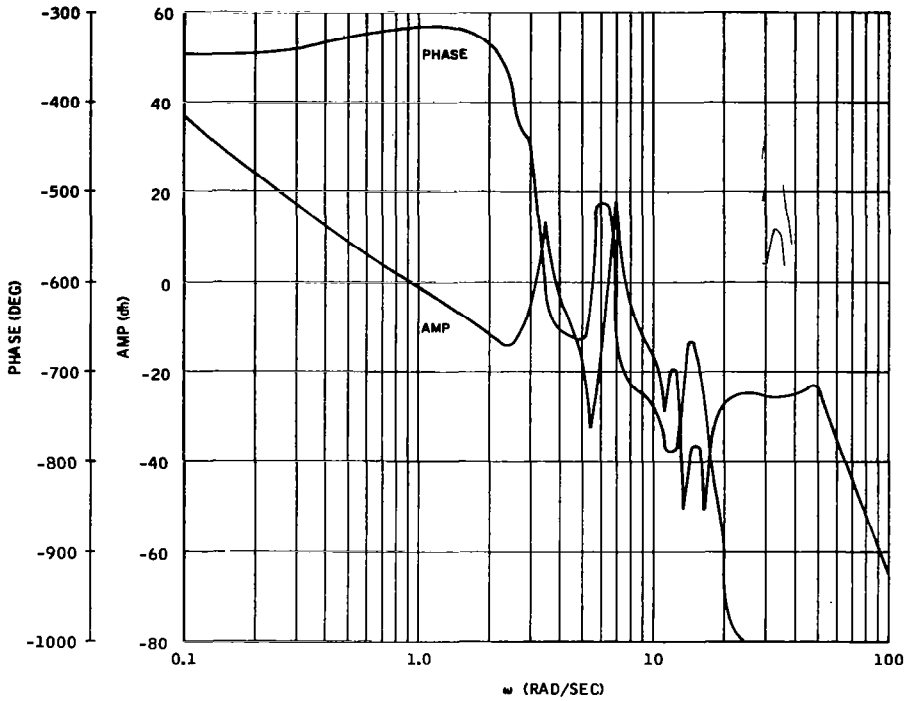

Figure E-39. t = 157 seconds, Nominal Multiple Blender System, $K_A = 0.21$, $K_B = 0.608$, $K_C = 0.40$